DEVELOPMENT OF DIRECT CURRENT HETEROPOLAR

MACHINES WITH SUPERCONDUCTING FIELD WINDINGS

by

Michael Jeffrey Ivo Green   B.E. (Hons)

submitted in fulfilment of the

requirements for the degree of

Master of Engineering Science

UNIVERSITY OF TASMANIA

HOBART

OCTOBER 1981

Conferred 1982

Except as stated herein this thesis contains
no material which has been accepted for the
award of any other degree or diploma in any
university, and that, to the best of my
knowledge and belief, the thesis contains no
copy or paraphrase of material previously
published or written by another person,
except where due reference is made in the
text of this thesis.

M.J.I. GREEN

"Antiphanes said merrily that in
a certain city the cold was so
intense that words were congealed
as soon as spoken."

PLUTARCH

ABSTRACT

A practical and theoretical study of direct current heteropolar machines with superconducting field windings was conducted with the aim of proving their technical feasibility and to indicate their advantages and disadvantages over machines of more conventional design. These studies were conducted in conjunction with extensive tests on small superconducting D.C. machines of various formats.

Three stages of machine development occurred. In the first stage machine the superconducting field winding was shielded from armature reaction fluxes with the aid of iron and compensating windings.

In the second stage machine the superconducting field winding was subjected to the full effects of the armature reaction fluxes.

Tests conducted with these machines indicated that the operation of the superconducting field winding was not influenced by the flow of armature currents. A third, four pole superconducting D.C. machine which exhibits all the advantages gained by using superconductors in the field windings has been constructed. This machine has most of the construction features of a full size prototype machine for future industrial applications. As a result of difficulties encountered in inducing the superconducting state into the field windings operational tests on this machine could not be conducted. Possible reasons for the difficulties are discussed with the result that some of the reasons are rejected and measures that could overcome the difficulties are forwarded.

The project began with no experience in cryogenics, cryostat design and construction nor superconductivity. Consequently details of practical techniques utilised during the project are included.

Continued development of superconducting heteropolar D.C. machines should prove that the design and operation of a prototype machine with a rating in excess of 10 MW is possible. This is essential if this type of machine is to make any impact in the future. Providing the expectation that voltage per commutator bar limits can be substantially increased is realised, machine ratings that are limited only by armature cooling should be possible.

ACKNOWLEDGEMENTS

TABLE OF CONTENTS

APPENDIX

LIST OF FIGURES

INTRODUCTION

1-1   A Brief History of Superconductivity

Onnes' discovery in 1911 of the disappearance of the electrical resistance in mercury at liquid helium temperatures (1-1) stimulated man's imagination in the use of this property in the field of electrical engineering. Soon after this discovery the basic characteristics of the phenomenon were determined: resistance vanished rapidly (apparently discontinuously for many pure metals) below a critical temperature; superconductors acted virtually as diamagnetics (Meissner effect); and the superconducting state could be destroyed in the presence of weak magnetic fields. The magnetic fields could arise from an external source or as a result of transport currents within the superconductor, Silsbee's rule (1-20).

However, progress in the field of superconductivity was very limited because few laboratories knew of the phenomenon, and it was not well under-stood within them. This position was partially reversed during the 1950's when the Bardeen, Cooper, and Schriefer theory was published (1-2) and new superconducting materials were being developed. The critical parameters of superconductors, namely temperature and magnetic field strength, were still very low and large scale applications were not feasible.

During the 1950's space technology developed to the stage where craft were being launched into orbit. From the space program further cryogenic technology evolved and improvements in heat insulation (1-53 to 1-56), and liquefaction techniques gave further impetus to research at cryogenic temperatures.

In 1961 Kunzler (1-3) published work which showed the existence of superconducting materials which could support large supercurrents in the presence of intense static magnetic fields. In the next five years many magnets were wound from single cored conductors of these materials, but difficulty was experienced in their operation. The coils would lose their superconductivity (quench) and often burn out at currents well below their design values.

In early 1964 the prospect of the application of superconductors in machines was considered to be very bleak (1-4). However, the application of superconductors was being pursued in the hope that the quenching problems would be overcome (1-5 to 1-8). The possibility of operating, at cryogenic temperatures, machines which retained conventional conductors and designs was also being studied (1-9).

The premature quenching problem was overcome with the advent of fully stabilised conductors (1-10), and the use of improved coil winding techniques. Also, during this time large helium liquefiers were further developed to a stage where they were becoming reliable. The next stage in the progress of superconductivity was the introduction of twisted, multifilament conductors which became available commercially in 1967.

In the succeeding years many texts on superconductivity and cryogenic engineering have been published (1-11 to 1-28), and the actual design and construction of many electrical devices have been accomplished (1-29 to 1-52). This upsurge in cryogenic investigation among other things was a direct result of man's ever increasing demand for energy which, in turn, demands the increase in the rating of system components. It was envisaged that superconductivity would provide the necessary technology to meet this increased rating demand more economically.

Further developments in the long term reliability of helium refrigerators, the production of conductors with higher critical temperatures and magnetic fields, and the improvement of cryogenic insulation (1-53 to 1-56), will ensure the future commercial applications of electrical equipment which employ superconductors.

1-2   Decision to do Research on Applied Superconductivity at the University of Tasmania

Because of the growing importance of the use of superconductors in the field of electrical engineering, a decision was made towards the end of 1972 to undertake cryogenic research within the Department of Electrical Engineering at the University of Tasmania, and that it should be done by a post-graduate student.

The initial task allotted to the author was therefore:-

(a)   to investigate whether or not it would be feasible to carry out research in the Department on the application of superconductors in the electrical engineering field;

(b)   to decide on the type of research to be undertaken; and

(c)   to undertake such research.

The constraints placed on the selection of the project were:

(a)   it should be capable of being carried out with a small budget;

(b)   it should be in an area which would lead to practical usefulness;

(c)   it should be in a more or less new area.

In addition, there was a complete lack of expertise in the Department and the University on low temperature work; and there were no existing facilities whatever for research into cryogenic engineering within the Department.

The initial investigation, which was conducted during the final year of the author's B.E. course, was a survey of the equipment needed to conduct worthwhile work on superconductivity, the possibility of constructing special equipment within the workshop of the Electrical Engineering Department, the availability of liquid nitrogen and helium and suitable superconducting wire and the order of the costs involved.

The results of this investigation (Appendix A) indicated that an initial equipment outlay of under $3,800 would be adequate and that an average running cost of $1,750 per annum would be sufficient for the purchase of the superconducting wire and helium required during the first three years of the research work into a number of possible fields. As these figures were acceptable and the workshop facilities were adequate, a decision was made to proceed with some research in the field of cryogenic engineering.

1-3   Field of Research

Apart from cost considerations the constraints upon the field of research listed in section 1-2 did not limit the choice of topics. However, it was considered that, to contain the costs, the cryostats should not be large. This eliminated the possibility of investigating cables and levitation systems. The consumption of helium had to be minimal because the supply was limited to thirty litres per experiment, for economic reasons, as it had to be air-freighted from mainland Australia-Sydney. Hence, the study of super-conductors subject to continuously alternating currents and alternating magnetic fields, for example a transformer, could not be considered. A remaining field which could be investigated was the use of superconductors in the field windings of machines. This was considered to be a field which would have important future applications in the utilisation and production of electrical energy at higher efficiencys and lower costs. The topic also

offered interesting challenges, consequently it was decided that research in this area would be pursued.

From the considerations set out below a decision was made to investigate the application of superconductors in D.C. heteropolar machines.

1-3-1 Synchronous Machine

To make a useful contribution in the design of synchronous machines with superconducting field windings there were problems, additional to those in D.C. machines, to be overcome in the areas of winding and supporting the field system and, if a rotating field was adopted, in the successful design and construction of rotating vacuum and liquid helium seals. As there was considerable research already in progress elsewhere in this area it was considered that a worthwhile new contribution in addition to that resulting from other organisations could not be made.

1-3-2 Homopolar Machine

Because of its apparent simple structure and international interest in this type of machine, it was decided to undertake some initial experiments on a homopolar machine with an improved and unconventional type of armature current collection. A system was devised to introduce an all-negative brush current collection system by using one set of rotating brushes and one set of stationary brushes and thus gain the advantage of the lower contact voltage drop under negative brushes - figure 1-1. Experiments were conducted with copper filament brushes which showed promise of satisfactory operation at high current densities, and high surface speeds, giving low values of friction and long wearing life.

FIG 1-1
LAYOUT FOR AN ALL NEGATIVE BRUSH MACHINE

Inner current collector

single sided rotor
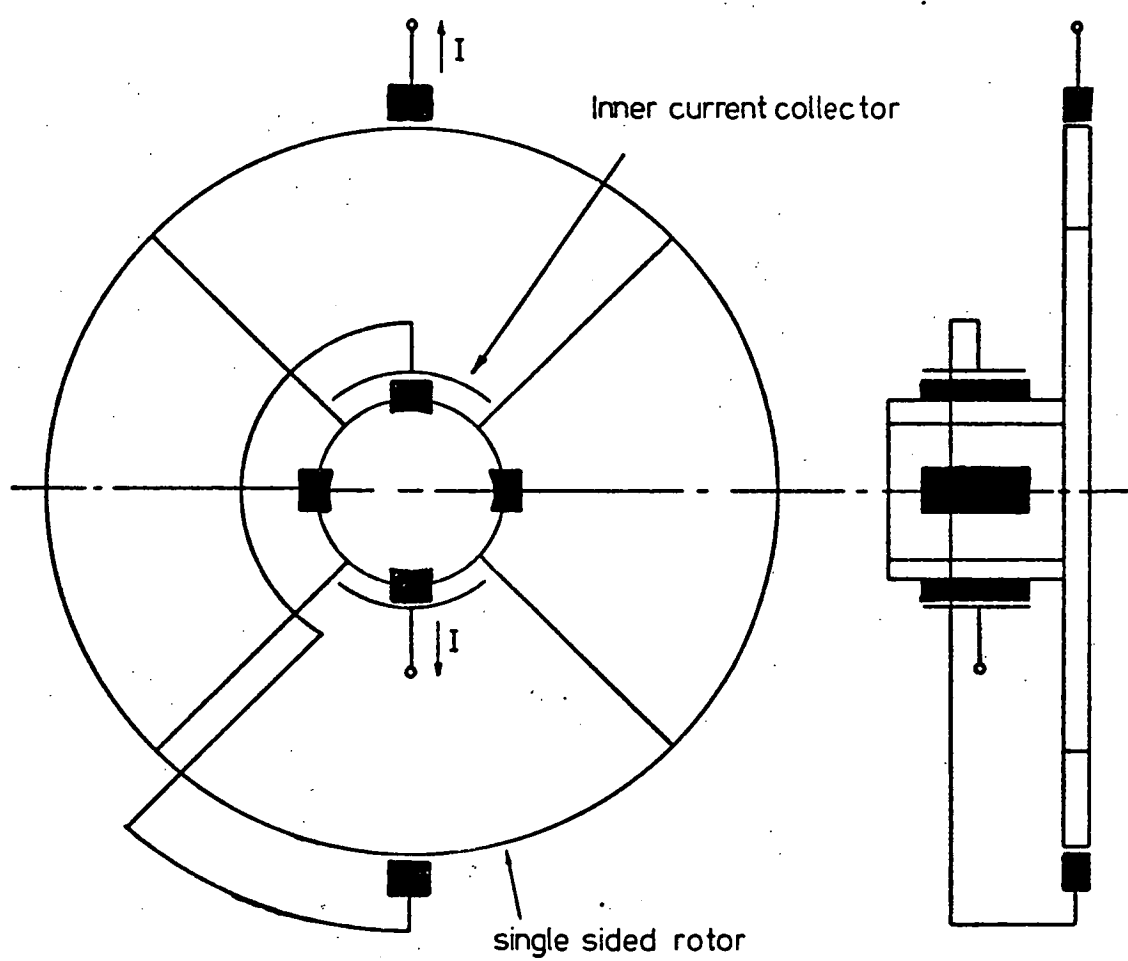
The need to gain first-hand knowledge on cryostat design, cryogenic insulation, and the necessity to determine possible problems associated with the vacuum sealing of joints subjected to cryogenic temperatures required a low cost introductory cryostat for initial experiments. Such a cryostat was constructed from galvanised iron - figure 1-2.

A solid coil of copper wire was housed within the cryostat so that possible advantages of operating conventional conductors at cryogenic temperatures and the effectiveness of the coil potting technique could be determined. Liquid nitrogen was used for all of the preliminary tests as it was in plentiful supply from within the University of Tasmania and it was considered that the experience gained could be related to liquid helium temperatures.

After this work was completed and the effects of low temperatures upon possible sealing materials were determined (Appendix C), a test homopolar machine with a segmented rotor was constructed. Liquid nitrogen cooled, copper pancake coils were used in the field so that the cryostat could be perfected and the armature tested before resorting to a superconducting field coil. The cryostat was partially insulated with polyurethane foam and very basic experiments on the current carrying capacity of the field coil were conducted.

The rating of the experimental machine with the superconducting field coil was to have been 1 kW at 2000 r.p.m. and 50 volts. The rotor disc diameter was 210 mm and to set up the magnetic field would have required over 1 km of superconducting wire. At this stage it occurred to the author that for practical applications it might be possible to produce a heteropolar machine, with a superconducting field winding, which could have advantages over the homopolar machine.

FIG 1-2
INITIAL CRYOSTAT

All dimensions mm
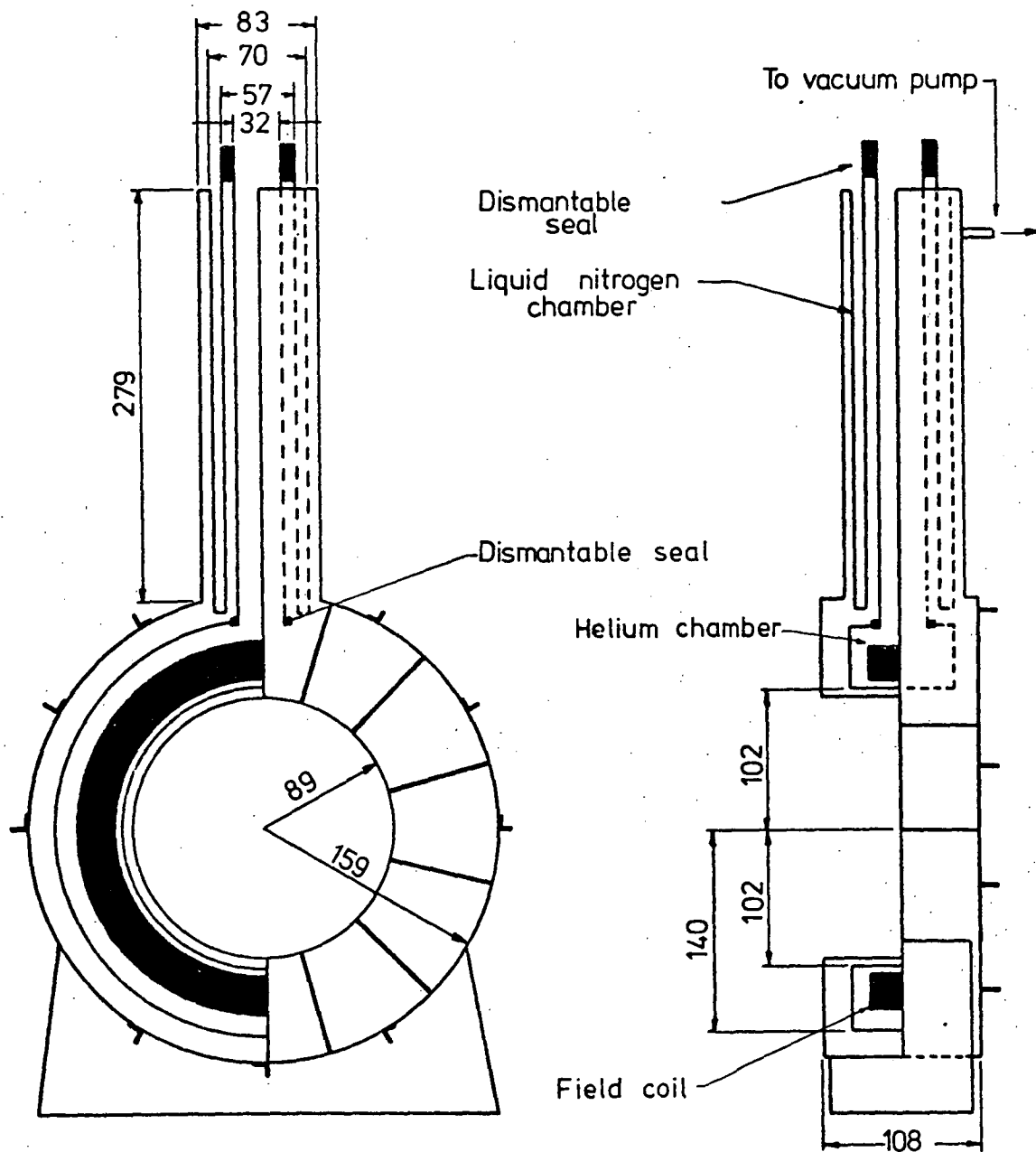
Because only one researcher would be working on the project it would not be possible to keep up with the rate of development on homopolar machines being conducted elsewhere in large laboratories (1-32), and therefore it would not have been prudent or relatively productive to continue into the investigations of homopolar machines. For these reasons a decision was made to discontinue further work on the homopolar machine. However, a great deal of experience had been gained from the initial work on the homopolar machine.

1-3-3 Heteropolar D.C. Machine

Researchers inferred (1-32, 1-44, 1-47) that it would not be practicable to build large heteropolar machines with superconducting field windings; the reasons given being

 (a) the unknown effect of armature reaction fluxes on the superconducting properties of the field windings;

 (b) the limits imposed upon the machine ratings because of inherent commutation problems;

 (c) the problems of supporting the field windings against the full load torque of the machine.

These three apparent disadvantages of the heteropolar machine and an awareness of other problems, such as the limits on the volts per commutator bar and the armature surface specific electric loadings, which limit the ratings of conventional heteropolar machines appeared to have combined to colour investigators' thinking. Hence the superconducting homopolar machine has been extensively studied by others and the heteropolar machine ignored until recently (1-46, 1-50 to 1-52).

Before the advent of superconductors, homopolar machines were not used extensively because of their excessive weight and the current collection

problems. However, when it became apparent that the field flux required could be obtained with the use of superconductors and without the large weight penalty of the iron in the magnetic circuit, the machine became a worthwhile proposition. The stability of superconductors in large windings was still questionable, and it was correctly thought that possible disturbances to the conductor should be minimal and hence the armature reaction-free, and torque reaction-free homopolar machine field winding was considered to be ideal for the first power engineering application of superconductors. In the view of the author it was these last few considerations alone which prompted some previous workers to decide that the homopolar machine should be investigated and that the heteropolar machine should not.

However, it was felt by the author that insufficient investigation had been conducted to overcome these problems. This was in direct contrast to the amount of work conducted on similar problems associated with the homopolar and synchronous machines. It was therefore considered to be a very worthwhile area in which to work.

In the opinion of the author the following points should be carefully considered together with the three previously mentioned arguments against the heteropolar machine when comparing the two forms of machine.

(a) The torque reaction disc (compensating winding) in a homopolar machine must be present to provide the return paths for the armature currents. Hence, as it is fundamental to the operation of the homopolar machine, it is not generally indicated that it is detrimental to machine efficiency. On the other hand the inclusion of a compensating winding (torque reaction winding) in a heteropolar machine is not fundamental, but may be necessary to the operation of the machine; hence it is

generally looked upon as being detrimental to efficiency but in effect is no more so than the torque reaction disc of a homopolar machine.

(b) The commutation and current collection problems in large heteropolar machines were thought by other workers to be insurmountable, but the current collection and commutation (drum type machine excluded) of much larger currents in the homopolar machine were not thought to be so.

(c) The stray flux outside a heteropolar machine is considerably less than that of a homopolar machine of comparable rating - figure 1-3. To obtain the same external flux densities with a homopolar machine a second "cancellation" winding would be required.

(d) The field system of a homopolar machine is not subjected to forces except for those caused by iron structures in the near vicinity. These forces can however be large - 1-40.

(e) The terminal voltage of the heteropolar machine, even with the use of a conventional type of commutator, can be many times that of the homopolar machine. The added expense and space requirements of the larger supply bus bars to a homopolar motor and the associated rectifying equipment, where required, could have disadvantages especially in situations where space is at a premium.

(f) A series of small field coils for a heteropolar machine would be easier to wind and pot than a single coil which surrounds the entire armature of a disc type homopolar machine. The jointing of the smaller coils could be a problem, but joints would also be required in the field coil of a homopolar machine. The use of brittle high

FIG 1·3
TYPICAL STRAY FIELD FLUX DENSITY
OF SUPERCONDUCTING MACHINE

A   Homopolar machine

B   16 pole heteropolar machine
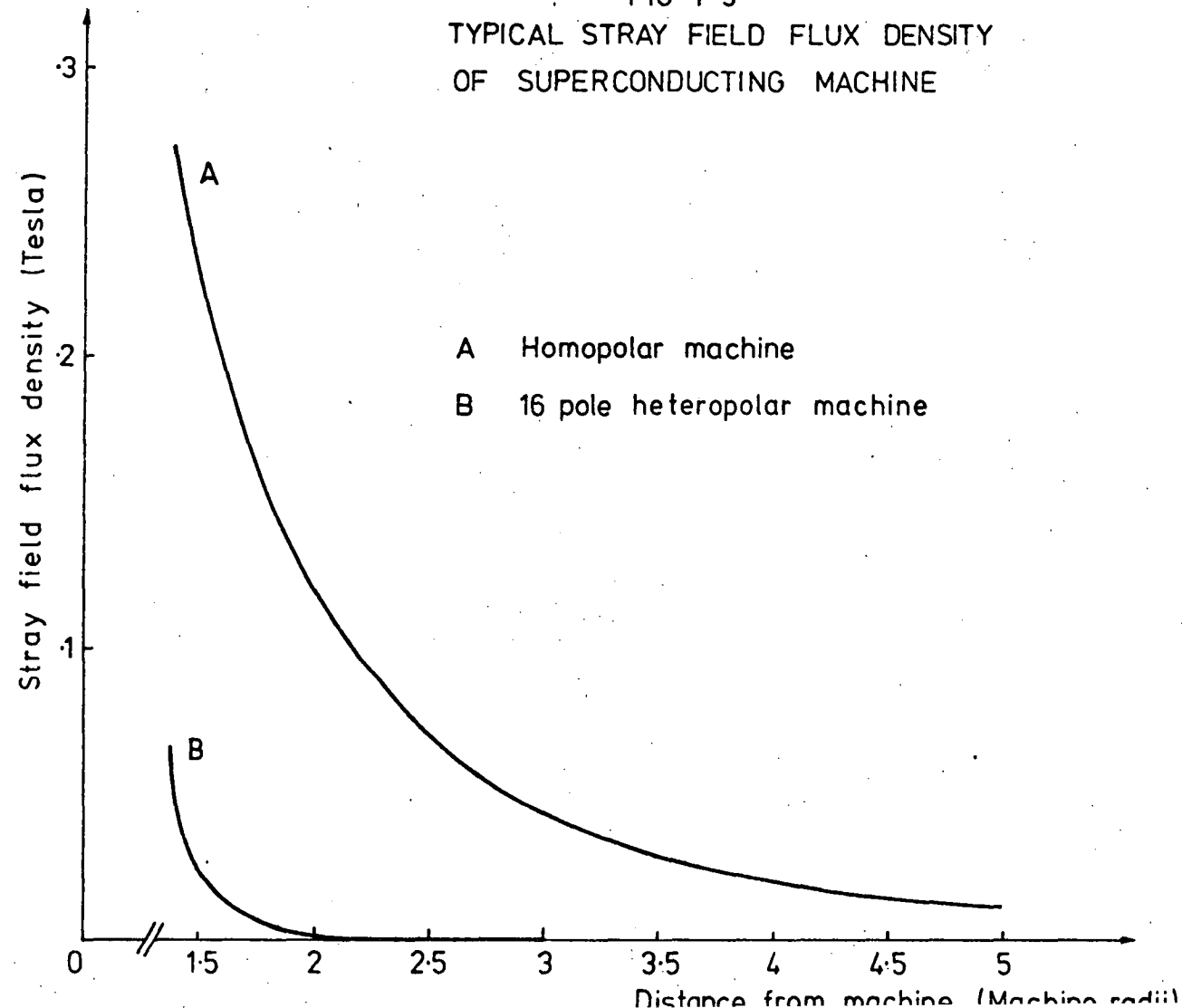
field superconductors which have high critical parameters
would be more attractive when small coils are required
because of the special curing techniques used during coil
construction.

Further preliminary studies indicated that useful results could be
obtained with small cryostats and coils which only required 100 metres
of superconducting wire.

In terms of a small laboratory the heteropolar machine also has cost
saving advantages over an equivalent homopolar machine required to obtain
similar experimental results. For example, a heteropolar machine has:

(a) considerably less superconducting wire than a comparable
     small homopolar machine;

(b) a smaller cryostat which does not have the helium
     consumption of a cryostat for a similar homopolar machine.

From the foregoing considerations it was apparent that the heteropolar
D.C. machine was an ideal project on which to conduct research in a
department of a small university.

1-4   The Advantages and Disadvantages of the use of Superconductors
      in Heteropolar Machines

There are fundamental reasons for investigating the use of super-
conductors in electrical machines: to determine whether higher rated
machines than those available using conventional construction techniques
can be economically constructed and whether more economic machines of the
same rating are possible.

The basic limitations of conventional design techniques on machine ratings were studied to determine how the application of superconductors could possibly increase machine ratings. Areas in which improvements and potential difficulties could occur with the use of cryogenic technology are discussed in the following paragraphs.

(a) The fundamental reason for considering the use of superconductors in the field windings of D.C. heteropolar machines was to reduce or eliminate the quantity of iron required in their construction. This possibility arises as a result of the large magneto motive forces possible with superconductors with negligible power loss. If the iron was eliminated the limiting saturation flux density of iron could be exceeded at the armature provided that the critical flux density of the superconductor is not exceeded. The higher field flux density would result in smaller machines than conventional machines of the same rating provided that other design limitations, especially the voltage between commutator segments, are not exceeded. The reduction in the iron content of a machine could eliminate the effect of the armature reaction saturation upon the voltage regulation. This would have advantages in the control of the machine.

(b) The use of high field superconductors carrying large transport currents in intense magnetic fields is at present limited to applications where the currents are essentially D.C. with little or no ripple. This constitutes the major reason why the use of superconductors in the armature windings, which are subject to both rapidly changing currents and magnetic fields, has not been considered. Therefore it does not appear at this stage that superconductors will be used in the armature windings of large machines. However, it would be possible to cool cryogenically,

conventional armature windings, thus increasing their current carrying capacity. This could produce a higher rated machine provided that successful commutation was possible.

(c) The major problem associated with increasing D.C. heteropolar machine ratings above their present limit is the commutation of the armature coil currents and the transfer of large quantities of electrical energy to and from rotating surfaces. It was in the improvement of commutation and transfer conditions that superconductors showed the possibility of increasing machine ratings. The reason for this is that, with the high field m.m.f.'s available with superconductors, the quantity of iron required to support the necessary field flux was reduced and large air gaps could be tolerated. This meant that the armature windings need not be embedded in armature slots; thus the armature coil reactance voltages would be reduced which would improve the commutation.

(d) The elimination of armature teeth provides more of the armature surface for armature conductors; hence increased armature specific electric loadings could be achieved which would result in increased machine ratings. With the conductors forming the armature surface, access for cooling media would be enhanced which, in turn, would reduce problems associated with the thermal performances of the higher specific electric loaded armature surfaces.

(e) In conventional machines the forces due to the load torques are largely carried by the iron armature teeth and little load torque is carried by the armature conductors. The armature teeth also act as supports for the armature conductors against forces such as a small percentage of the load torque and the centripetal forces. If full use is to be made of

the previously mentioned advantage, then adequate alternative means of support for the armature conductors, which now take the full load torque as well as the centripetal forces, have to be devised. The problem of conductor support could be partially overcome by producing machines with interlocking and suitably insulated copper bars as the armature conductors.

(f) The elimination of armature iron would lead to reductions in the inertia of the rotor of large machines and hence faster control of speed changes would be possible. This has advantages in marine, especially naval, and industrial (for example rolling mill) applications. The reduction in weight would also ease transport problems from machine manufacturing workshops to installation sites.

The drawbacks of a superconducting heteropolar machine are mainly associated with the production of a suitable environment so that the super-conducting state is maintained even under adverse conditions. The basic equipment to maintain the environment (for example helium recovery and liquefaction units, vacuum pumps and necessary protection and monitoring equipment) requires special attention by properly trained and experienced personnel to maintain reliable performance at optimum level. The installation of a cryogenic facility is expensive, hence introducing economic disadvantages as well as the previously mentioned operational difficulties. However, the advantages gained in other previously mentioned areas could outweigh these disadvantages.

Shunt or series operation of the field system of a superconducting machine is undesirable because of possible fluctuations in field currents (especially in the series connection) which could destroy the superconducting state; hence the separately excited mode of operation is required. This

necessitates a stabilizea high current, low voltage supply for the field system. In the event of a field quench the field supply would require a facility for reducing the field excitation current rapidly to prevent destruction of the field coil and sudden evaporation of liquid helium which could cause explosions within the cryogenic system. These difficulties are not insurmountable and proven techniques have been developed.

The above discussion indicates that the cost of a full scale, super-conducting D.C. heteropolar machine with a rating less than that which can be achieved with conventional machines could be in excess of the cost of a conventionally designed machine. However, as the machine ratings increase, the relative cost of refrigeration would decrease and the relative cost of the machine itself would decrease. Thus, above a certain rating the superconducting machine could show economic advantages.

1-5   Final Research Aims

Based on all the above considerations, the final aims set for the research project were:

(a) to develop and construct an economically and technically suitable heteropolar machine with superconducting field windings on which worthwhile research could be conducted. This included the design and development of the field winding cryostats and other components.

(b) to use this machine for research purposes and in particular to:

(i)   determine the practicability or otherwise of the heteropolar machine with superconducting field windings;

(ii) determine the factors which limit the upper rating of heteropolar superconducting machines;

(iii) make a comparison between conventional heteropolar, superconducting homopolar and heteropolar machines with a rating of near 10 MW;

(iv) determine the type of construction which could be adopted for large scale heteropolar machines;

(v) suggest lines of future research.

1-6 Procedure Adopted to Meet the Research Aims

The procedure adopted to meet the research aims progressed in the logical steps listed below.

(a) The cryogenic laboratory was established and introductory experiments at cryogenic temperatures were conducted - Chapter 2.

(b) A decision on the general format of an initial experimental machine was made based on flux density distributions obtained from models of many of the possible machine layouts - Chapters 3 and 4. The inclusion of some iron was considered to be necessary initially to ensure the least onerous operating conditions for the superconducting field winding and consequently we could be confident in the successful operation of the initial machine.

(c) An initial machine design was arrived at (Chapter 5) so that different quantities of included iron and the necessity or otherwise of a compensating winding could be systematically investigated. These investigations were designed so that a final format of a model of an actual prototype machine with a high MW rating could be determined.

(d) A design for field winding cryostats was arrived at after investigation work into insulation and construction techniques - Chapter 5.

(e) A design method was determined for the optimum leads which
supply the field current to the field coils - Chapter 6.

(f) A theoretical study resulted in an insight into the
processes involved in the cooling of cryostats from room
temperature to liquid nitrogen temperature and then to
liquid helium temperature - Chapter 7.

(g) All cryogenic components were tested with liquid nitrogen
prior to the experimental work which required liquid helium
so that the superconducting state could be achieved
- Chapters 8 to 12 inclusive.

(h) A comparison between the designs of superconducting
homopolar and heteropolar machines and a machine of
conventional design each with a rating of 10 MW was made
- Chapter 13.

(i) A model of the prototype machine with the format arrived
at as a result of the earlier tests was designed, constructed
and tested to confirm the viability of the superconducting
D.C. heteropolar machine - Chapter 14.

CHAPTER 2

ESTABLISHING THE CRYOGENIC LABORATORY

2-1   Introduction

The basic requirements of the cryogenics laboratory entail creating an environment in which superconductivity can occur. This required a suitable container (cryostat) in which temperatures near absolute zero could be maintained. It was envisaged that these conditions would be required for periods of not less than four hours so that there was sufficient time for new experimental work to be conducted. The only practical way of doing this was to use liquid helium as the cooling medium.

To attain this objective a few basic items were required:

(a) a source of liquid helium and a suitable storage vessel;

(b) a source of liquid nitrogen and a suitable storage vessel;

(c) a cryostat designed to accommodate the superconducting coil and in which the required environment could be produced;

(d) a vacuum pump capable of producing a pressure of 10^{-5} torr or less;

(e) adequate safety equipment to protect personnel;

(f) low temperature measuring equipment; and

(g) a source of high direct current at low voltage.

2-2   Supply of Liquid Helium

Liquid helium could have been obtained by two methods:

(a) to purchase a liquefication unit and produce liquid helium from a reservoir of gaseous helium when required;

(b) to purchase the liquid helium when required and vent boil-off gases to the atmosphere.

The first alternative would have been ideal because delays in transport and possible loss of helium during transport would have been avoided. The helium would be available almost as easily as "turning on a tap", but the major drawback of this alternative was the considerable capital outlay required for the liquefier and the helium recovery units; hence the second alternative had to be adopted. Even with the second alternative some capital outlay was required, mainly the purchase price of a suitable container for transportation of the helium; but this was only a small percentage of that required for the first alternative. Other costs with this alternative were the purchase price of the helium and the cost of air freighting the container to and from the supplier. Major disadvantages of this technique were: helium could be supplied only once a month by air freighter from Sydney; it was not economical to recover the helium gas and return it to the supplier and so it was lost to the atmosphere. To transport the liquid helium a thirty litre helium storage vessel was purchased.

2-3   Transfer of Helium

Two methods were available for transfer of the liquid helium from the dewar via a special transfer tube to the cryostat.

(a) To lower the pressure within the cryostat by pumping and hence the higher dewar pressure would force the helium across. This method lowered the boiling point of the helium within the dewar and could cause flash loss of helium if the pressure differential was excessive. This method also requires a pump with a pumping speed greater than 75 litres/min.

(b) To pressurize the dewar with boil-off gases from within the dewar. To augment this pressure a football bladder, which inflated from the boil-off gas from the dewar, was placed over one of the outlets of the dewar. Heat was then introduced into the dewar by squeezing the bladder, thus increasing the internal pressure of the dewar and hence the rate of liquid transfer. With this process the boiling point of the liquid helium within the dewar was raised and, on return to atmospheric pressure within the cryostat, flash boil-off was possible if the dewar pressure was excessive. This method was adopted and proved to give satisfactory rates and control over the transfer of helium with a dewar pressure of up to 100 mm gauge of mercury.

2-4   Supply and Usage of Liquid Nitrogen

A twenty litre dewar and a four litre stainless steel thermos flask were purchased for holding and transporting liquid nitrogen. These proved to be indispensable for initial work into the properties of materials at cryogenic temperatures and for the testing of equipment. Liquid nitrogen was readily available and could be obtained within an hour free of charge; hence it was possible to use liquid nitrogen virtually without restrictions during the project. The liquid nitrogen was also used as the coolant for the radiation shields in the cryostats.

2-5   Cryostats

Because of the specialized nature of the cryostats required, off-the-shelf cryostats could not be purchased and hence a decision had to be made on how the cryostats could best be manufactured. The alternatives were:

(a) to design them myself and get them custom built;

(b) to design them and manufacture them in our own workshops.

The latter was the obvious choice because it was cheaper and it had the advantage that design changes could be made as and when found necessary without incurring the high cost of external manufacture. In addition, if vacuum leaks formed within the custom made cryostats, it would have been necessary to return them to the manufacturer for repair - a time consuming and costly process. Alternatively, if we did the manufacturing any necessary changes could be made within the Department's workshops quickly and with little or no cost.

This decision necessitated the purchase of an argon arc welder for the workshop, as this was required for the special work involved in cryostat manufacture. A slow speed turntable, 2-10 r.p.m., was built to semi-automate the welding operation. For more detailed information regarding the construction and development of the cryostats see Chapter 4.

2-6   Vacuum Pump

The main form of insulation was vacuum insulation which required pressures of less than 5×10^{-5} torr to be effective. The lower the pressure the better the insulation, but other forms of heat inleak would tend to swamp that due to gaseous conduction at much lower pressures.

To obtain the required degree of vacuum it was essential to use some form of pumping other than just an oil sealed rotary pump. The two forms considered are listed below.

(a) To evacuate the cryostat initially to a pressure of near

0.001 torr with an oil sealed rotary pump and then completely

seal the cryostat and rely upon getters and cryopumping only to maintain the required vacuum. This method would have required extremely effective sealing of the cryostats and, unless there was special provision allowed to do so, there would be no easy way of monitoring pressures within the containers to be sure that the vacuum was maintained.

(b) To use a rotary backing pump, a diffusion pump, and a vapour trap which would stop pump vapours diffusing back into the cryostats. Cryopumping within the containers would also improve the final vacuum. With this method cryostats were continually pumped and with a gauge on the pump the pressure could be continuously monitored. This system had the advantage that it could tolerate very small leaks and still maintain the vacuum required. This technique was adopted.

The initial vacuum pump consisted of a very old rotary pump and a glass, mercury diffusion pump which was manufactured in the Chemistry Department. The system also had a liquid nitrogen vapour trap for cryopumping and to prevent the diffusion of mercury into the cryostats. This pump proved to be very useful in obtaining expertise and knowledge in the establishment of the vacuum; but the big drawback of the pump was its very low pumping speed. In fact it took nearly five hours just to pump itself down to a pressure of 5×10^{-5} torr. The use of glass proved to be a drawback as it was broken several times because of inexperienced handling. The glass however was easily repaired and components such as glass valves were quite cheap and easily replaced.

This pump was replaced with a commercially available system, which is shown diagramatically in figure 2-1, which had an ultimate vacuum of better than 10^{-7} torr and a pumping speed of 150 ℓ/min. The valving used enabled

FIG 2-1
VACUUM PUMP
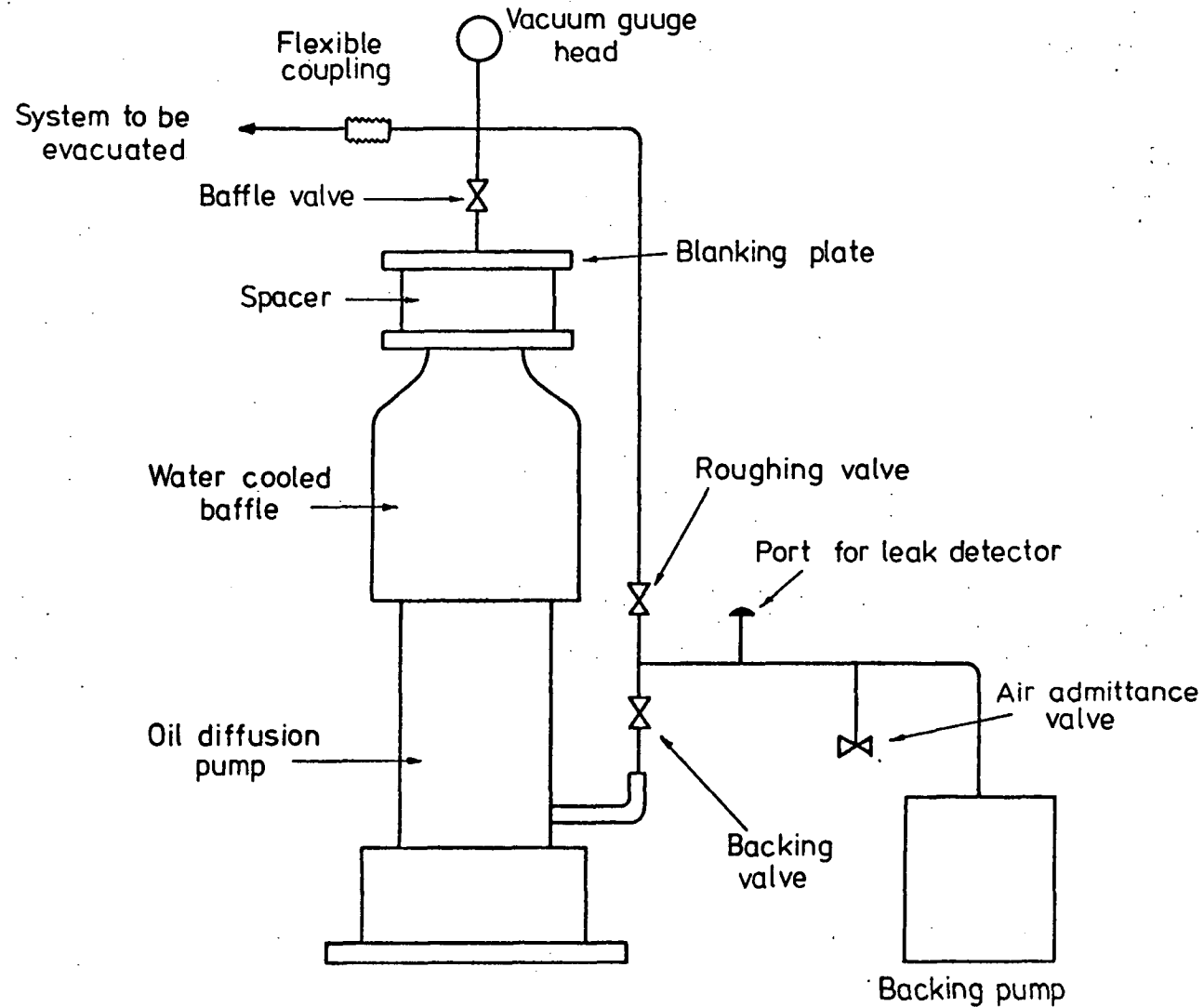
easy pumping and isolation of the pump from the cryostats. This meant that the cryostats could be left evacuated with the pump shutdown and let back to the atmosphere. A disadvantage of the system was that it required water as a coolant. This could have been avoided at a greater cost, but the saving in cost was more important than the inconvenience of cooling water. The final system gave a vacuum of 4×10^{-7} torr.

2-7   Leak Detection

The detection of leaks which cause loss of vacuum is an exacting task in itself. Three methods of leak detection were adopted:

(a) If the required vacuum was not achieved then this indicated the presence of a leak, or a virtual leak, but not its position. It should be noted that the required vacuum can be achieved even with leaks in the system, provided these are extremely small and therefore difficult to detect even with the most sensitive leak detecting apparatus.

(b) To pressurize the cans and then to spray a low viscosity and low surface tension liquid over the suspected leak area. The position of leaks was indicated by the formation of a foam. Such liquids were available commercially and detected surprisingly small leaks. This method was very fast because elaborate equipment was not required.

(c) A sensitive leak detector which operated by detecting the presence of halogens. This required the evacuation of the cryostat sections and spraying suspected leaks with halogen-bearing compounds such as freon or trichlorethylene. A detector, at the cryostat evacuation port, indicated that

the halogens had entered the containers. To use this
apparatus to its maximum capabilities required practice,
patience and a well ventilated area.

All these techniques were used in the early stages of the cryostat
development, but as experience was gained, leak-tight cryostats could be
produced by exercising care during their manufacture. No significant leaks
occurred in the later cryostats built within the Department.

2-8   Safety Precautions

An important part of the laboratory was the safety equipment, which
included:

(a) face shields which completely covered the face and
prevented anything getting into the operator's eyes;

(b) adequate gloves which covered the hands and forearms.

A dangerous possibility within any cryogenic laboratory is an explosion
which could be caused by the build-up of pressure within dewars and cryostats
or by the separation from the air of liquid oxygen which can spontaneously
ignite some organic compounds.

Pressure build-up can result from either the failure of insulation, thus
giving flash boiling of the liquid helium, or blockage in the boil-off
outlets. Blockages can arise from the freezing of condensation or from
atmospheric gases such as nitrogen or oxygen.

To prevent pressure explosions, gas release valves were incorporated
in the cryostats.

As liquid nitrogen and liquid helium will condense oxygen from the atmosphere, care was taken to ensure that any undesirable organic materials were excluded from any sections of equipment which could be exposed to low temperatures.

The research area was adequately ventilated to avoid any problems with asphyxiation.

2-9   Temperature Measurement

As it was not necessary to monitor the cryostat temperature precisely and only a reliable indication was required as to the conditions within the cryostat, carbon resistance thermometers were used. These thermometers required minimal cryostat space as well as providing a wide range of temperature measurement with more than adequate accuracy.

Auxiliary thermocouple thermometers made from copper-constantan junctions were used where the carbon resistors proved to be too bulky and to have too large thermal inertias. Thermocouple liquid nitrogen level detectors for the radiation shield coolant proved to be accurate within 2 mm and thermocouples were also used to measure coil temperatures during coil cooldown tests.

2-10   Current Supply

The supply and control of ripple-free direct currents of the order of 300 amperes was limited to three alternatives:

(a) a rectified and filtered twelve pulse supply, using

a variable A.C. source for control purposes;

(b) the output of a D.C. generator using field current

control;

(c)   paralleling banks of batteries and using a variable

water resistor as the means of control.

The last alternative was used initially as it did not require filtering and suitable batteries were available.

The resistor was made by dissolving potassium hydroxide in water in a 200 litre iron drum. Currents of up to 300 amperes were available from this system.

Control of the current was achieved by varying the immersed surface areas of a system of intermeshing iron plates. During current flow electrolysis of water took place; hence adequate ventilation for the resulting hydrogen and oxygen was necessary and the level of the water required topping up with hot water after every few hours of operation.

For later experiments a rectifier system was used.

2-11   Layout of the Laboratory

Figure 2-2 indicates the position of the cryogenic facility within a machines laboratory which is used for undergraduate experiments.

A photograph (figure 2-3) shows the layout of equipment in the laboratory.

FIG 2-2
UNIVERSITY POWER LABORATORY

22·86 m

CRYOGENICS LAB

3 m

4 m

14·94 m

POWER LAB
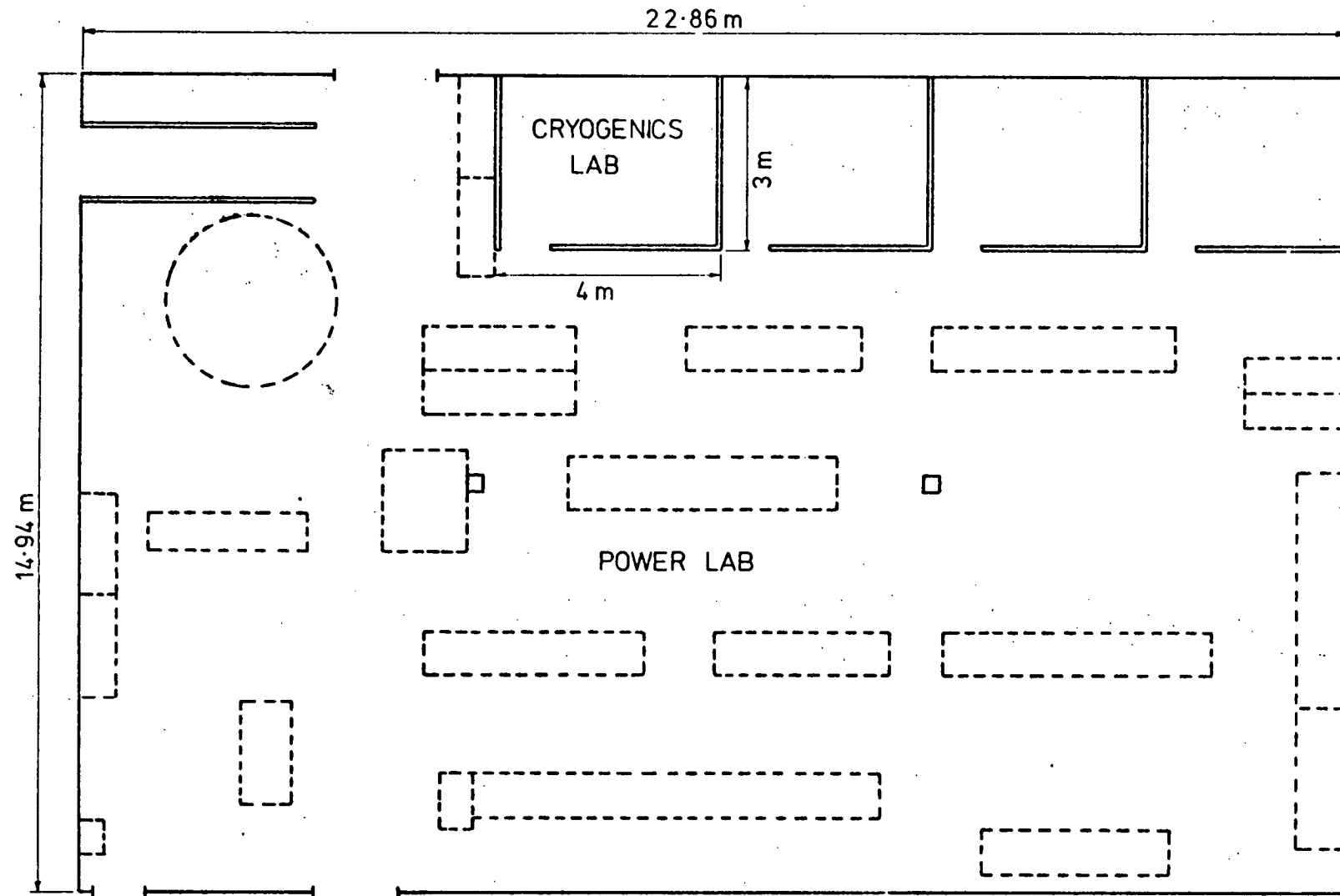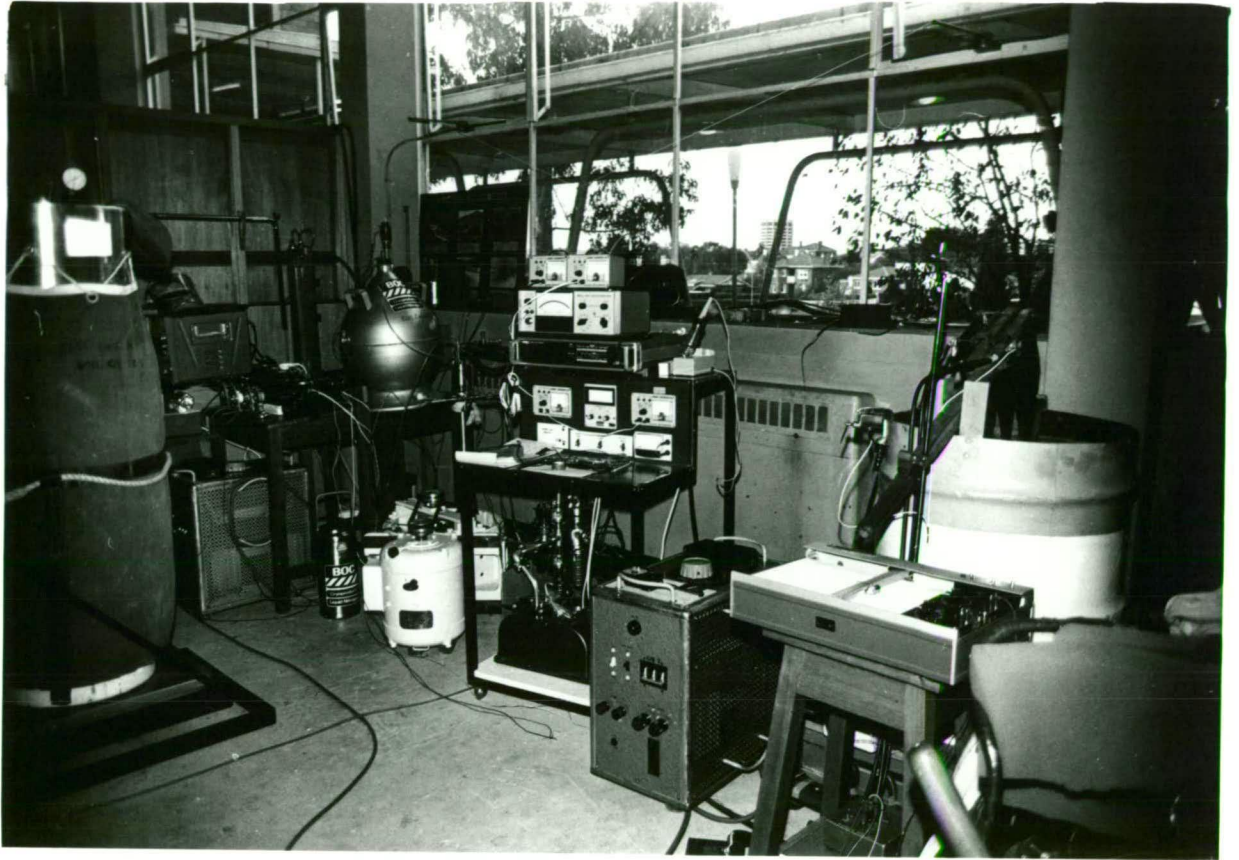
FIGURE 2-3

GENERAL VIEW OF THE CRYOGENICS LABORATORY

CHAPTER 3

INITIAL MACHINE FORMAT DEVELOPMENT

3-1   Introduction

The design for the initial machine was to ensure, in the first instance, the least onerous operating conditions for the superconducting field winding so that there was a high probability of successful operation. The format of the machine had to be such as to allow for the systematic study of the operation of the superconductor under progressively more onerous conditions.

To arrive at an appropriate format for the initial machine preliminary investigations into the flux distributions within models of the possible forms of the machine and basic theoretical studies were required. These investigations included the effects of the inclusion of iron and a compensating winding upon the flux distributions.

3-2   Necessity for Studies of Magnetic Flux Distribution

If a superconducting coil is subjected to a changing magnetic field above a certain, somewhat difficult to determine, magnitude, the superconducting properties can be lost due to heat generation within the winding. For this reason it was decided to reduce the armature reaction fluxes linking the superconducting field coil to a minimum possible in the initial machine.

It was considered necessary to adopt a design which reduced the force on the field windings (caused by the load torques) to a minimum. These forces are normally taken by the iron cores of the field poles in conventional

machines. The reason for this was that the support of the field winding against forces may have been difficult whilst maintaining suitable insulation of the helium chamber as they had to be supported through the vacuum chamber.

In order to determine the format of the machine which gave the minimum field coil flux linkage from the armature reaction fluxes, studies of magnetic flux distributions had to be made on the various possible forms of the machine. Later experimental work has indicated that a number of the above requirements were not as stringent as at first thought.

3-3   Compensating Winding

To reduce the effects of armature reaction on the superconductor an auxiliary winding which produced magneto-motive forces in opposition to those of the armature was utilised. The form of winding adopted was a stationary winding similar to the armature winding. This winding carried the load current or a percentage of the load current in the opposite sense to the current in the armature winding.

If the compensating and armature windings had the same number of coils and coil turns and they could be superimposed, the current carried by the compensating winding conductors required to give perfect flux cancellation would be 1/c of the load current, where c equals the number of parallel paths in the armature winding.

For a realistic compensating winding to cancel the armature reaction fluxes in the region of the superconductor, the ampere turns per pole required would be less than that of the armature because the compensating winding would have a larger diameter and hence be closer to the field windings.

A winding of this form would also reduce the armature reaction saturation effects on the back e.m.f. of the machine if iron was retained. However, if all of the iron was eliminated from the machine, the effects of the armature reaction upon the generated e.m.f. would be eliminated.

Another advantage of the compensating winding would be that it would counteract the force on the field windings produced by the armature winding and hence the forces due to load torques experienced by the field windings would be small.

The compensating winding could take the form of a second rotating armature winding. This could be achieved by winding the two armatures on separate and concentric shafts which would result in a machine with two outputs. The armatures would rotate in opposite directions, but they could be coupled together to give a single output shaft. If the two rotors were not coupled, the armatures could be connected electrically in series, thus producing a "constant" differential speed characteristic between the rotors.

This form of machine may well offer some interesting construction problems but it has the potential of making further use of the compensating winding by approximately doubling the output of a given size of machine. As the coils in the two armatures undergoing simultaneous commutations would be carrying currents in opposite directions, the mutual effects between the coils in the two armatures could have a beneficial influence on the commutation. A small experimental machine with a conventional field system and two concentric, contrarotating armatures was constructed and tested and successfully demonstrated the concept of using the compensating winding as a second armature.

The disadvantages of a compensating winding in a large machine are that there would be the added expense of providing the winding and that the extra copper losses generated in the winding would produce a drop in efficiency and hence an increase in running costs. The double armature suggestion would overcome these disadvantages. The concept was not investigated further as the potential benefit to the project was outweighed by the added construction complexity.

To investigate the effectiveness of the proposed fixed compensating winding an iron-free model consisting of an armature winding and compensating winding was constructed - see section 3-4 and figure 3-1.

3-4   Inclusion of Iron

The effect of any armature reaction flux cutting the superconducting field winding was not readily predicted with certainty since it depends heavily on the characteristics of the superconducting winding; for example, the ability of the winding to dissipate induced heat to the coolant. For this reason it was desirable to provide initially the best shielding possible by the most convenient method.

The results obtained from tests on the iron-free model of the armature reaction flux distributions, which are discussed in Chapter 4, revealed that perfect flux cancellation, using the discrete compensating winding, was not possible. This was particularly apparent in the region of the compensating winding where its discrete coil format produced ripples in the flux pattern. Further model tests finally led to the inclusion of iron pole faces in the initial machine to shunt armature reaction fluxes past the superconducting field coils.

FIG 3-1
IRON FREE MODEL

48 mm

Slots for the
compensating
winding

89 mm Dia

Slots for the
armature winding

16 Coils
2 Turns
18 SWG copper wire
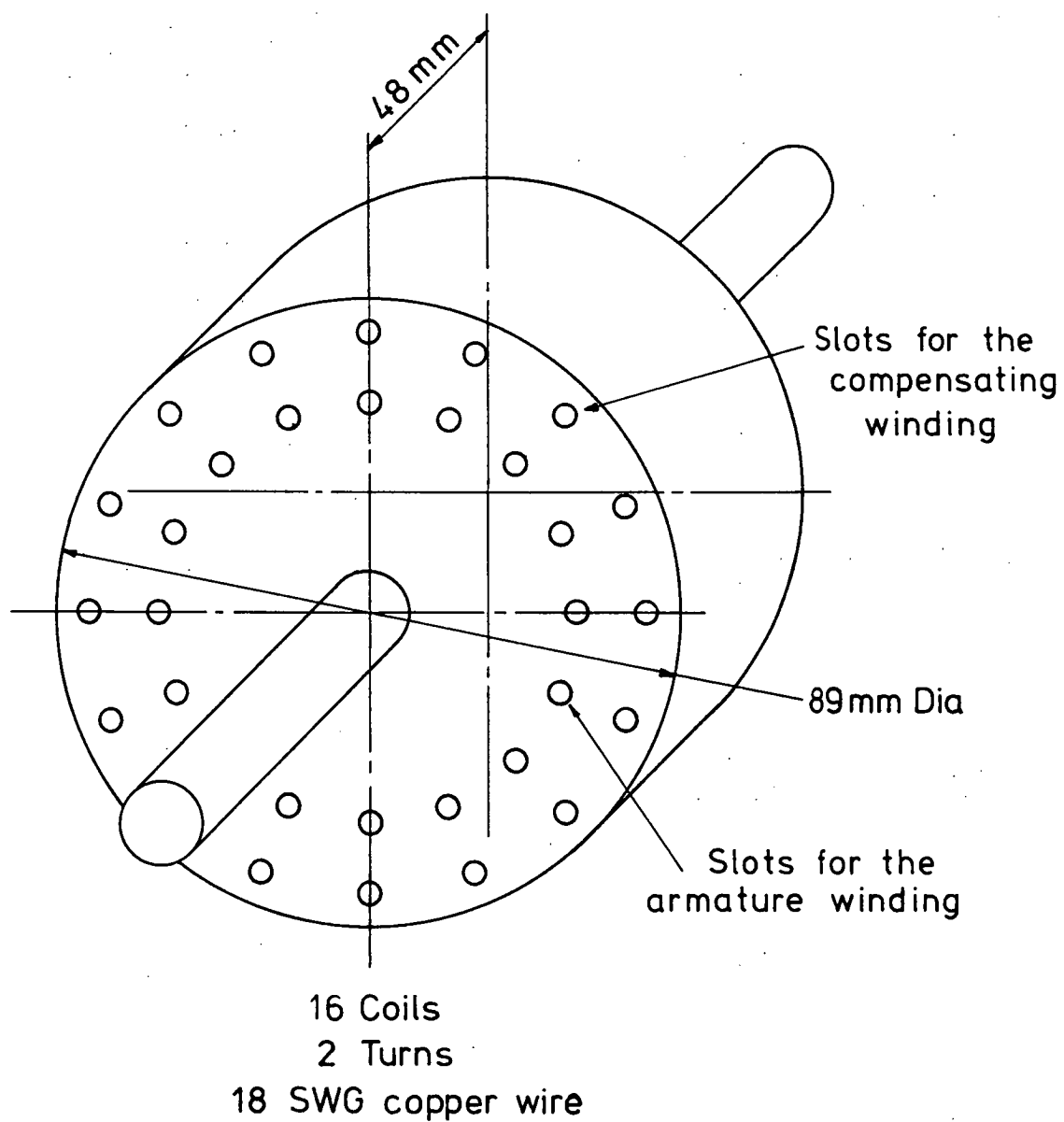
Iron was also retained in the yoke of the machine for the following reasons:

    (a) To protect the immediate environment around the initial machine from high flux densities. This may not be necessary in the proposed experimental machine but may be desirable in an industrial situation, such as the engine room of a ship, for health and safety reasons and possible effects on nearby equipment.

    (b) To reduce the quantity of superconductor needed to produce the required field flux and thus reduce the cost of the initial machine.

    (c) To provide a low reluctance path, for armature reaction fluxes, which bypasses the superconductor.

    (d) A suitable machine stator structure from a conventional machine was available which permitted a convenient machine size and the shortest construction time so that initial experience could be obtained quickly and at low cost.

The inclusion of iron did not vitiate the use of superconductors in the field windings because the machine had very large air gaps which are inherent in the envisaged design and so to provide the necessary field magneto-motive force using conventional conductors would have been out of the question.

3-5   Models for Magnetic Flux Distribution

The use of models in preference to complex calculations was considered to be the most appropriate method to obtain reliable flux density distribution information for the initial machine format envisaged. This approach

is desirable in the case of hybrid circuits which involve iron and air as the magnetic media and where the iron-air boundaries are difficult to describe mathematically. This was the case in this investigation and hence the use of models.

To maintain the quantity of superconductor and cryostat construction time to a minimum, the number of field windings was set at two; hence the armature and compensating windings of the initial machine and of the models were all two pole windings.

The first model (figure 3-1) consisted of a two pole armature and compensating windings with sixteen coils of two turns each and wound on a wooden former, using 18 SWG gauge copper wire. This model was used to determine armature reaction fluxes for an iron-free system and it was from results obtained with this model that the decision was made to investigate the effect of the inclusion of iron pole faces in the machine.

The final model (figure 3-2) was such that each section could be removed and hence different configurations were easily investigated. A six-inch diameter iron pipe fitted with an aluminium end bell and facilities for fixing pole pieces, field windings, armature and compensating windings into position was used. The armature and compensating windings were wound on the same wooden former. The armature wooden former was hollow so that the effects of inner cores of magnetic or non-magnetic materials could be investigated. The armature and compensating windings were not movable with respect to each other as this was not necessary because it was envisaged that the armature brushes on the actual machines would be fixed on the geometric neutral axis.

FIG 3-2
MODEL

Adjustable
Probe Holder

Angular Position
Potentiometer

Armature and
Compensating
Winding wound
together

Stator

Interchangeable
Rotor

Field Pole
Faces

Field
Coil

300mm

130 mm

170 mm OD
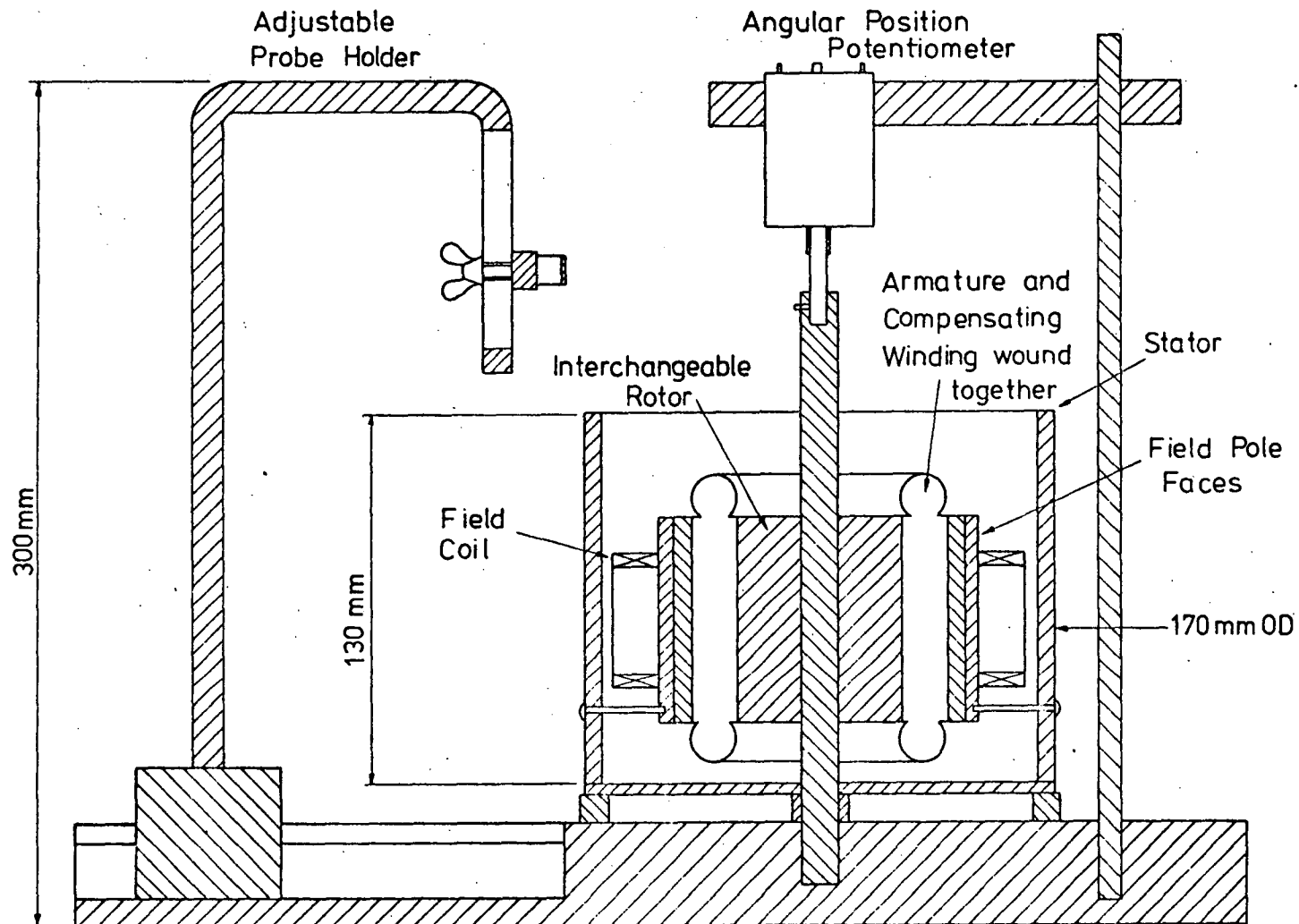
The model had three sets of windings: the armature, the compensating and the field windings. The armature and compensating windings were 16 coils of 5 turns each wound with 18 SWG gauge wire. The mean diameter of each winding was 76 mm and the length 64 mm. The field windings dimensions were 40 mm ID, 50 mm OD and 15 mm long with 6 layers of 19 turns per layer of 22 SWG wire. The dimensions of the model were chosen so that it would model the envisaged initial superconducting machine.

A Hall effect probe was used to measure the flux densities. Point by point hand measurement and plotting of the field patterns proved to be tedious and in fact missed some of the fine detail of the flux distributions and hence a continuous plot using an X-Y plotter was adopted.

The positioning of the probe was achieved with a simple holder which gave vertical and radial adjustment. The model assembly was free to rotate as a whole and the probe was fixed in place by the holder and hence flux density as a function of position was obtained.

A potentiometer gave a voltage proportional to the angular position. This activated the horizontal movement of the X-Y plotter.

The flux density was measured in two components: the radial and the circumferential components, from which both magnitude and direction of the flux density were obtained.

3-6   Format of the Initial Machine

From the preceding discussions and the tests on the models (which are discussed in chapter 4) the decision on the format of the initial machine was made.

The main aspects of the machine decided upon were that it should:

(a) have an iron yoke which, to save cost and time, was

a yoke from a scrap D.C. machine;

(b) have iron pole faces;

(c) be a two pole machine;

(d) have a compensating winding wound in a similar fashion

to the armature winding;

(e) have an armature with a changeable core;

(f) have easily removable and replaceable components so that

the different possible machine configurations and amounts

of iron could be easily investigated. See figure 3-3 for

a plan of the machine and figure 5-10 for a photograph.

FIG 3-3
INITIAL MACHINE
FORMAT
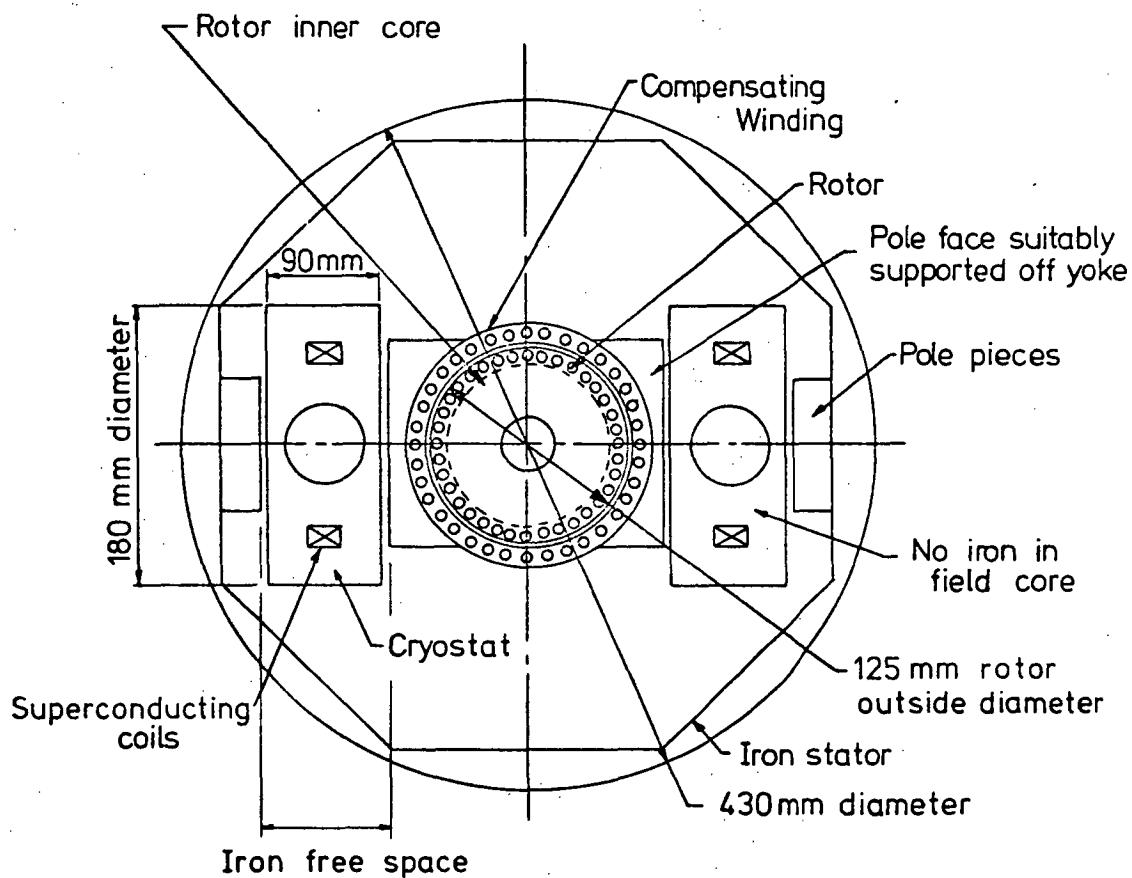
CHAPTER 4

RESULTS OF TESTS ON THE MODEL

4-1   Introduction

As a result of the decision to minimise initially the possibility of the superconducting coil quenching it was considered necessary to include iron in the initial machine. In order to obtain a clear picture regarding the effects of the iron, both on armature reaction and field flux distributions, tests were conducted with various quantities of iron included in a model of the envisaged initial machine.

The results of the tests lead to the decision that the initial machine would have an iron armature core and an iron yoke as they increased the field pole flux. Iron field pole faces and a compensating winding were selected to shield the superconducting field winding against armature reaction fluxes.

4-2   Armature Reaction

The magnitude of armature reaction fluxes, in the region of the field coils, is dependent on the different quantities of iron included in the machine. Studies were therefore carried out to determine the amount and arrangement of iron to be included in the test machine.

To ensure equal currents in all of the coils, the two halves of the model armature were connected in series - not in parallel as in an acutal two pole machine. Similar connections were also used in the compensating winding.

This form of connection meant that the currents measured in the following sections were actual armature conductor currents, or one-half (for a two pole machine) of the armature current of an actual machine.

4-2-1   Iron Free Model

Investigations into the armature reaction fluxes of the iron free armature winding, without the compensating winding energised, indicated how the armature flux patterns varied at different radii from the windings as a function of angular position - figures 4-1 and 4-2. Varying the position of the probe over the length of the armature, at a constant radius from the windings, showed little variation in the flux distributions. This meant that results obtained at mid-armature length would also apply at other lengths.

Tests also showed that the current in the compensating winding which gave the best overall flux cancellation was not necessarily the most suitable current as the machine required the best flux cancellation only in the region of the superconductor. For example, figures 4-3 and 4-4 for the iron-free armature, show the best overall flux cancellation with about 60% of the armature conductor current in the compensating winding and best cancellation in the field winding region with 70%.

Important results obtained were as follows:

(a)   The radial component of the flux density passed through a zero value near the centre of the field winding whereas the circumferential component passed through a maximum at this point.

(b)   In close proximity to the armature and compensating windings the discrete conductor nature gave rise to ripples in the flux distributions - as mentioned in Chapter 3. The compensating winding did not give complete flux cancellation due to the ripples and hence it was thought that another technique to help the cancellation was required in the initial machine.

FIG 4-1
ARMATURE RADIAL FLUX DENSITY
IRON FREE ARMATURE
current = 4 amps

FIG 4-2
ARMATURE CIRCUMFERENTIAL FLUX DENSITY
IRON FREE ARMATURE
current = 4 amps

FIG .4-3
RADIAL FLUX DENSITY CANCELLATION
WITH COMPENSATING WINDING
IRON FREE ARMATURE
current = 10 amps

$\frac{I_C}{I_A} = 0$

$\frac{I_C}{I_A} = \cdot 6$

$\frac{I_C}{I_A} = \cdot 7$

Flux Density (gauss)

field winding region

field winding region

θ

$\dfrac{\text{compensating winding radius}}{\text{armature winding radius}} = 1 \cdot 33$

$\dfrac{\text{probe position radius}}{\text{armature radius}} = 2 \cdot 2$

FIG 4-4
CIRCUMFERENTIAL FLUX DENSITY
CANCELLATION WITH COMPENSATING
WINDING
IRON FREE ARMATURE
current = 10 amps

$\frac{I_c}{I_a} = 0$

$\frac{I_c}{I_a} = \cdot 6$

$\frac{I_c}{I_a} = \cdot 7$

$\frac{\text{Compensating winding radius}}{\text{Armature winding radius}} = 1\cdot 33$

$\frac{\text{Probe position radius}}{\text{Armature radius}} = 2\cdot 2$

field winding region

field winding region

Flux Density (gauss)

If the superconducting field windings could have been placed at a sufficient distance from the armature windings, then the effects of the discrete armature windings would have been negligible and good cancellation would have been obtained. However, this would have resulted in field flux reductions at the armature. Alternatively, the ripple could have been reduced by evenly distributing the conductors over the armature surface in order to give a current sheet effect.

Before investigating the necessity or otherwise of using a more evenly distributed winding, it was decided to investigate the effects of the inclusion of iron, in the magnetic circuit of the machine, on the armature flux patterns.

4-2-2 Iron Yoke and Iron Armature Core

The introduction of the iron armature core and the iron yoke (but not pole faces) produced armature reaction flux distributions similar to those obtained with the iron-free armature but with a substantial increase in flux density magnitude - figures 4-5 to 4-8. Without the compensating winding energised, the peak circumferential component increased nearly ten times and the peak radial component increased nearly forty times the values obtained in the iron-free model. The increase obtained in the circumferential component was less because some of the flux was shunted by the low reluctance path of the iron yoke.

The increases in the armature reaction flux densities would also apply to the field pole flux, thus reducing the amount of superconductor required for producing the field flux.

The order of magnitude increase in the armature reaction flux was, however, detrimental to the flux cancellation as it required cancellation in the order of 100:1 to produce the same resultant flux densities as achieved with the iron-free model. This degree of cancellation did not

FIG 4-5
ARMATURE RADIAL FLUX DENSITY
YOKE , IRON CORE , NO POLE FACES
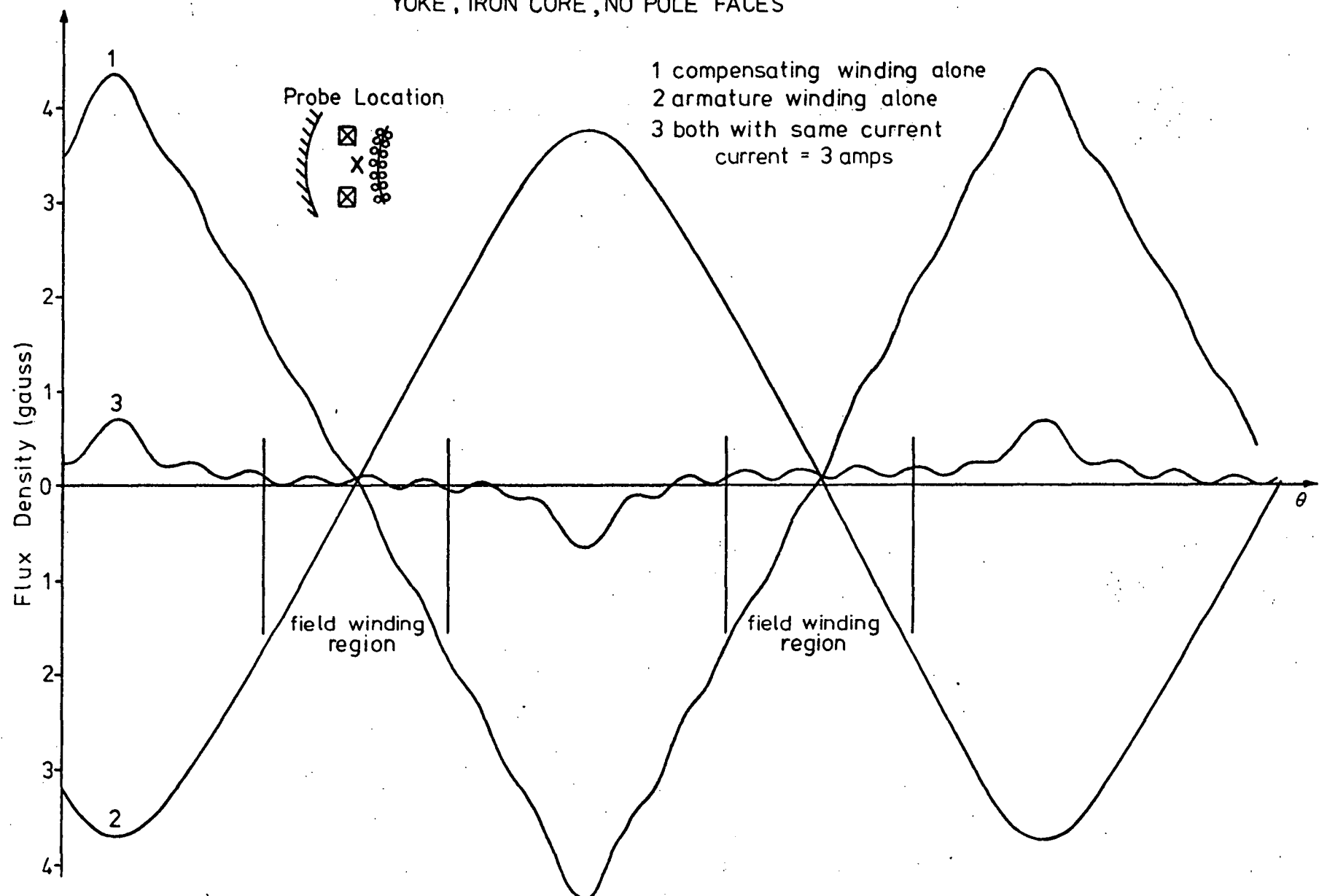
Probe Location

1 compensating winding alone
2 armature winding alone
3 both with same current
   current = 3 amps

field winding
region

field winding
region

Flux Density (gauss)

FIG 4-6
ARMATURE CIRCUMFERENTIAL FLUX DENSITY
YOKE, IRON CORE, NO POLE FACES

Probe Location

Flux Density (gauss)

90

60

30

0

30

60

90

1

2

3

θ

field winding region

field winding region

1 compensating winding alone
2 armature winding alone
3 both with same current
current = 3 amps
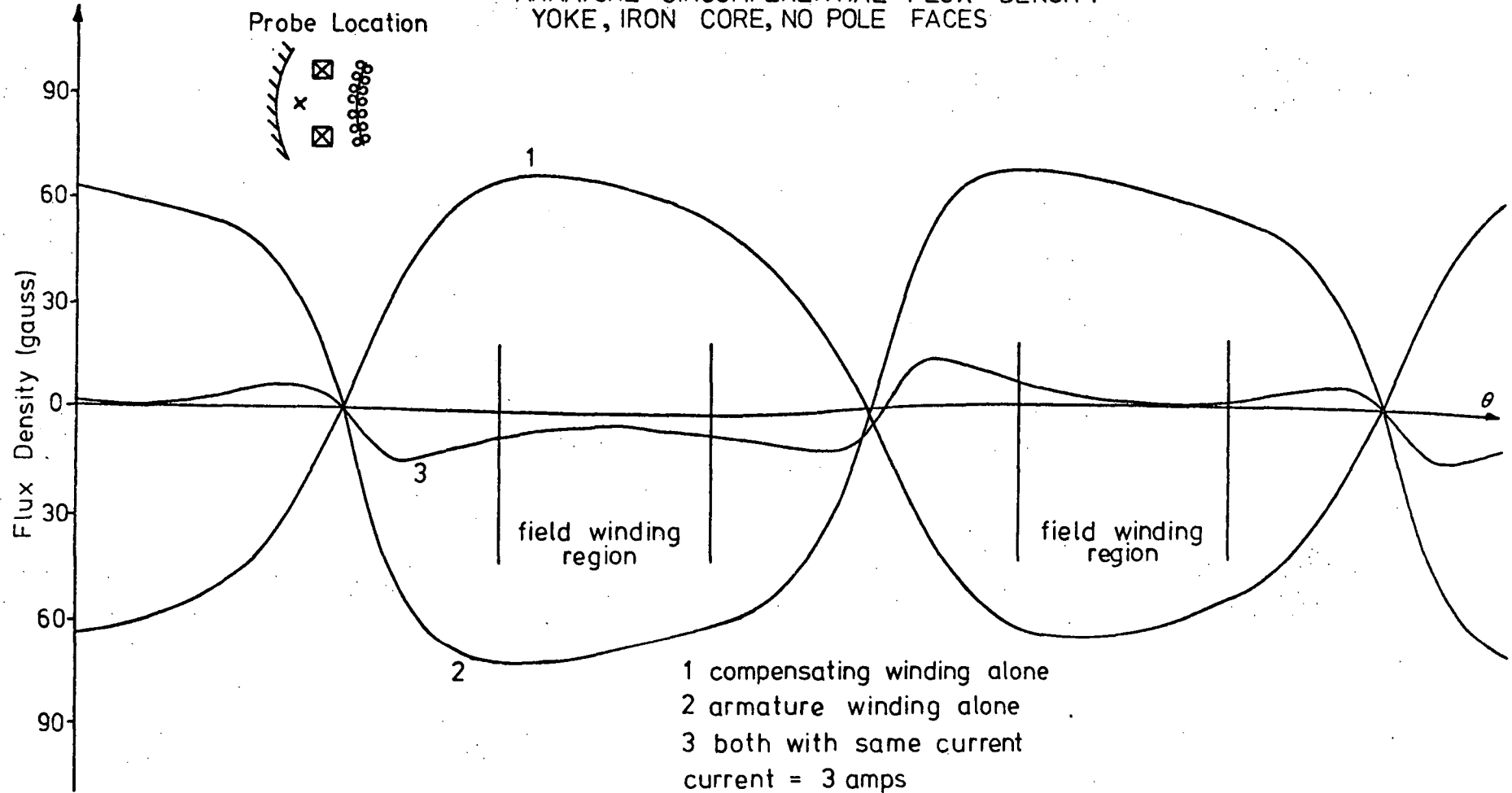
FIG 4-7
ARMATURE CIRCUMFERENTIAL FLUX DENSITY
YOKE, IRON CORE, NO POLE FACES

Pole Location
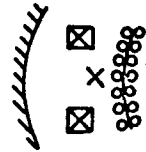
1 compensating winding alone
2 armature winding alone
3a both with same current
3b both but 5× scale magnification
current = 6 amps

4-10
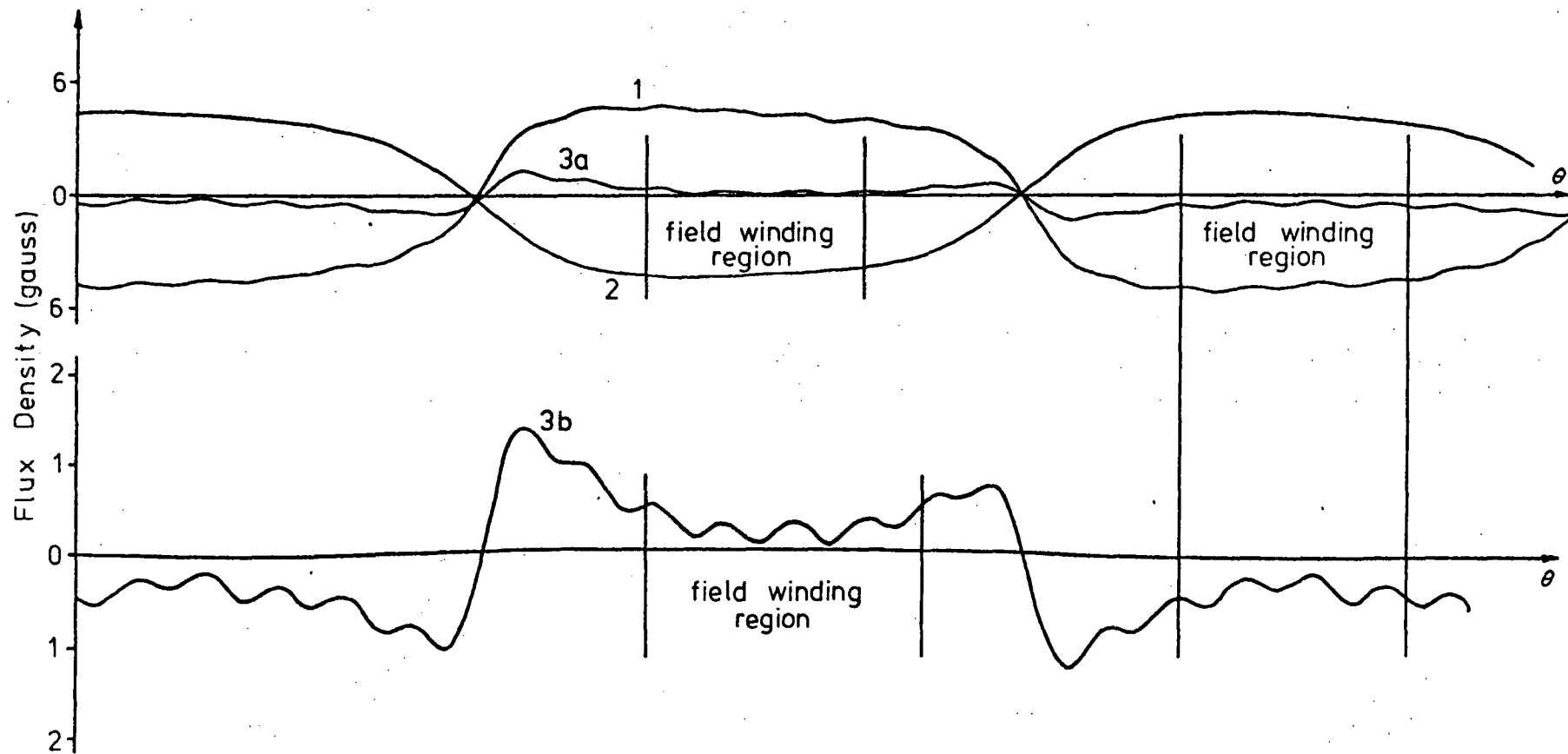
Probe Location
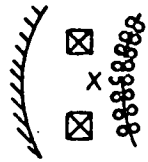
FIG 4-8
ARMATURE RADIAL FLUX DENSITY
YOKE, IRON CORE, NO POLE FACES

1 compensating winding alone
2 armature winding alone
3 both with same current
current = 3 amps

field winding region

field winding region
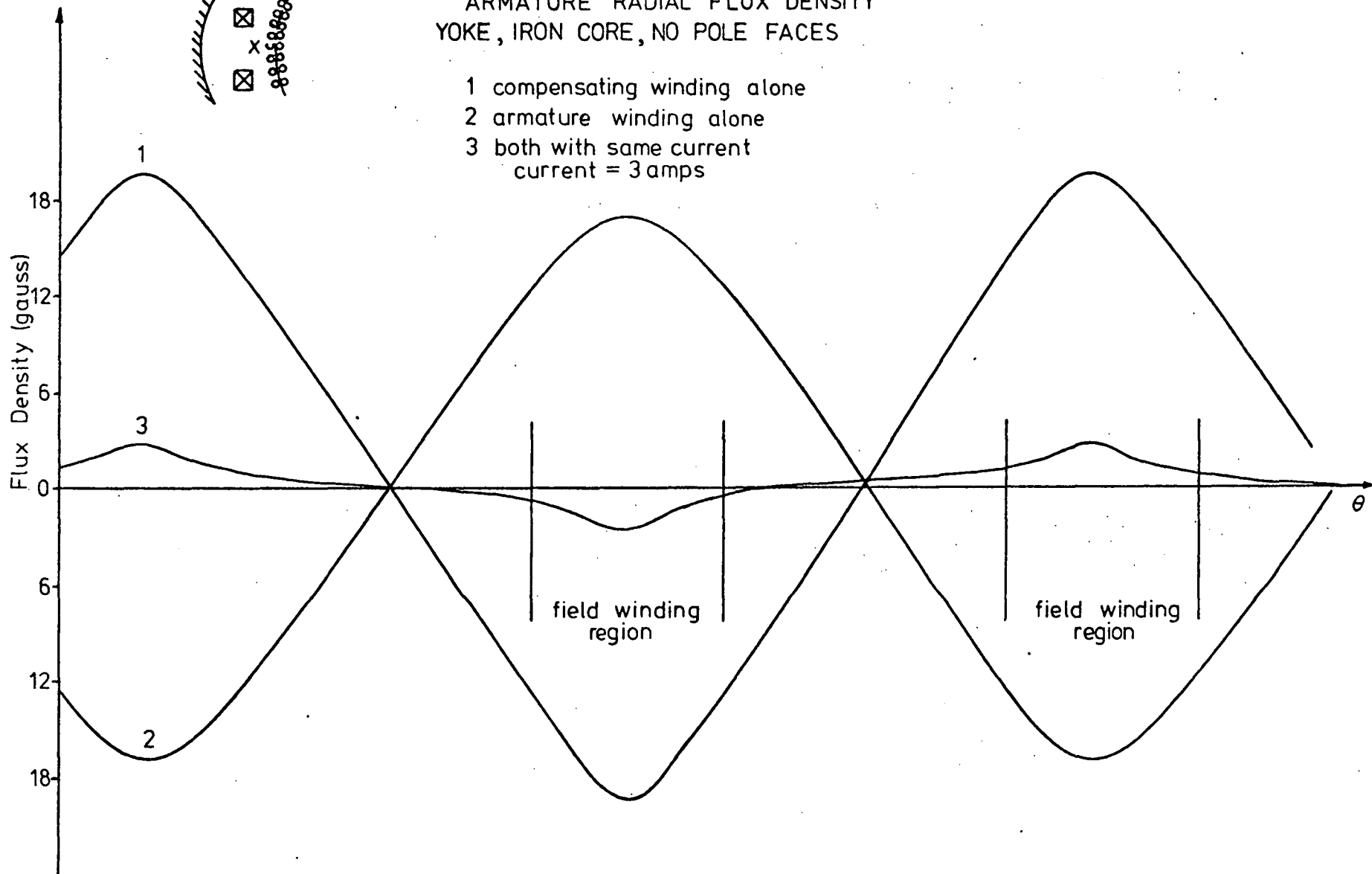
appear to be possible at the inner face of the field coil because of the ripple in the flux distributions of the compensating winding.

The curves in figures 4-5 to 4-8 indicated that the introduction of iron required a higher percentage of the armature current, as compared with the iron-free case, to flow in the compensating winding to give the best armature flux cancellation. Cancellations shown in figures 4-5 to 4-8 were not the best that could have been obtained because the windings were energised with the same current.

4-2-3 Iron Yoke Only

The removal of the armature iron core produced little change in the flux patterns. However, the radial and circumferential components of the armature reaction flux density were approximately half those obtained in the previous case. A notable difference between the curves of figures 4-5 to 4-8 and 4-9 to 4-12 was that, with the compensating winding energised, the percentage of armature current required for best cancellation without a rotor core was somewhat less than that required with a rotor core. Hence, if only an iron yoke was used and the flux cancellation was sufficient to prevent quenching of the superconductor a more efficient machine would result because of the lower loss in the compensating winding.

4-2-4 Iron Yoke, Pole Faces and Armature Core

To meet the initial aims mentioned previously, it was desirable to retain the iron in the magnetic circuit. As it was not possible to obtain complete armature flux cancellation with the combination of the compensating winding, the iron yoke, and the iron armature core, a further method of shielding was required. Hence the inclusion of the field pole faces. The field pole faces also provided a means for positioning and fastening the compensating winding. The idea behind the use of field pole faces was that they would provide a shunt for the armature reaction flux

FIG 4-9
ARMATURE RADIAL FLUX DENSITY
YOKE ONLY

Probe Location

1 compensating winding alone
2 armature winding alone
3 both with same current
current = 3 amps

field winding region

field winding region

Probe Location

FIG 4-10
ARMATURE RADIAL FLUX DENSITY
YOKE ONLY
1 compensating winding alone
2 armature winding alone
3 both with same current
   current = 3 amps

Flux Density (gauss)

18
12
6
0
6
12
18

1

3

2

field winding
region

field winding
region

θ

FIG 4-11
ARMATURE CIRCUMFERENTIAL FLUX DENSITY
YOKE ONLY
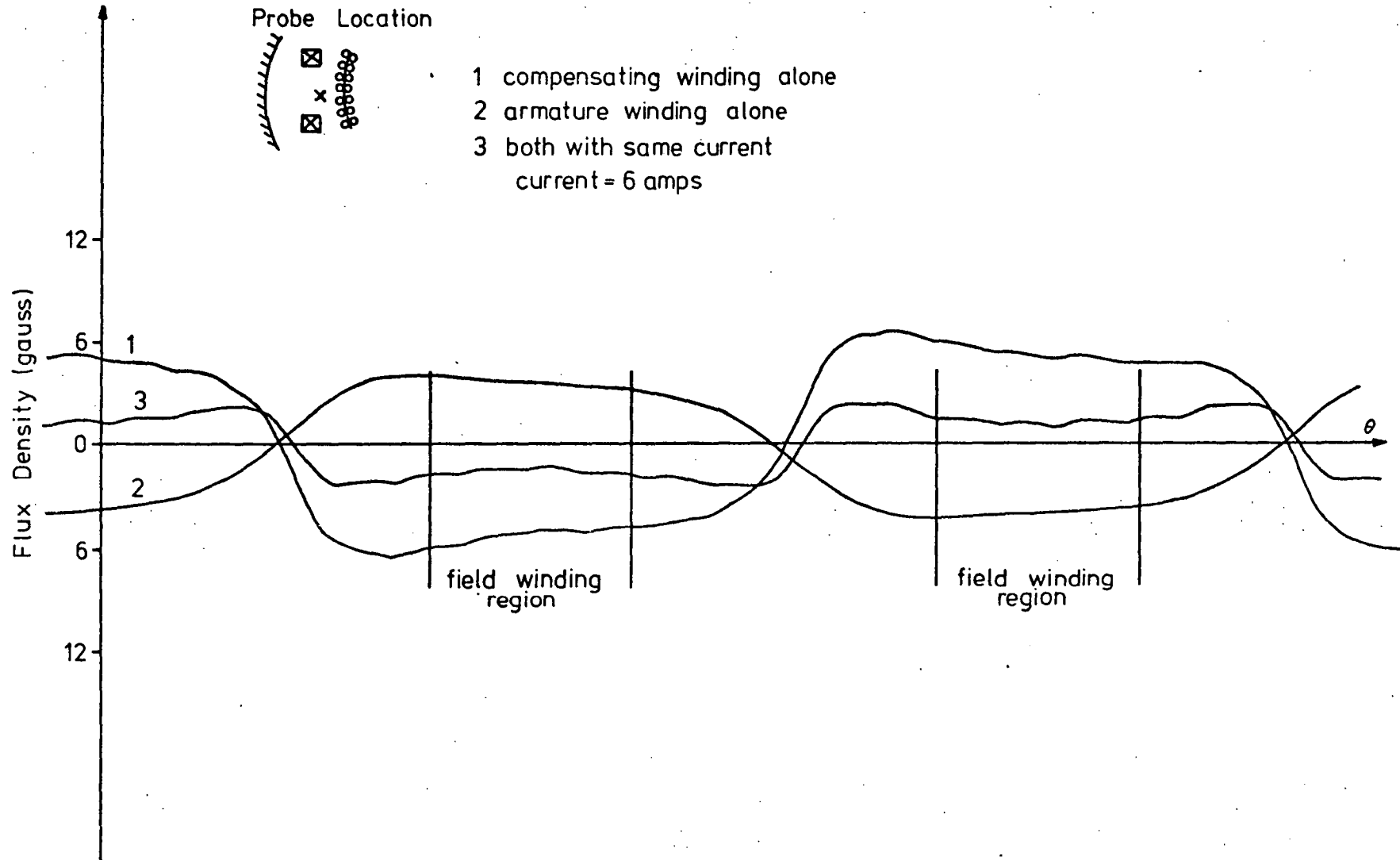
Probe Location

1 compensating winding alone
2 armature winding alone
3 both with same current
current = 6 amps

field winding region

field winding region

FIG 4-12
ARMATURE CIRCUMFERENTIAL FLUX DENSITY
YOKE ONLY

Probe Location

1 compensating winding alone
2 armature winding alone
3 both with same current
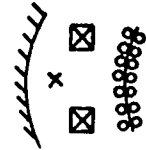
current = 6 amps

field winding region

field winding region

Flux Density (gauss)
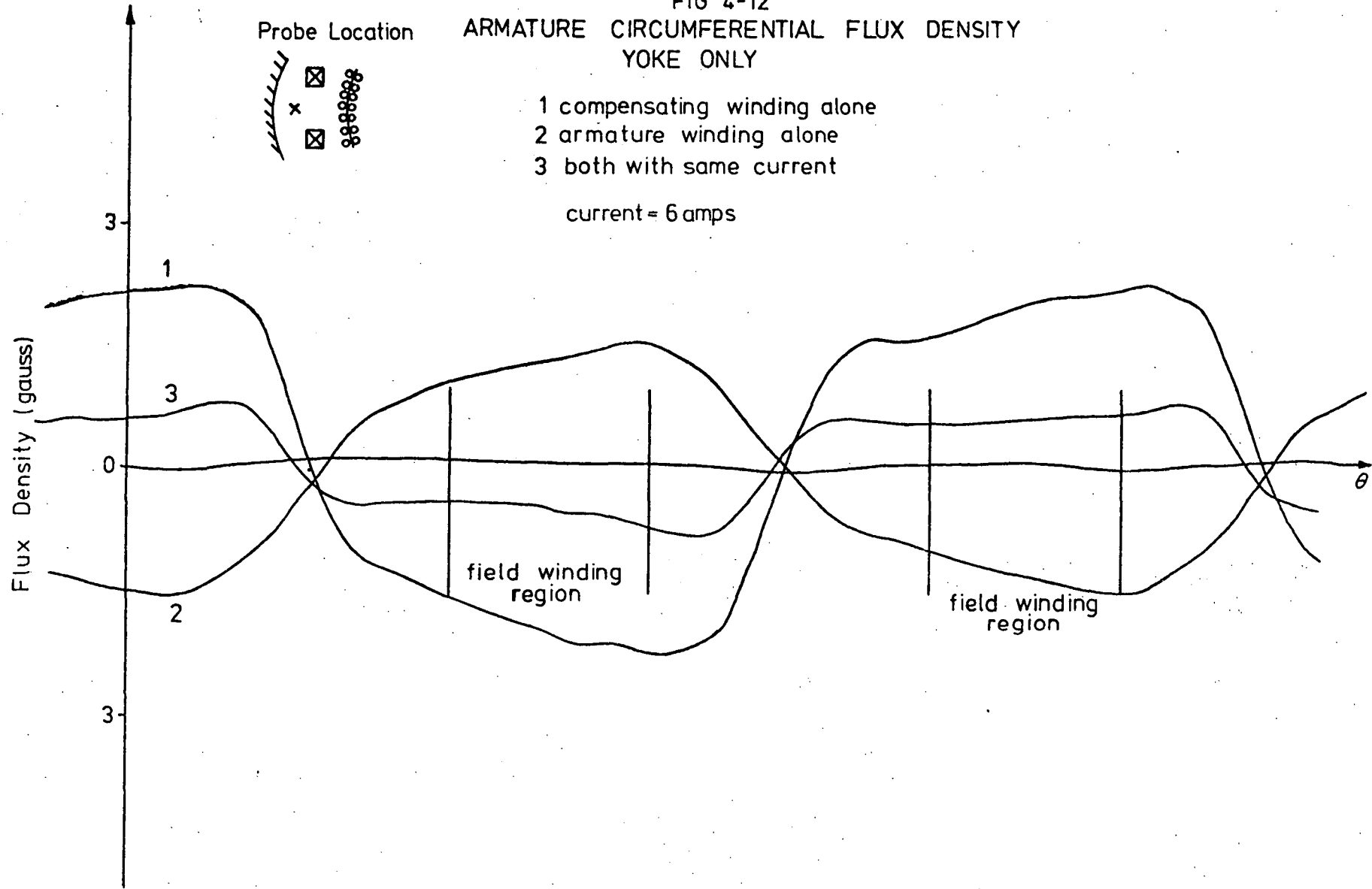
past the field windings. This applied particularly to the circumferential component which, without the pole faces, is at a maximum near the field windings.

Figures 4-13 to 4-16 indicated the dramatic change in the armature reaction flux patterns brought about by including the pole faces. The most notable change was in the circumferential component which dropped to a minimum in the region of the superconductor. This indicated that the field pole was acting as a magnetic flux shunt as planned.

The introduction of the field pole faces reduced the armature reaction flux in the superconductor region to such an extent that it may not be necessary to use a compensating winding. This would be verified after the test machine was constructed and operating.

The further cancellation obtained by passing equal currents through the armature and compensating windings was excellent. The combined use of iron pole faces and compensating windings gave better flux cancellations than those obtained under any other of the arrangements investigated. The tests indicated that a slight reduction in the compensating winding current would give almost perfect cancellation.

The good flux cancellation obtained by introducing the iron pole face led to the decision that the initial machine would have an iron armature core and iron pole faces which could be easily replaced by non-magnetic materials so that their necessity or otherwise could be investigated.

This permitted investigations on the initial machine into the operational characteristics of all possible machine configurations. In this way a final answer to the question: "How much iron is required to give adequate shielding to the superconductor from armature reaction fluxes?" would be obtained.

FIG 4-13
ARMATURE RADIAL FLUX DENSITY
POLE FACES ,YOKE,CORE

Probe Location

1 armature winding alone
2 compensating winding alone
3 both with same current
  current = 3 amps

Flux Density (gauss)

18
12
6
0
6
12
18

field winding region

field winding region

θ

Probe Location

FIG 4-14
ARMATURE RADIAL FLUX DENSITY
CORE, YOKE, POLE FACES

1 armature winding alone
2 compensating alone
3 both with same current
    current = 3 amps

Flux Density (gauss)

field winding region

field winding region

θ

4-19

FIG 4-15
ARMATURE   CIRCUMFERENTIAL FLUX DENSITY
POLE FACES , YOKE , CORE

Probe Position

1   armature winding alone
2   compensating winding alone
3   both with same current
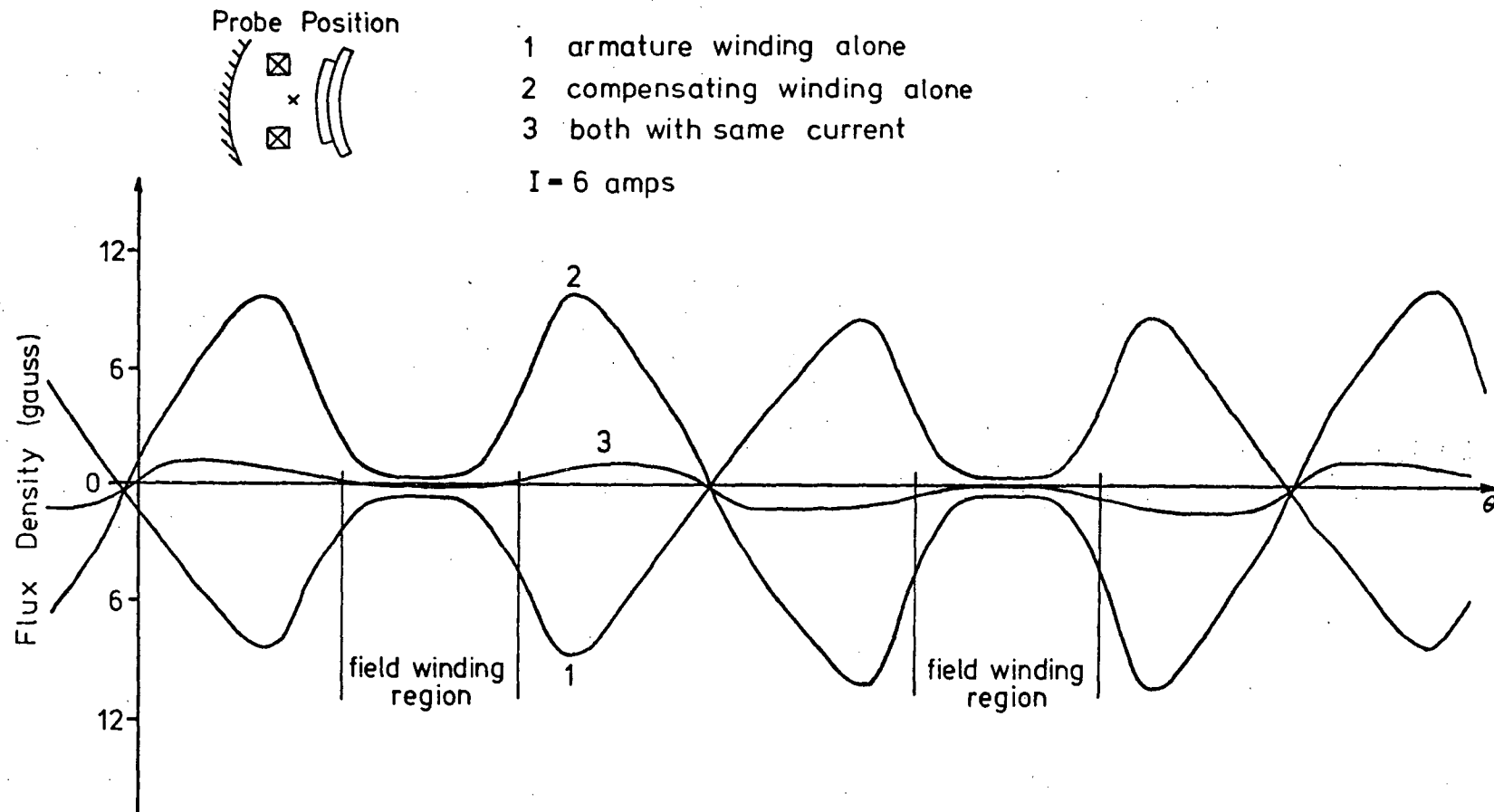
I = 6 amps

FIG 4-16
ARMATURE CIRCUMFERENTIAL FLUX DENSITY
CORE , YOKE , POLE FACES

Probe Location
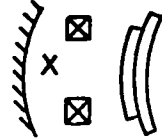
1 armature winding alone
2 compensating winding alone
3 both with same current
    current = 6 amps

Flux Density (gauss)

field winding region

field winding region
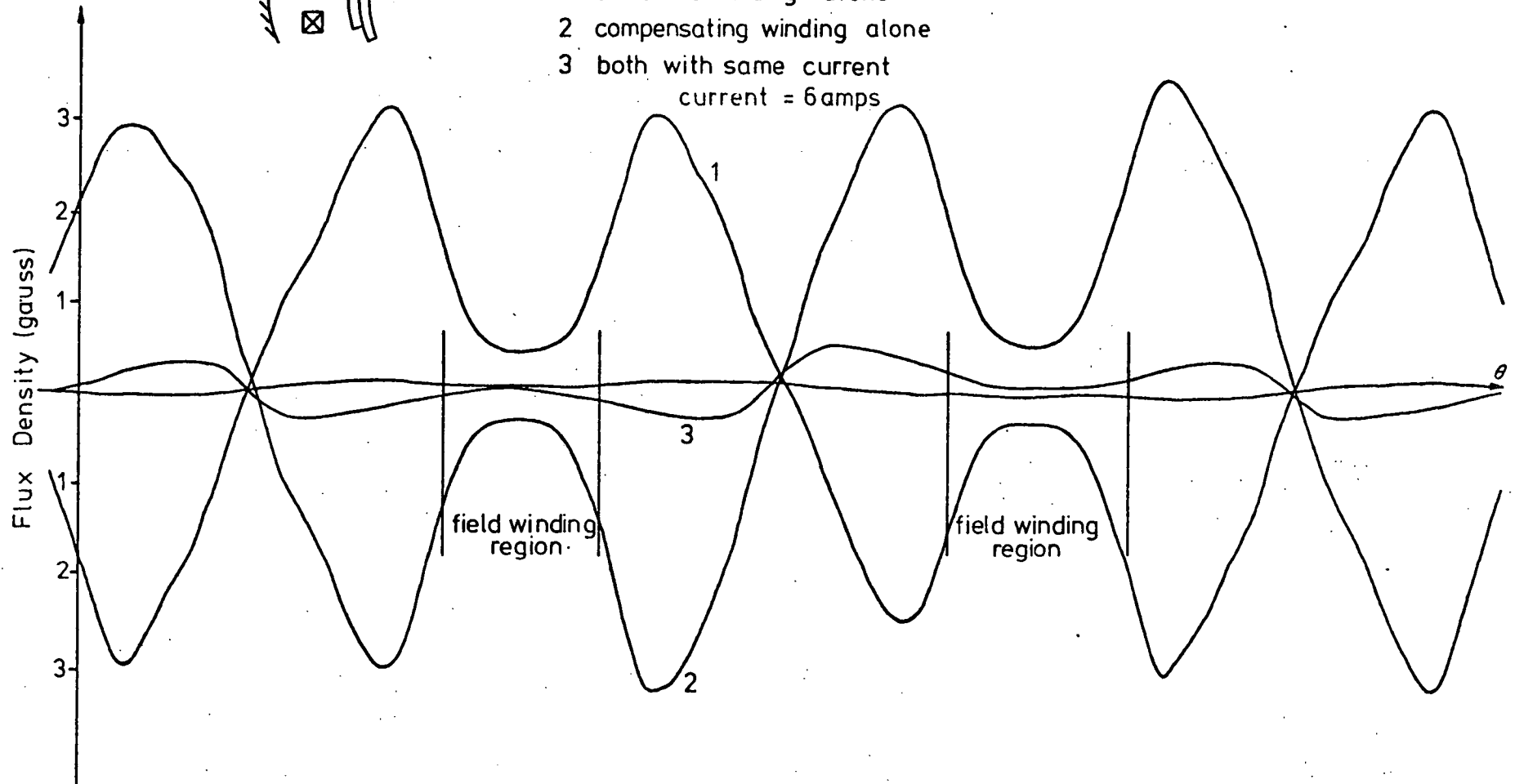
4-2-5   Iron Yoke and Pole Faces

The model armature flux distributions with this configuration were measured to determine the effects of the removal of the iron armature core on armature reaction cancellation. Comparing figures 4-13 to 4-16 with figures 4-17 to 4-20 indicated that the removal of the iron armature core produced little change in the shapes of the flux distributions. The good cancellation in the field winding region as obtained in the previous case was retained.   The magnitude of the armature reaction flux densities was reduced by a factor of approximately two, thus reducing the degree of cancellation required to obtain the same resultant flux as in the previous case. The further reduction of the armature reaction flux density in the region of the field windings may obviate the necessity for a compensating winding as mentioned in the previous section. This would improve machine efficiency and reduce costs and complexities in construction of such machines.

4-3   Field Pole Flux Distributions

To predict the machine voltage a knowledge of the total flux available for generation was required; hence field flux density distributions over the armature surface were measured. The field flux density varied over the length of the armature; hence plots for different axial positions of the probe were made. Flux plots at different radii were not necessary as only a knowledge of the flux at the armature windings was required. The model used in previous investigations was used for this purpose.

The magnetic flux due to the field windings can be split into three components: the axial, circumferential and radial components. The component of interest which gives rise to the machine voltage is the radial component; thus only its investigation was necessary.

FIG 4-17
ARMATURE RADIAL FLUX DENSITY
YOKE , POLE FACES

Probe Location

1 armature winding alone
2 compensating winding alone
3 both with same current
    current = 6 amps

field winding region
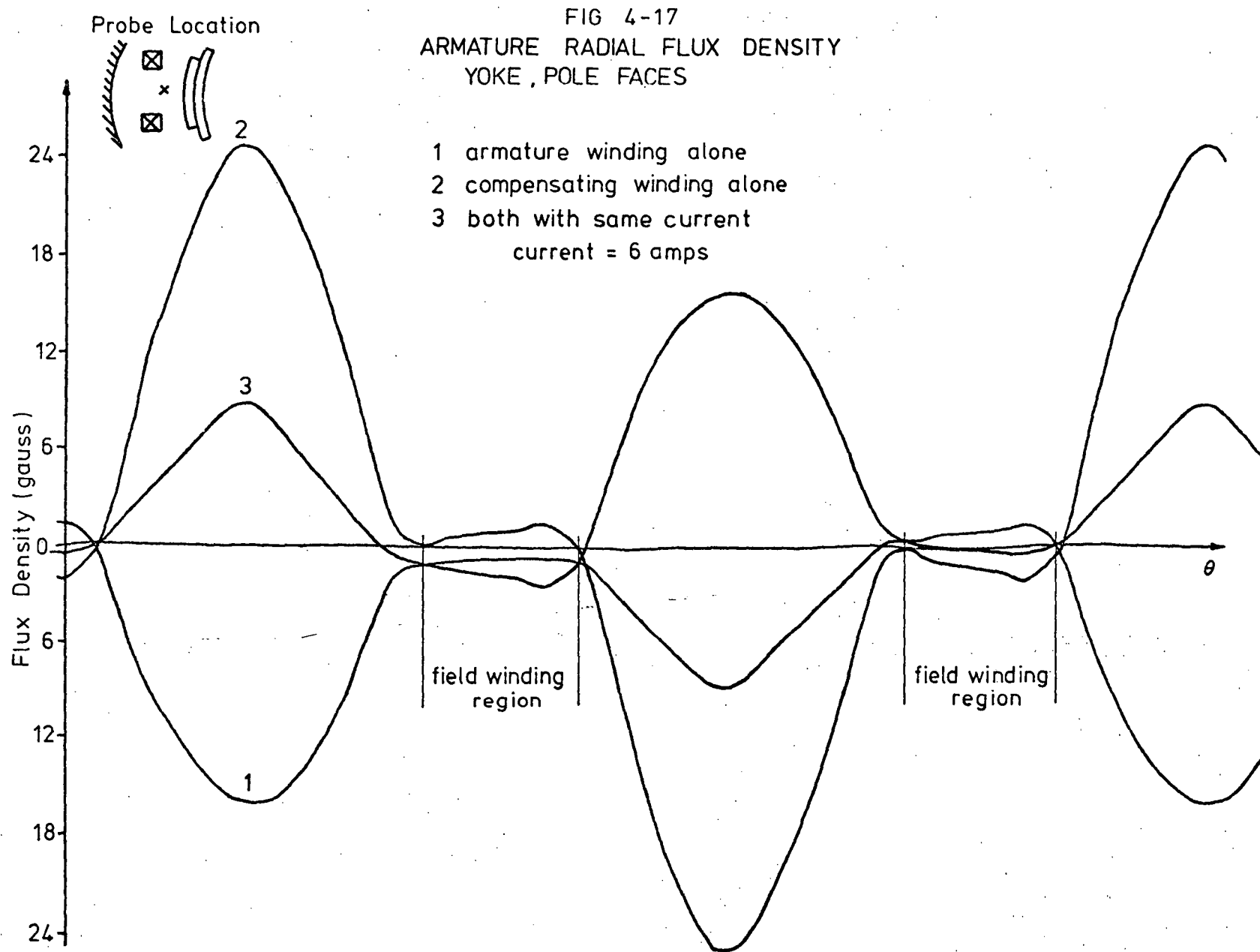
field winding region
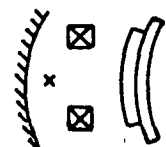
FIG 4-18
ARMATURE RADIAL FLUX DENSITY
YOKE, POLE FACES

Probe Location

1 armature winding alone
2 compensating winding alone
3 both with same current
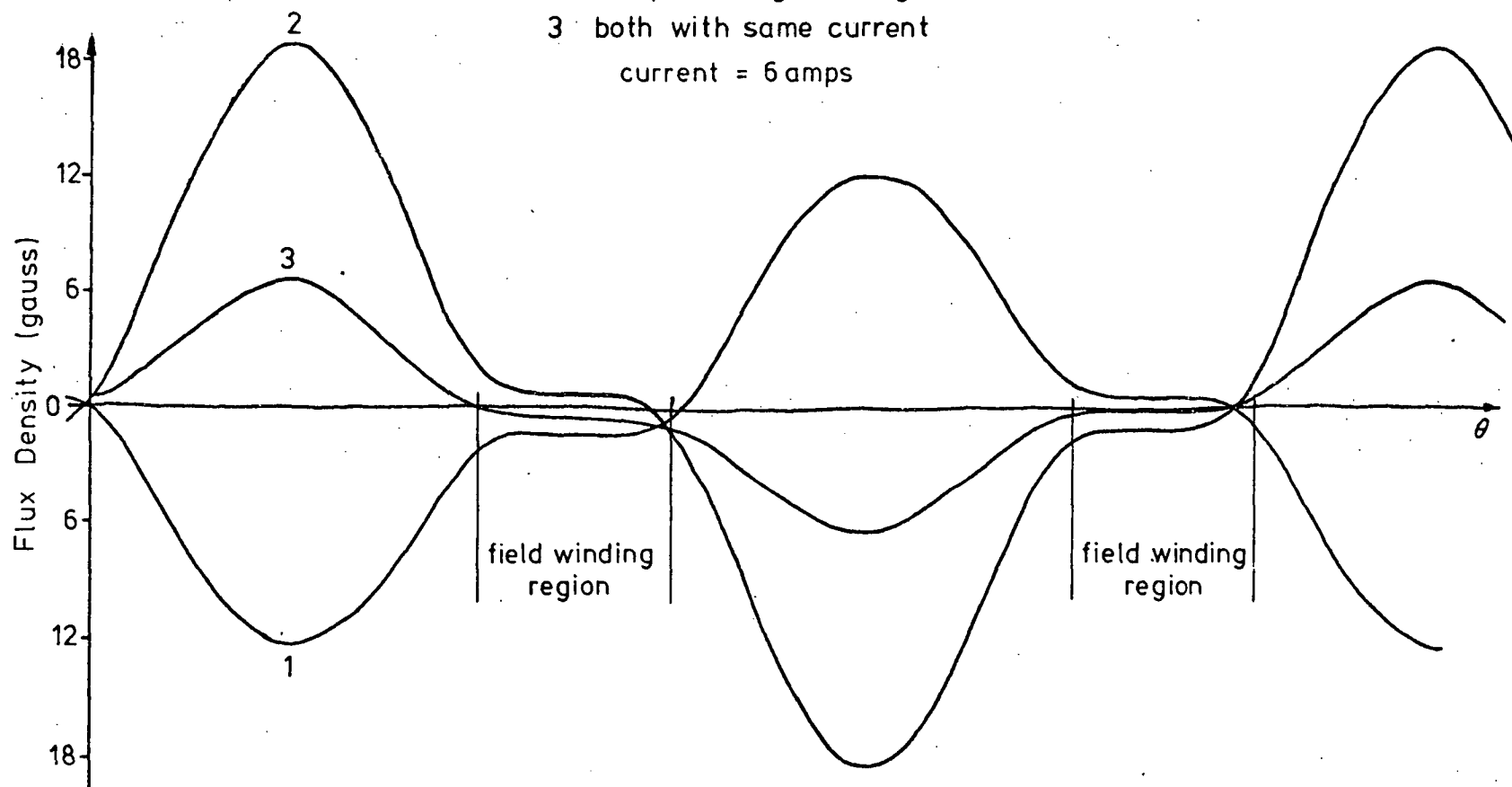
current = 6 amps

FIG 4-19
ARMATURE CIRCUMFERENTIAL FLUX DENSITY
YOKE , POLE FACES
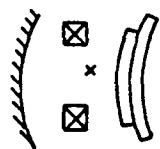
Probe Location

1 armature winding alone
2 compensating winding alone
3 both with same current
current = 6 amps

field winding region
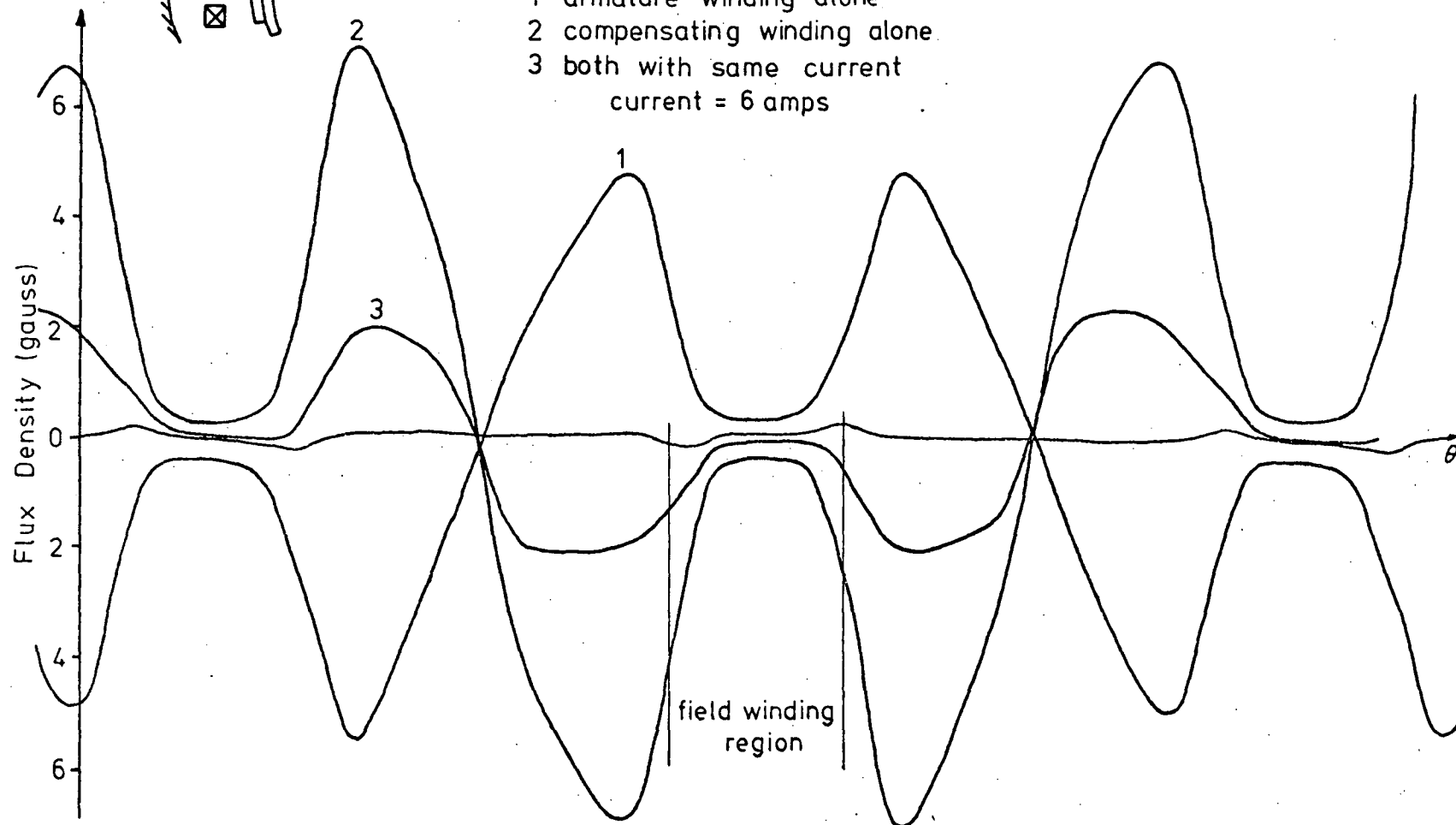
Probe Location
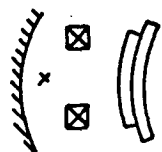
FIG 4-20
ARMATURE CIRCUMFERENTIAL FLUX DENSITY
YOKE , POLE FACES

1 armature winding alone
2 compensating winding alone
3 both with same current
   current = 6 amps

Flux Density (gauss)

field winding
region
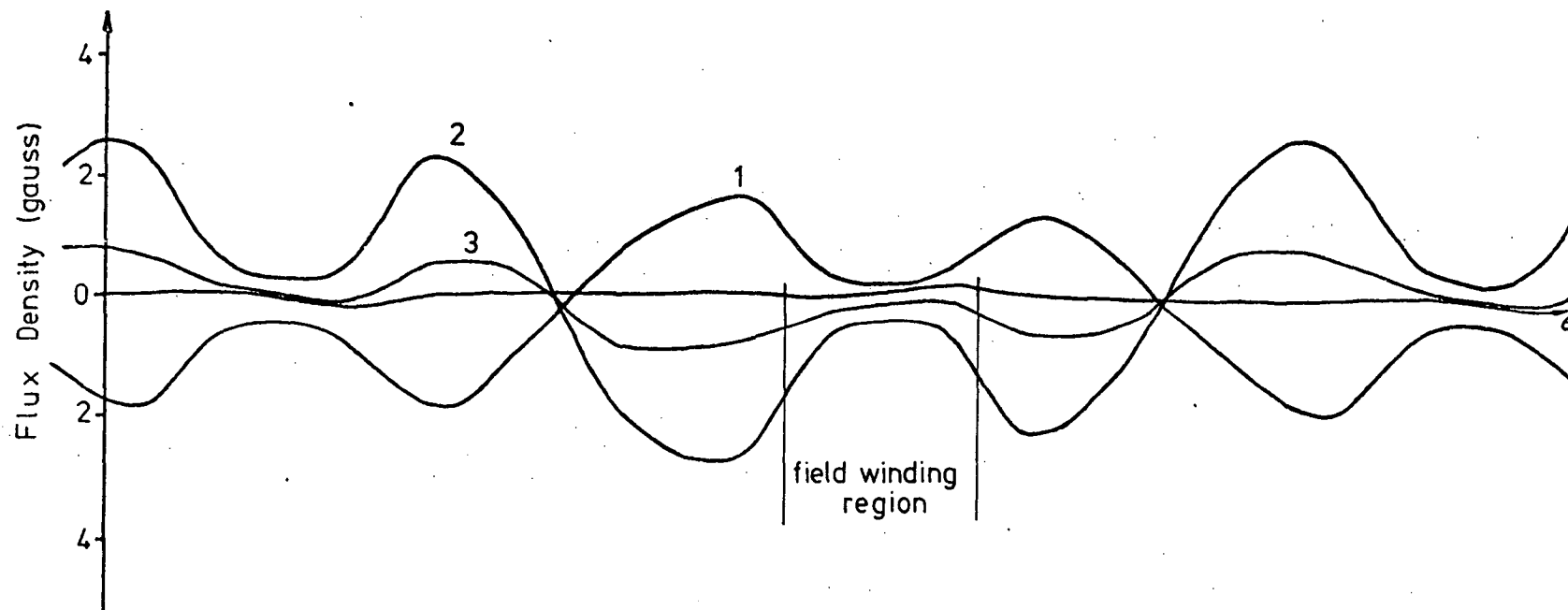
The distributions of flux were studied for different machine configurations and the results obtained are discussed in the following sections. Table 4-1 summarizes the quantitative results obtained from the plots so that comparisons between the different machine configurations could be made. For explanations of the quantities tabulated, see Appendix D on flux distributions and calculations.

4-3-1 Armature Core and Yoke Only

The flux density patterns (figure 4-21) obtained for this machine configuration were not ideal distributions for a D.C. machine because they would result in a high generated voltage in the coil under the centre line of the field pole and rapid decrease in coil voltage the further the coil was positioned from the pole axis. This is undesirable because it leads to non-uniform voltage differences between the commutator segments. Since the voltage rating of D.C. machines is limited by the allowable voltage between commutator segments; the maximum voltage that could be obtained for a given commutator, with a uniform flux distribution, would not be possible with this flux distribution.

The peaking in the flux distributions would also lead to peaking in the mechanical forces experienced by the armature conductors when not located in a slotted iron armature. This would require mechanical support considerably greater than the support required if the flux was more evenly distributed.

Another disadvantage of peaking on the flux distributions was that the large variations in flux density magnitude with axial and circumferential positions could give partial magnetic saturation of the inner iron rotor core. Hence the iron armature core would not have been used with maximum effectiveness. The fact that the ratio $B_{MAX}/\bar{B}$, where $\bar{B}$ is the specific magnetic loading, equalled 4.37 for the model (Table 4-1) indicated the ineffective usage of the armature surface with this machine

FIG 4.-21
MODEL FIELD POLE RADIAL FLUX DENSITY
ARMATURE CORE AND YOKE ONLY
0,1,2 one winding only
3 position 0 both windings
current = 2 amps

Field Pole Radial Flux Density (gauss)

Probe Height

rotor
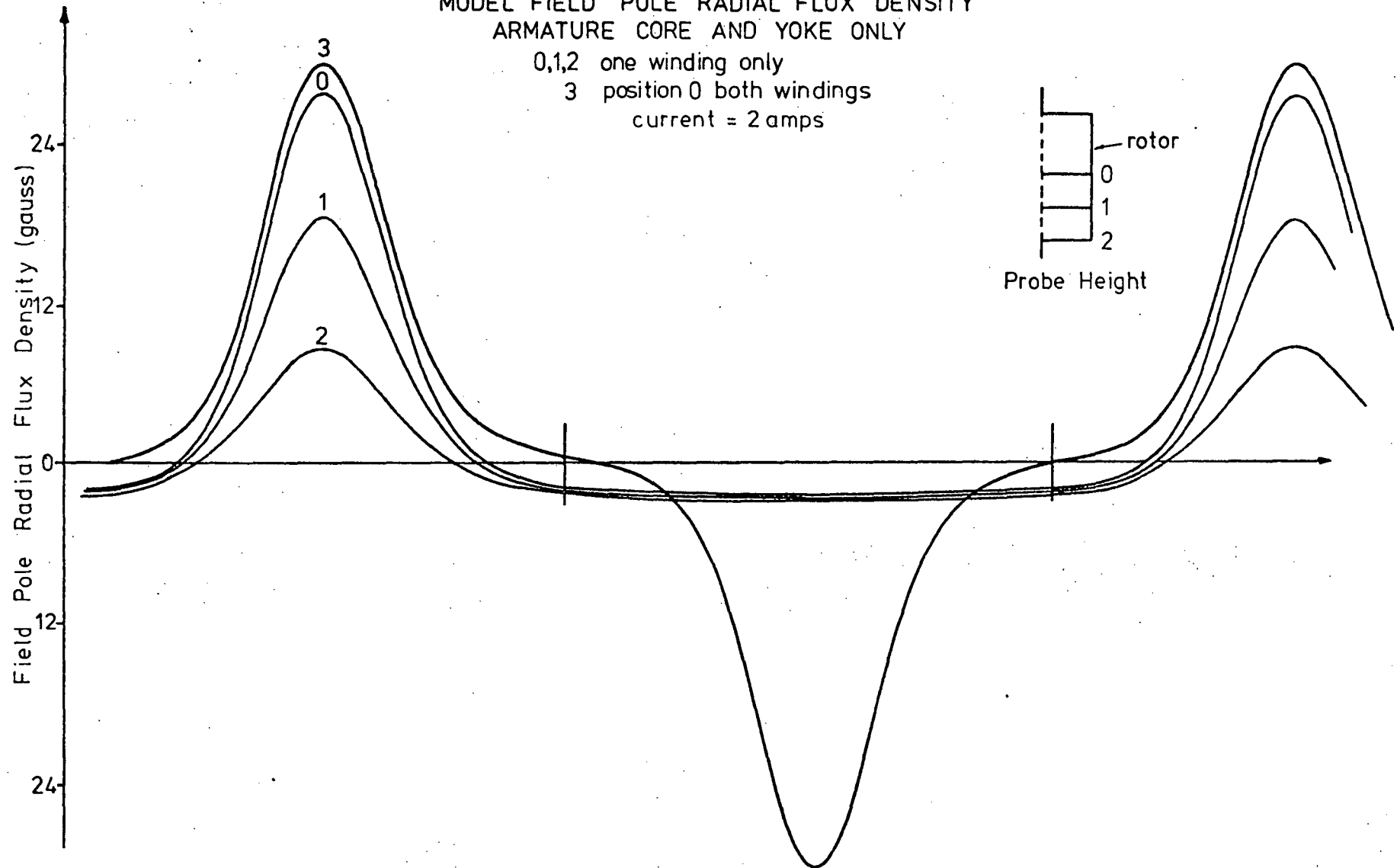
TABLE 4-1

MODEL TESTS

RADIAL COMPONENTS OF FIELD POLE FLUX

		Armature Core and Yoke only	Armature Core, Yoke and Pole Faces	Yoke only	Yoke and Pole Faces only
Field pole flux	$\phi \mu W$	2	2.78	1.11	1.27
Average field pole flux density	$\bar{B}$ gauss	3.54	4.84	1.96	2.24
Maximum field pole flux density	B_{MAX} gauss	15	9.8	9.14	4.35
	$B_{MAX}/\bar{B}$	4.24	2.02	4.66	1.94
	$\bar{B}_R$	1.75	2.51	1	1.15
	B_{MAXR}	7.65	4.91	4.66	2.17

$$B_{MAXR} = B_{MAX}/\bar{B} \text{ with yoke only}$$

$$\bar{B}_R = \bar{B}/\bar{B} \text{ with yoke only}$$

configuration. However, the flux distributions gave small flux densities in the vicinity of the magnetic neutral axis. This was regarded as being desirable for good commutation because of the decrease in field induced armature coil voltages at the completion of the commutation cycle.

4-3-2 Armature Core, Yoke and Pole Faces

The pole faces were introduced as flux shunts to shield the super-conductor from armature reaction fluxes. Hence, unlike the pole faces of conventional two pole D.C. machines, which shadow nearly 50% of the rotor surface, they shadowed only 30% of the rotor surface. If the pole faces were too large, then a large percentage of the field flux would leak between the pole tips rather than pass through the rotor because of the large airgaps between the rotor inner core and the pole faces. This leakage would increase if an iron-free rotor was used.

The flux was more evenly distributed over the entire pole face area (figure 4-22) and the ratio $B_{MAX}/\bar{B}$ was 1.95. This was large when compared with values obtained in conventional machines but was still an improvement on the previous case discussed.

The more evenly distributed field flux was an important improvement obtained with the introduction of the field pole faces because it reduced the effects of peaks in the field flux densities. For the same field magneto motive force the iron pole faces increased the useful field flux above the value obtained in the previous case whilst a reduction in the peak flux density occurred. These results indicated that the introduction of the field pole faces was beneficial in many areas and would result in a higher rated initial machine. In the initial machine saturation of the pole face could occur in the immediate vicinity of the field coil. However, the saturation would extend only a short distance into the back surface of the field pole face; hence the field pole faces would retain their advantages. The introduction of the field pole faces had a dis-

FIG 4-22
MODEL FIELD FLUX DENSITY DISTRIBUTION
YOKE, CORE AND POLEFACES
current = 2·5 amps

rotor
0
1
2

Probe Height

RESIDUAL

1 positions 0 and 1 both windings
2 positions 0 and 1 one windings
3 position 2 both winding
4 position 2 one winding

Field Pole Radial Flux Density (gauss)
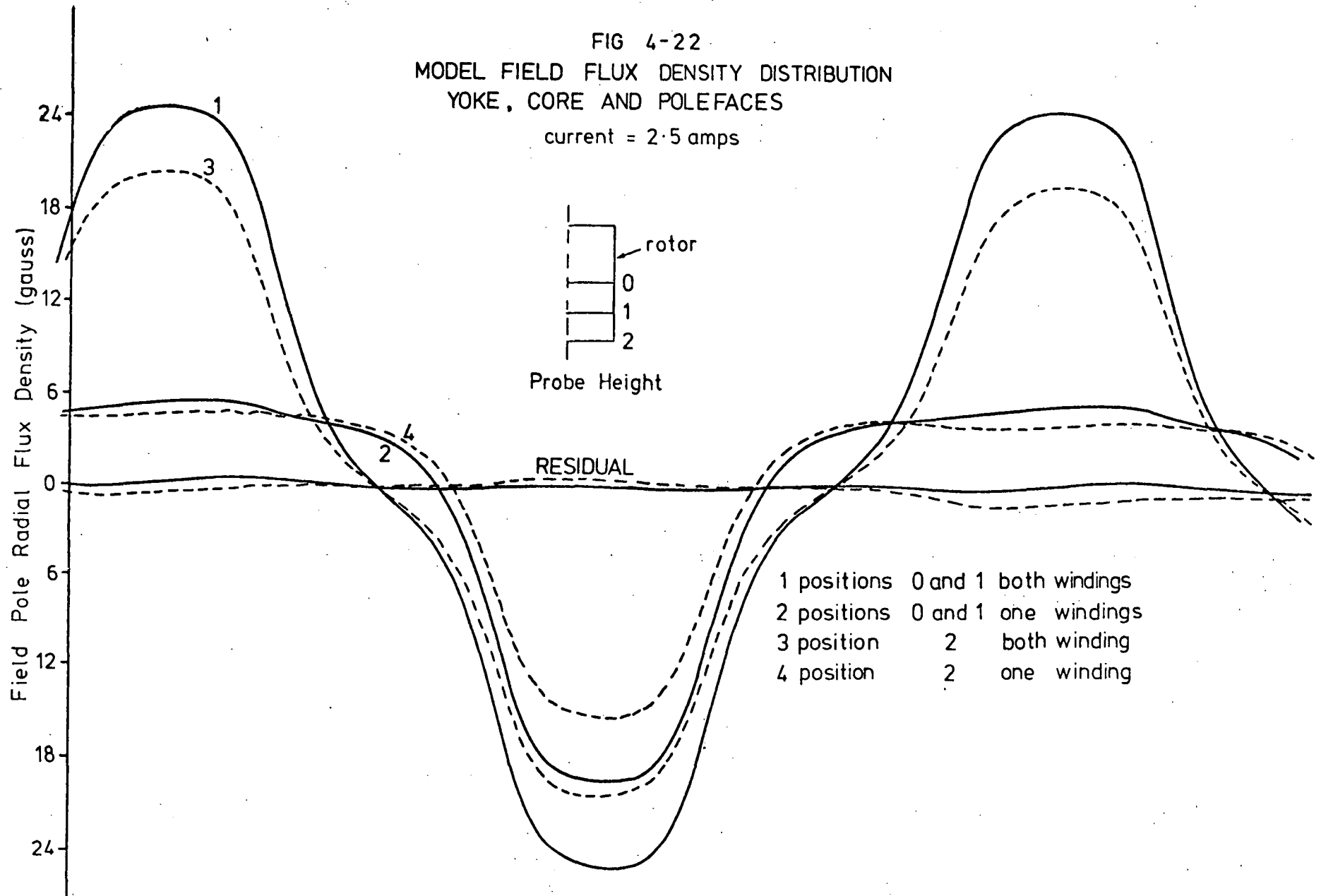
advantage in limiting the allowable peak field flux to near 1.2 tesla which reduced the fundamental advantages of higher flux densities available with superconductors with suitably designed field coils. However, for the purposes for which the initial machine was intended the disadvantage did not arise because flux densities of this magnitude were difficult to achieve whilst maintaining the peak flux density at the superconductor below the critical value. This is also true to a lesser extent in full scale machines, in which critical flux densities can be exceeded at the field winding with field flux densities at the armature of near one tesla.

4-3-3 Yoke Only

The field pole flux distribution (figure 4-23) in a machine with only an iron yoke was characterised by its high peak flux density, its high ratio of peak flux density to average flux density, and the very small radial component of flux density in the vicinity of the magnetic neutral axis. These have the disadvantages and the advantages as discussed in the previous sections.

The penalty for the absence of the iron armature core and iron pole faces would be the necessity for more ampere turns to produce the field flux. But an important advantage was that effects due to magnetic saturation in the rotor were absent. Hence the peaking in flux density can be tolerated to a greater extent than in the case discussed in section 4-2-1.

For a given number of ampere turns in the field winding the flux was reduced by a factor of 2.5 of that obtained when using an iron armature core, yoke, and pole faces. Provided adequate shielding of the super-conductor could be obtained using the compensating winding, the disadvantage could be obviated by the use of a larger quantity of super-conductor and the advantages obtained from the elimination of iron could be retained.

FIG 4-23
MODEL FIELD FLUX DENSITY DISTRIBUTION
YOKE ONLY
current = 2 amps

1 position 0 both windings
2 position 0 one winding
3 position 1 both windings
4 position 2 both windings

Probe Height

Field Pole Radial Flux Density (gauss)
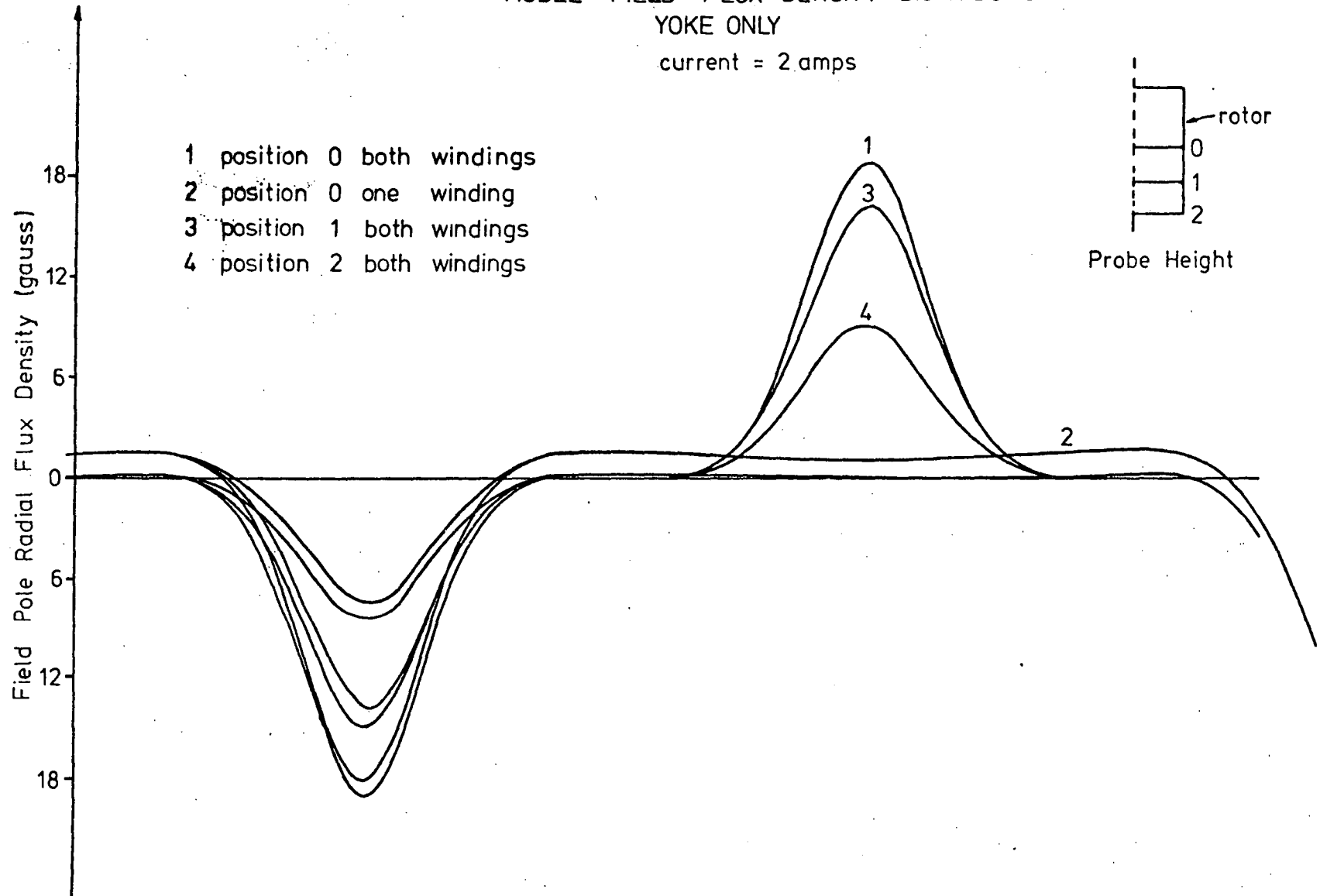
4-3-4 Yoke and Pole Faces Only

The pole faces distributed the pole flux more evenly over the rotor surface (figure 4-24) and the peak flux density to average flux density ratio was the smallest of all the cases considered - Table 4-1. However, the total flux was only marginally greater than the previous case. Due to the uniformity of the flux density, large voltage variations between commutator segments would not occur, and the low flux density in the region of the magnetic neutral axis was retained.

Because of these characteristics, this layout for a large machine may be the best. The amount of iron required in the pole faces would be small. In addition, the large magneto motive forces available with superconductors could be used to the utmost and at the same time the iron would give the required shielding of the superconductor. However, the same limitation in field flux density as discussed in section 4-2-2 applies.

Without an iron armature core the possibility of induced currents in the shaft of the machine would need to be investigated.

4-4 General Comments

The preceding investigation into field pole flux distributions in large air gap machines revealed two characteristic properties:

(a) There was a low value of the ratio of average flux density to peak flux density.

(b) Low flux densities were produced in the region of one field winding by the m.m.f. of the other field winding. This was a result of the many leakage paths inherent in a large air gap machine - figure 4-25.

FIG 4-24
MODEL FIELD FLUX DENSITY DISTRIBUTION
POLE FACES AND YOKE
current = 3 amps

1 position 0 one winding
2 position 0 both windings
3 position 1 both windings
4 position 2 both windings

Probe Height

Field Pole Radial Flux Density (gauss)
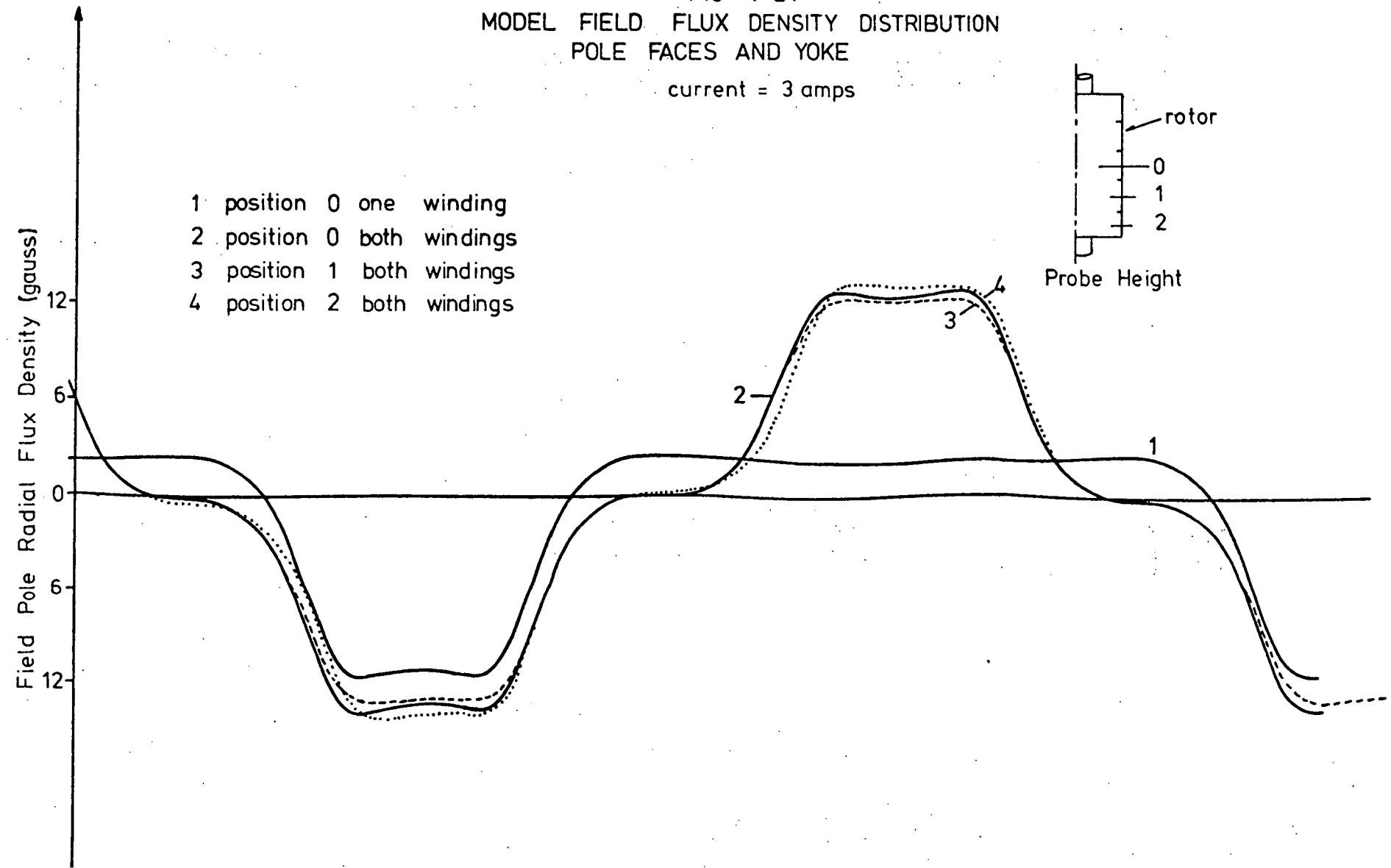
FIG 4-25
FIELD FLUX LEAKAGE PATHS

SECTION X-X

iron armature core

pole face

field winding

yoke

shaft

flux acting in oposition to main field flux
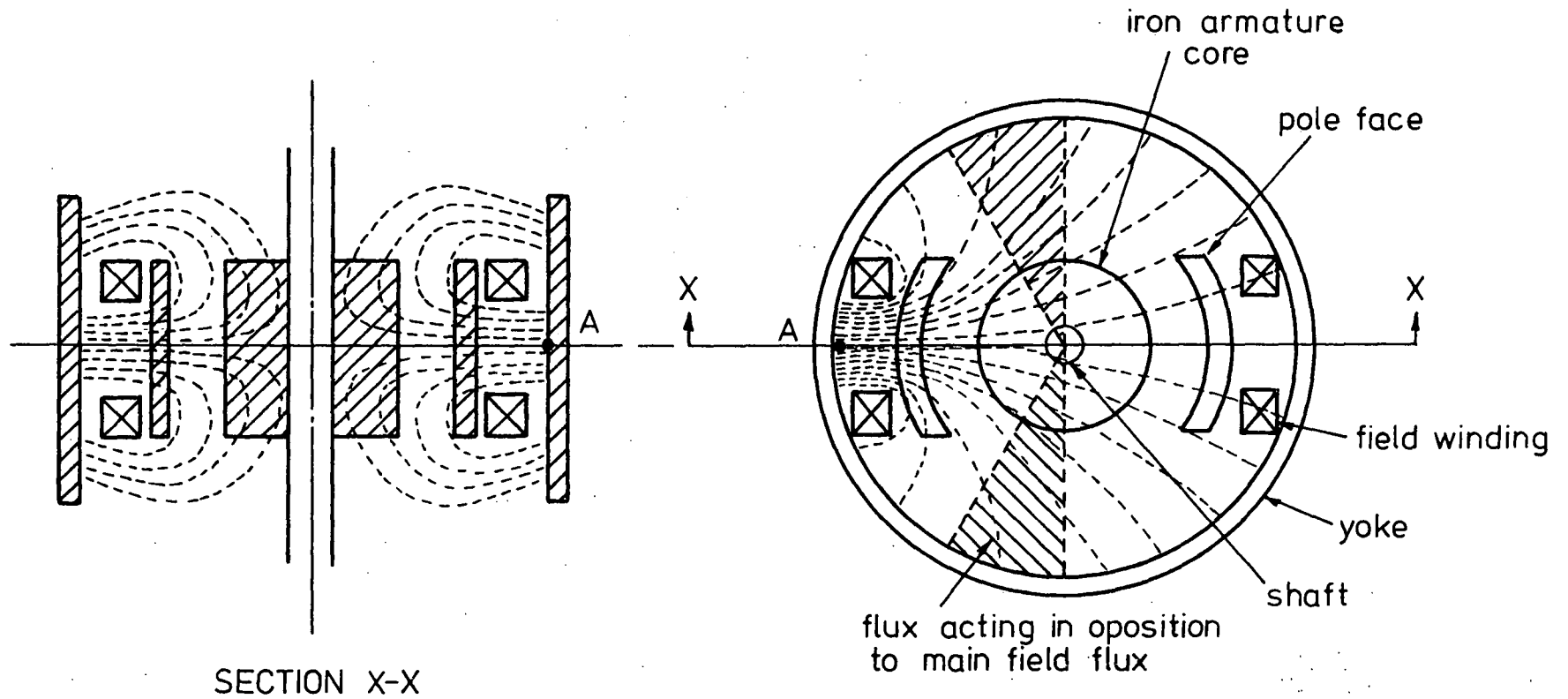
The leakage pattern shown in figure 4-25 leads to higher field flux densities in the region of the field coil than at the armature windings. This tends to give magnetic saturation of the yoke near point A. Figures 4-21 to 4-24 show regions in which the flux actually acts in opposition to the main flux which tends to reduce the e.m.f. of the machine.

The leakage is unavoidable in large air gap machines. Although the leakage is undesirable it has one advantage: that is, the force of attraction between field coils is smaller than if all the flux from one coil was concentrated in the vicinity of the other. This requires less structural support for the field coils which, in turn, would give less heat influx to the liquid helium. In a conventional machine the pole core carries the flux; hence the forces on the field windings are small.

To maintain the shunting effect of the field pole faces on the armature reaction fluxes, it was necessary that the iron pole faces were not saturated. The use of the field pole faces for shielding purposes thus imposed a lower upper limit than the saturation level of the iron on the possible pole flux density.

4-5   Conclusions

The tests on the model have shown that the basic format as visualised for the test machine was satisfactory. It was appreciated that the design may not resemble that finally selected for a model of a prototype, but it was suitable for conducting the necessary experiments to investigate the problems to be considered in arriving at an optimum design of a heteropolar machine with superconducting field windings. The aim at this stage was to construct a satisfactory machine at minimum cost so that planned research could be conducted to gain the basic information for the design of a final model research machine.

CHAPTER 5

DESIGN OF THE INITIAL MACHINE

5-1   Introduction

This chapter discusses the factors which were considered in the selection of the size and current rating of the initial machine.

The design of the cryostats and the problems encountered during their construction and testing are covered. The chronological stages in the development of the cryostats, the techniques attempted to obtain successful vacuum seals (which led to the use of argon arc fusion welding to the exclusion of other possible forms of permanent jointing), and the details of two developmental cryostats built, are provided as a summary of the path of progress towards the choice of the design of the cryostat first adopted.

It is stressed that the objective of the initial machine was to obtain basic data related to the influence of armature reaction on the operation of the superconductor and to gain experience in the design, construction and operation of cryostats.

5-2   Selection of the Physical Size of the Machine

The size of the initial machine was determined from the requirement that maximum utilisation of readily available and suitable components be made. On the basis of the results obtained from the tests on the models, an iron stator was required for the test machine. An iron stator with what were considered to be satisfactory dimensions was obtained from an old four-pole D.C. machine and formed the basis of the initial machine. An available thirty-one segment commutator which was

suitable for the test machine determined the number of armature coils.
The major dimensions of the stator are listed below:

internal diameter	400mm
external diameter	470mm
overall length	254mm

The components of the machine which had to be mounted within the
iron stator were:

(a) field coil cryostats;

(b) armature;

(c) compensating winding;

(d) field pole faces.

The necessary space had to be provided for each of these.

The basic form of the cryostats was determined from the consider-
ations discussed in sections 5-3-1 and 5-3-2. The availability of "off
the shelf" stainless steel tubing in various wall thicknesses and
diameters and the envisaged size of the superconducting field coils
determined the dimensions of the cryostats. These considerations
required that 90mm of the stator inside diameter be set aside for each
cryostat. Standard "off the shelf" tubing and container sizes were
selected to minimise the possibility of faulty vacuum leaks occurring
in the cryostats. Standard materials also reduced the complexity of
construction thus further reducing the possibility of faulty cryostats.

The dimensions of the remaining components were chosen to obtain
the maximum armature diameter consistent with convenience of construction
and the provision of adequate clearance between the end windings of the
armature coils and the compensating winding former. The field pole
faces acted as supports for the compensating winding. Hence, the outside
diameter of the compensating winding former determined the curvature of
the field pole faces.

The length of the armature was set at 127mm (5"). This left
sufficient space for the armature winding end connections, the commutator
and the brush holder. The lengths of the compensating winding and the
field pole faces were the same as those of the armature so that each
shadowed the other.

This approach for the selection of the physical size of the machine
was adopted so that a suitable and low cost initial machine could be
constructed to allow the various problems associated with the development
of such a machine to be fully investigated. The general proportions of
the initial machine are indicated in figure 3-3 and a photograph of the
completed machine is given in figure 5-10.

5-3   Cryostats and Field Coils

To hold helium in the liquid state for sufficiently long periods so
that useful experimental results can be obtained requires containers
(cryostats) which have only small heat inleaks to the cold region.
A heat inleak of 1 watt to liquid helium produces a boil-off rate of
liquid of 1.4 litres per hour. This indicates the necessity for good
thermal insulation to prevent excessive loss of coolant. The construction
and designs of two developmental cryostats and the first adopted cryostat
are described in the following sections.

5-3-1 Cryostat Design Considerations

The means by which heat transfers to the cold region of a cryostat
are conduction, convection and radiation.

Vacuum insulation around the inner cold region virtually eliminates
convection heat inleak and gaseous conduction heat inleak. The vacuum
required in order to achieve this is in the range of 10^{-4} to 10^{-5} torr.
Pressures below these values further reduce these heat inleaks but at

these vacuum pressures other forms of heat inleak, such as radiation, dominate the total heat inleak, thus offsetting any advantages gained by the further pressure reduction. The technology to obtain these pressures was readily available, but to obtain adequate vacuum sealing of containers is an exacting task from the practical point of view.

Conduction heat inleak due to the structural materials can be reduced by using materials of low thermal conductivity (for example nylon, teflon, and stainless steel), maximizing the path lengths for such heat inleaks, and minimizing the cross sectional areas of the paths. This is one of the reasons for a long chimney from the liquid helium chamber to room temperature and the light gauge stainless steel used for the inner chimney pipe. The determination of heat inleak due to current leads to the superconducting coil is covered in Chapter 6.

The heat conducted to the liquid helium via the stainless steel chimney pipe (figure 5-1) can be estimated as follows:

For a constant cross sectional area of the chimney material:

$$Q = \frac{A}{\ell} \int_{Tc}^{Th} KdT$$

where

A = area

ℓ = length

K = thermal conductivity

Q = heat conducted

Tc = lower temperature

Th = higher temperature

For stainless steel $\int_{4.2}^{300} KdT = 30.5 \text{w-cm}^{-1}$ and $\int_{4.2}^{77} KdT = 3.17 \text{w-cm}^{-1}$

FIG 5-1
'A' CRYOSTAT

O ring
O ring
Chimney
Shield plug
Indium seal
Tie point
Threaded
89mm
64mm
Polished copper

Weld
Nitrogen tie point
Indium seal
Coil former fitted to end plate for centralising
coil
coil
Indium seal
Weld
Radiation shield
Demountable covers 6·35 mm s/s plate
Tap 8 BA

Weld
Thin walled s/s tube
Weld
Indium seal
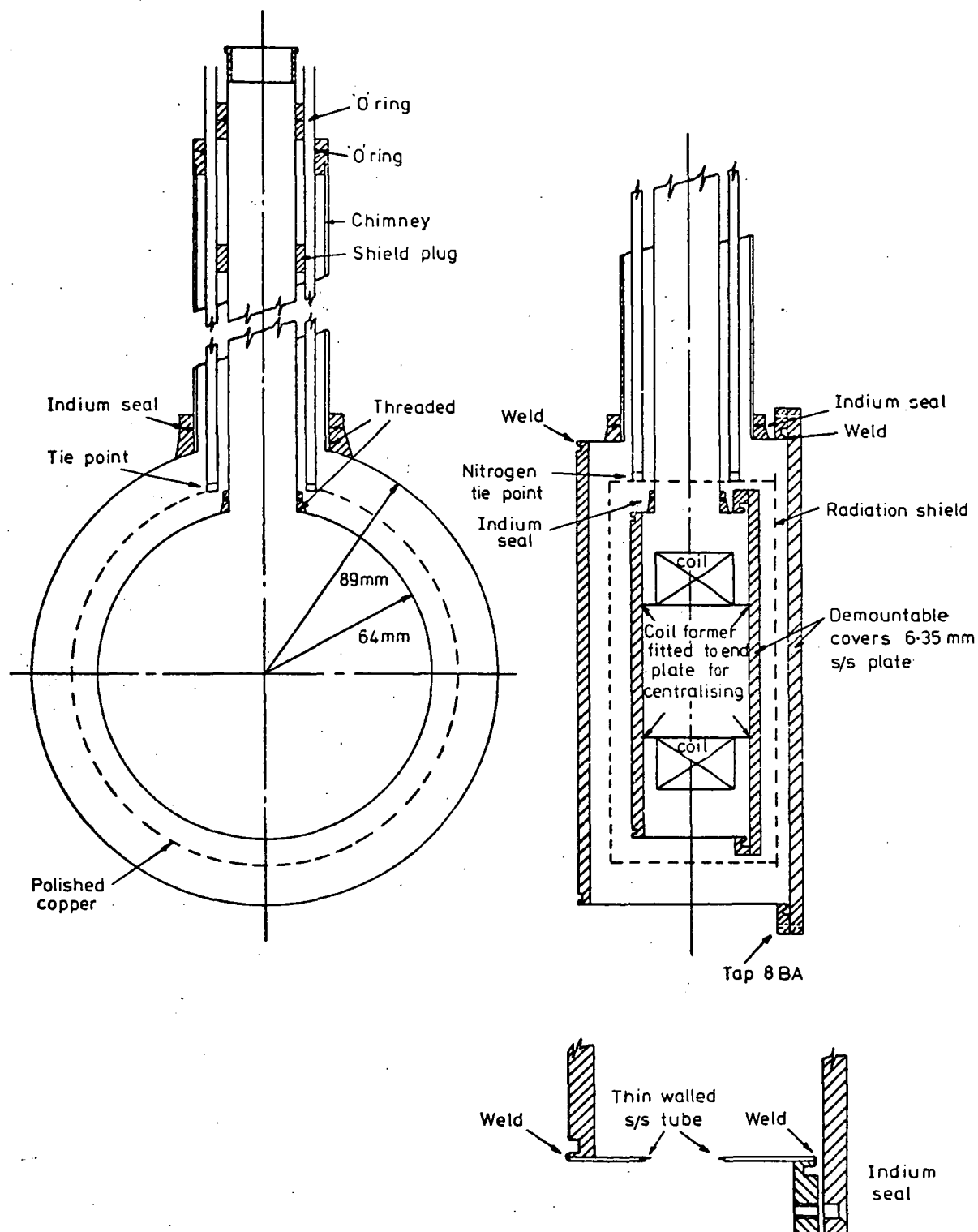
Details for argon arc welding
of stainless steel joints

These results indicate that if the chimney tube could be held at 77K near its room temperature extremity, conduction heat losses down the chimney could be reduced by a factor of ten. To achieve this, a stainless steel plug was positioned in the vacuum space between the radiation shield coolant chamber (discussed next) and the inner tube. The plug diverts the heat conducted via the chimney from its room temperature extremity into the radiation shield coolant chamber. The resulting increase in the rate of loss of liquid nitrogen was acceptable because of the ready availability of liquid nitrogen and because of the decrease in the rate of loss of liquid helium.

Thermal radiation heat inleaks are dependent on absolute temperature differences:

$$\frac{Q}{A} \propto \delta \, (T_h^4 - T_c^4)$$

δ = Stephan-Boltzmann constant

A = area

For a black body, the constant of proportionality (emissivity) is unity, but for real bodies, the constant of proportionality is less than one. Hence, an upper bound to thermal radiation heat inleak can be found using an emissivity of unity.

If T_h = 300K and T_c = 4.2K then for a black body,

$$\frac{Q}{A} = 5.67 * 10^{-12} * 300^4 \text{ watt/cm}^2$$

$$= 45.9 \text{mW/cm}^2$$

If A = 500cm^2 as a representative value,

Q = 23 watts.

Heat inleaks of this magnitude are totally unacceptable and hence a shield was used to intercept the heat radiation. This shield was constructed from 26 gauge copper sheeting because of its high thermal conductivity. The high thermal conductivity material was used so that

the thickness of the radiation shield could be minimised whilst main-
taining a uniform radiation shield temperature of near that of the
liquid nitrogen shield coolant. The shield completely surrounded the
inner vessel and was cooled by joining it to the bottom of the liquid
nitrogen chamber in the chimney section - figures 5-1, 5-2, and 5-3.

To indicate the effect of cooling a radiation shield with liquid
nitrogen, consider the above example but with T_h = 80K.

$$\frac{Q}{A} = 0.232 mW/cm^2$$

$$Q = 0.116 \text{ watt if } A = 500 cm^2$$

That is the inclusion of the radiation shield would lead to a reduction
in the radiation heat inleak to the liquid helium by a factor of two-
hundred.

The above results were obtained assuming black body emissivities.
This was assumed so that the importance of using materials with low
emissivities would be illustrated. The black body radiation heat inleak
to the shield of 23 watts was excessive. However, the emissivities of
the stainless steel and copper used in the cryostat were approximately
.05 and .03 respectively. With these figures, the above heat inleaks
would become about 1 watt and .005 watt respectively, which were
acceptable.

An intercepted heat inleak to the liquid nitrogen-cooled shields of
1 watt, even if concentrated at the furthest extremity of the shield
from the nitrogen, would produce a temperature difference of less than
7K across the shield. In actual fact, the temperature difference would
be considerably smaller because of the distributed nature of the heat
inleak. Hence, the assumption that the shield was at 77K was justified
and the method of cooling was effective.

FIG 5-2
'B' CRYOSTAT

Chimney structure and inner can from a single unit

51mm

Silver soldered into position

Vacuum outlet

Shield plug

650 mm

'O' ring

Tie point

Silver solder

89mm

64 mm

Polished copper

Liquid nitrogen

Weld

'O' ring

Weld

Tie point

Silver soldered

Copper radiation shield

coil

coil former fitted to end plate for centralising

Demountable covers 6·35mm s/s plate

coil

Indium seals

Tap 8 BA

'O' ring

25·4 mm R

Tapped

Silver soldered on to 51 mm pipe

Silver soldered on to 178 mm pipe

Weld

Thin walled s/s tube

Weld

Indium seal

Details of argon arc welding of stainless steel joints

FIG 5-3
'C' CRYOSTAT

Teflon plug

Grindable fusion welds

Vacuum port

Radiation shield coolant chamber

Shield Plug

Grindable fusion weld

s/s steel ring f/welded to tubes blind tapped holes for radiation shield tie point

70 mm dia × 16 g s/s steel

Indium seals

51 mm

83 mm   89 mm

64 mm

Helium   container

127 mm

159 mm

178 mm

210 mm

Liquid   & coil

Radiation shield 165 mm dia × 76 mm dia polished copper

12 - 3·175 mm dia holes on 200 mm P.C.D.

12 - 3·175 mm dia holes on 149 mm P.C.D.

Small container 127·2 mm OD   Large container   179·1 mm OD
                 125 mm ID   176·9 mm ID
         Depth   57 mm   Depth   89 mm

In later tests (Chapters 10 and 11) and cryostat designs (Chapter 12) an additional technique of shielding using alternate layers of low emissivity material and low conductivity material was used between the radiation shield and the helium chamber. The materials used were aluminized mylar and fibreglass mat. They were packed so that they filled the vacuum space. A problem with operating the "Super Insulation" was to maintain good vacuum between the insulation layers as mylar degasses considerably. The degassing and difficulty with pumping such insulations has led to the manufacture of self-pumping super insulations which incorporate getter materials such as activated carbon in the spacer material (5-1). These were not used during this project.

It was necessary to use the same construction material throughout the sections of the cryostat which were joined and exposed to low temperatures if excessive stresses due to differing thermal contraction rates were to be avoided. These stresses, if present, could cause cracking of materials and hence failure of the cryostats.

Thermal contraction for stainless steel between 293K to 77K and 293K to 4.2K results in changes in lengths given by:

$$\frac{L_{77} - L_{293}}{L_{293}} = -270 * 10^{-5}$$

$$\frac{L_{4.2} - L_{293}}{L_{293}} = -300 * 10^{-5}$$

The radiation shield coolant chamber was selected to be 650mm in length and almost its entire length was to be maintained at 77K with liquid nitrogen. The decrease in its length during cooldown was estimated at near 1.75mm. The radial clearance between the radiation shield and the room temperature outer container was only 5mm; hence the cryostat was constructed so that, after cooling, contraction centralized the radiation shield (and the coil chamber) within the outer can. This

method of allowing for differential contraction at the construction stage reduced the risk of thermal short circuits between sections of the cryostat at differing temperatures.

In sections which were not subject to the low temperatures, differing materials could have been used, provided they could have been joined satisfactorily for vacuum operation.

The radiation shields were made of copper, for the reasons mentioned earlier, yet they were at liquid nitrogen temperature. This appears to contradict the above statement as they were joined to stainless steel which has different thermal contraction properties to those of copper. However, the joint did not have to be mechanically strong, as the shield did not have a pressure difference across it and the dimensions did not result in significant differential expansions; hence the joining of these dissimilar materials was possible. The join needed to be a good thermal contact so that effective heat transfer from the shield to the liquid nitrogen could occur. The effectiveness of the thermal contact would be unaffected by small differential movements as it was a screw and not a welded joint.

The cryostats were dismantable, or in the final cryostat design, semi-dismantable for two reasons:
  (a) If leaks occurred, it was not a difficult task to locate and repair them.
  (b) Easy access to the superconducting coils was available for inspection and replacement purposes.

The requirement of dismantable cryostats necessitated the design of seals which could be dismantled and readily reassembled.

This preliminary discussion indicates the reasons for the complexity of a cryostat and the reasons for the choice of stainless steel as the main construction material.

It was envisaged that most of the difficulties involved in the construction and operation of the test machine would be with the cryostats; hence their design requirements took priority over other factors. The diameters of the armature and the compensating windings were selected after the dimensions of the cryostats were determined.

5-3-2 Dimensions of the Cryostat and Field Coil

Because of the lack of experience in the construction and behaviour of superconducting coils, it was decided initially to make smaller coils than would be required to produce the maximum flux density which could be achieved in the test machine. Allowing for some failures of coils, adopting this approach gave the required experience at minimum cost.

The possible causes of coil failure are:
(a) failure of the coil potting materials which could allow
     movement of the coil conductors - for example, cracking
     of the material when subjected to liquid helium temperatures;
(b) incomplete coil penetration of the potting material;
(c) operation of the conductor outside its critical parameters.

Any one of these points could lead to the loss of the superconducting property of the wire (quenching) and consequent possible damage to the coils.

The field coil shape chosen required approximately eighty metres of wire. With 400 turns in each field coil and 300 amps excitation current, the field pole m.m.f.'s were 120,000 ampere-turns, which was considered ample for initial work with the test machine.

The dimensions of the field coils were:

Inside diameter   = 51mm

Outside diameter   = 78mm

```
Coil length              = 38mm
Number of layers         = 11
Number of turns per layer = 36
```

The size of the inner container of the cryostat was determined by
the dimensions of the coil and, as with the other sections, the avail-
ability of "off-the-shelf" stainless steel tubing. The inner container
was also made larger than required for the initial field coil so that
larger coils could be fitted as experience was gained with the test
machine.

The dimensions of the outer container were chosen so that clearance
was provided between the inner and outer containers for the copper
radiation shield and for ease of construction. The spacing between
components was sufficient so that movement of sections with respect to
each other as a result of thermal contraction should not form thermal
short circuits and failure of the insulation.

The chimney section served three purposes:

(a) to reduce the thermal heat conduction via the inner stainless
     steel tube to the helium;

(b) to give an effective transition path from room temperature
     to the liquid helium for the current supply leads and to help
     minimize the heat inleak via the leads;

(c) to form the liquid nitrogen vessel for radiation shield
     coolant.

The length of the chimney was chosen from examination of the length
of frost deposits on a copper conductor which had one extremity immersed
in liquid nitrogen and which was approximately the size envisaged for
the current leads. The bar was not cooled with the nitrogen boil-off
gases. In fact, the boil-off gases were separated from the bar. The
length of the frosted section gave what might be called the natural

transition length and was therefore considered to be a guide to a minimum chimney length. The length selected was approximately twice this value as the calculated diameter of the optimum current leads of length 650mm was considered to be a convenient and realistic value (see Chapter 6).

The diameter of the inner pipe had to be large enough to accommodate the two copper current leads: the helium transfer tube, the leads for the temperature monitoring resistor, and to allow for flow of the boil-off gases. It had to be small enough so that there would be adequate space for the nitrogen vessel inside the outer 50.8mm (2") diameter pipe. The diameter of the outer pipe was chosen as 50.8mm because this was the largest manufactured tubing available which suited the cryostat. The diameters of the tubing for the nitrogen vessel were chosen to give adequate clearance between sections as well as allow for a sufficient capacity of liquid nitrogen coolant. The major dimensions are indicated in figure 5-1.

5-3-3 Cryostat Development and Construction

The first cryostat for the heteropolar machine was designed so that it could be easily dismantled as it was envisaged problems in making vacuum-tight joints would be encountered and subsequent re-jointing would be necessary, see figure 5-1. Thin walled stainless steel tubing was used to minimise liquid helium loss during initial cooldown and to minimise heat inleaks during operation. This cryostat indicated a number of construction difficulties and deficiencies in the demountable seals as discussed below.

The major difficulty was the welding of the stainless steel sections to ensure that they were vacuum tight. The difficulty was aggravated by the fact that the wall thickness of tubing to be joined onto bottom plates was only 0.2mm. Where thin sections were to be welded to thicker

sections, the latter were prepared, as shown in figure 5-1. The first cryostat was sent to a local firm to be argon arc welded, but it proved to be a failure because of lack of knowledge on the part of the firm. However, parts of the weld which were satisfactory indicated that a properly applied argon arc weld would be successful. Attempts by a second firm to weld the cryostats also proved unsatisfactory. In this case electric rod welding using flux-coated rods was used even though instructions issued to the firm were for an argon arc weld. Further inquiries indicated that satisfactory welding of the cryostats could not be done by local firms. It was thus decided that welding techniques would have to be developed within the Department of Electrical Engineering. An attempt was made to make the rod-welded cryostat cans vacuum tight. To patch the cans required a form of silver solder as more suitable alternatives were not available to the workshop. As it was desirable not to heat the cans excessively - as this would cause buckling of the machined surfaces - a low melting point silver solder, which could be made to flow by using an electric hot plate, was thought to be ideal. This proved not to be the case. The solder flowed well in some places but would not wet the stainless steel in other places, even though special care was taken in cleaning the stainless steel and not over-heating the flux.

The solder was removed as efficiently as possible and normal silver solder was used. This no longer avoided over-heating but sealed the leaks. The sealing of the leaks proved very tedious and took many hours of labour. As soon as the can appeared sealed, another flux intrusion from the initial arc weld leaked.

As this process was not giving the desired result and since the appearance of the cryostat gave the impression of a bad job, it was decided to construct new cans and to silver solder the sections together. At this stage, it was thought that argon arc welding would give the best

results but the equipment for such a weld was not available. The silver soldered cryostat proved that silver solder would seal the cans if care was taken, but construction was not easy as the process was not clean and buckling of thin sections occurred.

With the glass vacuum pump available, this system attained a vacuum of 10^{-3} torr at room temperature after five hours pumping. This appeared to suggest a substantial leak in the system, but it should be noted that the pump was very slow and took around six hours to pump itself out to $5 * 10^{-5}$ torr.

Tests under semi-operational conditions, using liquid nitrogen, indicated that the positioning of the chimney upper "O" ring seals, and the helium chamber threaded seal, which used teflon tape as the sealant, were unsatisfactory.

When the cryostat was being filled with liquid nitrogen, the top "O" ring seals failed because they froze. The "O" rings were replaced with extruded indium wire; but the inner top chimney seals proved to be unreliable and difficult to make because the indium did not remain in position during the making of the seal.

The outer threaded seal appeared to work well, but during the tightening process, the "O" ring experienced shear forces between the stationary and rotating sections of the seal which could have eventually caused failure of the seal. A successful point was that the indium seals proved to work well and hence these were included in future designs.

The second design (figure 5-2) eliminated all but one of the dismantable "O" ring seals and was designed to have silver solder joints.

The cryostat was still dismantable but the important change was that the chimney section and the inner can were all permanently joined as one piece by soldering the sections together. This change required only the

one outer "O" ring seal as indicated in figure 5-2. This "O" ring seal relied on clamping rather than a threaded tightening technique. The materials used for construction were the same as the previous design.

Because of the troubles experienced with soldered joints and the knowledge that argon arc welding produced superior joints, the possibility of purchasing an argon arc welder was investigated. It was found that our budget allowed the purchase of a suitable welder. This completely changed the thinking on the design of the cryostats and combined with the experience gained with the previous designs a third design, as shown in figure 5-3, was produced. Instead of using thin-walled tubing and welding on bases to form the containers, stainless steel surgical bandage holders of suitable dimensions were used. However, these were of heavier gauge metal than the tubing, hence incurring increased cooldown loss of liquid helium but eased welding and reduced construction problems.

The final design (figure 5-3) was only semi-dismantable because of the problems experienced previously with dismantable joints. In fact, to dismantle the cryostats it was necessary for welds to be ground away. This was allowed for in the design so that if necessary, dismantling was not difficult; hence the fluting of the chimney tubing and the format of the lower chimney weld as indicated. The indium seals were retained so access to the superconducting coil was available without grinding any of the welds. The cryostats were entirely argon arc welded, thus avoiding the use of silver solder and possible problems with flux inclusions.

A variable speed, slowly rotating, welding turntable was built to ensure the uniformity of the welding procedure. With the turntable, circular welds were done in one operation. This avoided undesirable stopping and starting during a weld. It was also found necessary to clamp copper heat sinks to the material to be welded to prevent excessive differential expansions.

The argon arc process proved to be successful and had the following advantages over other welding techniques:

(a) The weld was clean in that it avoided the use of flux.

(b) Welds that are found to leak can be easily re-done without any detrimental effects.

The fluting of the stainless steel tubing was achieved by rotating the tubes in a lathe and, whilst heating to a cherry red, forming the tubes to a desired shape. In the case of the larger diameter tubes, a pre-shaped flaring tool was used. Special care was taken to ensure that the tubing did not get too hot or heated too far along the tube, thus preventing possible wrinkling or fracturing of the tube. With the smaller tube, the diameter of which had to be reduced, a tool constructed from a roller bearing was allowed to roll on the outer surface of the cherry red, rotating tube and by increasing the pressure on the bearing, the tubing was forced into the shape of a brass former which was inserted inside the tubing. The tool was gradually worked along the heated section of the tubing repeatedly until the tubing contoured around the brass former.

5-3-4 Cryostat Safety

The possibility of the cryostat containers rupturing due to excessive pressure within the helium chamber had to be considered to prevent possible personal injury. Causes of excessive pressure within the cryostat were:

(a) blockage of the boil-off gas escape path; for example, by solidified air or solidification of the nitrogen used to pre-cool the cryostats;

(b) extreme heat inleak or sudden dumping of energy, from a coil quench, into the liquid helium which could cause rapid liquid boil-off.

Possible blockages of the gas escape path were prevented by ensuring that atmospheric gases were prevented from entering the cryostat by the escaping helium gases and that all of the liquid nitrogen used in the initial cooldown of the coil container to 77K was removed before the transfer of liquid helium commenced.

The most likely cause of excessive pressure within the cryostat was considered to be the resistive losses within the coil as a consequence of the coil undergoing a quench. The worst case under these conditions occurs when all of the losses are dissipated into the liquid helium and when little helium can escape as a result of the current leads restricting the escape path.

The resistance of the coil after a quench would be less than 0.01Ω and hence the power loss within the coil at 300 amps would be less than 900 watts. If the current was cleared after three seconds, the resulting pressure for an initial charge of 600ml of liquid helium would be as determined by the following.

Total energy dissipated in the helium = 2700 Joule

As no helium escapes from the cryostat, the increase in enthalpy:

$$\Delta H \: = \: \frac{2700}{600 * 0.125} \text{ Joules per gram}$$

$$= \: 36 \text{ Joules per gram.}$$

The enthalpy-entropy diagram for helium gave the resultant pressure as $2.5 * 10^6 \text{N/m}^2$.

The hoop stress on the wall of the inner container at $2.5 * 10^6 \text{N/m}^2$ internal pressure is given by:

$$\frac{\text{radius * pressure}}{\text{wall thickness}} \: = \: \frac{0.13 * 2.5 * 10^6}{0.9 * 10^{-3}} \text{ N/m}^2$$

$$= \: 3.6 * 10^8 \text{N/m}^2$$

The yield stress of stainless steel at 4.2K is greater than $6 * 10^8 N/m^2$ (references 5-2, 5-3, 5-4).

The stainless steel screws used to bolt the container lid into position were tested at room temperature and failed at a load of 4200N. The load on each screw at an internal pressure of $2.5 * 10^6 N/m^2$ would be 3750 Newtons. This was considered to be sufficiently below the thread failure load at a temperature of 4.2K. The extension of the screws under a load of 3750 Newtons would result in the venting of helium into the cryostat vacuum space. In the event of this happening, the blow-off valve fitted to the outer chimney would operate, thus preventing rupture of the cryostat. The blow-off valve design used is shown in figure 5-4.

To conclude: the previous results indicated that the cryostats for the initial machine were safe in that they should not rupture even under the worst conditions considered above.

5-3-5 Superconducting Coil

The wire selected for the superconducting field coils was the Imperial Metal Industries (Kynoch) Limited 1mm diameter NIOMAX FM C361 Niobium-Titanium, multifilamentary wire. This wire has a critical temperature of 9.5K and its critical flux density at 4.2K was considered more than adequate for the application under investigation.

The length of wire required for the field coil was such that no superconductor-to-superconductor joints were required as 100 metre lengths of wire were available from the suppliers. Stainless steel formers lined with fibreglass mat were used for coil support during the winding process and they were also used for positioning the coil within the cryostat.

The material used for potting the coil was CIBA-GEIGY araldite. The reactants used in the araldite and the proportions of each are listed below:

FIG 5-4
SAFETY VALVE

"o" ring

41 mm

20 mm

10 mm

75 mm
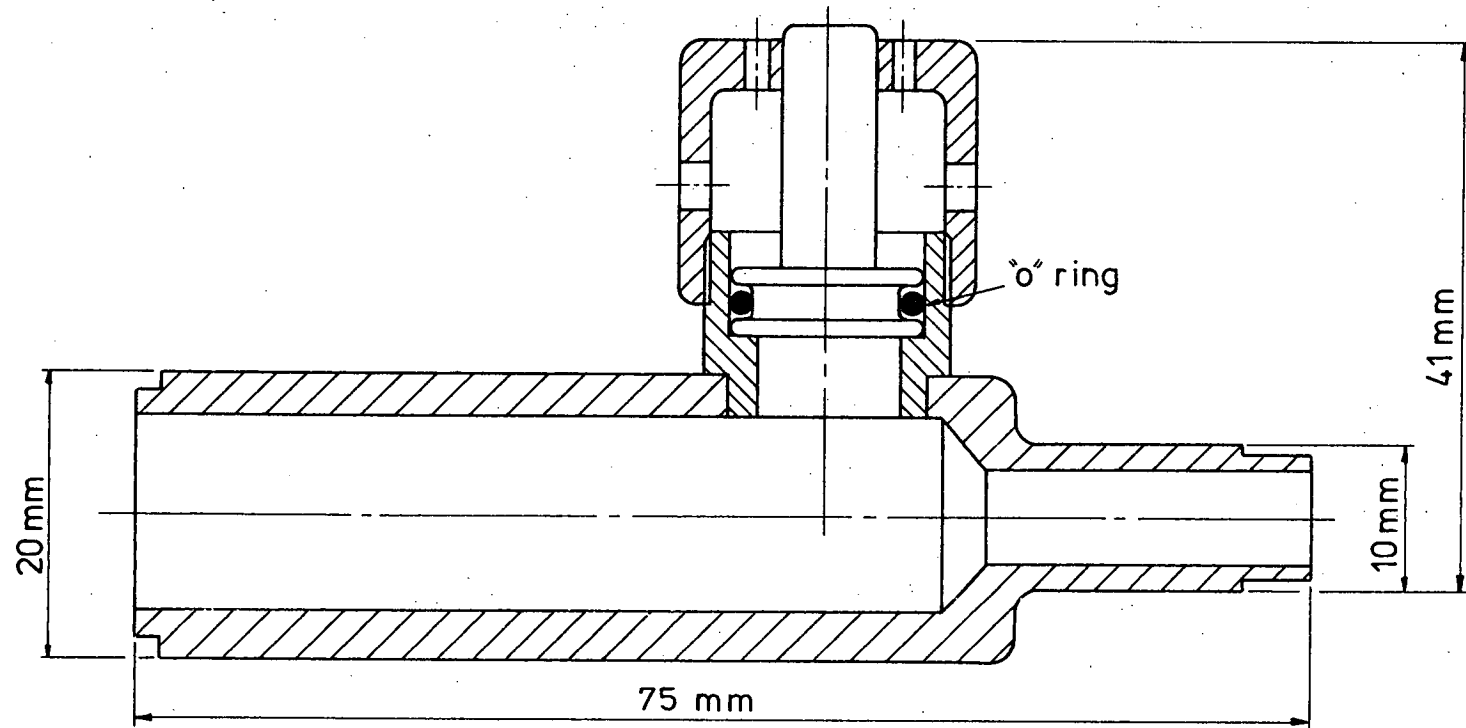
HARDNER   HY 906   80 parts by weight

EPOXY   MY 740   100 parts by weight

ACCELERATOR DYO 62   0.5 parts by weight

The reactants were thoroughly mixed and then the coil whilst immersed in the reactant mixture was heated to 60°C for two or three hours. Curing was achieved by heating the coil, after removal from the reactants, to 100°C for ten hours.

A trial coil, wound with a varnish insulated copper wire of the same diameter as the superconducting wire, when put through the preceeding potting process, showed good penetration of the araldite. As this procedure proved adequate, elaborate coil potting techniques involving araldite impregnation under vacuum were not used. Complete penetration of the potting material was of prime importance so that flux jumping due to wire movement was reduced to a minimum.

An important consideration in a large superconducting coil is the amount of energy stored in the magnetic field of the coil and how best to dissipate this energy safely and to prevent the conductor overheating and melting in the event of the coil quenching. This was not considered to be a problem with the test machine as the inductance of the coil was only 8.2mH. With a current of 300 amperes, the stored energy was only 360 joules (negligible when compared with the 2700 joules considered in section 5-3-4). If all this energy were suddenly dissipated within the coil, the temperature rise would result in a final temperature of less than 40K, hence overheating of the coil should not occur. It is of interest to note that to raise the temperature of 100 metres of the superconductor used from 4.2K to 77K requires approximately 3200 joules of energy.

Two alternative techniques for connecting the superconductor to the copper supply leads were considered to provide a suitable transition

from superconduction to resistive conduction:

(a) To spiral the superconductor around the copper current leads
and solder into position - figure 5-5.

(b) To drill a hole deep into the length of the copper lead and
solder the superconductor into the hole - figure 5-6.

The first alternative has better heat transfer between the super-
conductor and the coolant because of the intimate contact, while the
second alternative requires no more space than that taken by the leads
themselves.

The first alternative was adopted as the diameter of the leads was
too small to allow the drilling of the required size hole to an adequate
depth and because of the superior conductor cooling.

5-4 Armature and Compensating Windings

The current ratings of the armature (and hence the compensating
winding) had to be sufficiently high so that the effects of armature
reaction on the field coils, the necessity or otherwise of a compensating
winding, and problems associated with commutation could be investigated.

5-4-1 Armature

Superconducting field windings enable the use of non-magnetic and
non-electrically-conducting construction materials in the magnetic circuit
of armatures of machines. These eliminate the necessity for iron armature
teeth. The winding of armature coils directly onto the surface of a
cylindrical former results in higher specific electric loadings and would
also result in better armature reaction cancellation (by means of a
similarly wound compensating winding) because slot ripple in the flux
distributions would be eliminated. Disadvantages of this design included
the difficulty in supporting the armature coils during assembly of the

SUPERCONDUCTION TO RESISTIVE CONDUCTION TRANSITION CONNECTIONS

copper lead

40 mm

40 mm

1mm diameter superconductor
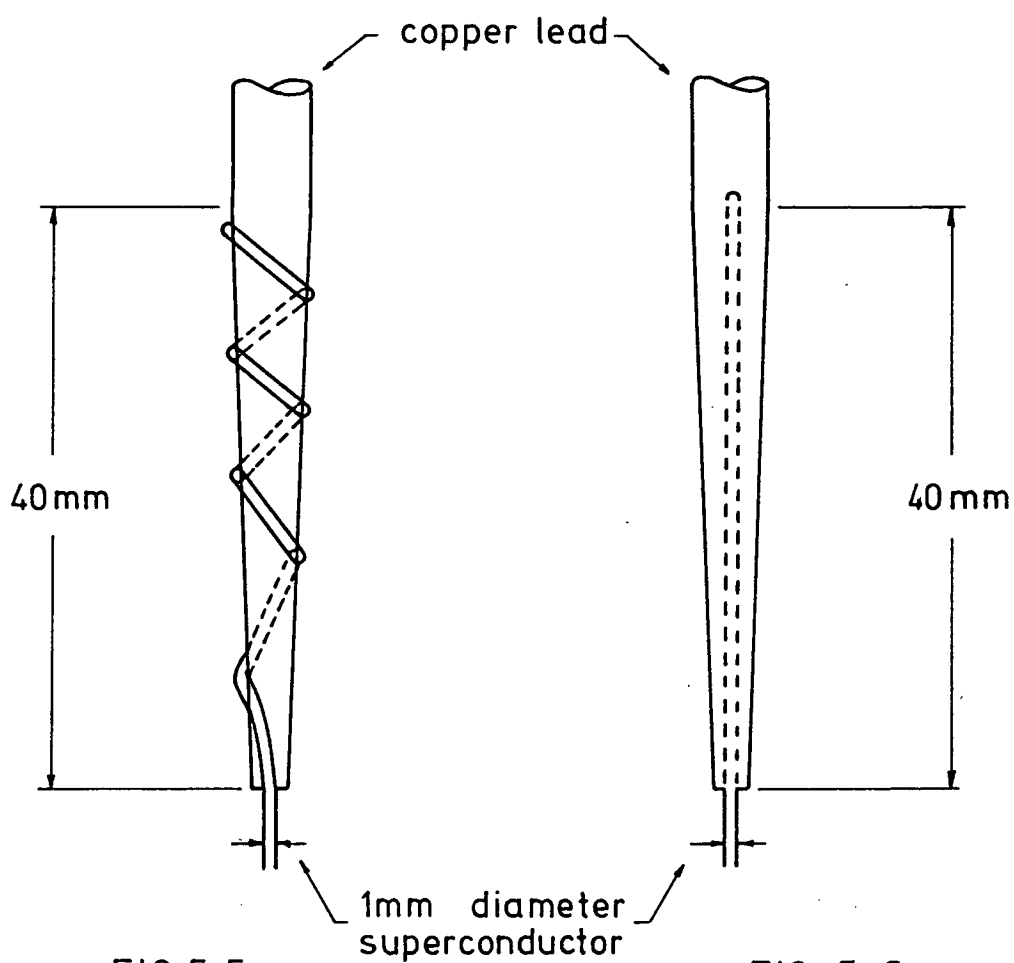
FIG 5-5
Spiral Transition

FIG 5-6
Internal Transition

armature and in large machines an increased difficulty in providing adequate support for the coils against loading torques.

Because of the intricacy associated with the construction of a small slotless armature, a slotted former made from varnished hardwood was used to wind the armature of the initial machine. The ratio of slot width to tooth width was three to one or greater than that possible in conventional machines. The number of slots selected was thirty-one to suit the available thirty-one segment commutator. The inner diameter of the wooden former was machined out so that interchangeable armature cores of iron or wood could be machined to fit. This feature enabled different configurations of the machine to be investigated. Figure 5-7 shows an exploded diagram of the armature. To ensure the correct method of assembly of the armature structure, locating pins were used.

The design of the cryostats took priority and the remaining machine components were designed to maximise the specific electric loading of the armature surface. The aim was to allow the possibility of producing sufficient armature reaction fluxes so that their influence on the operation of the superconducting field coil could be investigated and extrapolated to the operation of a model of a prototype machine.

The selection of the wire size and the number of turns per armature coil necessitated a compromise between the current rating, voltage rating, and the space available, as determined by the armature slots, for the conductors. A continuous current rating of 6 amperes and a short time current rating of 10 amperes was chosen because D.C. supplies were available which could meet this demand. The wire size selected for the armature coils was $19\frac{1}{2}$ B & S which had a current carrying capacity of 3 amperes at a typical machine current density of near 420 amps/cm^2, thus giving the two pole machine a continuous current rating of 6 amperes.

FIG 5-7
WOOD FRAMED ARMATURE

125 mm

Locating holes

Interchangeable wood & MS core 76 mm d × 125 mm long

Locating holes

Commutator

120mm

25 mm

Armature winding slots

Armature:
31 coils 20 turns per coil
$19\frac{1}{2}$ B & S
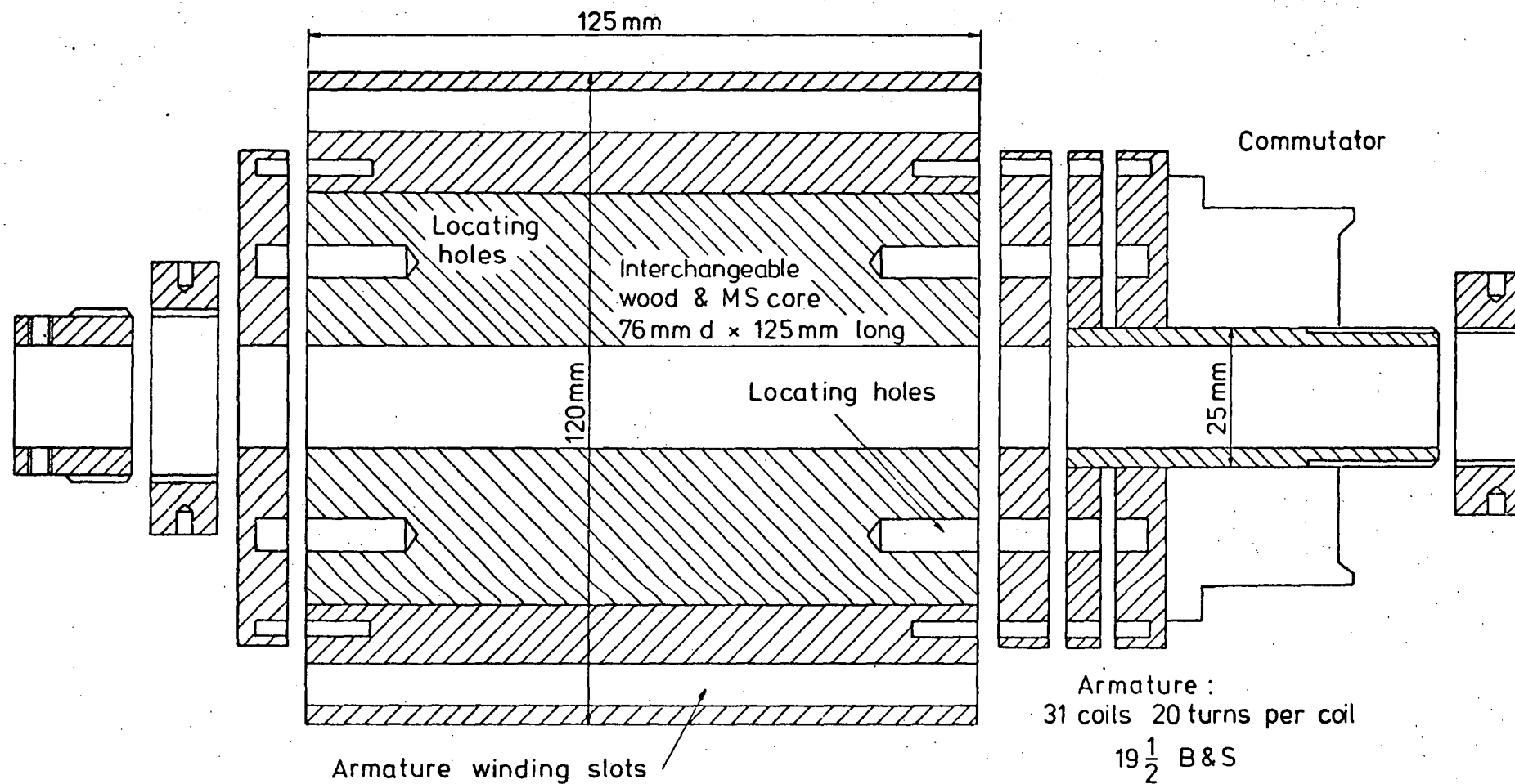
For the initial machine the spaces allowed for both the armature and compensating windings and the removable iron armature core were proportioned so that the maximum number of armature turns per coil could be reasonably accommodated. This resulted in twenty turns per coil using $19\frac{1}{2}$ B & S wire. The armature resistance was calculated at 3.1 ohms at 20°C.

5-4-2 <u>Estimated Flux In and Armature Voltage Of the Initial Machine</u>

Even though the model was not intended for obtaining magnitudes of pole fluxes, a check of the voltage of the initial machine was obtained by first estimating its flux per field pole. The flux per field pole of the initial machine was estimated from the flux plots obtained from the model by using appropriate scaling factors as determined below.

Neglecting any possible effects of saturation in the iron sections the total flux is directly proportional to the field current times the number of turns in the field coil. From this, if the ratio of the machine's dimensions to the model dimensions is l_1/l_2 and the field currents I_{F1}/I_{F2}, then the flux density ratio B_1/B_2 and flux per pole ratio Φ_1/Φ_2 are:

$$\frac{B_1}{B_2} = \frac{I_{F1}}{I_{F2}} \frac{n_1}{n_2} \frac{l_2}{l_1} \qquad \qquad \dots 5\text{-}1$$

$$\frac{\Phi_1}{\Phi_2} = \frac{I_{F1}}{I_{F2}} \frac{n_1}{n_2} \frac{l_1}{l_2} \qquad \qquad \dots 5\text{-}2$$

This only applies if the model is an exact replica of the machine and as this was not the case between the model used and the initial machine, the previous results were used only as a rough guide.

With $\dfrac{n_1}{n_2} = \dfrac{400}{114}$ and $\dfrac{l_1}{l_2} = 2.5$

$$\frac{B_1}{B_2} = \frac{400}{114} * \frac{1}{2.5} \frac{I_{F1}}{* I_{F2}} = 1.4 \frac{I_{F1}}{I_{F2}} \qquad \ldots 5\text{-}3$$

$$\frac{\Phi_1}{\Phi_2} = \frac{400}{114} * 2.5 \frac{I_{F1}}{I_{F2}} = 8.7 \frac{I_{F1}}{I_{F2}} \qquad \ldots 5\text{-}4$$

The E.M.F. equation for a direct current heteropolar machine is:

$$E = \frac{2p}{a} Z_a \Phi_p N_s \quad \text{volts}$$

where E = E.M.F.

p = number of pairs of field poles

Z_a = number of armature conductors

Φ_p = flux per pole in Weber

N_s = speed in revolutions per second

a = number of parallel paths in the armature winding

  = 2 for a wave winding

  = 2p for a lap winding

The number of armature conductors was determined from the consider-
ations given in the previous section. The field pole flux of the initial
machine depended on the configuration adopted but the relationship
between the field fluxes of the model and the initial machine, as
determined previously, is applicable for all configurations. Hence:

$$\frac{\Phi_1}{\Phi_2} = 8.7 \frac{I_{F1}}{I_{F2}} \quad \text{for all configurations} \qquad \ldots 5\text{-}4$$

Values of Φ_2 and I_{F2} were obtained from Table 4-1 whilst at the stage
of designing the machine I_{F1} was assumed to be near 300 amperes. The
flux per pole, as determined from equation 5-4, for the different machine

configurations is given in Table 5-1. A comparison between the estimated
values and the observed values is given in Chapter 8.

Table 5-1

Predicted Pole Fluxes

	IRON INCLUDED IN THE MACHINE			
	YOKE, CORE and POLE FACES	YOKE and CORE	YOKE and POLE FACES	YOKE
Φ_p milliweber	7.2	5.2	3.3	2.9
E.M.F. volts	220	160	102	90

The first tests on the initial machine were conducted with the iron
yoke, armature core and the pole faces positioned. The approximated
generated voltage of 220 volts (Table 5-1) indicated a continuous rating
of 1.1kW and a short time rating of 1.7kW. The rating with just the
iron yoke would have been about forty percent of the above values. Low
ratings at this stage were of little consequence as the armature reaction
depends on the armature current and not the rating of the machine.

5-4-3 Compensating Winding

The compensating winding was wound on a cylindrical wooden former of
the dimensions shown in figure 5-8. The former had 31 slots which
coincided with the 31 slots of the armature winding. The winding was the
same as the armature winding with 20 turns per coil of $19\frac{1}{2}$ B & S copper
wire. The winding was split into two halves; they could be series or
parallel connected. The series connection ensured equal currents in all
of the compensating winding conductors but resulted in a high resistance.

Current division in the parallel connection was not equal between the
two halves of the compensating winding because one half had 16 coils and

FIG 5-8
COMPENSATING WINDING

150mm
130mm
31 SLOTS

125 mm

FIG 5-9
FIELD POLE FACE

125 mm
75 mm
165mm
15 mm
60mm
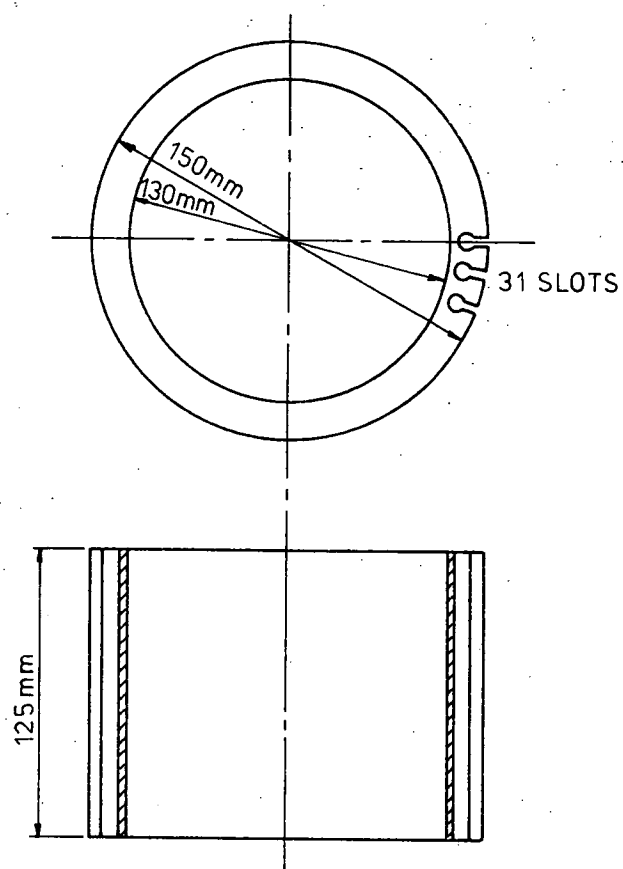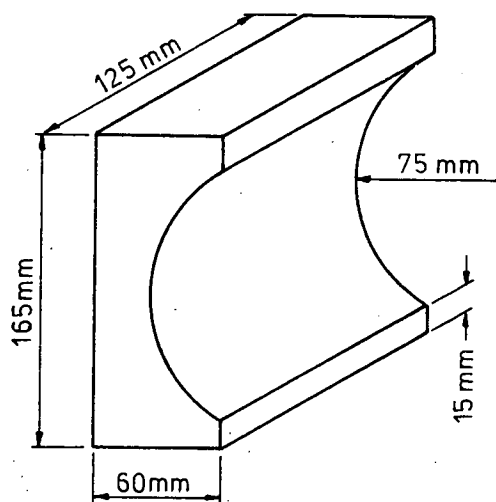
the other had 15 coils. This, however, did not affect the operation of the compensating winding because the number of ampere-conductors per slot was independent of how the current divided as all but one of the slots contained coil sides from each of the two halves of the winding. The slot with coil sides from the same half (16 coil half) had a net ampere-conductor value of zero and was positioned in the centre of one of the poles of the compensating winding.

The armature reaction cancellation tests of Chapter 4 indicated that, in some configurations, 60 to 70% of the armature conductor current (or 30 to 35% of the armature current) was required in the conductors of a similarly wound compensating winding. This result meant that the compensating winding could have been wound with only 30 to 35% of the number of armature coil turns (with a larger wire) for a series connected winding or 60 to 70% (with the same wire) for the parallel connected winding - both cases carrying the full armature current. If these designs were adopted, problems with obtaining the best cancellation for each of the machine configurations could result because of a lack of compensating winding m.m.f.

The design of the compensating winding selected was chosen because it was intended that a variable bypass resistor would shunt much of the armature current past the winding, giving the best possible flux cancellation for each of the machine configurations possible with regard to the quantity of iron retained.

The estimated resistance of the compensating winding and bypass resistor was obtained as follows:

(a) Series Connected

Resistance of winding $\simeq$ 4 * armature resistance. Assume that 35% of the armature current was required in the winding. Hence, the bypass resistance required was $\frac{35}{65}$ * 4 * armature resistance.

Therefore the total resistance $= \dfrac{4 * \frac{35}{65} * \text{armature resistance}}{4 \left(1 + \frac{35}{65}\right)}$

$= 1.4 * \text{armature resistance.}$

(b) Parallel Connected

Resistance of winding $\simeq$ armature resistance. Assume that 70% of

the armature current was required in the winding (or 35% in the

winding conductors). Hence the bypass resistance required was

$\frac{70}{30} * $ armature resistance.

Therefore resistance $= \dfrac{\frac{70}{30} * 1}{\frac{70}{30} + 1} * \text{armature resistance}$

$= 0.7 * \text{armature resistance.}$

These results indicate that the parallel connection was preferred

because of the lower resistance but it should be noted that the series

connected winding was capable of providing a greater cancellation

m.m.f. than the parallel connected winding if it was required. This

could best be determined from tests conducted on the test machine.

5-5 Field Pole Faces

The field pole faces were cast from iron, then machined to the

desired dimensions as shown in figure 5-9. Each field pole face was

positioned using three 0.75 inch diameter threaded brass rods, which

also acted as supports for the cryostats.

5-6 Conclusion

The design adopted resulted in a machine which would allow the

different possible configurations, with regard to the quantity of iron

retained, to be investigated. Figure 5-10 is a photograph of the

completed machine.
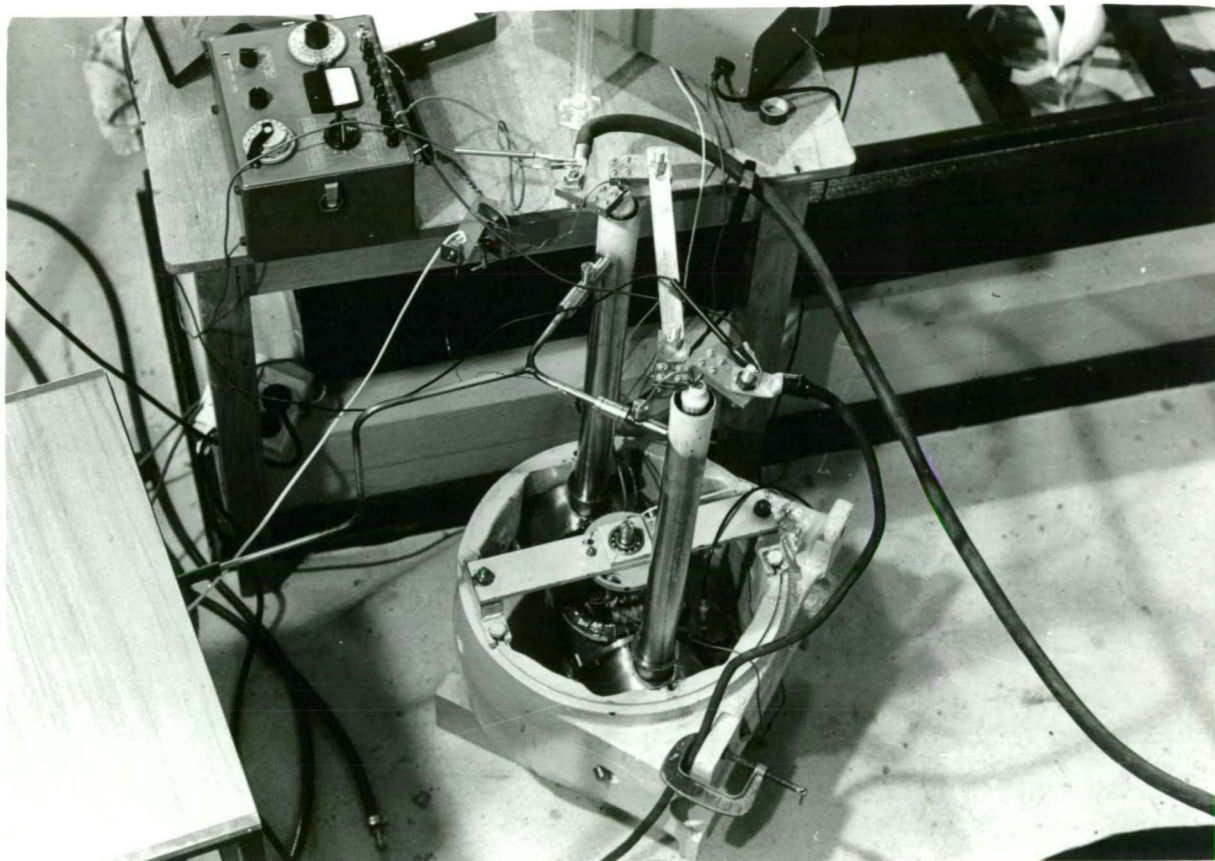
FIGURE 5-10

INITIAL MACHINE

CHAPTER 6.

CRYOGENIC CURRENT LEADS

6-1 Introduction

A major source of heat inleak into the liquid helium is via the leads which supply current to the superconducting coil. The lead heat inleak introduced by a set of uncooled leads carrying current to the superconducting field coil is shown to be unacceptable - section 6-7. For this reason it was essential, if the liquid helium loss is to be kept to a minimum, to optimize the design of the leads. The problem of optimizing the dimensions for the leads led to the conflicting requirements of large cross sectional area to minimise the electrical I^2R losses and small cross sectional area to minimise the heat conduction inleak. Another conflicting requirement was that, ideally, a material with a high electrical conductivity and low thermal conductivity should be used; however, high electrical conductivity generally implies a high thermal conductivity.

The heat required to raise liquid helium at one atmosphere pressure to a gas at normal temperature and pressure is approximately 1500 J/g or for a heat inleak to the liquid helium at the rate of 1 watt requires heat transfer to the resultant helium gas at the rate of 72 watts to raise the boil off gases to room temperature. This indicates the effectiveness of using the boil off-gas to cool the leads and remove much of the heat inleak and the I^2R losses in the leads, and at the same time reducing the I^2R losses by reducing the lead temperature and so its resistance.

In this chapter two methods are examined by which the design of the leads with a minimum heat inleak can be obtained. Details of the lead design are provided as are the results of tests conducted to verify the

assumptions made in arriving at the optimum lead design and the design of the leads adopted.

To reduce or possibly eliminate heat inleak via current leads a superconducting switch was considered. A superconducting switch consists of a length of superconductor connected between the terminals of the super-conducting field coil. During energisation of the field coil the switch would be maintained at a temperature greater than the transition temperature by a small heater. At completion of energisation the heater is turned off and the switch becomes superconducting. The external supply to the field coil can be disconnected and the leads to the field coil can be removed from the cryostat. The field current continues to flow through the superconducting switch.

A superconducting switch was not used because of the difficulty with controlling the field current and, as the switch joins the terminals of the field coil, voltages induced into the field coils cannot be measured.

6-2   Optimization of the Leads

The problem of accurately describing the properties of gas cooled counterflow cryogenic current leads mathematically and solving the resultant equations is difficult because many of the parameters are variable functions of temperature.

A differential equation describing the system can be obtained if the following assumptions are made:

(a) There is perfect heat transfer between the boil-off gases and the leads; that is, the boil-off gases are at the same temperature as the leads.

(b) The boil-off gases are at a constant pressure of one atmosphere hence the rate of heat transfer required to raise the temperature of the boil-off gases is given by differences

in enthalpy.

(c) Thermal conductivity and electrical resistivity are
     related by the Wiedemann-Franz Law.

These assumptions are not strictly true but give a basis for estimat-
ing the heat inleak. Experimental testing of lead designs determined
the error introduced by the assumptions, section 6-9.

FIG 6-1
CRYOGENIC CURRENT LEADS
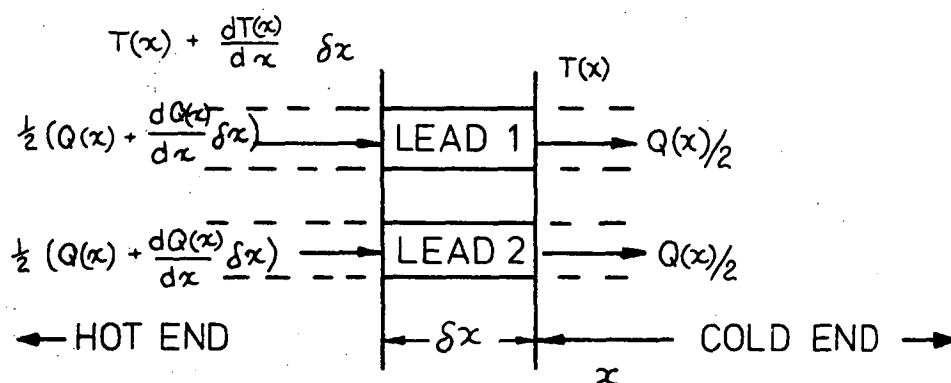
6-2-1 Differential Equation

Variables:

x   = distance from liquid helium to point being considered on the
        lead   cm

T(x) = temperature profile on the leads in K

A(x) = cross sectional area of lead conductor cm^2

Q(x) = rate of heat conduction down the leads   watts

h(T) = enthalpy of the boil-off gases at temperature T   J/gm

K(T) = thermal conductivity of the lead material $watt\text{-}cm\text{-}K^{-1}$

ρ(T) = electrical resistivity of the lead material   ohm-cm

C_p(T) = specific heat at constant pressure of the gases $J\text{-}gm^{-1}\text{-}K^{-1}$

T_o = helium temperature K

Q_L = lead heat inleak to the liquid helium watts

Q_a = ambient heat inleak without leads watts

C_L = latent heat of vaporization of liquid helium Joule-gm^{-1}

n = total boil-off rate of liquid helium gm-sec^{-1}

Q_o = total heat inleak to the liquid helium watts

ℓ = lead length cm

I = electrical current in the leads ampere.

Consider the case of two conductors which are required to supply the current to the superconductor. From figure 6-1 have:

$$Q(x) = 2 * K[T(x)] * A(x) * \frac{dT(x)}{dx} \qquad (6-1)$$

In the steady state the net rate of heat generation and transfer into and out of an element of the leads must be zero, hence:

$$Q(x) = Q(x) + \frac{dQ(x)}{dx} * \delta x + 2I^2 \frac{\rho[T(x)]}{A(x)} * \delta x - n \frac{d\,h(T)}{dT} * \frac{d\,T(x)}{dT} \delta x$$

$$\therefore \frac{d\,Q(x)}{dx} + 2I^2 \frac{\rho[T(x)]}{dx} - n\,C_p \frac{d\,T(x)}{dx} = 0 \qquad (6-2)$$

Where $C_p = \frac{d\,h(T)}{dT}$

substitute 6-1 into 6-2 have:

$$\frac{d}{dx}\left(2A(x) * K[T(x)] \frac{dT(x)}{dx}\right) + 2I^2 \frac{\rho[T(x)]}{A(x)} - n\,C_p \frac{dT(x)}{dx} = 0 \qquad (6-3)$$

The Boundary Conditions are:

at $x = 0$ $T = T_o$

and $\frac{dT}{dx} = Q_o/[2A(0) * K(T_o)]$

where $Q_o = C_L\,n - Q_a$ 　　　　　　　　　　　　　　　(6-4)

6-2-2 Solution to the Differential Equation

Equation 6-3 is in general difficult to solve formally but by assuming

a constant value for C_p and that the lead material obeys the Wiedemann-Franz Law it can be reduced to a simple harmonic oscillator equation by substitution from J.P. Scott - reference 6-1. See also references 6-2 to 6-9.

$$\text{Let} \quad \frac{dZ}{dx} = \frac{n \, C_p}{2A(x) \, K[T(x)]} \tag{6-5}$$

at $x = 0$ $x = 0$

The Wiedemann-Franz Law gives

$$K(T) \, \rho \, (T) = T \, L$$

where L = Lorenz Number $(2.4 * 10^{-8} \, W \, \Omega \, K^{-2})$

The Equation thus obtained is:

$$\frac{d^2T}{dZ^2} - \frac{dT}{dZ} + \frac{4I^2L}{n^2C_p^2} T = 0 \tag{6-6}$$

The boundary conditions are:

at $z = 0$ $T = T_0$

and $\quad \dfrac{dT}{dZ} = \dfrac{C_L}{C_p} - \dfrac{Q_a}{n \, C_p} = B = \dfrac{C_L}{C_P} (1-N)$ $\tag{6-7}$

where N = fraction of total boil-off due to ambient heat inleak.

$$\text{With} \quad D = 4I^2 \, \frac{L}{n^2 C_p^2} \tag{6-8}$$

it follows that:

$$\frac{d^2T}{dZ^2} - \frac{dT}{dZ} + D \, T = 0 \tag{6-9}$$

The solutions to equation 6-9 are:

$$D > \tfrac{1}{4} \quad T(Z) = EXP(Z/2) * \{ T_0 \cos[(D-\tfrac{1}{4})^{\frac{1}{2}}Z] + \frac{B - T_0/2}{(D-\tfrac{1}{4})^{\frac{1}{2}}} \sin[(D-\tfrac{1}{4})^{\frac{1}{2}}Z] \} \tag{6-10}$$

$$D = \tfrac{1}{4} \quad T(Z) = T_0 + (B - T_0/2) * Z * EXP(Z/2) \tag{6-11}$$

$$D < \tfrac{1}{4} \quad T(Z) = \frac{EXP(Z/2)}{(1 - 4D)^{\frac{1}{2}}} [\alpha + \beta] \tag{6-12}$$

where

$$\alpha = \{\frac{T_o}{2} * [(1 - 4D)^{\frac{1}{2}} - 1] + B\} * EXP[(1 - 4D)^{\frac{1}{2}} * Z/2]$$

$$\beta = \{\frac{T_o}{2} * [(1 - 4D)^{\frac{1}{2}} + 1] - B\} * EXP[-(1 - 4D)^{\frac{1}{2}} * Z/2]$$

These solutions are plotted in figure 6-2 for various values of

$$4LI^2/n^2C_p^2 = D \quad \text{and} \quad Q_a = 0,$$

i.e. the gases cooling the leads are due to lead boil-off only with T_o = 4.2K and C_L/C_p = 3.9K. The curves show that the leads are optimized if $4LI^2/n^2C_p^2 \simeq 0.31 = D$ or $n/I = 1.01 * 10^{-4}$gm-sec^{-1}-amp^{-1} or the optimized heat inleak is 2.12mW per amp for the two conductors.

This minimum heat inleak is independent of the shape of the leads and can be obtained, for example, by tapered or constant diameter leads.

To actually determine optimum lead proportions firstly consider constant diameter leads, i.e. A(x) = constant.

It thus follows that:

$$\frac{dZ}{dx} = \frac{n \ C_p}{2A(x)K[T(x)]} \tag{6-5}$$

$$\therefore \quad K[T(Z)]dZ = \frac{n \ C_p}{2A(x)} \ dx$$

$$\therefore \quad \int_0^{Z_1} K[T(Z)] \ dZ = \frac{n \ C_p \ell}{2A} \tag{6-13}$$

where Z_1 is such that $T(Z_1)$ = 300K and ℓ = length of the leads.

The integral $\int K[T(Z)]dZ$ can be numerically evaluated provided K(T) is known. For the thermal conductivity of copper as given in Appendix E:

$$\int K[T(Z)]dZ \simeq 50 \ watt\text{-}K^{-1}\text{-}cm^{-1} \quad \text{at optimum lead design.}$$

$$\therefore \quad \frac{n \ C_p \ell}{2A} = 50 \ watt\text{-}K^{-1}\text{-}cm^{-1}$$

FIG 6-2
COUNTER-FLOW CRYOGENIC
LEAD z TEMPERATURE PROFILES
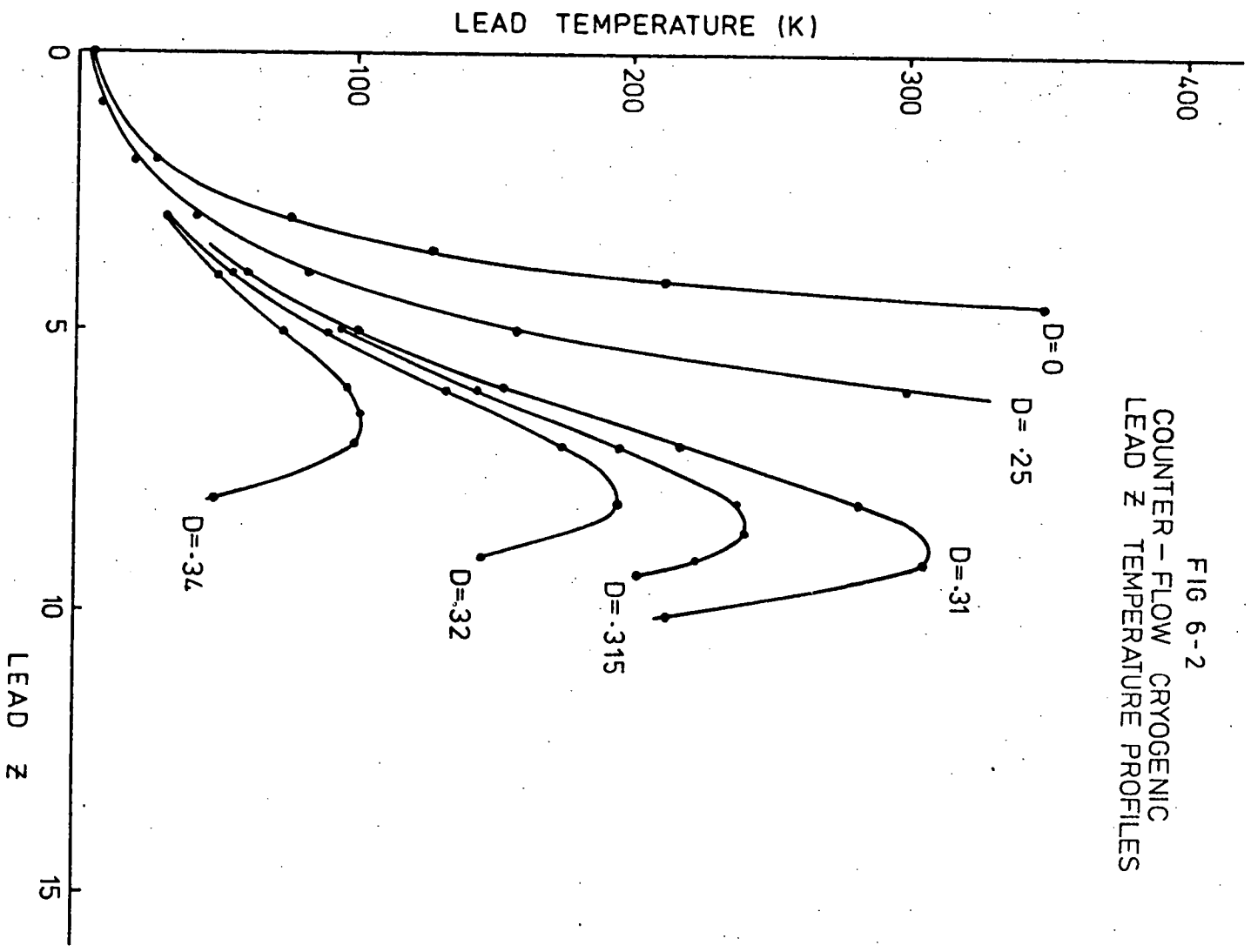
If I = 300 amps → n = 3.03 * 10^{-2} gm/sec.

$$\therefore \ \frac{\ell}{A} \ = \ \frac{100}{3.03*10^{-2}*5.4} \ = \ 6.11 \ cm^{-1}$$

If ℓ = 65cm, as selected in section 5-2-2, then A = 0.106cm^2 for optimum. The corresponding lead diameter was 0.368cm and Q_o equalled 0.636 watts at a current of 300 amperes. This was a reasonable cross-sectional area so that the length of 65cm was retained in the design.

6-3 Temperature Profile of the Optimized Lead

The lead temperature profile was calculated as follows to determine whether the assumption of perfect heat transfer to the boil-off gases was reasonable.

To calculate the temperature profile of the constant cross-sectional area, optimized lead requires the relationship:

$$\frac{dZ}{dx} \ = \ \frac{n \ C_p}{2A(x) \ K[T(x)]} \tag{6-5}$$

From the solution curves the data for T as a function of Z was available: thus, from thermal conductivity data the thermal conductivity of the lead material as a function of Z was determined - figure 6-3.

Equation 6-5 can be rewritten as an integral equation

$$x \ = \ \int_{Z=0}^{Z_T} \frac{2A(Z)}{n \ C_p} K[T(Z)] \ dZ \qquad \text{where temperature at Z = } Z_T \text{ is T K}$$

or $\quad x \ = \ \frac{2A}{n \ C_p} \int_{Z=0}^{Z_T} K[T(Z)] \ dZ \qquad$ if A(Z) and C_p are constants.

If A(Z) and C_p are constants then values of x can be calculated by numerical integration of $\int K[T(Z)] \ dZ$ from figure 6-3b.

The curve $\int K(Z)dZ \simeq Z$ is plotted in figure 6-3a. The resulting temperature profile of the optimized lead with no ambient heat inleak is

FIG 6-3a
INTEGRAL PROFILE
OPTIMIZED LEAD
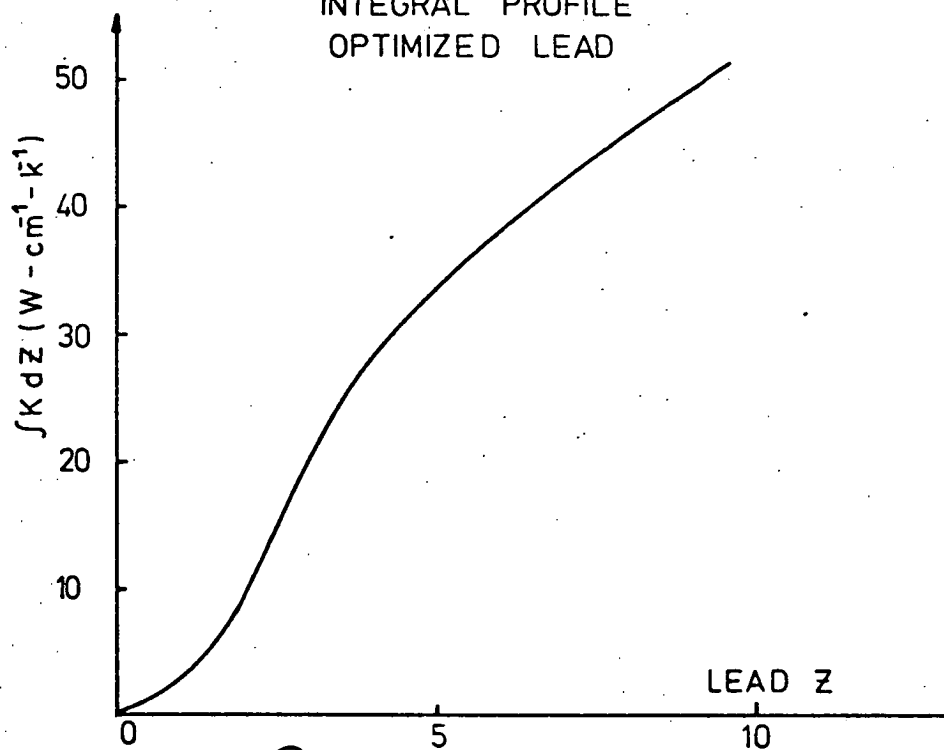
FIG 6-3b
THERMAL CONDUCTIVITY PROFILE
OF OPTIMIZED LEAD
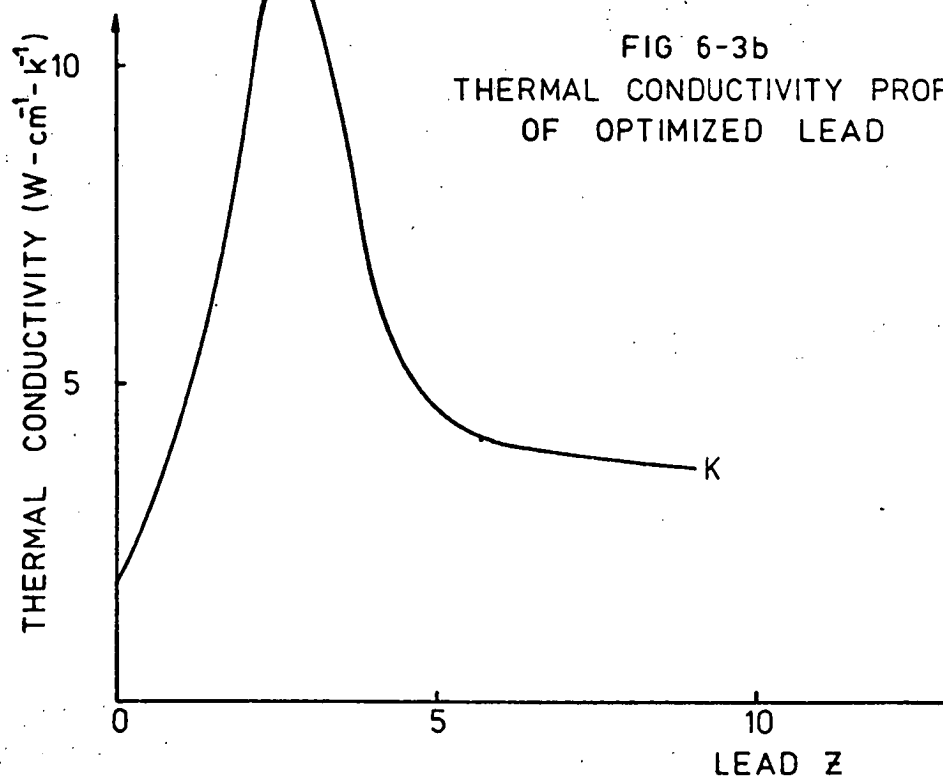
plotted in figure 6-4.

The predicted temperature gradient along the leads at the helium end was approximately 1 K/cm and at the room temperature end was 10 K/cm. With the small temperature gradients at the cold end and the fact that the speed of the boil-off gases would be low, heat transfer per unit volume of boil-off gas at the cold end should prove to be adequate. At the room temperature end of the leads the gas speed and temperature gradients were predicted to be higher; hence ideal heat transfer could be difficult but not impossible to obtain.

6-4 Effects of Ambient Heat Inleak on the Design of the Optimized Lead

The effect of ambient heat inleak would be to change the value of B in equation 6-7 which changes the Z temperature profiles for a given lead as indicated in figure 6-5. The resulting changes in the Z temperature profile also changes the lead design for optimum conditions.

With an increase in the ambient heat inleak-fraction the value of D for the optimum lead decreases as given in figure 6-6. These results were calculated using an iterative process by assuming a value of D and finding the value of N for optimum conditions.

From equation 6-8 $D = 4I^2L/n^2C_p^2$; hence, if D decreases then n must increase. This give a higher total inleak which equals $nC_L = Q_T$ (figure 6-7) and hence it is necessary to keep the ambient heat inleak as small as possible. Although the total heat inleak increases as ambient heat inleak Q_A increases, the heat inleak due to the leads themselves decreases, that is $(1-N)nC_L = Q_L$ decreases - figure 6-7.

This can be hypothetically explained by the fact that the greater the ambient heat inleaks other than via the leads to the liquid helium,

FIG 6-4
TEMPERATURE PROFILE OF OPTIMIZED
LEAD

$Q_A = 0$ $I = 300$ amp
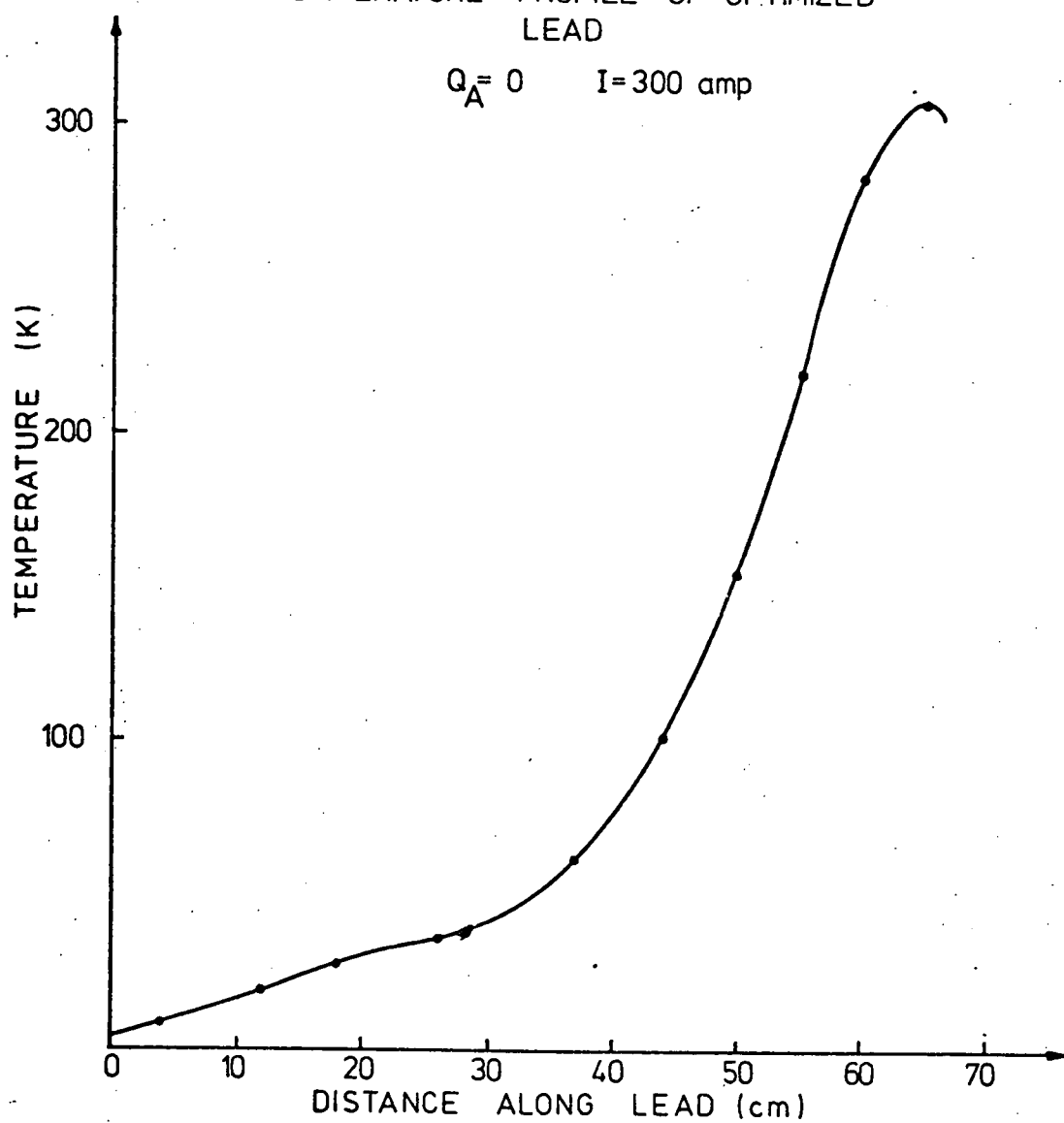
FIG 6-5
Ƶ   TEMPERATURE PROFILES
WITH AMBIENT HEAT INLEAKS
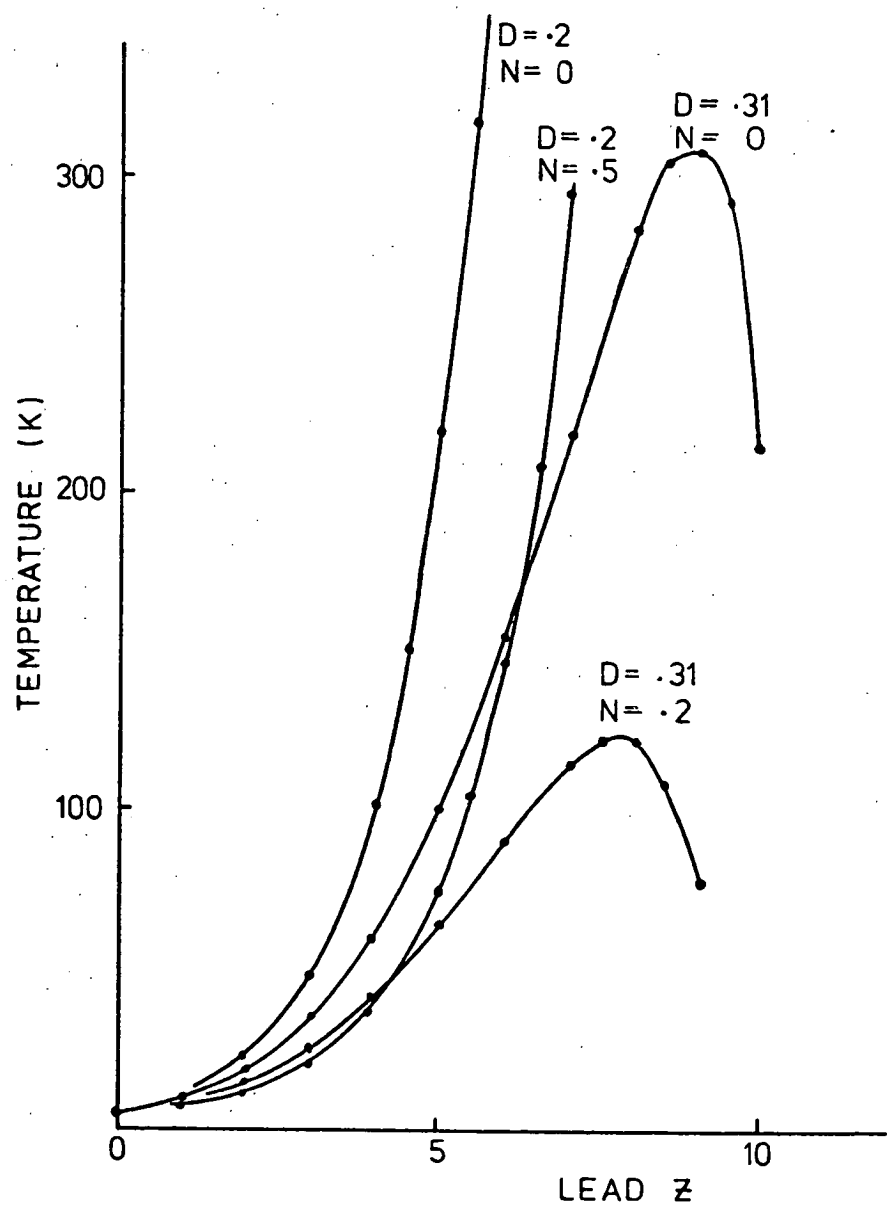
FIG 6-7
OPTIMUM MODIFIED HEAT INLEAKS
VERSUS AMBIENT HEAT INLEAK
FRACTION
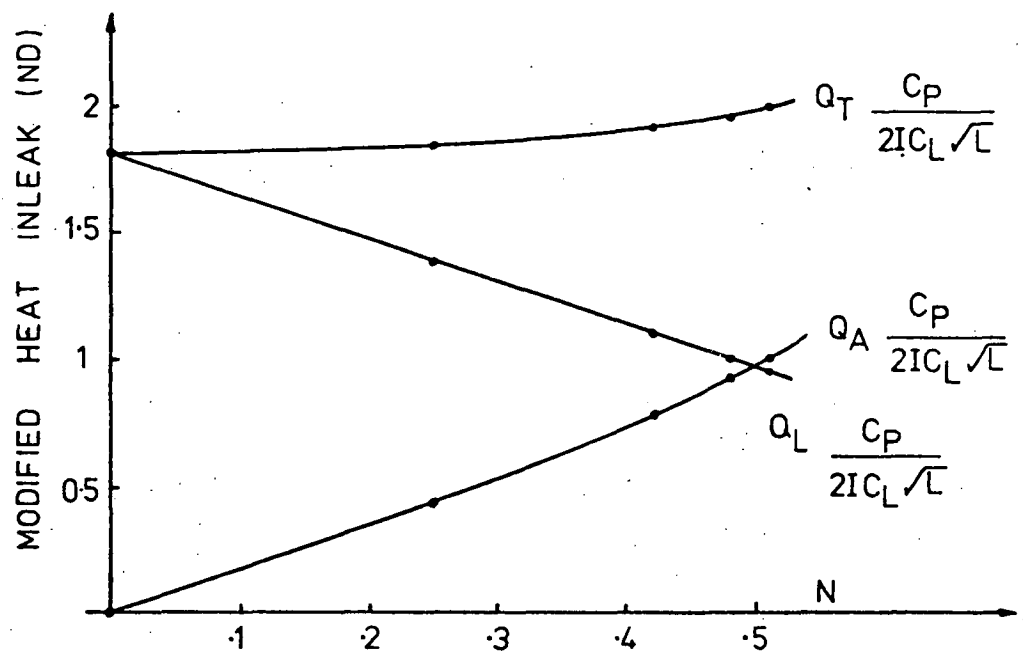
FIG 6-6
OPTIMUM 'D' FOR GIVEN 'N'
CRYOGENIC CURRENT LEADS

FRICTION OF HEAT INLEAK DUE TO AMBIENT
HEAT INLEAK
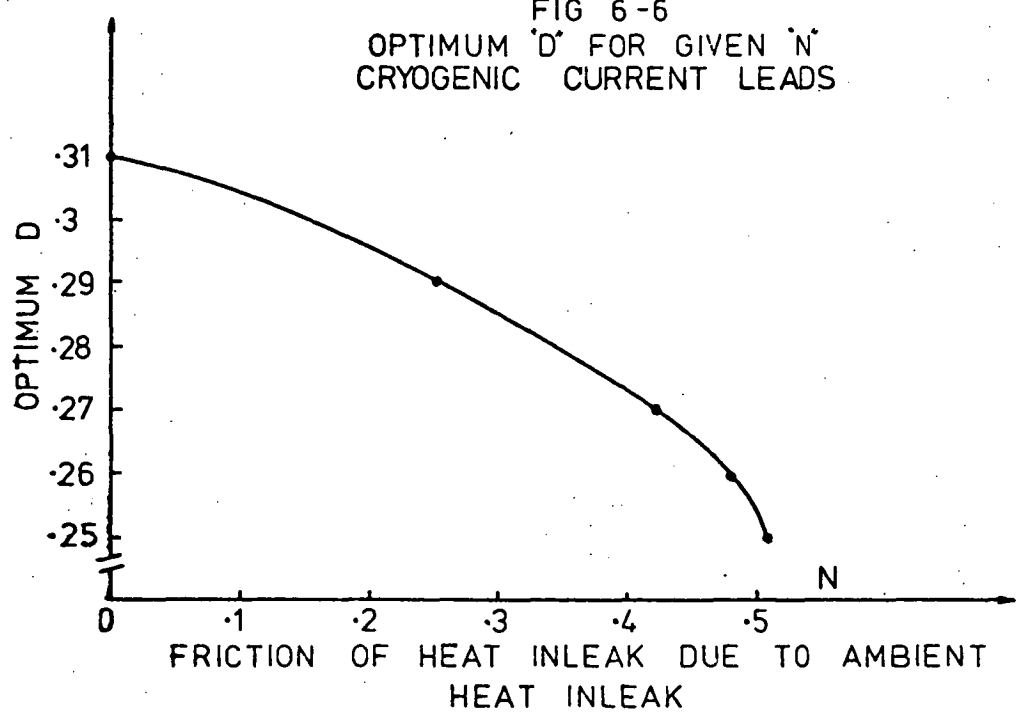
the greater the boil-off and thus more heat would be extracted from the leads by the helium gas to raise its temperature to room temperature; hence less heat inleak via the leads to the liquid helium. The non-dimensional quantities in figure 6-7

$$\frac{C_p Q_A}{2IC_L\sqrt{L}} \ , \quad \frac{C_p Q_L}{2IC_L\sqrt{L}} \ , \quad \frac{C_p Q_T}{2IC_L\sqrt{L}} \qquad \text{were evaluated from}$$

$$n = \frac{2I\sqrt{L}}{C_p\sqrt{D}} \quad \text{and} \quad Q_T = nC_L, \quad Q_A = NnC_L, \quad \text{and} \quad Q_L = (1 - N)nC_L$$

and are plotted for each optimum condition.

6-5 Design of Optimum Lead with Known Ambient Heat Inleak

The optimization applies for only one value of current; hence the current must be known.

From the given values of ambient heat inleak, Q_A, and current, I, the quantity $\dfrac{Q_A C_p}{2IC_L\sqrt{L}}$ can be evaluated and from the curves on figure 6-7 corresponding values of N and D can be found.

From these values of N and D the Z temperature profile for the optimum lead can be calculated from equation 6-10, 6-11, or 6-12, whichever applies. Note that figure 6-6 only allows for D > 0.25; hence equation 6-10 applies.

The Z temperature profile supplies the data for the evaluation of the expression

$$\int_{Z=0}^{Z_1} K(Z) \, dZ \qquad \text{where } T(Z_1) = 300 \text{ K.}$$

Finally from equation 6-13 either the area of the conductors or their length can be calculated, depending upon which has been pre-determined by other conditions.

An example of the above calculation follows:

find the optimum leads of length 65cm to carry 300 amperes if the ambient heat inleak is, for example, 0.18 watts.

$$\text{Modified heat inleak} = \frac{0.18 * 1/3.9}{2 * 300 * 1.55 * 10^{-4}} = 0.495 \text{ watts.}$$

From figure 6-6, N = 0.27 and D = 0.2877 and the temperature profile is hence given by:

$$T(Z) = EXP(Z/2) \{4.2 * \cos(0.1942Z) + 3.847 * \sin(0.1924Z)\}$$

This is plotted in figure 6-8 with the thermal conductivity and integral profiles. From figure 6-8 the value of

$$\int KdZ = 56 \text{ watts-cm}^{-1}\text{-K}^{-1}, \text{ therefore}$$

$$\frac{nC_p}{2A} = 56 \text{ watt-cm}^{-1}\text{-K}^{-1}$$

From the definition of n and N it follows that:

$$Q_T = nC_L = \frac{Q_a}{N}$$

$$nC_p = \frac{Q_a C_p}{NC_L} = 0.191$$

$$A = \frac{0.191 * 65}{2 * 56} = 0.111 \text{ cm}^2$$

This lead is not very different from the optimum lead with N = 0, a fact which indicates that the optimum lead remains the same for a considerable range of ambient heat inleak.

6-6 Effects of Operating Away from the Optimum Current for a Given Lead

In this problem the cross-sectional area and the length of the leads are constant and the current carried is the variable. The question to be answered is: "How does the lead heat inleak vary as the current

FIG 6 - 8
OPTIMUM LEAD Z PROFILES
Q_A = 0.2 watt
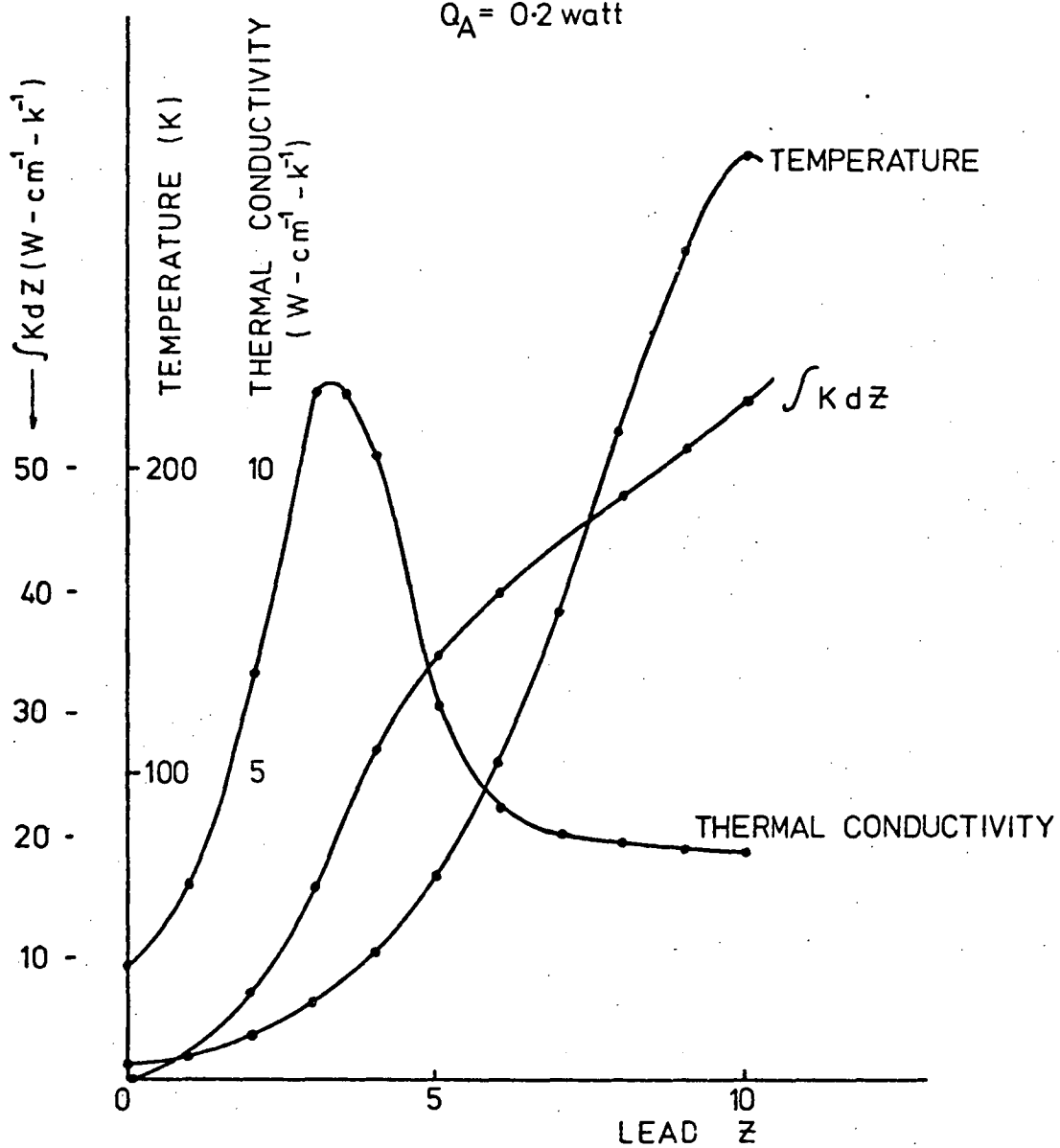
is increased from zero to the optimum and beyond with ambient heat inleak negligible?"

The difficulty in solving this problem arises because the value of D in equation 6-9 is unknown. A solution follows the lines of guessing the heat inleak, calculating n and hence D for a given current and solving the equation 6-9 for the temperature profile as a function of Z. From this profile the temperature as a function of distance "X" above the level of the liquid helium can be calculated from equation 6-5. And if the temperature is 300 K when X equals the lead length then the guess of n is correct. This process requires a knowledge of thermal conductivity as a function of temperature.

Another method of solving this problem uses an indirect approach but requires no iteration as above. Instead of assuming a lead current, then calculating the heat inleak, as above, assuming heat inleaks and calculating the corresponding currents gives a curve from which the answer can be determined without iterations. The method is as follows:

assume a value of D and evaluate T(Z), then calculate n

from equation 6-13 which requires the evaluation of integral:

$$\int_{Z=0}^{Z_1} K(Z) \, dZ = \frac{nC_p \ell}{2A}$$

From the values of n and D, the current I can be calculated from equation 6-8. This process was carried out for the optimum leads and the results plotted in figure 6-9.

In the range $0.25 < D < 0.31$, for an ambient temperature of 300 K, there are two values of Z_1 such that $T(Z_1) = 300$ K - figure 6-2. Hence in this range there are two values of current which satisfy the boundary conditions: one value is greater than the optimum current and the other less than the optimum current.

FIG 6-9
OPERATION OF LEADS AWAY
FROM THE OPTIMUM
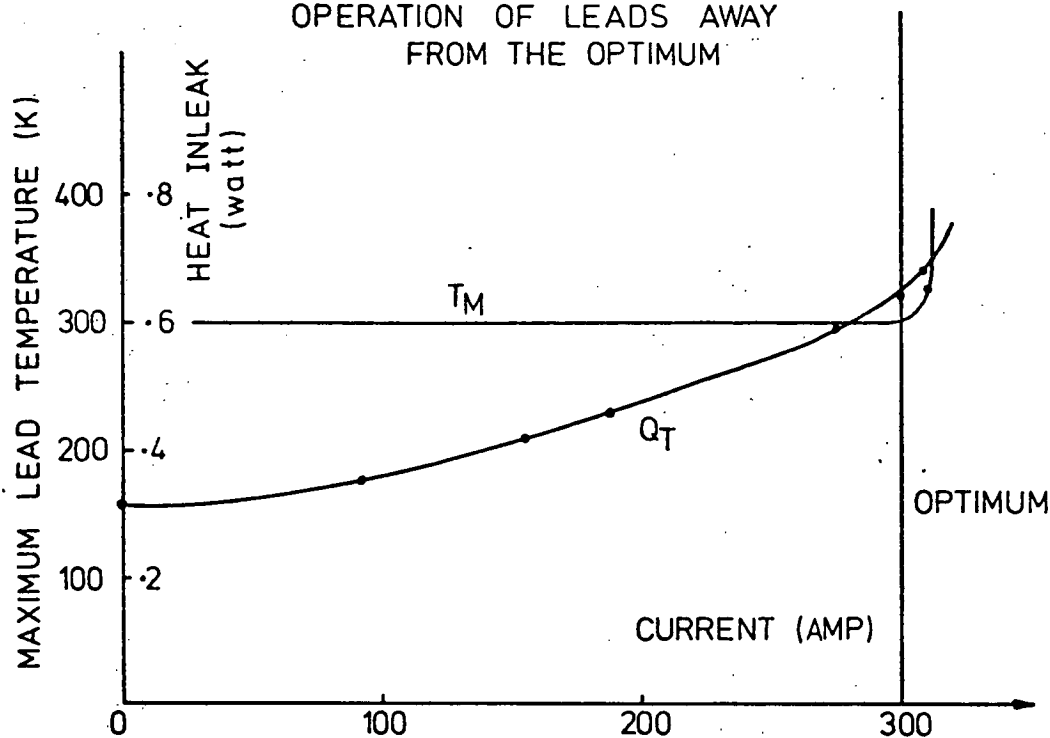
FIG 6-10
'OPTIMUM' LEAD PERFORMANCES

A WIEDEMANN FRANZ LAW
B ITERATIVE SOLUTION
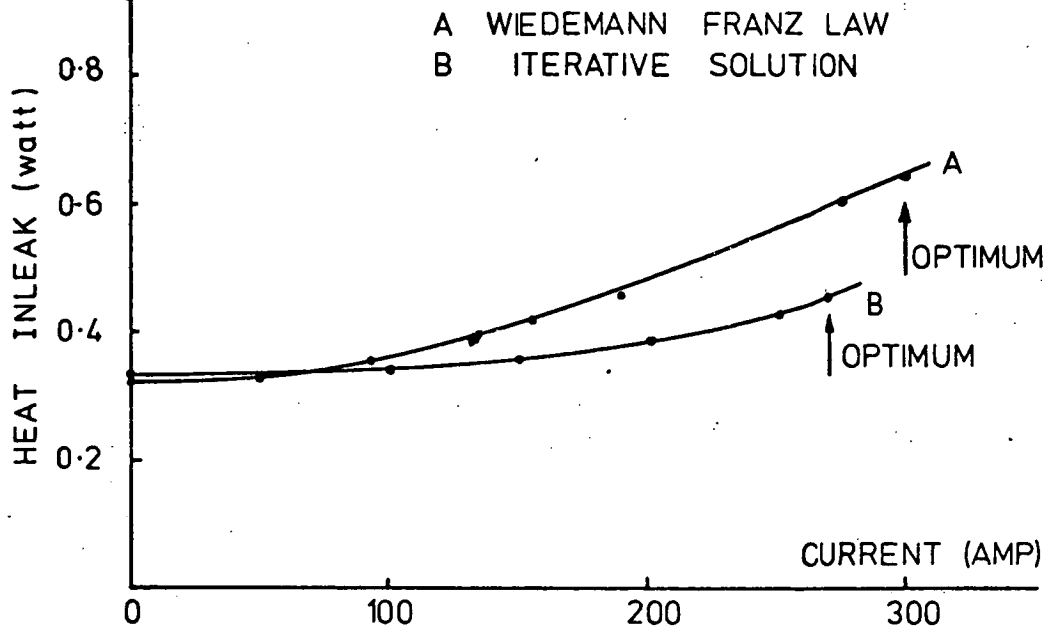
For lead currents greater than the optimum value the temperature profiles predict lead temperature in excess of the ambient room temperature. These effectively shorten the lead length (as suggested by S.P. Scott) and hence the boil-off increases rapidly with increased current above the optimum.

The predicted peak hot spot temperature reached by the leads increases rapidly with lead current in excess of the optimum value. For example, with only 5% excess current the predicted peak temperature is 345 K. This indicates that to avoid increased lead heat inleaks currents in excess of the optimum should not be used. This predicted "cooking" of the lead occurs within very close proximity to the room temperature end of the copper lead.

6-6-1 Alternative Solution

An iterative solution to the problem can be achieved with the only assumption being that perfect heat transfer between leads and the cooling gas occurs. The other variables need only be tabulated or described mathematically if a digital computer is used - see Appendix E.

The equations used for the two leads were:

$$T_{j+1}(x + \delta x) = T(x) + \frac{\delta x * [Q_j(x + \delta x) + Q(x)]}{[A(x + \delta x) + A(x)] * [K_j(x + \delta x) + K(x)]} \quad (6-14)$$

$$Q_{j+1}(x + \delta x) = Q(x) - 2 * I^2 * \delta x \frac{[\rho_j(x+\delta x)+\rho(x)]}{[A(x+\delta x)+ A(x)]} + t*[h_j(x+\delta x)-h(x)] \quad (6-15)$$

where subscripts j and $j+1$ refer to the iteration steps. By assuming a lead heat inleak and a value of n, a solution can be obtained without assuming C_p constant and without assuming that K and ρ obey the Wiedemann-Franz Law. The value of n was calculated from the guess value of the lead heat inleak (Q_o) and

the ambient heat inleak (Q_a), using equation 6-4.

The method of solution was first to guess the lead heat inleak Q_o to the helium and for the first iteration step the values of $Q_o(\delta x)$ and $K_o(\delta x)$ were assumed to be the values obtained with $T = 4.2K = T(0)$. $T_1(\delta x)$ was then calculated using equation 6-14 and values of $\rho_1(\delta x)$, $h_1(\delta x)$, and $K_1(\delta x)$ were determined from the tabulated values. This enabled $Q_1(\delta x)$ to be calculated.

Using the values $Q_1(\delta x)$ and $K_1(\delta x)$ the second iterated value of temperature $T_2(\delta x)$ was calculated and, as before, values of $\rho_2(\delta x)$, $h_2(\delta x)$, and $K_2(\delta x)$ were determined and hence $Q_2(\delta x)$ was calculated. This process was continued until differences in values were small.

Similarly the next step was to calculate $Q(2\delta x)$ and $T(2\delta x)$, but this time $Q_o(2\delta x) = Q(\delta x)$ and $K_o(\delta x)$ for the first iteration.

This was continued until the lead length was reached and if $I = 300K$ then the original guess for Q_o was correct: otherwise another estimate of Q_o had to be made and the entire process repeated.

To do this by hand is obviously tedious, so to speed up and simplfiy the calculations for the process, curves were fitted to the thermal conductivity, electrical resistivity, and enthalpy data and the solution carried out on a digital computer. Even then the time taken for each guess of Q_o on a PDP8E computer was five minutes or so depending on the value of δx chosen.

The equations which were used to describe the various properties are given in Appendix F in addition to tabulated data.

6-6-2 Comparison Between Results

The iterative solution predicted smaller current lead heat inleaks

than those predicted by the optimized leads obtained from the Wiedemann-Franz Law - figure 6-10. The reason for this result was that the tabulated values of thermal and electrical conductivity deviate considerably from the Wiedemann-Franz Law. If the tabulated values of thermal conductivity were used to calculate electrical resistivity using the Wiedemann-Franz Law, then the resulting calculated values would be, in some cases, considerably larger than those tabulated. This then gives rise to higher Joule heating losses using the Wiedemann-Franz Law case than for the tabulated values and hence the predicted heat inleak for the "optimized" leads was greater than that for the iterative solution.

The iterative solution also gave the result that the "optimum" leads obtained using the Wiedemann-Franz Law were not the optimum. The iterative solution predicted the optimum current for the "optimum" leads to be 270 amps and for a current of 300 amps the leads required shortening to near 59cm to be optimized.

Although the iterative solution does not give the optimum lead design directly, once a design has been chosen, say using Wiedemann-Franz Law, its performance without the Wiedemann-Franz Law approximation can be determined and a comparison made between results.

6-7 Uncooled Leads

The heat inleak due to uncooled leads can be easily calculated and shows the necessity for counterflow leads.

The differential equation can be derived with reference to figure 6-11.

$$\frac{Q(x)}{2} + \frac{I^2 \rho (T) \delta x}{A(x)} = \frac{Q(x + \delta x)}{2}$$

$$\Rightarrow \frac{dQ}{dx} = \frac{2I^2 \rho (T)}{A(x)} \qquad (6-16)$$

and $$Q(x) = -2K(T) A(x) \frac{dT(x)}{dx} \qquad (6-17)$$

FIG 6-11
CRYOGENIC CURRENT LEADS
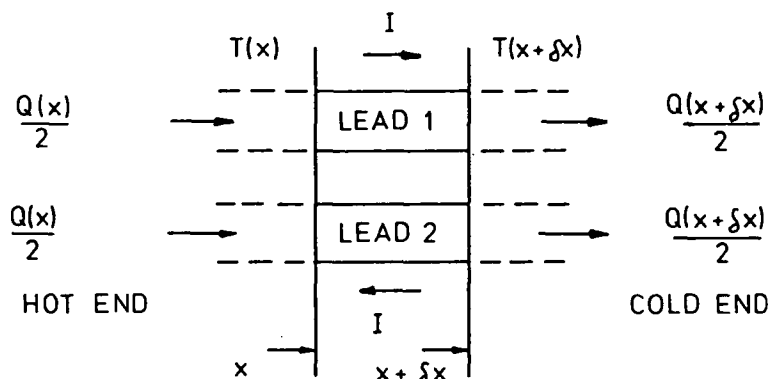
Eliminate A(x) between equations 6-16 and 6-17.

$$Q(x) \; \frac{dQ(x)}{dx} \;\; = \; - 4I^2 \; \rho(T) \; K(T) \; \frac{dT(x)}{dx}$$

Integrate with respect to x

$$\int_0^x Q(x) \; \frac{dQ(x)}{dx} \;\; = \; - 4I^2 \int_0^x \rho(T) \; K(T) \; \frac{dT(x)}{dx} \, dx$$

$$\Rightarrow \; \tfrac{1}{2}\{Q^2(x) - Q^2(o)\} \;\; = \; - 4I^2 \int_{T_{MAX}}^{T(x)} \rho(T) \; K(T) \; dT$$

Assume $\rho(T)$ and $K(T)$ obey the Wiedemann-Franz Law

$$\Rightarrow \; Q^2(x) - Q^2(o) \;\; = \;\; 4I^2 L[T^2_{MAX} - T^2(x)]$$

$$\Rightarrow \; Q(\ell) \;\; = \;\; \{4I^2 L[T^2_{MAX} - T^2_{MIN}] + Q^2(o)\}^{\frac{1}{2}}$$

$Q(o)$ is the heat inleak when $I = 0$ and was determined as follows:

Equation 6-16 gives $\frac{dQ}{dx} = 0 \;\Rightarrow\; Q(x)$ is constant

Equation 6-17 gives $Q(x) = -2A(x) \; K(T) \; \frac{dT}{dx}$

Integration gives
$$\int_0^{\ell} \frac{Q(x)}{2A(x)}\, dx = \int_{T_{MIN}}^{T_{MAX}} K(T)\, dT$$

Since $Q(x)$ = constant the left hand side can be evaluated if $A(x)$ is variable. If $A(x)$ is constant then the result below follows:

$$Q(o) = \frac{2A}{\ell} \int_{T_{MIN}}^{T_{MAX}} K(T)\, dT$$

Using values of ℓ and A as determined from the optimum leads

$$Q(o) = 2 * 0.106 * \frac{1492}{65} \text{ watts}$$
$$= 4.87 \text{ watts}.$$

For $I = 300$ amps, $T_{MAX} = 300K$, $L = 2.4 \times 10^{-8}$ and $T_{MIN} = 4.2K$

$$Q_o = \{4 * 9 * 10^4 * 2.4 * 10^{-8} * 9 * 10^4\}^{\frac{1}{2}}$$
$$= 28.3 \text{ watts}.$$

A heat inleak of 28.3 watts was completely unacceptable because the resultant loss of liquid helium would be excessive; hence the simultaneous operation of the two cryostats would be impossible from the supply of helium available. Comparing this result with 0.636 watts for the optimized counterflow lead shows the importance of using the boil-off gases to cool the leads.

6-8 General Comments

The method of analysis used to predict the heat inleak rested heavily on the assumption of perfect heat transfer between boil-off gases and the leads. Temperature profiles obtained assuming constant lead cross sectional areas tend to be very steep with temperature gradients in excess of 10K/cm near the room temperature and hence difficulties with heat transfer to the gas could occur in this region. At the other end of the

leads the predicted slope was small, approximately 1K/cm. At the cost of ease of construction the temperature difference could be more evenly distributed by using a varying lead cross sectional area, hence reducing potential problems arising from inadequate heat transfer.

To obtain effective heat transfer, the boil-off gases should be maintained in turbulent flow. This can be achieved by using metal gauze in the path of the boil-off gases; but adequate electrical insulation would be required to isolate the leads from each other and the metal of the cryostat.

Since the object of this investigation was to arrive at the simplest design of a lead operating at, or near, optimum conditions a fixed diameter, 9 SWG gauge conductor was selected as the lead for the test machine. This conductor has an area of $0.108cm^2$ compared with the area of an optimised lead of $0.106cm^2$, as derived in section 6-2-1.

The design of the cryostat provided only limited space for the leads; hence inclusion of the most effective heat transfer surface between the leads and the boil-off gases, such as copper gauze, was not practicable. Copper fins were soldered onto the leads at 7mm intervals to improve the heat transfer and teflon spacers every 100mm prevented electrical short circuits between the cryostat and the leads - figure 6-12. The lead assembly thus constructed was rigid and hence easily positioned in the cryostat. The number of fins selected was the maximum number consistent with the requirement of ease of manufacture of the leads.

6-9 Liquid Nitrogen Lead Test

The design of the leads and their calculated performance rested heavily on assumptions which were only approximations to what actually occurs; hence testing was necessary. Tests in liquid helium were not possible because of the high cost involved; hence it was necessary to

FIG 6-12
A SECTION OF THE 300 AMPERE CURRENT LEAD

21 gauge copper
heat exchangers

17.5mm

7.5mm

Teflon alignment spacers
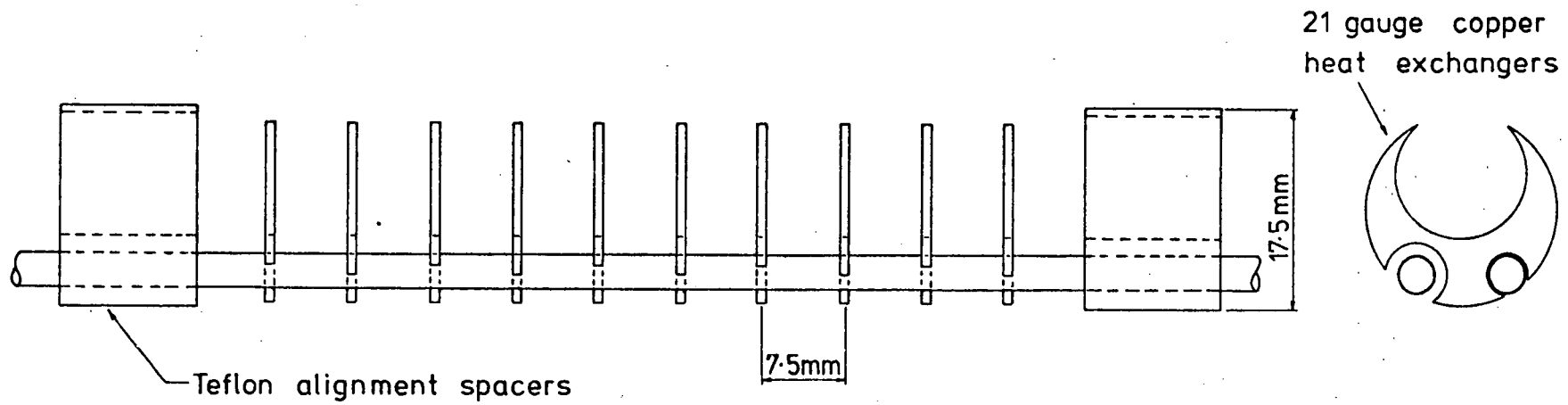
perform tests with liquid nitrogen, and interpret the results for operation into liquid helium.

Heat inleaks to the liquid nitrogen with the leads terminated in a short circuit and carrying different currents were measured (Appendix F). The results were compared with predicted heat inleaks calculated using the iterative technique - figure 6-13. The measured results compared favourably with the computed heat inleaks although they were generally greater. This was to be expected because of imperfect heat transfer between the leads and the boil-off gases. This was apparent with the larger lead heat inleaks at the higher currents. The measured results indicated the effects of exceeding the optimum current. For example, with currents less than the optimum (I_{opt} = 80 amp for liquid nitrogen) the heat inleaks decreased as the lead length increased, as a result of the drop in liquid level. The opposite occurred for currents greater than approximately 80 amp and the temperature of the ambient extremity of the leads increased above room temperature. The predicted heat inleak curves (figure 6-14) indicated that variation of lead length and ambient heat inleak result in small changes in total heat inleak to the liquid nitrogen.

The maximum rate of nitrogen gas flow from the cryostat during the tests was approximately 30cc/sec with a current of 100 amps. With the optimized leads supplying 300 amps to the superconducting coil (and assuming negligible ambient heat inleak) the rate of helium gas flow would be 180cc/sec or six times that encountered during the nitrogen tests. This larger volumetric flow rate may result in problems with heat transfer and with the transfer of liquid helium from the dewar to the cryostat; however, from the small temperature difference between the leads and the escaping gas (as estimated in Appendix N) the heat transfer was shown to be satisfactory.

FIG 6-13
LIQUID NITROGEN
LEAD RESULTS
MEASURED

1 Lead length 65cm calculated using program
2 Measured inleak showing range over which Q varied. Arrow indicates lead length increase
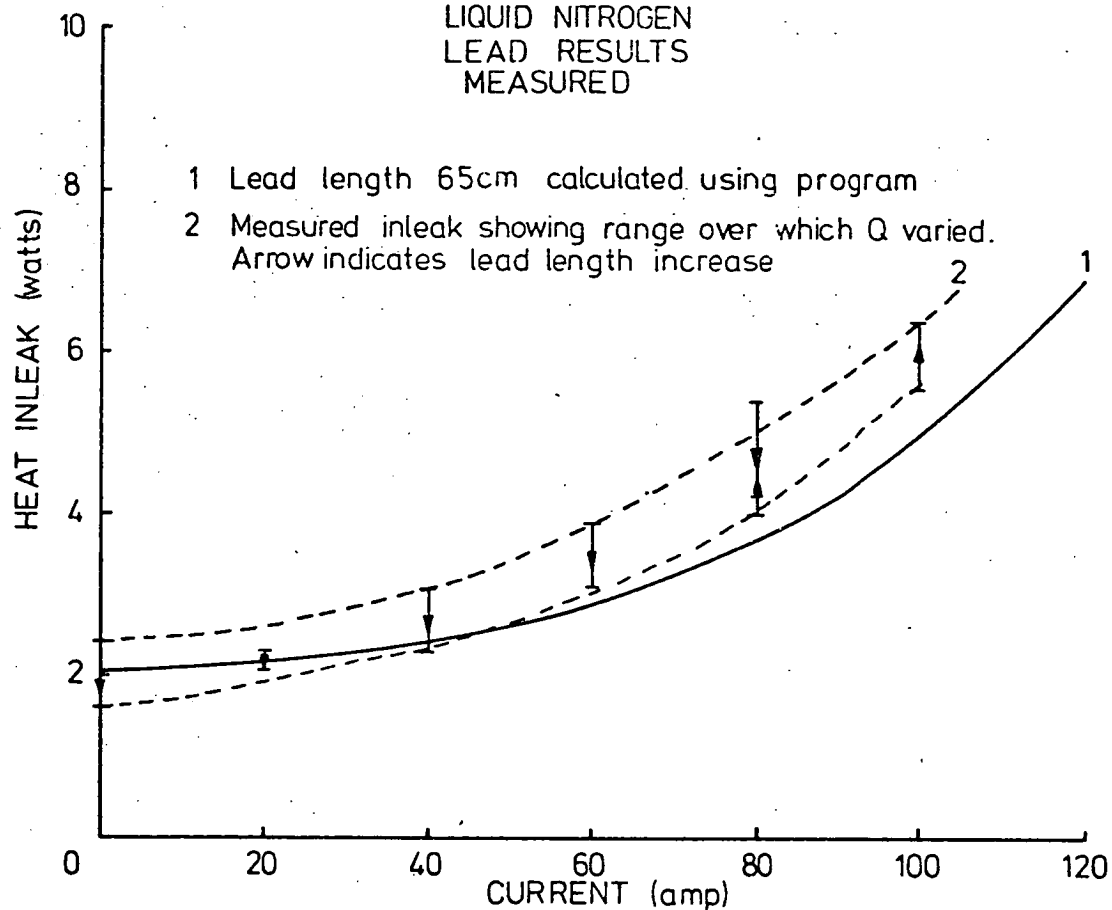
FIG 6-14
LIQUID NITROGEN
LEAD RESULTS
CALCULATED

$l = 75\,cm\ Q_A = 0$
$l = 65\,cm\ Q_A = 1\,watt$
$l = 65\,cm\ O_A = 0$
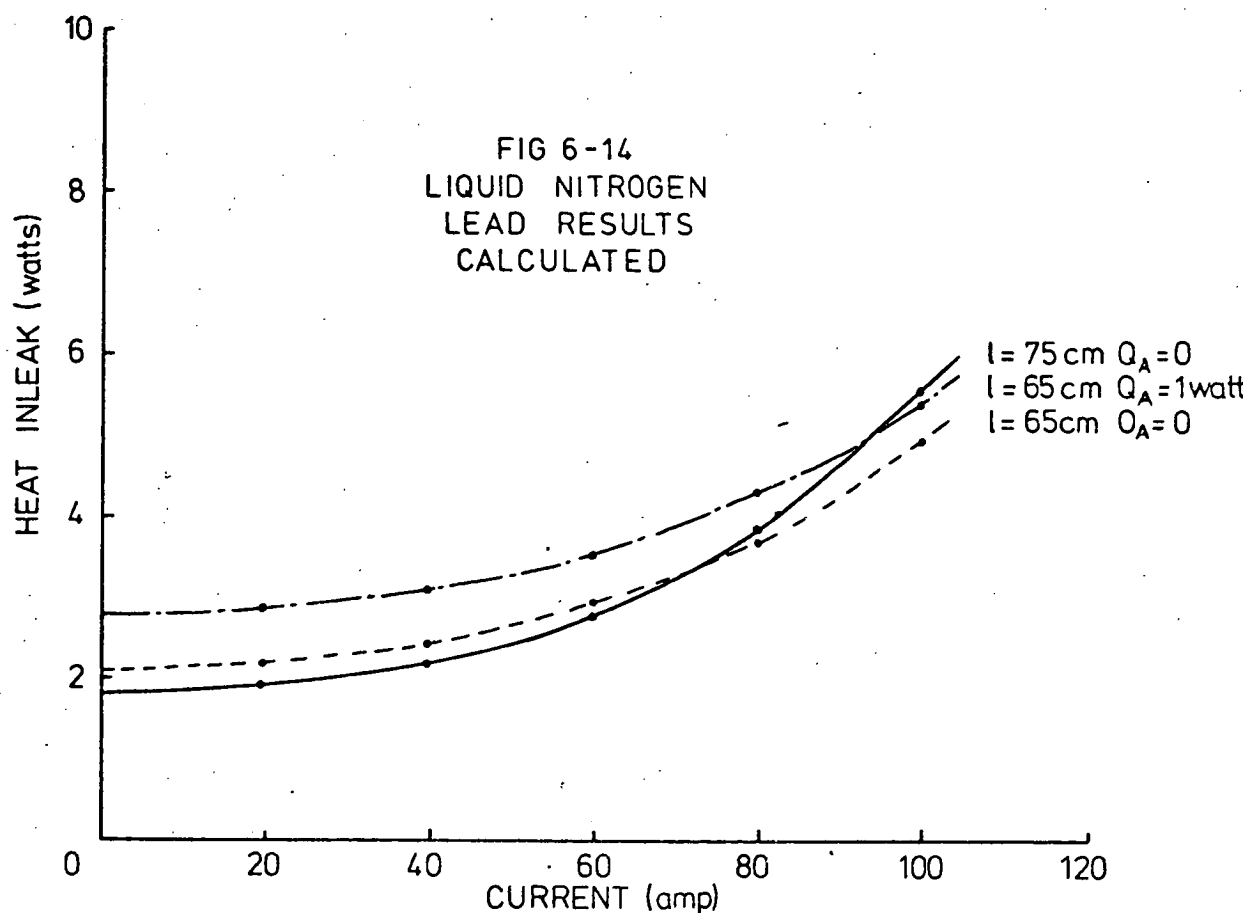
As the leads operated as predicted into liquid nitrogen, and taking into consideration the possible difficulties with helium, it was decided to retain the adopted lead design for operation of the superconducting field coil.

CHAPTER 7

CRYOSTAT AND COIL COOLDOWN

7-1   Introduction

Initial cooldown calculations (Appendix B) estimated the quantities
of liquid helium required for the cooldown of the coil and cryostat from
77K to 4.2K. In this chapter a method is established to relate the time
required to cool the coil to a temperature at which it becomes super-
conducting with the rate of flow of liquid helium and other parameters
which affect the rate of cooldown. It shows that the time lag for the
bulk of the coil to attain equilibrium with the surface temperature of
the coil is only a matter of seconds and that the overall cooldown time
is dependent on the rate at which heat can be transferred from the *surface*
of the coil to the liquid helium and so removed from the interior of the
cryostat.

7-2   Describing Cooldown

7-2-1   Model

The first step in determining the time required for the bulk of the
coil to reach equilibrium with the surface temperature was to satisfact-
orily model the thermal properties of the coil and cryostat sections to
be cooled. The cryostat was manufactured from thin stainless steel;
hence cooldown times for the stainless steel would be short in comparison
with the relatively bulky superconducting coil. Thus as a first approxi-
mation the problem was reduced to the cooldown of the coil only.

The thermal characteristics of the coil were complicated by the
different materials in the coil; for example the copper matrix, the
niobium-titanium superconducting alloy, the insulation of the conductor,
and the coil potting material. The second approximation replaced the

non-homogeneous coil materials with a homogeneous material with properties strongly biased towards those of copper.

Thirdly, to simplify the calculations a circular coil section was adopted in which the heat flow would be radial only.

The resultant model decided upon was hence equivalent to an infinitely long, homogeneous cylinder. This eased the mathematical description, and resulted in a temperature distribution which was a function of radial position and time only.

7-2-2 Differential Equation

The differential equations describing the cooldown were obtained from consideration of heat flows within the cylinder. This resulted in equations 7-1 and 7-2.

$$\frac{\partial Q}{\partial r} = -2\pi r \frac{\partial h}{\partial t} \tag{7-1}$$

$$Q = -2\pi r \frac{\partial V}{\partial r} \tag{7-2}$$

Q = outward flow of heat per unit time per unit length (watts/cm)

r = radial position (cm)

h = enthalpy (joule/cm^3)

t = time (sec)

V = temperature (K)

K = thermal conductivity (watt-cm^{-1}-K^{-1})

The heat flow was eliminated to give:

$$\frac{\partial}{\partial r} \left\{ Kr \frac{\partial V}{\partial r} \right\} = r \frac{\partial h}{\partial t} \tag{7-3}$$

The boundary conditions were:

(a) at time t = 0 the coil was at a uniform temperature of V_o

$$\implies V(0,r) = V_o$$

(b) no heat could flow from the centre of the cylinder

$$\implies \frac{\partial V}{\partial R}\bigg|_{R=0} = 0$$

(c) at the outer radius the temperature was assumed to be the same as that of the coolant.

7-2-3 Solution Technique

Over the temperature range which was under consideration the thermal conductivity (K) cannot be considered as constant and the constant specific heat representation of enthalpy is not precise. However, as the previous assumptions reduced the accuracy of the model, it was considered appropriate that representative equivalent constant values of specific heat and thermal conductivity be chosen. If the assumptions made model the cooldown accurately then the values of specific heat and thermal conductivity chosen would result in an over-estimate of the time required for cooldown.

Using the simplification of constant specific heat and thermal conductivity, equation (7-3) reduced to:

$$\frac{\partial^2 V}{\partial r^2} + \frac{1}{r}\frac{\partial V}{\partial r} = \frac{\bar{C}_p}{\bar{K}}\frac{\partial V}{\partial t} \qquad (7-4)$$

$\bar{C}_p$ = representative specific heat (Joule/cm^3/K).

$\bar{K}$ = representative thermal conductivity (watt/cm/K^{-1}).

Or in non-dimensional form:

$$\frac{\partial^2 U}{\partial R^2} + \frac{1}{R}\frac{\partial U}{\partial R} = \frac{\partial U}{\partial T} \qquad (7-5)$$

where $U = V/V_0$

$R = r/r_0$

$T = (\bar{K}/\bar{C}_p r_0^2) * t$

$V_0 =$ non-dimensionalising temperature (i.e. the initial temperature of the coil)

$r_0 =$ non-dimensionalising radius (i.e. the outer radius of the cylinder).

Equation 7-5 could have been solved analytically using the technique of separation of variables. This would have resulted in Bessel's equation which would have involved unwarranted numerical work.

Solutions of equation 7-5 were obtained using forward difference representations for the partial derivatives, hence solving the resulting difference equations with the aid of a digital computer. The Crank-Nicholson representation of partial derivatives gave the following set of derivatives at the $1^{\underline{th}}$ non-dimensional time interval and $j^{\underline{th}}$ radius position.

$$\frac{\partial^2 U}{\partial R^2} = \frac{1}{2 \Delta R^2} [X + Y] \qquad (7\text{-}6)$$

$X = U(I, J + 1) - 2U(I, J) + U(I, J - 1)$

$Y = U(I + 1, J + 1) - 2U(I + 1, J) + U(I + 1, J - 1)$

$$\frac{\partial U}{\partial R} = \frac{1}{2 \Delta R} [U(I, J + 1) - U(I, J - 1)] \qquad (7\text{-}7)$$

$$\frac{\partial U}{\partial T} = \frac{1}{2 \Delta T} [U(I + 1, J) - U(I - 1, J)] \qquad (7\text{-}8)$$

where $\Delta R =$ non-dimensional radius step length

$\Delta T =$ non-dimensional time step length

Substitution into the partial differential equation 7-5 gave:

$$U(I + 1, J + 1) - U(I + 1, J) * (2 + 1/a) + U(I + 1, J - 1) = B(I + 1, J)$$

(7-9)

where $a = \Delta T/\Delta R^2$

$$B(I + 1, J) = -U(I, J + 1) * (I + 1/J) + 2U(I, J) - U(I, J - 1) * (1 - \frac{I}{J})$$

$$-U(I - 1, J)/a$$

for $J = 1, 2, \ldots (n - 1)$

   n = number of radius steps $= 1/\Delta R$

   The term $\frac{1}{R} \frac{\partial U}{\partial R}$ led to difficulty at $R = 0$ hence equation 7-5 was adjusted to give a usable equation with $R = 0$.

   From the Maclaren expansion:

$$\frac{\partial U}{\partial R}_{(R,T)} = \frac{\partial U}{\partial R}_{(0,T)} + R \frac{\partial^2 U}{\partial R^2}_{(0,T)} + \frac{1}{2} R^2 \frac{\partial^3 U}{\partial R^3}_{(0,T)} + \ldots\ldots\ldots$$

Have that $\frac{\partial U}{\partial R}_{(0,T)} = 0$ hence:

$$\frac{1}{R} \frac{\partial U}{\partial R}_{(R,T)} = \frac{\partial^2 U}{\partial R^2}_{(0,T)} + \frac{1}{2} R \frac{\partial^3 U}{\partial R^3}_{(0,T)} + \ldots\ldots\ldots\ldots$$

with $R = 0$ the result follows:

$$\frac{1}{R} \frac{\partial U}{\partial R}_{(0,T)} = \frac{\partial^2 U}{\partial R^2}_{(0,T)}$$

So at $R = 0$ equation 7-5 becomes:

$$2 \frac{\partial^2 U}{\partial R^2}_{(0,T)} = \frac{\partial U}{\partial T}$$

(7-10)

It thus follows at $R = 0$:

$$\frac{\partial^2 U}{\partial R^2} = \frac{1}{2\Delta R^2} [U(I,1) - 2U(I,0) + U(I, -1) + U(I + 1,1) - 2U(I + 1,0)$$

$$+ U(I + 1, -1)]$$

The values of U(I, -1) and U(I + 1, -1) were obtained from:

$$\left.\frac{\partial U}{\partial R}\right|_{R=0} = \frac{1}{2\Delta R}[U(I,1) - U(I,-1)] = 0$$

Hence U(I,1) = U(i, -1) for all I and equation 7-10 becomes:

$$U(I + 1,1) - U(I + 1,0) * (1 + 1/4a) = B(I + 1,0) \tag{7-11}$$

where $B(I + 1,0) = U(I,0) - U(I,1) - \frac{1}{4a} U(I - 1,0)$.

Equations 7-9 and 7-11 gave rise to equations in the unknowns U(I + 1,J), J = 0, 1, ...(n-1) and in matrix form, taking into account that U(I + 1, n) equals the coolant temperature U_c, they are:

$$
\begin{bmatrix}
-(1+\frac{1}{4a}) & 1 & 0 & 0..0 & 0 & 0 \\
1 & -(2+\frac{1}{a}) & 1 & 0..0 & 0 & 0 \\
0 & 1 & -(2+\frac{1}{a}) & 1..0 & 0 & 0 \\
\cdot & \cdot & \cdot & \cdot \ \cdot \ \cdot & \cdot & \\
\cdot & \cdot & \cdot & \cdot \ \cdot \ \cdot & \cdot & \\
0 & 0 & 0 & 0..1 & -(2+\frac{1}{a}) & 1 \\
0 & 0 & 0 & 0..0 & 1 & -(2+\frac{1}{a})
\end{bmatrix}
\begin{bmatrix}
U(I+1,0) \\
U(0+1,1) \\
U(I+1,2) \\
\cdot \\
\cdot \\
U(I+1,n-2) \\
U(I+1,n-1)
\end{bmatrix}
=
\begin{bmatrix}
B(I+1,0) \\
B(I+1,1) \\
B(I+1,2) \\
\cdot \\
\cdot \\
B(I+1,n-2) \\
B(I+1,n-1)-U_c
\end{bmatrix}
$$

Values of the U(I + 1,J) were obtained using the Gaussian elimination technique which was rapid because of the simple nature of the matrix.

7-2-4   Results

The calculations were carried out as if the coil, initally at room temperature, was suddenly immersed in the coolant and the surface of the coil instantly adopted the same temperature as the coolant. The cooldown curves from room temperature to liquid nitrogen temperature for R = 0, 0.5 and 1 (figure 7-1) were obtained with values of 0.05 and 0.1 for $\Delta T/\Delta R^2$ and ΔR^2 respectively which meant that $\Delta T = 5 * 10^{-4}$.

FIG 7·1
COIL COOLDOWN
ROOM TEMPERATURE TO 77K
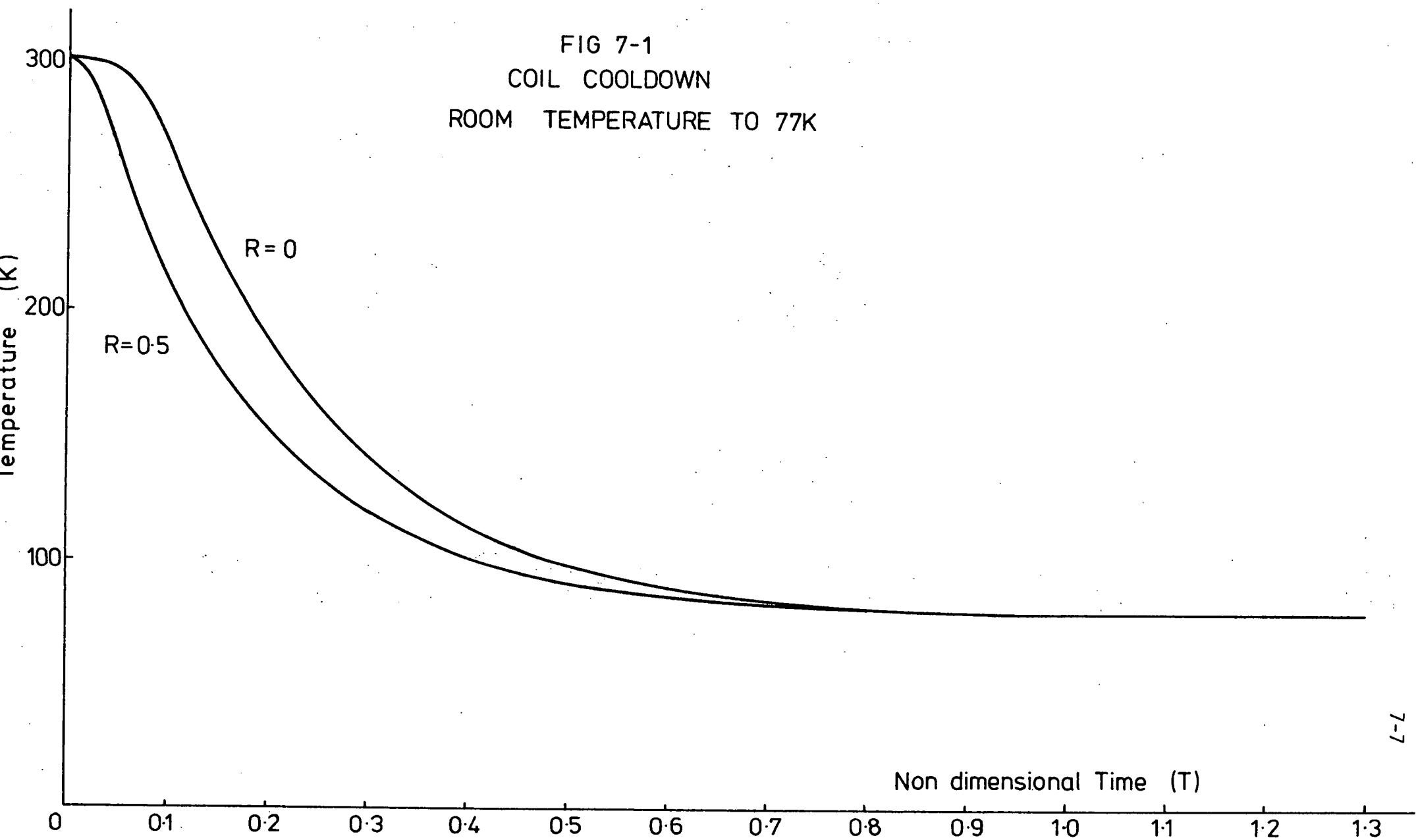
The approximate value of the non-dimensional time for complete cooldown was 1.25 and to convert this to real time for the liquid nitrogen case:

$$t = T * \frac{\bar{C}_p r_o^2}{\bar{K}}$$

$$= 1.25 * \frac{3.2}{4} * r_o^2$$

$$t = r_o^2 \text{ seconds } (r_o \text{ in cm.})$$

For a rod of solid copper of radius 1cm the estimated cooldown time from room temperature to 77K was 1 second. As C_p decreases substantially and K, for pure copper, increases substantially with decrease in temperature the predicted cooldown time from 77K to 4.2K would have been less.

7-3 Cooldown Tests

The properties of the superconducting coil were different from those of copper because of the wire insulation, potting material, and the relatively poor thermal contact between coil turns. Since the shape of the cooldown curves were independent of the type of material (provided that C_p and K could be assumed constant); by conducting nitrogen cooldown tests on the coils a representative value of $\bar{C}_p/\bar{K}$ could be determined, hence the time for cooldown from 77K to 4.2K could be estimated.

The measurement technique adopted was to pass a small, constant current (10 mA) through the coil and record, on an X-Y plotter, the coil terminal voltage as a function of time after the coil had been immersed in a bath of liquid nitrogen.

7-3-1 Test Results

The cooldown curves obtained (figure 7-2) gave cooldown times over

FIG 7-2
SUPERCONDUCTOR COIL COOLDOWN
ROOM TEMPERATURE TO 77K
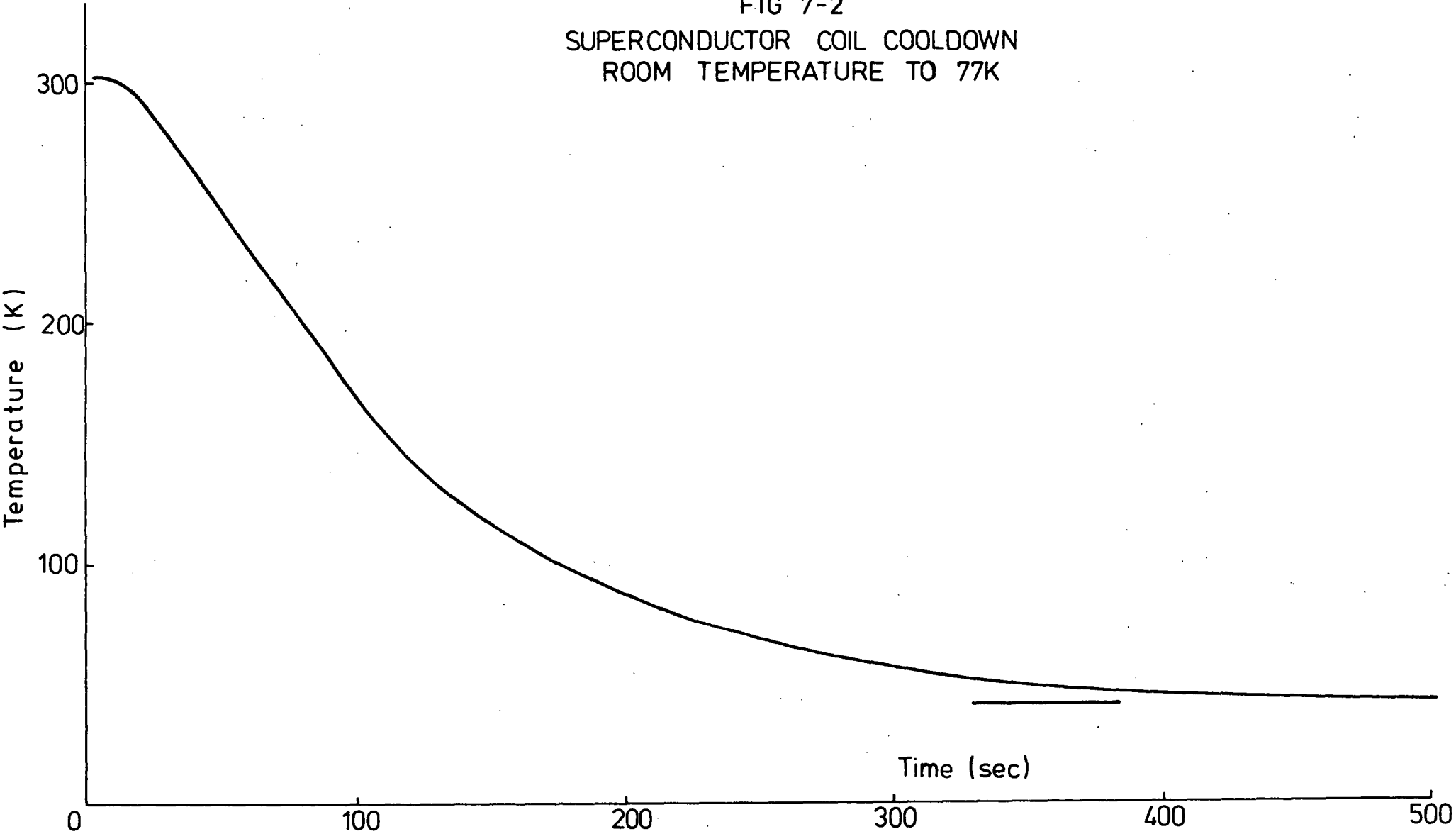
two orders of magnitude greater than those previously predicted in section 7-2-4. Representative values of C_p and K indicate that the discrepancy could not be explained by $\bar{C}_p/\bar{K}$ being 300 to 400 times larger, hence another explanation was necessary.

The cause contributing most to the discrepancy was that the surface temperature of the coil was not 77K as soon as it was immersed in the liquid nitrogen. This would have been caused by the violent boiling of the liquid on immersion of the coil, thus producing poor thermal contact between the liquid and the surface of the coil.

To test this hypothesis, a thermocouple was soldered onto the surface of a 7mm diameter copper rod and the surface temperature monitored, as a function of time, as the rod cooled. The resulting curve (figure 7-3) verified the hypothesis and it also indicated that as the surface temperature neared 77K, cooldown proceeded more rapidly and as soon as the surface temperature reached 77K, the entire bar was at 77K.

The time taken for the rod to cooldown was near 60 seconds, or over 350 times larger than predicted. The factor of 350 was much the same as in the case of the coil cooldown test.

7-4 Discussion

Although the predicted times for cooldown bore little relationship to the actual cooldown times (primarily due to the invalid assumption that the coil surface temperature was the same as the coolant temperature), the calculations and the tests showed that the coil cooled rapidly to its surface temperature. This was an important result because it showed that the cooldown times were determined by the rate of coolant flow into the coil chamber (the rate at which heat could be removed from the chamber) rather than by the time required for temperature of the coil to

FIG 7-3
COPPER ROD COOLDOWN
ROOM TEMPERATURE TO 77K

Thermocouple soldered onto the
surface of the copper rod

Rod diameter 8mm
Rod length 150mm

Cooldown completed
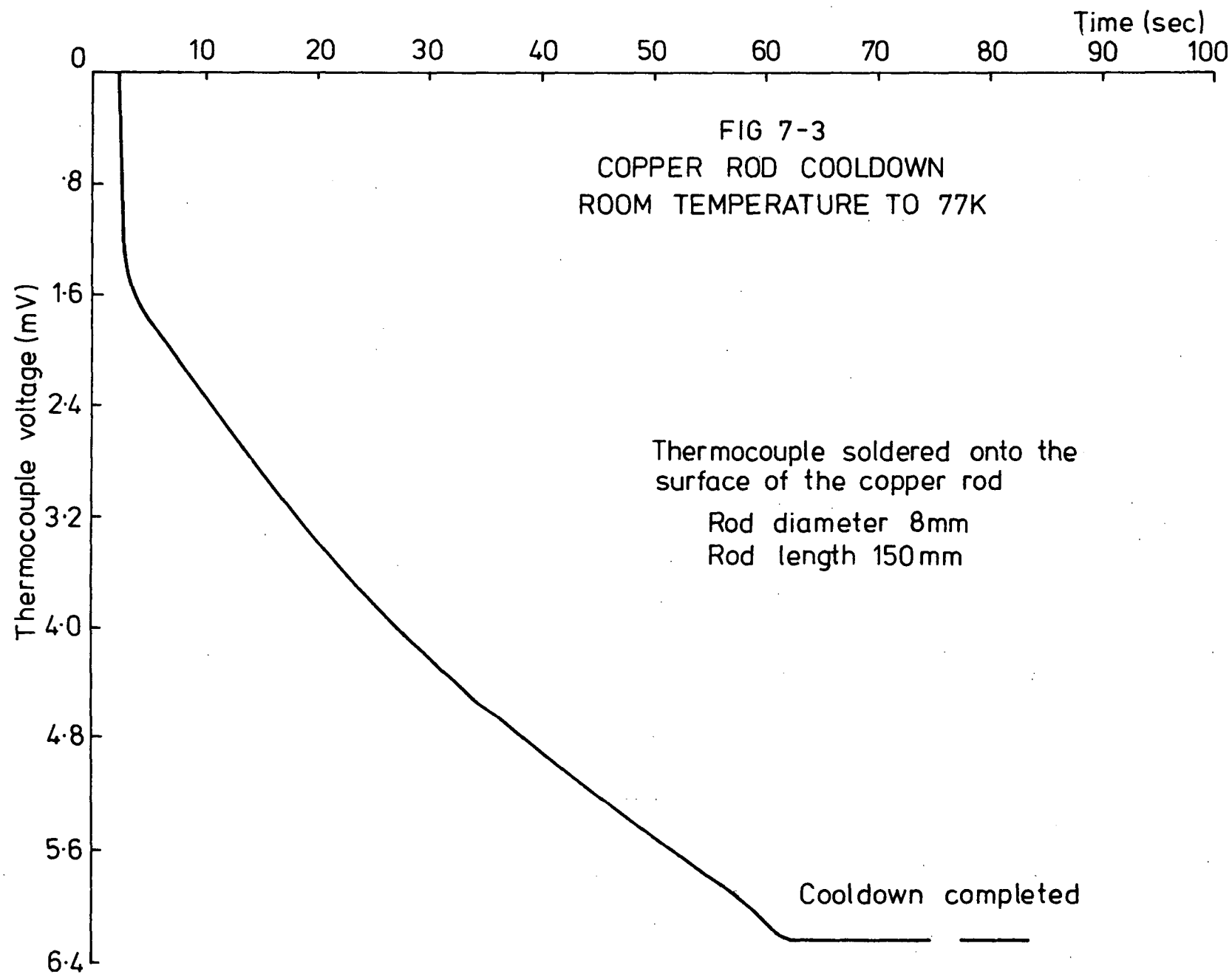
become uniform. However, this result only applied when the coolant flow rate was insufficient to give cooldown times comparable with times obtained by immersion of coils into a bath of coolant. This restriction applied because the maximum possible rate of liquid helium transfer was limited by the bore of the transfer tube and consequently was below that required to produce cooldown times comparable with those possible from sudden immersion into the coolant.

As the rate of cooldown depends almost entirely upon the rate of transfer of coolant, approximate times for cooldown can be calculated from the coil and cryostat enthalpy difference, the latent heat of vaporization of the coolant, and the rate of coolant transfer - equation 7-12.

$$\text{Time} = \frac{\Delta h}{QC_L - W} \qquad (7\text{-}12)$$

Δh = total enthalpy difference (joule)

Q = rate of liquid transfer (litre/hour)

C_L = latent heat of vaporization (joule/litre)

W = heat inleak to helium chamber (joule/hour)

As an example, the following data applied to the successful second helium experiment

Δh = 6500 joule

Q = 3 litre/hour

C_L = 2610 joule/litre

W = 0.5 watt = 1800 joule/hour

The estimated time for cooldown was thus 65 minutes which compared favourably with the observed value of 77 minutes.

Pressures within the helium dewar ranging from 20 to 130mm of mercury above atmospheric pressure were used to transfer the liquid

helium at a rate of three litres per hour. The lower pressure was sufficient with the 100 ampere leads in position, the higher pressure was necessary with the 430 ampere leads used in the test machine. The increased pressure was required as a result of the increased restriction to the escape of the boil off gases.

7-5 Conclusion

The time required for the bulk of the coil to attain equilibrium with its surface temperature was small; hence the time between the surface of the coil becoming superconducting and the entire coil becoming super-conducting would be short. This will result in a rapid drop in the apparent resistance as the coil goes into the superconducting state. This was found to be the case during the successful experiment in which the transition occurred within a matter of a second. This was an excellent and positive indication that the transition to superconductivity had taken place.

CHAPTER 8

CRYOSTAT AND INITIAL MACHINE PRELIMINARY TESTS

8-1 Introduction

Testing of the initial machine and the cryostats with liquid nitrogen
prior to the use of liquid helium was essential so that unforseen operational
difficulties were revealed and corrected. This chapter describes the
preliminary tests conducted and the results obtained. Tests were undertaken
to determine:

(a) the electrical and magnetic performances of the armature,
    compensating winding, and the field system;

(b) the dynamic performance of the armature;

(c) the possible effects of armature currents and commutation on
    the performance of the superconducting field coils;

(d) the heat inleaks to the field coil chamber of the cryostats;

(e) whether any modifications were required to remedy unforseen
    design errors or to simplify experimental procedures.

8-2 Armature and Compensating Winding

The initial machine was assembled but with the superconducting field
windings replaced, for testing purposes, with similar 400 turn, 21 B & S gauge
copper wire coils. Special care was taken during the assembly to ensure
that the compensating winding was positioned so that its magnetic field was
correctly aligned with the magnetic neutral axis of the field system.
On motoring the machine problems with the thrust bearing and armature
balancing were revealed. The correct positioning of the armature brushes
was obtained after noting that with incorrect brush positioning the
compensating winding acted as a source of field flux and the machine
motored without field excitation. The brushes were thus adjusted until
motoring without field excitation was eliminated.

The armature was driven by an auxilliary motor and readings of open circuit voltage for various field currents were taken. From these results the voltage rating of the machine, with the superconducting coils carrying a field current of 300 amperes and an armature speed of 1500 rpm, was calculated to be 70 volts - Appendix G. This is lower than the voltage estimated in section 5-4-2. The estimation of the voltage of the initial machine which was based upon the results of the tests on the model was only intended as an indication of the order of the voltage possible with the quantity of superconductor considered to be expendible if unforseen problems arose. As discussed in Chapter 4 the purpose of the model was to obtain flux distribution patterns and not precise magnitudes of flux densities.

The armature resistance was 2.9Ω and the resistance of the compensating winding, with the parallel connection, was 3.35Ω. Hence, the maximum possible generator armature current on short circuit, with a field current of 300 amperes and with the compensating winding in circuit, was limited to eleven amperes. The maximum output power as a generator available from the machine (with a load resistance of 6.4Ω) was approximately 200 watts. However, at this stage this limitation was not of importance in the initial helium test as it was concerned with testing of the cryostat and the investigation of the effects of armature reaction on the operation of the superconducting field coil with rated armature current.

8-3 <u>Field Coils</u>

To maintain the superconducting state in the field coils depended on ensuring that the temperature and maximum flux density were below their critical values.

The maximum magnetic field density occurred at the inner surface of the field coil. The maximum flux density produced by the substitute copper field coils was measured and then corrected for 300 ampere operation with the superconducting coil - Appendix G.

The maximum flux density thus calculated was 2.82 tesla, which was well below the critical value of 6.5 tesla at 300 amperes field current - Appendix H. Plotting of the coil load line on the critical current - flux density characteristics of the superconductor indicated that a current in excess of 400 amperes would be possible before the coil would quench due to excessive magnetic field - Appendix G. The margin between the working peak flux density at the field winding and the critical flux density was consistent with the design philosophy adopted at this stage in the research project.

8-4 Armature Reaction Cancellation

The armature reaction flux densities for the test machine configuration were predicted (Chapter 4) to be very small in the region of the super-conductor and the necessity for a compensating winding was thus questioned and investigated as discussed later.

The measured flux distributions in the region of the field coils of the test machine (figure 8-1) revealed armature reaction flux densities near ten gauss which was more than three orders of magnitude below the critical field of the niobium-titanium superconductor. The flux distributions also indicated that complete cancellation was not possible with the configuration adopted and in fact the compensating winding flux reinforced the armature flux in some areas instead of cancelling it. However, with such small flux densities complete cancellation was not considered as necessary as originally envisaged for the correct operation of the superconductor. The unsymmetrical flux distribution about the field pole centre line was caused by the combination of the odd number of armature and compensating winding coils and irregularities in the iron stator.

The purpose of the compensating winding was to protect the field coils from changing armature fluxes caused by varying armature load currents and to reduce forces on the field coils due to the load torque of the machine.

FIG 8-1
INITIAL MACHINE
ARMATURE FLUX DISTRIBUTION
IRON CORE, YOKE, AND POLE FACES

Field plots along A-A
mid-height

—— Radial Component

--- Circumferential Component

Exitation current 6 ampere
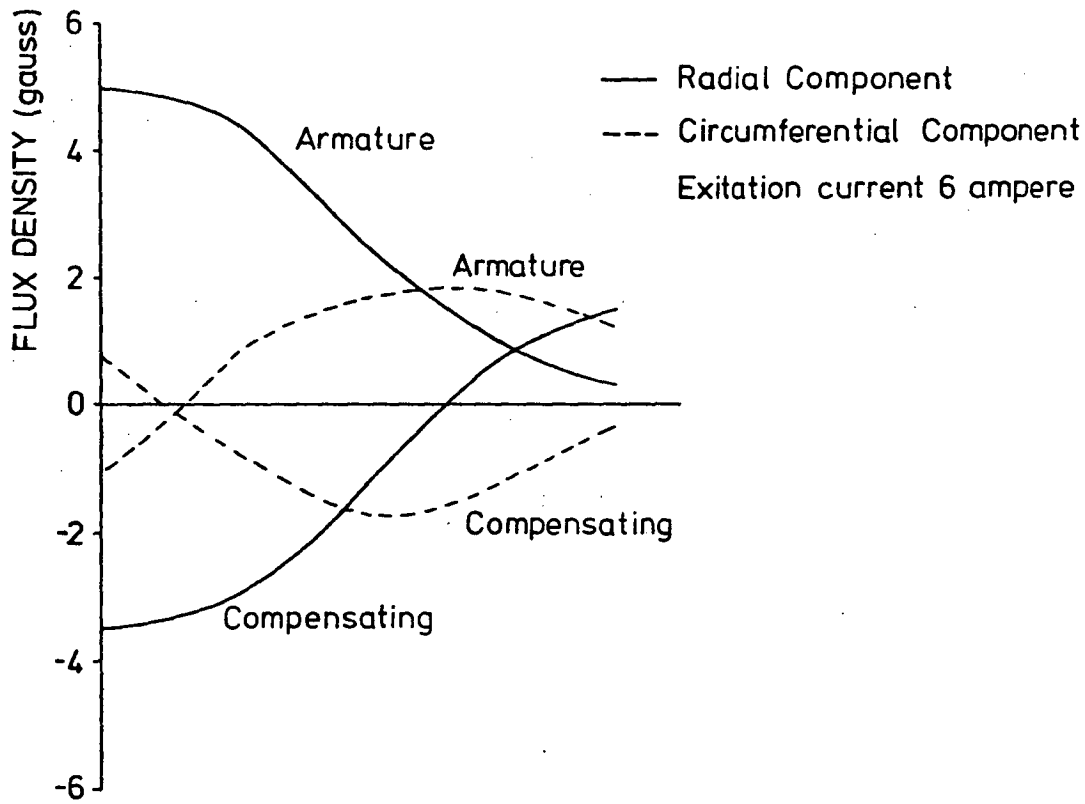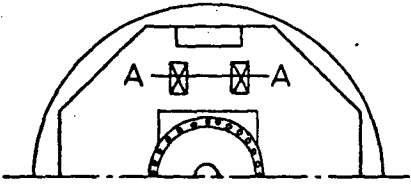
The compensating winding, however, did not shield the field coils from fluxes due to changing current in the coils undergoing commutation. Measurement of the voltage induced in the field coil from these currents revealed the following:

(a) The compensating winding had little or no effect on the induced voltage with a steady armature current.

(b) The induced voltage had two frequency components. One component corresponded to the commutation frequency, which produced spikes in the induced voltage, and the other component corresponded to the speed of rotation.

The induced voltage was near 10mV at 1500 rpm and 5 ampere armature current which corresponded to a very small flux density. Hence, losses induced into the superconductor as a result of armature coil commutation were considered to be negligible. It should be noted that a secondary effect of the copper radiation shield in the cryostat would be to shield the coil from alternating fluxes.

8-5 Cryostat Tests

The first cryostats completed relied only on vacuum and the nitrogen cooled radiation shield for thermal insulation. It was intended that the cryostats were to be continuously pumped so bake-out procedures were not used. With the cryostats filled with liquid nitrogen a vacuum pressure of 2 x 10^{-6} torr was obtained after forty-eight hours of pumping. It was evident that to maintain this low pressure, continuous pumping was necessary as degassing within the cryostats was considerable. Superinsulation was used in subsequent cryostats - Chapters 10 and 12.

The vacuum gauge head was positioned for convenience near where the vacuum line to the cryostat was connected to the pump. This meant that the gauge reading could have been different from the actual pressure within the cryostats. It was considered that the indication given by the vacuum

gauge was sufficient to determine the adequacy or otherwise of the vacuum within the cryostat. For example, with the gauge reading a pressure of 1.5×10^{-5} torr, a mist formed on the chimney of the cryostat when the radiation shield was cooled to 77K but with a vacuum reading of 5×10^{-6} torr, no mist formed. The corresponding heat inleaks, with the inner container approximately half filled with liquid nitrogen, were 2.4 watts and 1.45 watts respectively.

The method adopted for determining the heat inleak to the cryostat relied on the volumetric ratio of gaseous nitrogen at room temperature and pressure and liquid nitrogen temperature of 77K. The time taken for the boil-off gases to displace a predetermined fixed volume of water was recorded and, taking into account the saturation vapour pressure of water in air, the heat inleak was calculated.

For the heat inleak experiments, the liquid helium section of the cryostat was initially filled to within 200mm of the top of the chimney section with liquid nitrogen and the heat inleak was recorded as the level of the liquid nitrogen fell, both with and without the radiation shield cooled with liquid nitrogen. The patterns of the heat inleaks with and without the radiation shield cooled as the level fell were similar; starting at a high heat inleak (which was to be expected because of the close proximity of ambient conditions) and falling to a final constant value which was taken as the heat inleak for the conditions under investigation. The heat inleaks stabilised with the liquid nitrogen level at the lower extremity of the counter flow cryogenic current leads.

The effect of an inadequate vacuum and the cooling of the radiation shield with liquid nitrogen on the heat inleak into the coil chamber of the cryostat indicated the necessity for a vacuum, as indicated by the gauge head, of below 2×10^{-6} torr as well as the cooled radiation shield - figure 8-2. Pressures below 10^{-6} torr were not necessary as the heat

FIG 8-2
FIRST CRYOSTAT HEAT INLEAK
300 ampere leads in position
but not carrying current
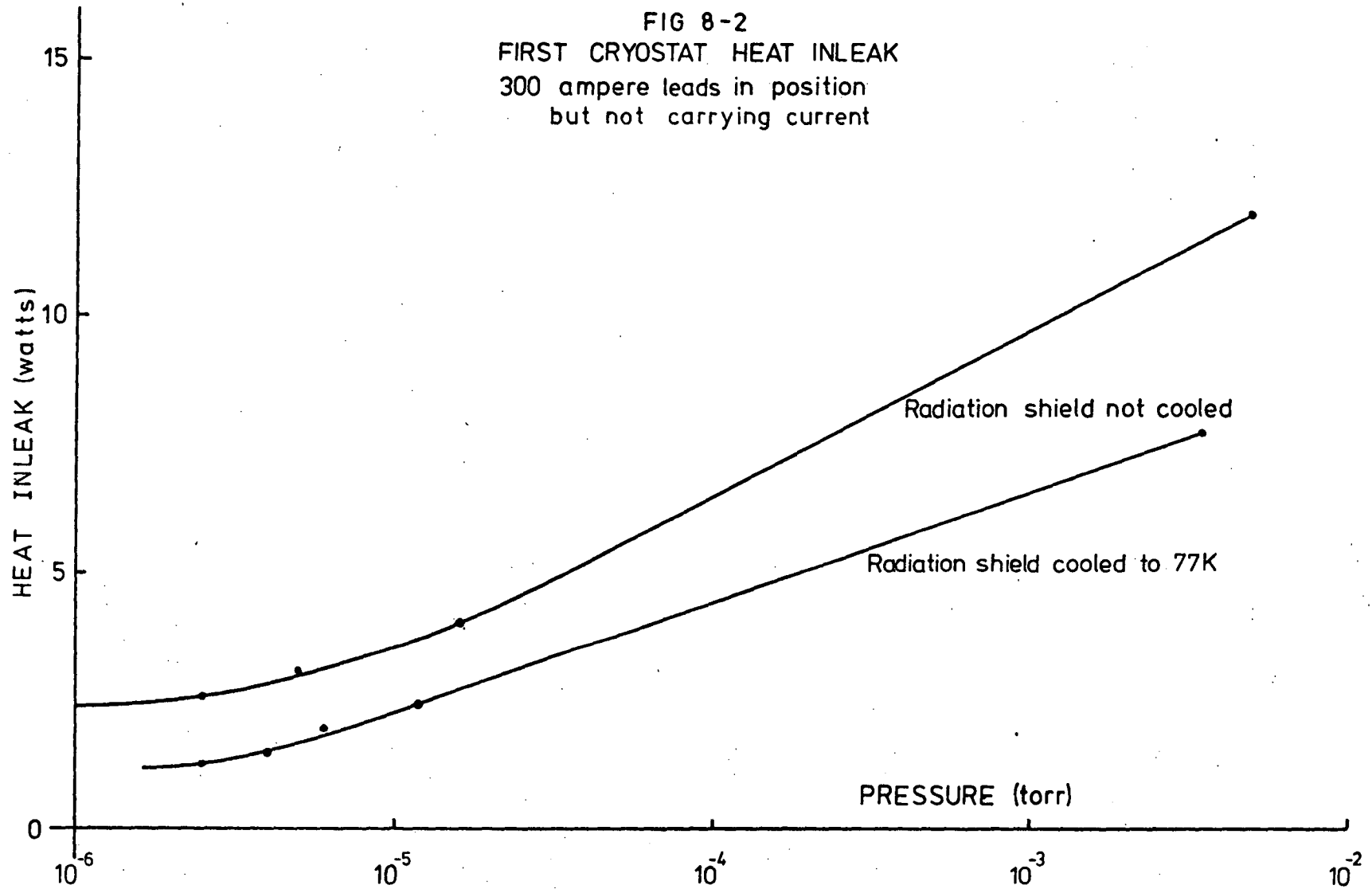
inleak did not decrease significantly with further reductions in the pressure.

The liquid nitrogen tests indicated that the welds in the cryostats were free from leaks which only appeared at cryogenic temperatures, and that the demountable indium seals were performing as required.

8-6 Conclusions

The design of the initial machine allowed flexibility in its operation in that many configurations could be investigated. The armature and the compensating windings had sufficient ampere conductors so that useful results would be obtained on the influence of armature reaction fluxes on the superconducting field coil.

The observed magnitude of the heat inleak was very near that calculated in Chapter 6 with the leads operating into liquid nitrogen. As the leads are the primary source of the heat inleak and the heat inleak into liquid nitrogen is greater than that into liquid helium, as indicated in Chapter 6, it was evident that the cryostats were satisfactory for a run with liquid helium.

CHAPTER 9

FIRST LIQUID HELIUM RUN

9-1 Introduction

After the tests with liquid nitrogen indicated that adequate vacuum could be maintained in the insulation space of the cryostats, shown in figure 5-3, and that the heat inleak to the coil chamber could be attributed to the expected heat inleaks introduced by the coil cryogenic supply leads, a dewar of liquid helium was imported.

The superconducting state was not achieved because a thermal short circuit occurred within the cryostat. However, the experience gained in the handling of liquid helium and the design and operation of the cryostats was invaluable. As a result of the experiment a number of alterations were made to the design of the machine and cryostat.

9-2 Test Run

A forty volt, 350 ampere battery supply with a variable water resistor was used for the supply of the superconducting coil excitation current. A twelve channel ultra-violet light recorder was used to record:

(a) the armature terminal voltage;

(b) the armature current;

(c) the voltage between the terminals of the superconducting coil;

(d) the superconducting coil current, and

(e) the flux density in the vicinity of the superconducting coil.

9-2-1 Coil Supply Lead Voltage Drop

To give an indication as to the state of superconduction in the field

coil and the operation of cryogenic supply leads, it was necessary to have an estimate of the voltage drop between the cryogenic lead terminals at the top of the chimney under normal operating conditions.

The voltage drop was calculated from

$$V = 2 \int_0^{\ell} \rho \frac{I}{A} dx \tag{9-1}$$

where V = voltage drop (volt)

ρ = resistivity (ohm-cm)

ℓ = lead length (cm)

A = cross sectional area of the cryogenic leads (cm^2)

I = current (amp)

x = distance from the helium extremity of the lead (cm).

For the lead design A was a constant, hence equation 9-1 became:

$$V = \frac{2I}{A} \int_0^{\ell} \rho \, dx \tag{9-2}$$

From the optimum lead temperature profile (figure 6-4) and the resistivity data (Appendix E), the resistivity profile of the leads was approximated, as given below, for the evaluation of the intergration.

From figure 6-4 the temperature profile was approximated by:

$$\begin{matrix} 0 < x < 40\text{cm} & T = 1.45x + 4.2K \\ 40 < x < 65\text{cm} & T = 10x - 350K \end{matrix} \tag{9-3}$$

From the resistivity data,

$$\begin{matrix} T > 45K & \rho/\rho_{300} = T/255 - 0.1765 \\ T < 45K & \rho/\rho_{300} = 0 \end{matrix} \tag{9-4}$$

Combining sets of equations 9-3 and 9-4 the resulting resistivity profile was:

$$0 < x < 35.6\text{cm} \quad \rho/\rho_{300} = 0$$

$$35.6 < x < 40\text{cm} \quad \rho/\rho_{300} = \frac{1}{255}(1.145x - 40.8) \quad (9-5)$$

$$40 < x < 65\text{cm} \quad \rho/\rho_{300} = \frac{1}{255}(10x - 395)$$

The value of the intergration in equation 9-2 was $2.17*10^{-5}$ $\Omega\text{-cm}^2$, with $\rho_{300} = 1.7*10^{-6}$ $\Omega\text{-cm}$. The voltage drop for the optimized leads with the optimum current was hence calculated as 0.12 volts.

The lead voltage drop was also estimated as follows. Using the Wiedemann-Franz Law in equation 9-1,

$$V = 2I \int_{0}^{\ell} \frac{TL}{AK} \, dx \qquad (9-6)$$

T = temperature (Kelvin)

K = thermal conductivity (Watt-cm)

L = Wiedemann-Franz constant

Substituting for $\frac{I}{AK}$ from equation 6-5 and using the value of D_{opt}, equation 9-6 becomes:

$$V = 2 \sqrt{L \, D_{opt}} \int T(Z) \, dZ \qquad (9-7)$$

Since equation 9-7 is independent of current and the Z temperature profile for optimum conditions is invariant, the lead voltage drop under optimum conditions is independent of the lead design and current. The voltage obtained from equation 9-7 was 0.167 volts which compares favourably with the previously obtained value of 0.12 volts. A loss of the superconducting state would be indicated if the voltage between the lead terminals exceeds these values.

9-2-2 Vacuum

After twenty-four hours of continuous pumping, a pressure of $7*10^{-6}$ torr was achieved with the cryostat at room temperature. With the

radiation shield nitrogen chambers filled, the pressure dropped to $2*10^{-6}$ torr. Three times during the course of the experiment the pressure increased for periods of less than fifteen seconds to 10^{-4} torr. The pressure returned to $2*10^{-6}$ torr each time. The losses of vacuum were attributed to sudden degassing within the cryostats rather than the formation of leaks at the reduced temperatures.

9-2-3 Pre-Cooling

Liquid nitrogen was introduced into the coil chambers to pre-cool the superconducting coils to a temperature of near 77K. The resistance of the coil was monitored so that the transfer of nitrogen could be stopped as soon as the temperature of the coil, as indicated by the resistance, was just in excess of 77K. This method of pre-cooling ensured that very little or no liquid nitrogen remained in the cryostats before the transfer of the helium into the cryostat was commenced.

Throughout the experiment the liquid nitrogen level in the radiation shield coolant chamber was maintained above the heat plug.

9-2-4 Coil Cooldown

The method adopted for transferring the helium was to pressurise the helium dewar with its boil-off gas, hence forcing the helium into the cryostats. The pressure was maintained by periodically squeezing an inflated football bladder which was connected over one of the outlets of the helium dewar - thus introducing heat into the dewar - Chapter 2.

To prevent an excessive build-up in pressure within the helium dewar, as a result of the rapid cooling of the end of the transfer tube, the transfer tube was slowly lowered into the liquid helium. The only escape paths for the resultant helium gas were via the transfer tube and via a pressure release valve which was an integral part of the dewar. Operation

of the pressure relief valve was not wanted as it meant the loss of a small quantity of coolant which could aid the cooling of the transfer tube and cryostat. During transfer of the helium, the release valve was permanently closed unless an over-pressure occurred whence it was opened manually. The pressure within the dewar was monitored continuously and maintained at a safe level. In the event of a sudden and dangerous over-pressure within the dewar, a secondary, high pressure release valve, which was also an integral part of the dewar, would operate.

The pressure required to maintain the transfer of helium was 16 to 22 mm of mercury. If the pressure rose to near 26 mm of mercury the rate of transfer was excessive and led to inefficient cooling of the cryostat. At a lower pressure of 13 mm of mercury the transfer of helium ceased. A carbon resistor thermometer situated near the outlet of the helium transfer tube in the cryostat indicated whether or not helium at 4.2K was being transferred.

The helium boil-off gases were necessarily allowed to escape from the top of the cryostats after passing over the leads to the atmosphere with consequent freezing of external sections. This was, however, character-istic of the cooldown process because as soon as any liquid helium came in contact with the coil it would immediately vaporize, thus leading to large quantities of gaseous helium which escaped from the cryostats.

With the equipment available only one cryostat at a time could be filled; hence it was necessary that the heat inleaks to the cryostats would be small enough to allow one cryostat to be filled whilst the other maintained its charge of helium. A hoist was built so that the dewar and the transfer tube could be lifted together, thus avoiding the wasteful process, in terms of liquid helium consumption, of removing the transfer tube from the dewar. Estimated heat inleaks to the cryostats indicated this would have allowed the alternate filling and topping up of the cryostats

without incurring excessive losses of helium.

The resistance of the superconducting coil was monitored with a sensitive resistance bridge to give an indication as to the progress of the cooldown and to indicate the transition to the superconducting state. The resulting cooldown curve (figure 9-1) gave the ratio of the coil room temperature resistance to the lowest resistance obtained when the liquid helium was exhausted as 182 which corresponded to a mean coil temperature of approximately 20K. The transition to the superconducting state was not achieved for the unforeseen reasons given below.

In the later experiments the coil resistance was monitored by measuring the voltage drop on the coil cryogenic supply leads and the field coil constant current of 10mA. This technique was adopted as the voltmeter did not require balancing, unlike the resistance bridge, and it was also used to monitor the performance of the superconducting coil whilst carrying the required machine field excitation current.

The irregular section of the cooldown curve after two hours of cooling was due to the liquid helium level in the dewar falling below the extremity of the transfer tube; hence causing the cessation of the transfer of helium. This was rectified by lifting the dewar with the hoist until the transfer tube rested on the bottom of the dewar. This should have been done when the transfer tube was initially inserted into the helium dewar, but was overlooked.

Midway through the cooldown, frost formed at the lower end of the chimney. This had not occurred during the previous liquid nitrogen tests and it was assumed that relative contraction due to the further reduction in temperatures had caused contact between the radiation shield and the lower end of the chimney. The effectiveness of the radiation shield was thus greatly reduced. Susequent dismantling of the cryostat showed the above explanation of the frosting to be correct.

FIG 9-1
FIRST LIQUID HELIUM RUN
SUPERCONDUCTINC COIL COOLDOWN
COIL RESISTANCE ~ TIME

Loss of helium transfer

Helium exhausted

SUPERCONDUCTING COIL AND CRYOGENIC LEAD RESISTANCE (ohm)

TIME (minute)
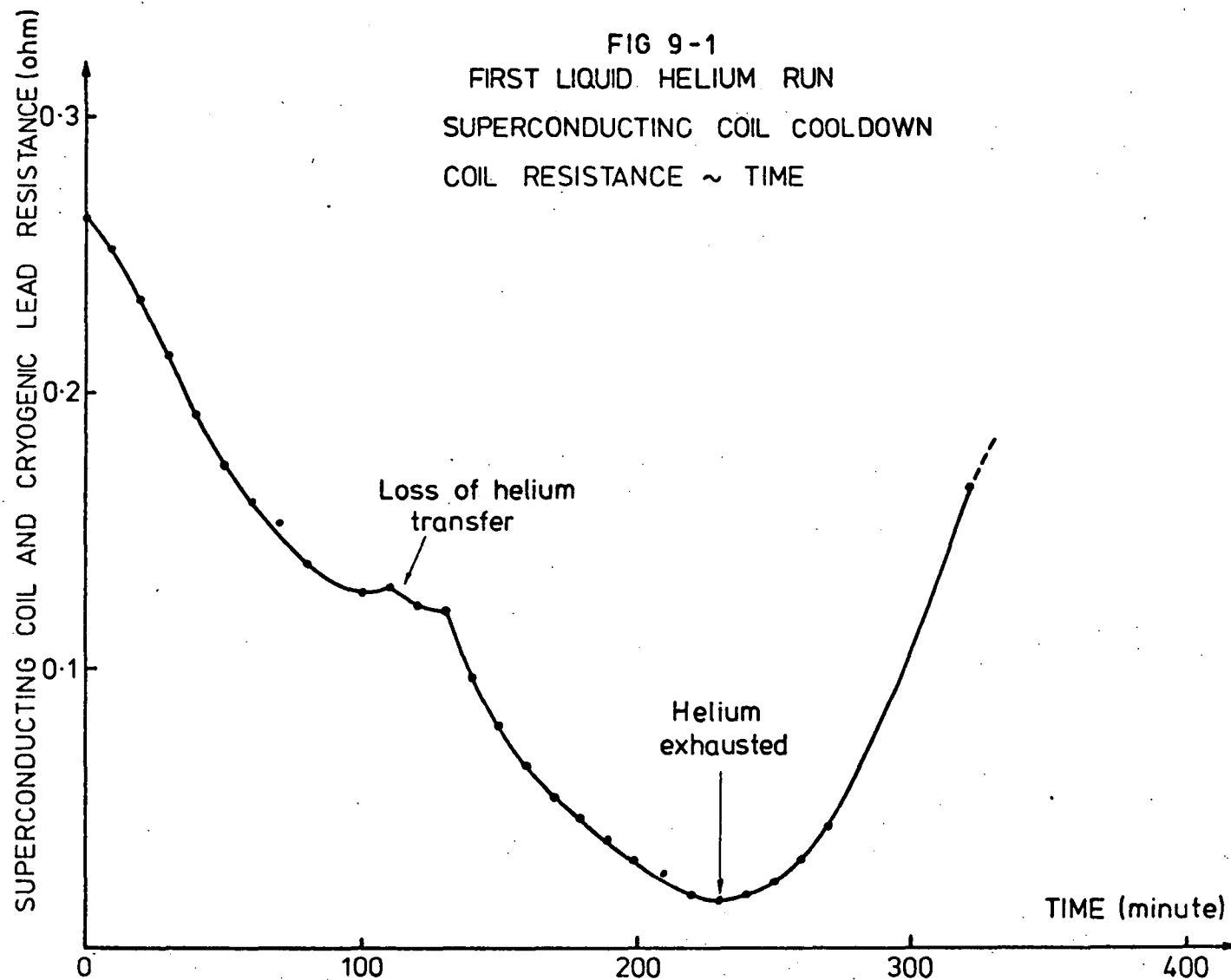
9-3 <u>Results</u>

The cooldown curve (figure 9-1) indicated that a mean coil temperature of near 20K was achieved. This meant that only one to two litres more of liquid helium should have been required to reduce the temperature into the superconducting region. The difference between the weights of the dewar before and after the test revealed that only twenty-two litres of liquid helium were supplied instead of thirty litres which was the capacity of the dewar. Thus it was apparent that with a full dewar the superconducting state would have been achieved despite the thermal short circuit and therefore with the correct allowance for contraction in the cryostat the experiment would have been successful.

Before the experiment was conducted, it was estimated that the cool-down from near 77K to 4.2K should have taken approximately one and a half hours. This time was based on estimated rates of helium transfer and the amount of heat to be removed during cooldown. Even with a heat inleak of 0.5 watts to the coil chamber, the cooldown of one cryostat should have required approximately five litres of liquid helium - not the twenty-two litres as indicated by the test run. This showed that the thermal short circuit resulted in excessive heat inleak to the helium chambers.

9-4 <u>Discussion</u>

The experience gained during the run was invaluable as it highlighted a number of points in connection with the design and the operation of the cryostats. For example, the unwarranted fears that the insertion of the transfer tube into the dewar would result in large quantities of helium gas and consequent high pressures within the dewar and that the method of helium transfer may not work were quelled. However, problems associated with the operation of the superconducting field coil remained unanswered and they could not be readily answered until the superconducting state

was achieved.

A critical look at the entire system revealed that further improvements could be made in the insulation of the cryostats, prevention of the thermal short circuit at the lower extremity of the cryostat chimney and in the insulation of the transfer tube which was uninsulated at its end sections.

Further tests revealed that the frost deposit which formed at the bottom of the chimney did not occur until the radiation shield coolant chambers were filled with liquid nitrogen. The movement of the radiation shield with the contraction of the shield coolant chambers caused the radiation shield to come into contact with the room temperature sections of the cryostat. This would have caused the temperature of the radiation shield to be well above 77K, hence nullifying the effectiveness of the radiation shield. This fault was rectified by providing more clearance between the radiation shield and the outer sections of the cryostat which was later successfully operated.

The insulation of the cryostat used during this test relied entirely on vacuum and the radiation shield. The tests with liquid nitrogen indicated that this insulation was adequate, but as a result of the test with the helium it was prudent to further reduce all sources of heat inleak. Further improvements in the insulation were possible with the use of layers of superinsulation within the vacuum space. This improved method of insulation was used in subseqeunt cryostats.

The transfer tube had uninsulated end sections which were approximately 200 mm long. This, in effect, exposed the liquid helium within the transfer tube which was entering the cryostat to the boil-off gases which had temperatures above the boiling point of liquid helium. This exposure would have introduced unnecessary losses of liquid helium during the

transfer process and had to be rectified. The temperature between the boil-off gases and the transfer tube is maintained by the heat inleak from the cryogenic leads. As the difference in the temperatures between the liquid and the gaseous helium, at the extremity of the transfer tube, was not large it was sufficient to insulate the end sections with teflon tubing.

It was apparent that simultaneous operation of two cryostats from the single dewar of liquid helium would not be possible unless rates of helium loss and the cooldown time could be greatly reduced. This led to the decision to redesign the machine and to incorporate a normal conducting field winding, thus eliminating the need to operate two superconducting field coils simultaneously. This would operate as satisfactorily from the machine point of view as all the information concerning the operation of the superconducting field coil would be obtained with one coil as with two.

9-5 Conclusion

The great value of this test was mainly in the experience obtained in the operation of the cryogenic components, the highlighting of defects in the design of the cryostat, and the consequent decision to alter the designs of the machine and cryostat. It was also concluded that even more stringent testing with liquid nitrogen would in future be carried out on the cryostats so that problems, such as that experienced with the radiation shield or any other problem, should not occur during future liquid helium runs.

CHAPTER 10

INITIAL MACHINE RE-DESIGN AND TESTS

10-1 Introduction

It was apparent from the first test with the liquid helium that
modifications in the design of the initial machine were necessary. The
modifications were required to reduce the demand for liquid helium below
that encountered during the cooldown and operation of the superconducting
coils in the first helium test. This was achieved by introducing super-
insulation, improving the design of the cryostats, rectification of the
fault with the shield coolant chamber, and replacing one of the super-
conducting coils and cryostat with a conventional field winding. The
following chapter discusses the implementation of the improvements and the
tests which were conducted to verify their effectiveness.

10-2 Cryostat Helium Loss Reduction

The demand for liquid helium was halved when the decision to use only
one superconducting field coil was made; however, further reductions in
helium demand below that with the thermal short were necessary. The heat
inleaks to the cryostat were through the insulation, through the current
leads and through the thermal short. The insulation was improved upon by
the introduction of alternate layers of fibreglass matting and aluminized
mylar sheeting which completely occupied the vacuum space between the
radiation shield and the outer and inner sections of the cryostat.

Although the counterflow current leads were designed to give the
minimum heat inleak, they still introduced the majority of the total heat
inleak to the helium in a properly insulated cryostat. The only option
available to further reduce the heat inleak introduced by the leads was to
redesign them for a reduced operating current. A reduction in the operating
current to one-hundred amperes was decided upon as it was considered that

initially it was important to achieve the superconducting state. Attempted operation at the higher current would have incurred the possibility of not achieving the state of superconduction because of the higher lead heat inleak associated with the 300 ampere current, three times that for 100 ampere, and the subsequent faster consumption of the liquid helium.

The design of the 100 ampere leads was along the same lines as the 300 ampere leads, but the cross-sectional area of the 100 ampere conductors was one-third that of the 300 ampere conductors. As both leads were optimized, the temperature profile and the voltage drop with optimum current flowing were the same. The reduction in the current by two-thirds theoretically reduced the lead heat inleak by two-thirds.

The unmodified cryostat was insulated with superinsulation and reassembled, but without the coil and leads in position. This enabled the ambient heat inleak of the cryostat alone to be measured. The cryostat was reassembled unmodified so that a check on the validity of attributing the excessive heat inleak encountered during the helium test to the thermal short.

With the radiation shield cooled with liquid nitrogen, it was evident that the problem of the frost formation at the base of the chimney section remained as expected. Tests were conducted without the cryogenic leads and the heat inleaks to the liquid nitrogen in the coil chamber were 0.41 watt and 1.08 watt with and without the radiation shield cooled. The vacuum gauge indicated a pressure in the range of 4×10^{-7} torr to 6×10^{-7} torr. With the one-hundred ampere leads in position and carrying no current, the heat inleaks were 0.77 watt and 1.30 watt respectively.

Inspection of the cryostat with the nitrogen chamber filled indicated that the resulting contraction of the nitrogen chamber was greater than that allowed for. This, combined with an incorrectly positioned radiation shield, caused contact between the radiation shield and the lower end of the outer chimney section.

The cryostat was rebuilt with the coil and the leads in position. A greater clearance between the radiation shield and the outer sections of the cryostat was provided, thus eliminating the possibility of contact between these sections as a result of differential thermal contraction.

Tests on the cryostat showed that the problem with the differential thermal contraction, which led to the thermal shorting and consequently the reduction in the effectiveness of the copper radiation shield, had been successfully eliminated; as a result the heat inleaks were reduced. With liquid nitrogen in the coil chamber and the 100 ampere leads positioned, the heat inleaks were 0.97 watt without the shield cooled with liquid nitrogen and 0.57 watt with the shield cooled. Prior to the cryostat reconstruction, the corresponding heat inleaks were 1.3 watt and 0.77 watt. The heat inleak with the shield cooled was actually below the estimated value of 0.68 watt, which was calculated as the 100 ampere lead heat inleak to liquid nitrogen with no current flow.

With the radiation shield cooled to a uniform temperature equal to that of liquid nitrogen the only heat inleak to the coil chamber with it filled with liquid nitrogen would be via the cryogenic leads and the stainless steel of the chimney. With the thermal short circuit and without the leads the heat inleak was measured as 0.41 watt with the shield cooled. With this configuration the heat inleak should have been less than 0.1 watt. With the leads in position and the thermal short removed the corresponding heat inleak was 0.57 watt which could all be attributed to the leads. It was quite clear that the thermal short removed the effectiveness of the shield even at liquid nitrogen coil chamber temperatures. The reduction in effectiveness would have been amplified with the coil chamber at liquid helium temperatures. The conclusion can be made that the thermal short was the major contributing factor to the excessive heat inleak encountered during the helium test.

The above results also indicated that the cryostat had been significantly improved and that it was ready for a second attempt at achieving the super-conducting state and tests on the machine with the superconducting coil in operation.

10-3 Field Flux Patterns

To reduce the demand for liquid helium, one of the superconducting field coils was replaced with a conventional type of field coil. The replacement coil was obtained from an old machine and had 3935 turns of 25 B & S copper wire. The conventional field coil required an iron core to produce the necessary field flux; hence the field flux density distributions produced by the conventional and superconducting coils were different.

The field flux pattern of the superconducting coil (figure 10-1) had a similar shape to that obtained with the model - figure 4-22. The introduction of the iron core resulted in the component of the field flux near the conventional pole due to the superconducting coil being a larger fraction of the total superconducting coil field flux than obtained in the model. The field flux pattern of the conventional pole (figure 10-2) indicated that a current of 0.215 amperes in the conventional winding resulted in equal total pole fluxes with a superconducting coil excitation current of 100 amperes.

To avoid circulating armature current in D.C. machines with more than two poles, the field flux of each pole must be equal. As this is not always possible, armature equalising connections are used to avoid excessive current densities at the brushes of the machine due to circulating currents. Circulating currents cannot occur in two pole D.C. machines, unless a gramme ring type winding is used; hence unequal pole fluxes can be tolerated. Difficulty with operation under this condition could arise from uneven torque loading of the armature surface and different attractive forces, if iron is retained in the armature, between poles and the armature.

FIG 10-1
SUPERCONDUCTING COIL FIELD
FLUX DISTRIBUTION

Current 100 ampere

Centre of the superconducting field
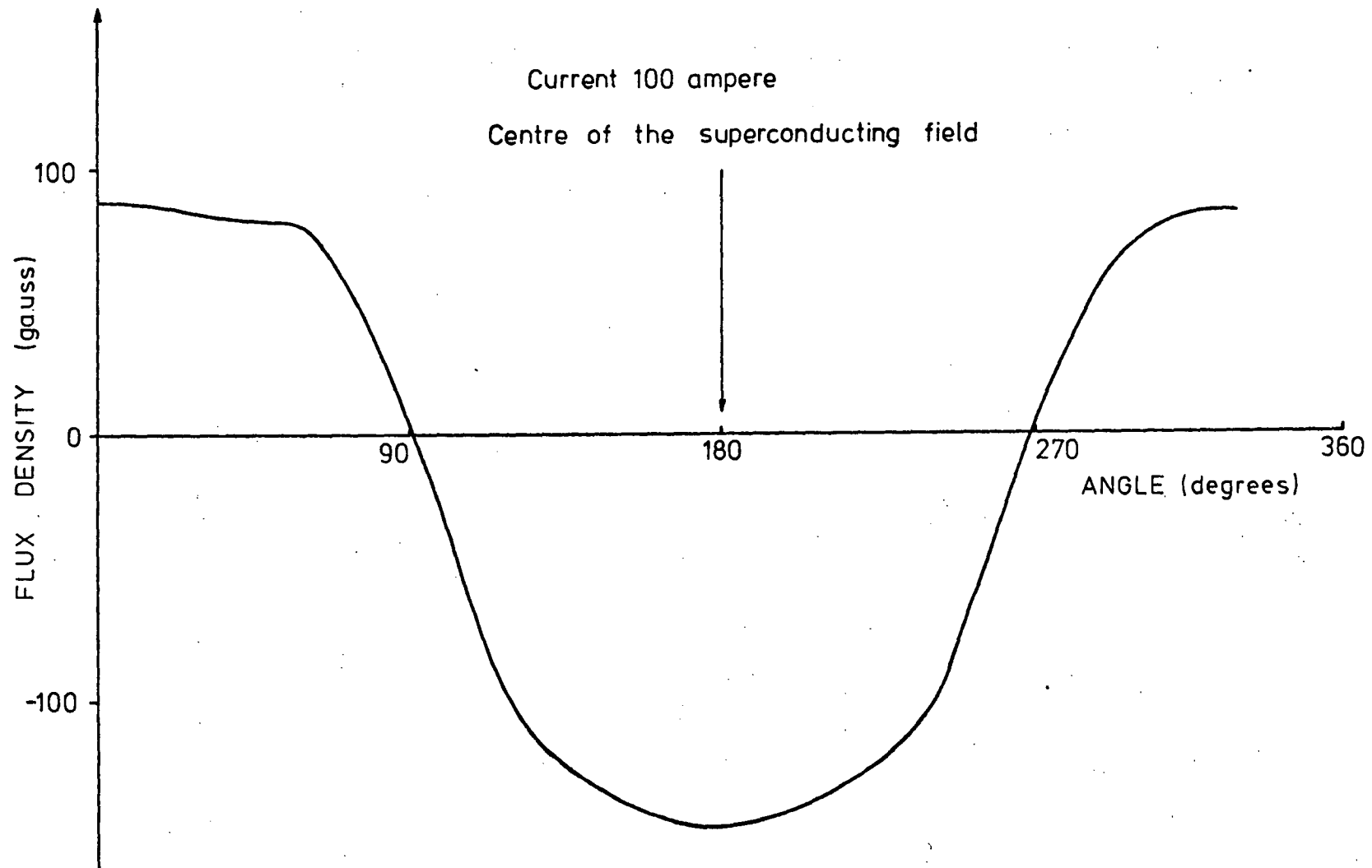
FIG 10-2
CONVENTIONAL FIELD
FLUX DISTRIBUTION

Current 0·25 ampere

Centre of superconducting field
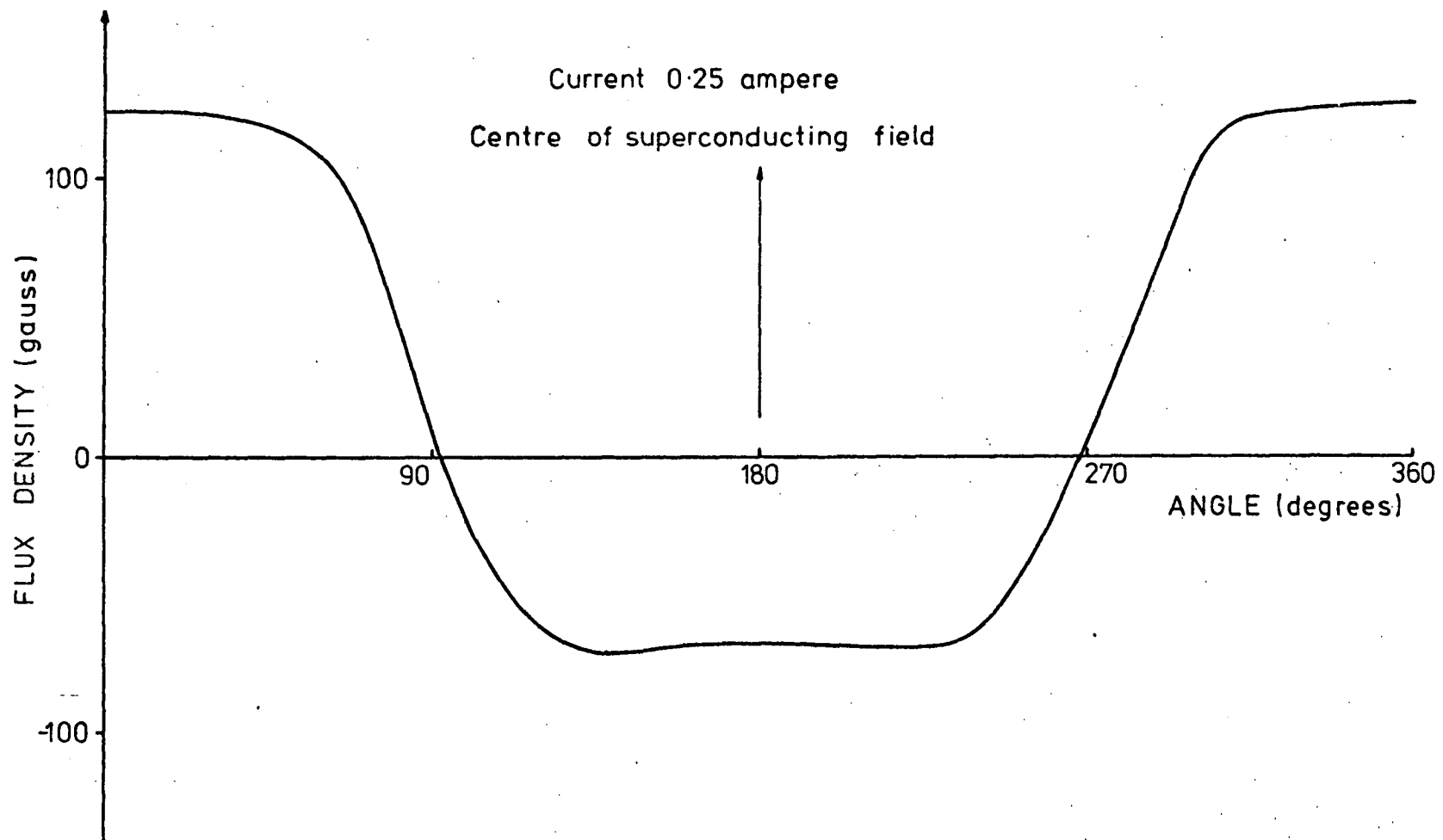
Further tests indicated that with 100 amperes flowing in the super-
conducting coil, the generated voltage would be 17 volts which, although
an order of magnitude below that initially aimed for, was in accordance
with the estimates in Chapter 8.

As discussed in Chapter 8, at this stage in the project the rating of
the machine was of secondary importance to achieving the superconducting
state and the collection of initial data on the influence of armature
reaction on the operation of a superconducting field coil.

10-4 Moisture Problem

A cause of loss of vacuum was the freezing of moisture which had
collected between the surfaces of the indium seals. During the tests on
the initial cryostat to determine the cause of the frost deposit it was
found that after several cooling cycles loss of vacuum occurred during the
cooldown process. On returning the cryostat to room temperature, the
vacuum leaks self sealed and the required vacuum was again achieved. The
loss of vacuum made the operation of the cryostat impossible; hence it
was dismantled and the cause of the problem was found to be moisture which
had collected between the stainless steel sealing surfaces of the indium
seals. On cooling, the moisture froze and expanded, thus breaking the
indium wire seals.

The problem was solved by introducing further control over the ingress
of moisture and fitting top pieces to the cryostat which prevented the
entry of moisture into the cryostat.

10-5 Automatic Radiation Shield Coolant Transfer

To eliminate the manual refilling of the radiation shield coolant
chamber and to allow extended periods of unattended cryostat precooling,
a controller which maintained the required level of liquid nitrogen was
developed. A simple controller based on copper-constantan thermocouple

detectors and high gain amplifiers maintained the required precoolant level except in the presence of strong electromagnetic wave interference, such as close proximity radio frequency transmissions, which caused false triggering of the logic circuitry. Normal local radio station transmissions had no effect on the operation of the automatic filler.

A thermocouple within the nitrogen supply dewar was used as a reference and two thermocouples within the nitrogen chamber of the cryostat were used for the high and low detectors. A fourth thermocouple near the bottom of the dewar served as a master shut down if the liquid nitrogen supply was exhausted. After amplifying the thermocouple voltages by a factor of 250, the logic section controlled the power supply to a nitrogen transfer valve. A schematic diagram of the automatic filler is given in figure 10-3.

10-6 Conclusion

The substantial reduction in the heat inleak to the cryostat and the improvements made in the operating techniques combined with the fact that the superconducting state was very nearly achieved during the first test with liquid helium to indicate that the machine was ready for a second test with liquid helium and that the superconducting state would be achieved. A plan of the rebuilt machine is given in figure 10-4 and a photograph in figure 10-5.

FIG 10-3
NITROGEN LEVEL CONTROLLER

High
level

Low
level

Reference

Supply
dewar
empty

Amplifiers

Comparitors

Logic

Nitrogen
transfer
solenoid

Copper constanton
thermocouple level
detectors
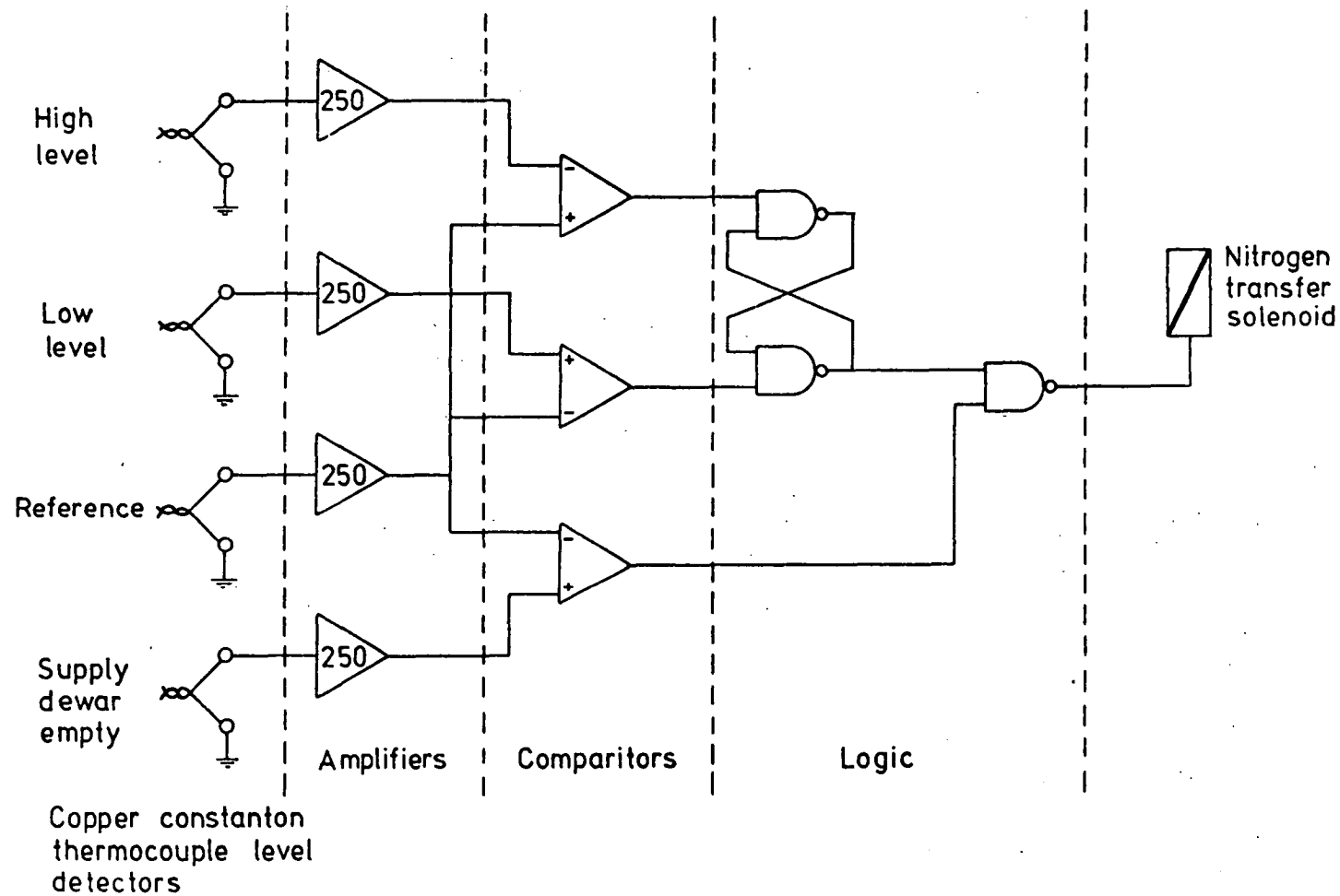
FIG 10-4
SECTION THROUGH MODIFIED MACHINE
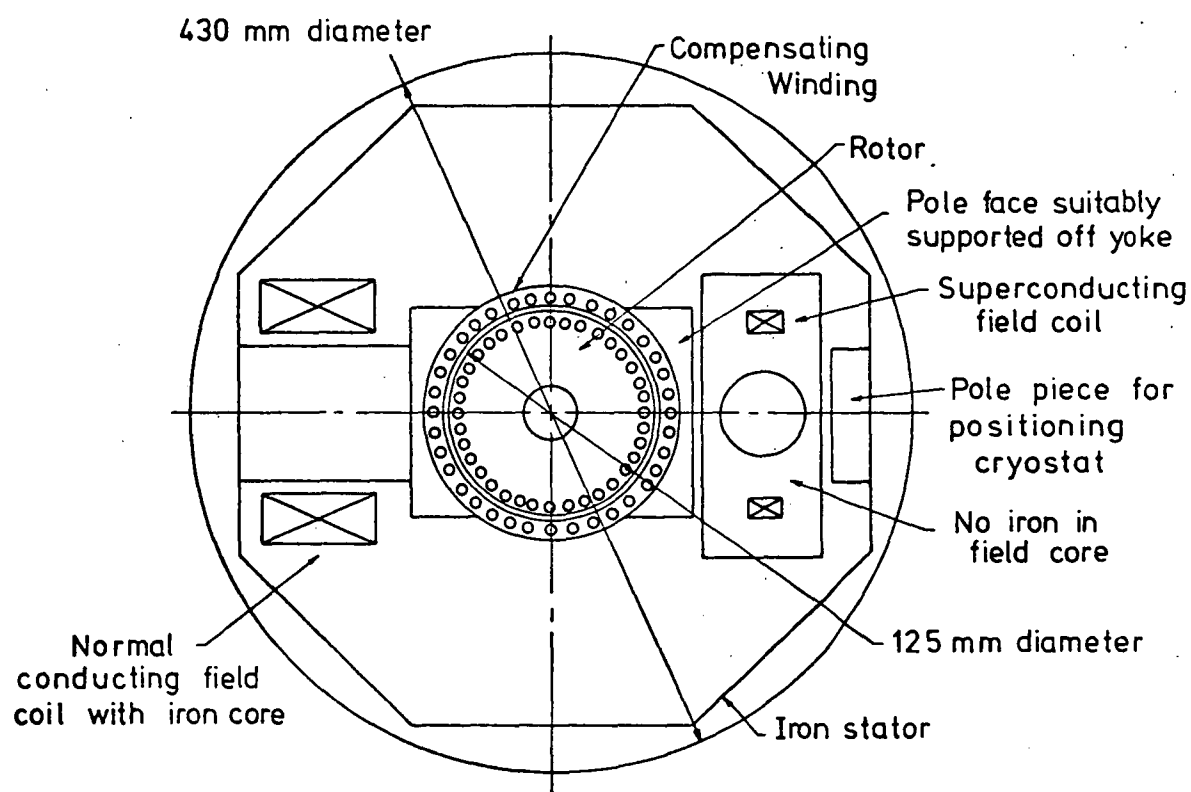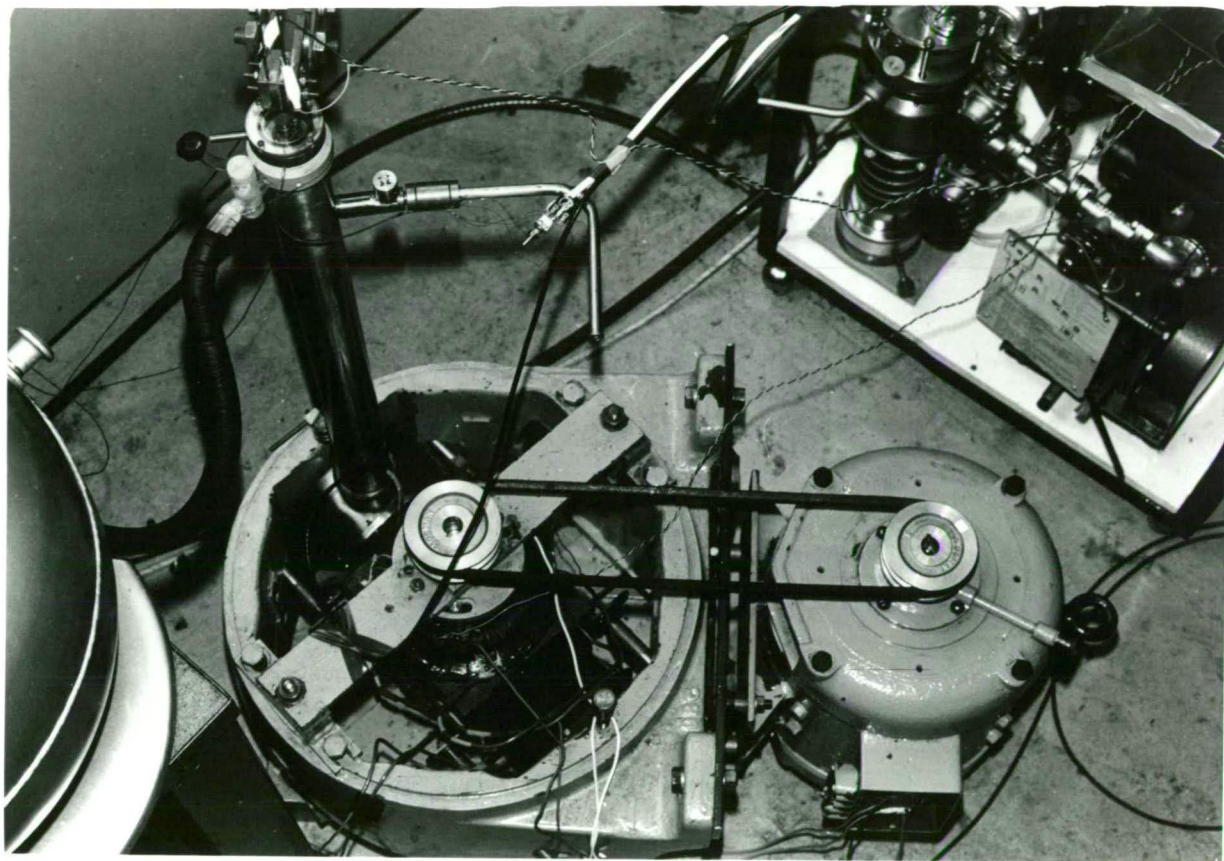
FIGURE 10-5

INITIAL MACHINE

AFTER FIRST MODIFICATION

CHAPTER 11

SECOND AND THIRD LIQUID HELIUM RUNS

11-1 Introduction

The following chapter discusses the operation of the machine and the superconducting coil during two successful attempts to obtain the superconducting state. Excitation currents in excess of 100 amperes were achieved. For the first test, the excitation current was supplied from a bank of lead acid batteries and for the second, a D.C. generator was used. A single, thirty litre dewar of liquid helium was sufficient for both tests. Selection of the armature control circuitry and aspects associated with the operation of the cryostats are included.

The aim of the experiment was to conduct qualitative tests on the initial machine so that an indication of the direction in which the project should proceed would be apparent. The initial machine provided the maximum shielding for the superconducting field winding against armature reaction fluxes. The intention was to progressively remove the shielding so that a format for a model of a prototype machine would be obtained. For these reasons quantitative comparisons between the results obtained from the experiments on the initial machine are not compared with expected values in a prototype machine. It is therefore sufficient to discuss the operation of the machine in a qualitative manner.

11-2 Machine Preparation

Previous tests on the characteristics of the machine showed that the maximum generated voltage would be only 17 volts. This was insufficient to produce the rated armature current in the generating mode. To obtain the rated armature currents in both the generating and motoring modes the ± 26 volt circuit shown in figure 11-1 was used. This circuit

FIG 11-1
MACHINE ELECTRICAL SUPPLY
FROM THE BATTERIES

ARMATURE SUPPLY

MOTOR   GENERATOR

+26 Volts○   ○   Knife switch

Armature

Compensating winding
with shorting switch

Central zero
10 amp

1·6Ω, 25 amp   6·5 amp, 11·5Ω

1·7Ω, 20 amp

Battery neutral

-26 Volts

FIELD   SUPPLY

762Ω, 1 amp

+106 Volts   0·25 amp

Normal
field

+26 Volts
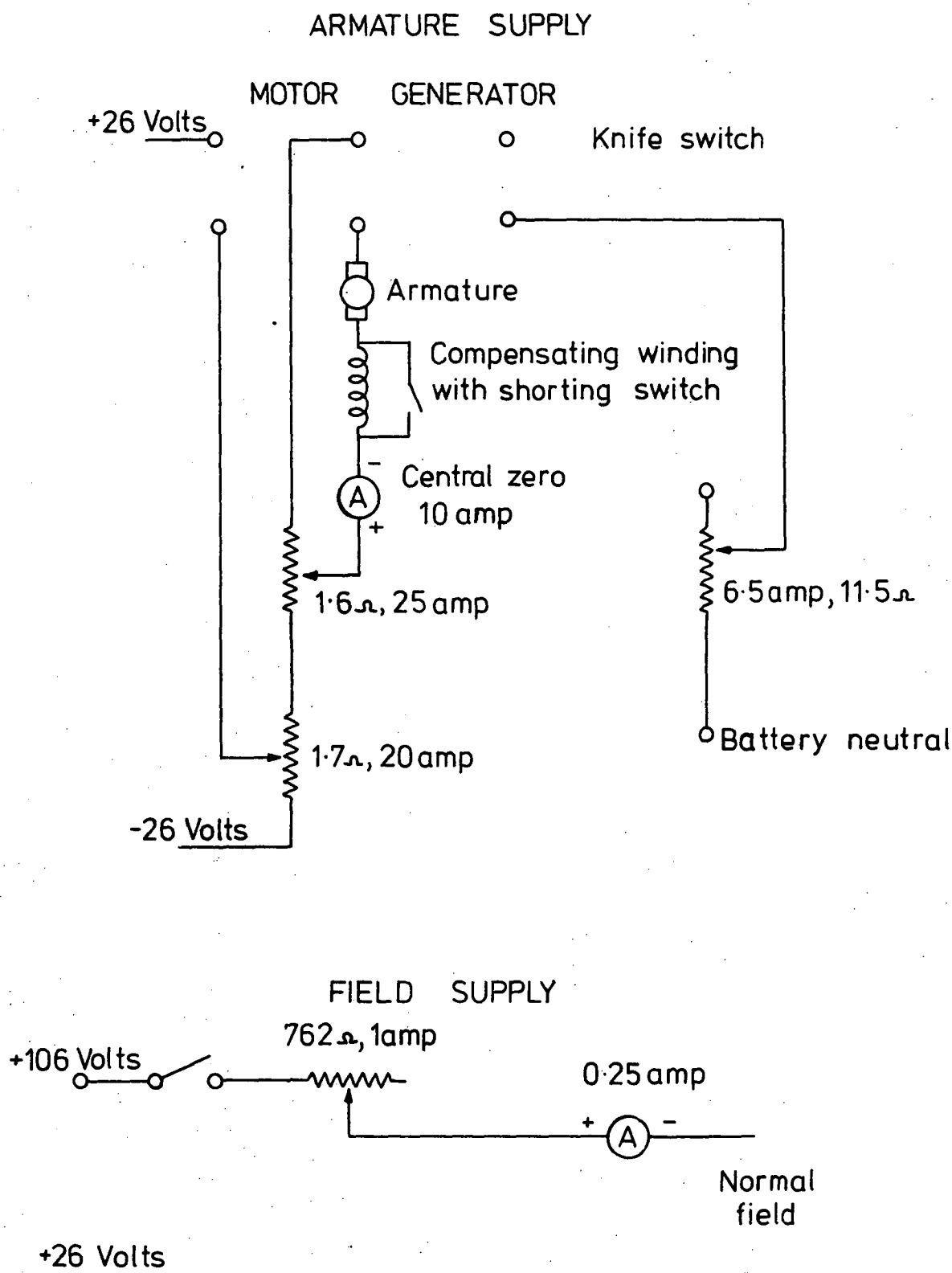
was designed so that transient testing of the machine both with and without the compensating winding in circuit was possible.

The compensating winding was connected in series with the armature winding; hence the full armature current was carried by the compensating winding. The compensating winding conductor current was approximately half the total current because the parallel internal connection was used - Chapter 5.

A 2300 r.p.m., 1kW, D.C. machine which was belt coupled to the test machine maintained a speed of 2000 r.p.m. for generation testing. For much of the motor testing it was found necessary to maintain speed using the drive motor because of the low rating of the test machine.   Motor tests were carried out with the drive machine electrically isolated and acting as a frictional load. Tests with the drive motor uncoupled from the test machine were also conducted.

11-3 Data Recording

An ultra-violet light recorder enabled a continuous record of the following variables to be taken:

(a) The radial component of flux density between the superconducting coil and the ion pole face. A Hall plate was used as a transducer.

(b) The machine armature voltage.

(c) The machine armature current.

(d) The superconducting field coil current.

(e) The superconducting field coil and cryogenic lead voltage.

(f) The normal field coil current.

11-4 Second Liquid Helium Run

The second liquid run was designed to confirm the liquid nitrogen

tests which indicated that the rebuilt cryostat was capable of maintaining the necessary conditions for superconductivity for some hours from the single thirty litre dewar of liquid helium and to permit the study of the effects of armature reaction fluxes on the superconducting field coil. Other questions which required answers were:

. How can the transition from normal conduction to superconduction be detected?

. What rates of increase of the current in the superconducting field coil can be achieved?

The pressure in the vacuum spaces of the cryostat was maintained at less than $8 * 10^{-7}$ torr during the experiment.

11-4-1 Superconducting Coil Current Supply

Eight, two volt, 500 ampere-hour batteries were connected to give an eight volt D.C. source which was capable of supplying a current in excess of 100 amperes to the superconducting field coil. A water resistor with variable, intermeshing iron plates was used to regulate the current in the superconducting field coil.

11-4-2 Cryostat Pre-Cooling

To ensure the best possible pre-cooling of the superinsulation the liquid nitrogen level in the radiation shield coolant chamber was continuously maintained for four days prior to the helium test. An automatic filler described earlier maintained the level of nitrogen above that of the heat plug. This method of cooling maintained a temperature of near 110K in the helium chamber.

Prior to the transfer of liquid helium, the helium chamber was further pre-cooled with liquid nitrogen supplied directly into the helium chamber. To ensure the removal of the pre-cooling nitrogen from within the helium chamber, the internal pressure of the chamber was reduced to

100 mm of mercury. The resultant lowering of the boiling temperature of the nitrogen increased the effectiveness of the pre-cooling by reducing the coil temperature a further 2K below 77K.

11-4-3 Cryostat and Coil Cooldown

Once the cryostat was correctly pre-cooled, the liquid helium transfer tube was slowly lowered into the helium dewar and the machine cryostat. The resulting evaporation of liquid helium caused the pressure within the dewar to exceed 65 mm of mercury above atmospheric pressure which initiated the transfer of liquid helium to the cryostat.

The pressure within the dewar was allowed to drop to 12 mm of mercury above atmospheric pressure and this was found to be sufficient to initially sustain the transfer of liquid helium. As the liquid level within the helium dewar dropped, the pressure required increased slightly.

The resistance of the coil was monitored by passing a current of 10 mA through the coil and measuring the applied voltage. Carbon resistor thermometers indicated the temperature at the top and at the centre line of the superconducting coil. The cooldown curves thus obtained are plotted in figures 11-2 and 11-3.

The significant features of the cooldown curves are that they clearly indicate the transition to superconduction and the greatly shortened cooldown time when compared with that of the first helium run when the superconducting state was not achieved.

The transition to the superconducting state was easily detected by a drop in the coil plus supply lead resistance from a steady value of near 0.025 ohm whilst the temperature of the coil fell from 25K to below 10K to a value which was below 0.0015Ω. The temperature within the cryostat was allowed to rise above the transition temperature of 9.2K

FIG 11-2
SECOND LIQUID HELIUM RUN
COIL COOLDOWN
COIL RESISTANCE ~ TIME

FIG 11-3
SECOND LIQUID HELIUM RUN
CRYOSTAT COOLDOWN
TEMPERATURE ~ TIME

A   Middle of the coil
B   Top of the coil

superconducting
transition
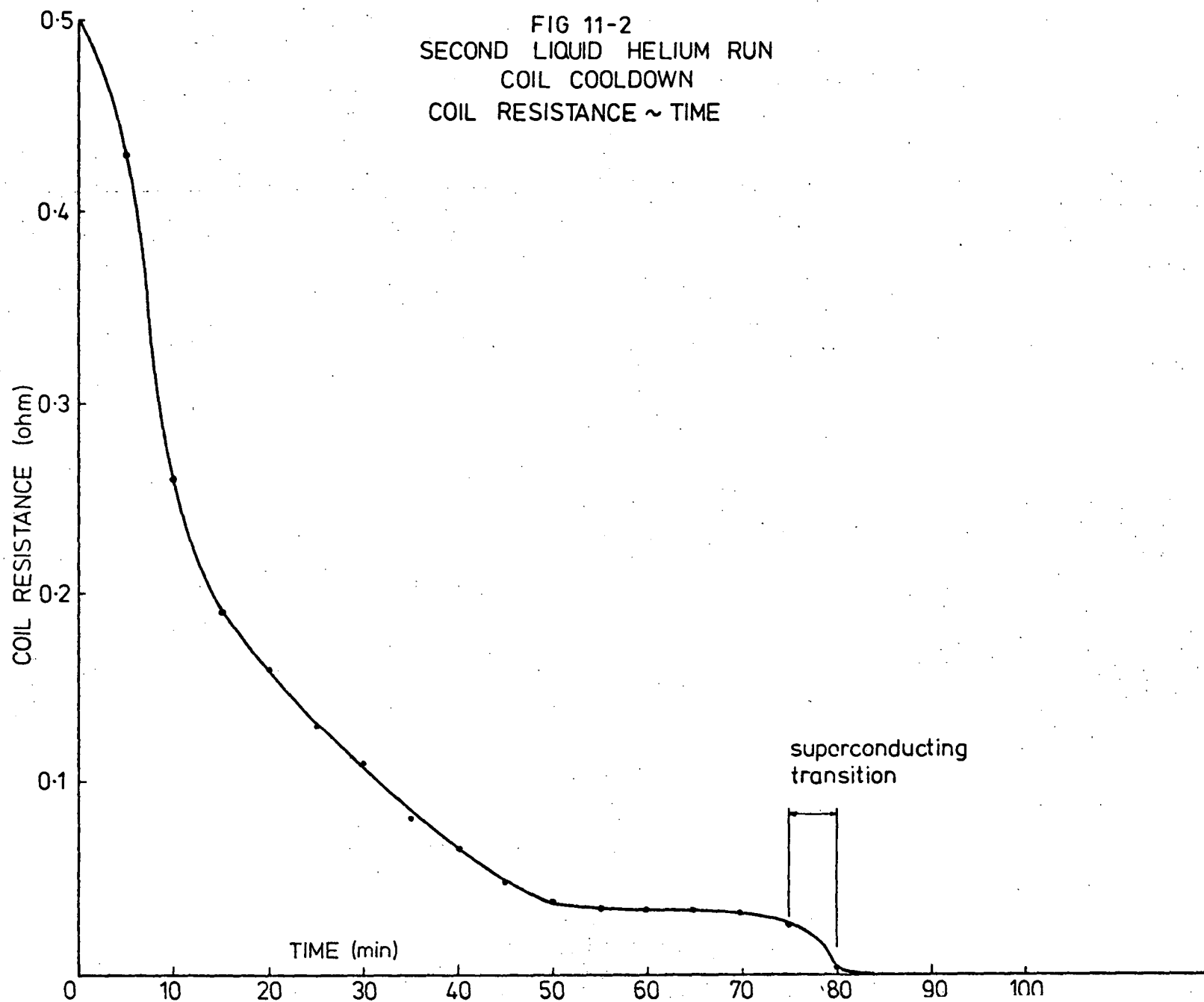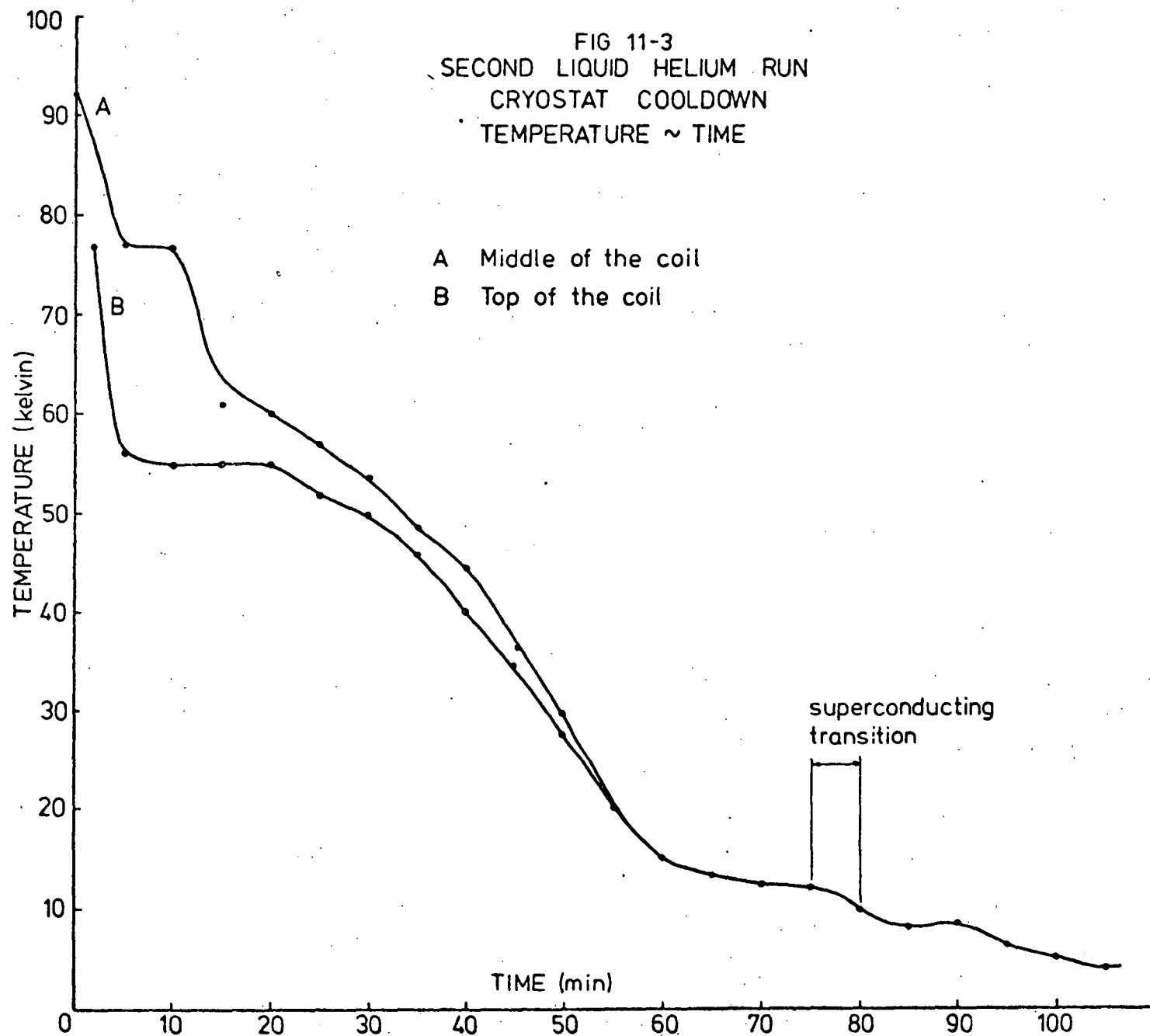
and there was a sudden rise in the resistance to near 0.025 Ω. Sudden return to superconduction occurred on subsequent cooling.

11-4-4 Superconducting Coil Excitation

Previous calculations indicated that the lead resistance at 95 amperes, the theoretical optimum for the lead cross sectional area selected, current would be 0.00128Ω - section 9-2-1. To determine the state of the super-conducting coil, the voltage across the coil and leads was recorded as the excitation current was increased. If this voltage had exceeded 0.12 volts, the estimated voltage drop on the leads at 95 amperes excitation current, it would have been assumed that the coil had quenched and the field current supply would be switched off. The observed lead voltages are discussed in Section 11-4-15.

To avoid a possible quench due to an excessive rate of increase of superconducting coil current, the coil current was initially increased very slowly - figure 11-4. Backlash in the mechanism of the motor driven, variable water resistor gave rise to the oscillatory increase in the excitation current of the superconducting coil.

The required superconducting coil current was achieved without diffi-culty within fifteen minutes. This suggested higher coil charging rates could be used in subsequent tests. After the tests on the machine had been completed, the rate of excitation was increased and the required current was obtained after six minutes. Higher rates of excitation could not be obtained during this experiment because of the limitation of the maximum speed of the driving motor of the variable water resistor. The maximum excitation current achieved during the experiment was 120 amperes which was obtained with the water resistor at its minimum resistance.

11-4-5 Field Coil Flux Density

The flux density on the axis of the superconducting field coil in

FIG 11-4
SECOND LIQUID HELIUM RUN
SUPERCONDUCTING COIL EXCITATION
EXCITATION CURRENT ~ TIME
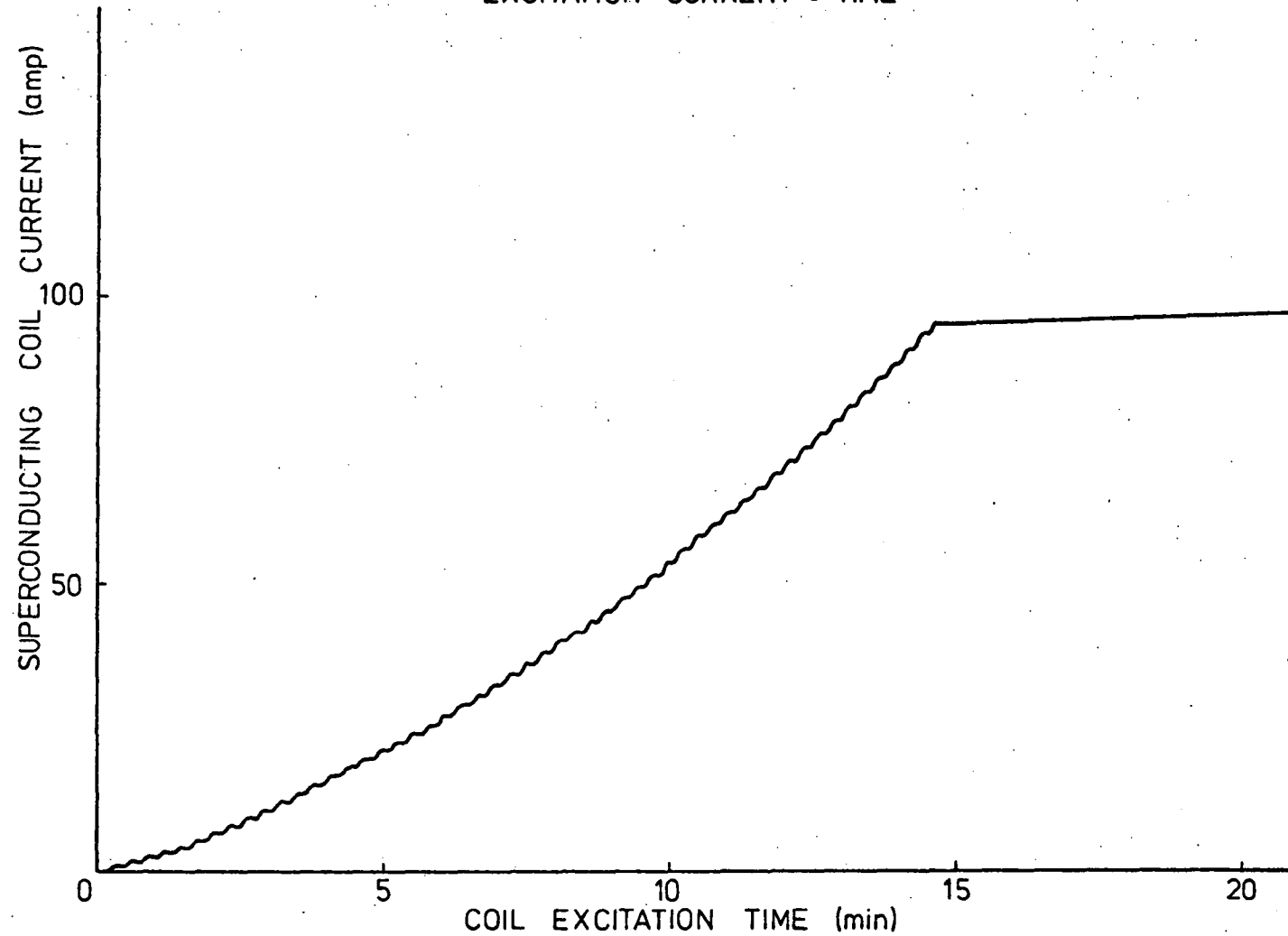
the region between the cryostat and the iron field pole face was recorded as the superconducting coil current was increased - figure 11-5.

If the flux density obtained at the armature windings was the same as at the above position, then the generated voltage would have been over 100 volts at 2000 r.p.m. However, this was not the case because of the loss of flux due to the inherent leakage paths in machines with reduced iron contents.

11-4-6 Machine Tests

The aim of the following tests was to reveal the conditions, if any, under which the superconducting coil would quench as a result of current magnitudes and changes in the currents flowing in the armature windings of the machine.

The current in the normal field coil was set at 0.215 amperes which resulted in equal field fluxes from the superconducting field coil, when excited with 95 amperes, and the normal field coil, see Chapter 10.

11-4-7 Motoring Tests with Compensating Winding

For the first set of tests, the machine was driven by the auxiliary motor at 2000 r.p.m. so that the rated speed could be maintained during armature current variations. With the test machine drawing the rated armature current, the speed of the machines increased to 2200 r.p.m., that is, the test machine was motoring but being driven at the same time.

Although it was expected that the very small armature reaction fluxes in the region of the superconducting field coil (Chapter 8) would not cause the coil to quench, the armature current was slowly increased the first time the machine was operated - figure 11-6. This load cycle proved that with the compensating winding in circuit the machine was operational for smooth changes in the armature current and that the superconducting field coil was not affected by either steady armature reaction fluxes of

FIG 11-5
SECOND LIQUID HELIUM RUN
SUPERCONDUCTING COIL FLUX DENSITY
FLUX DENSITY ~ EXCITATION CURRENT
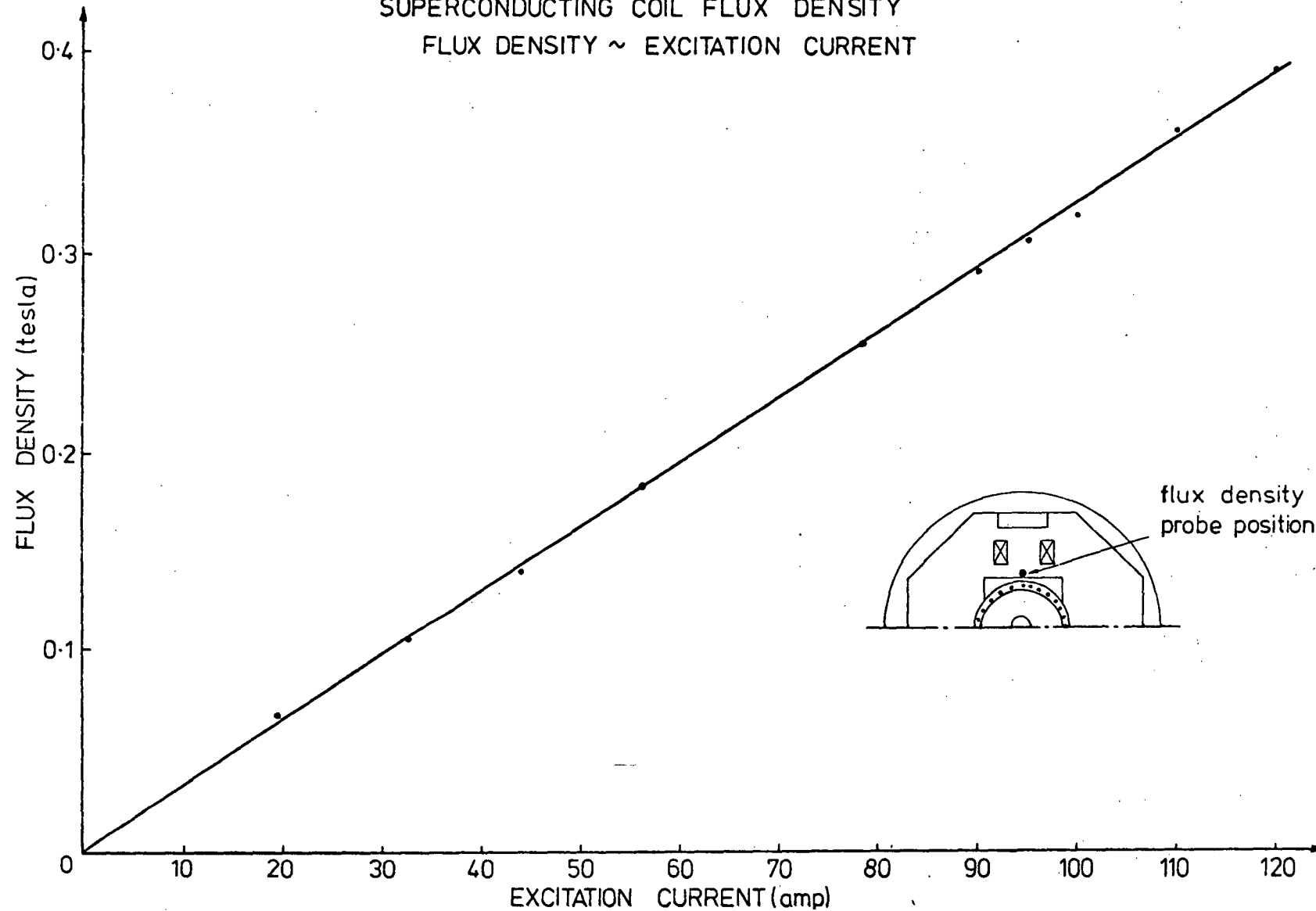
FIG 11-6
SECOND LIQUID HELIUM RUN
FIRST MACHINE LOAD CYCLE
ARMATURE VOLTAGE AND CURRENT~TIME
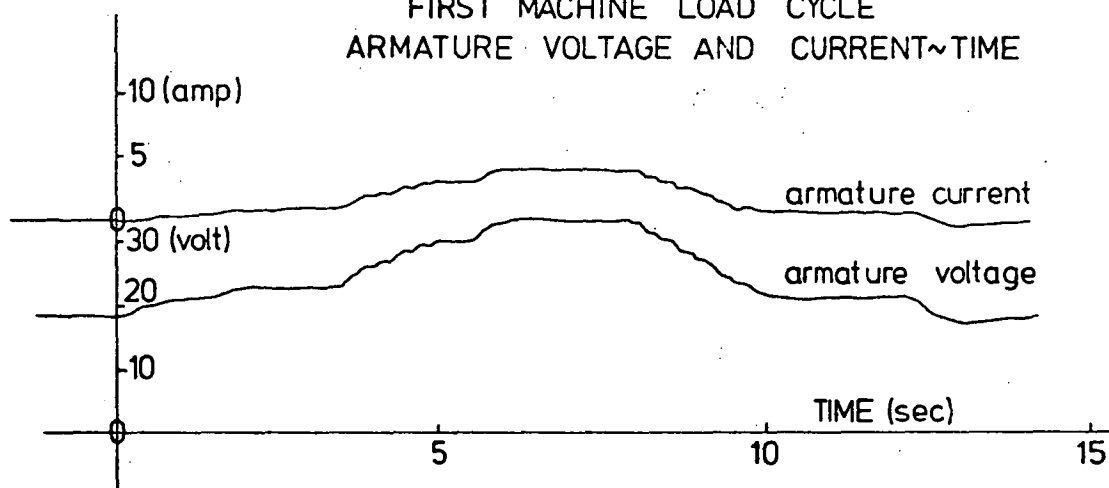
near 15 gauss or changing fluxes or near 6 gauss per second.

Subsequent increased rates of change of armature current had little effect on the field coil voltage and supercurrent.

Sudden applications of the armature supply (figure 11-7) induced transients in the superconducting coil voltage and almost imperceptible spikes in the supercurrent traces. The transients did not cause any apparent malfunctions, a fact which allayed fears that the coil would quench during such abnormal operations of the machine. The entire super-conducting coil was subjected to armature reaction flux densities of up to fifteen gauss which was very small, as initially aimed for, when com-pared with the critical flux density of the superconductor.

11-4-8 Motoring without Compensating Winding

The machine load cycles in the previous section were repeated but with the compensating winding short circuited. With the compensating winding short circuited, larger armature voltages and armature currents were achieved than in the motor test with the compensating winding connected in series with the armature.

Gradual increase and decrease in the armature current (figure 11-8) did not affect the operation of the superconducting coil as indicated by the steady supercurrent and coil voltage traces produced during the load cycle. The sudden application and removal of the armature supply (figure 11-9) produced little change in the supercurrent, but transient voltages were induced in the superconducting coil.

The induced voltage transients in the superconducting coil contained two time constants: one short time constant which was associated with the time constant of the armature circuit and hence the initial rise time of the armature currents and another larger time constant which was associated with the superconducting coil inductance and external power supply resistance. The copper radiation shield and the short circuited

FIG 11-7
SECOND LIQUID HELIUM RUN
MOTOR TRANSIENT TEST
WITH COMPENSATING WINDING
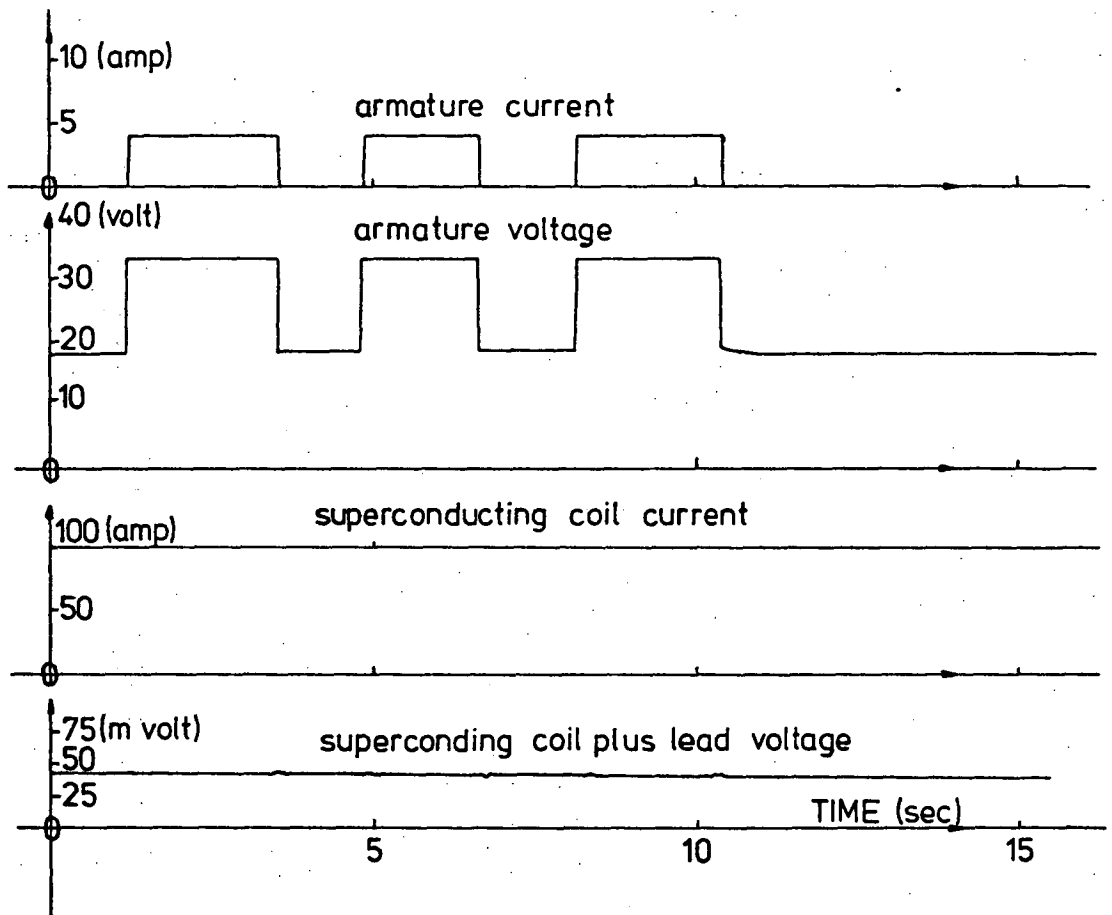
FIG 11-8
SECOND LIQUID HELIUM RUN
MOTOR LOAD CYCLE WITOUT COMPENSATING WINDING
ARMATURE VOLTAGE AND CURRENT ~ TIME
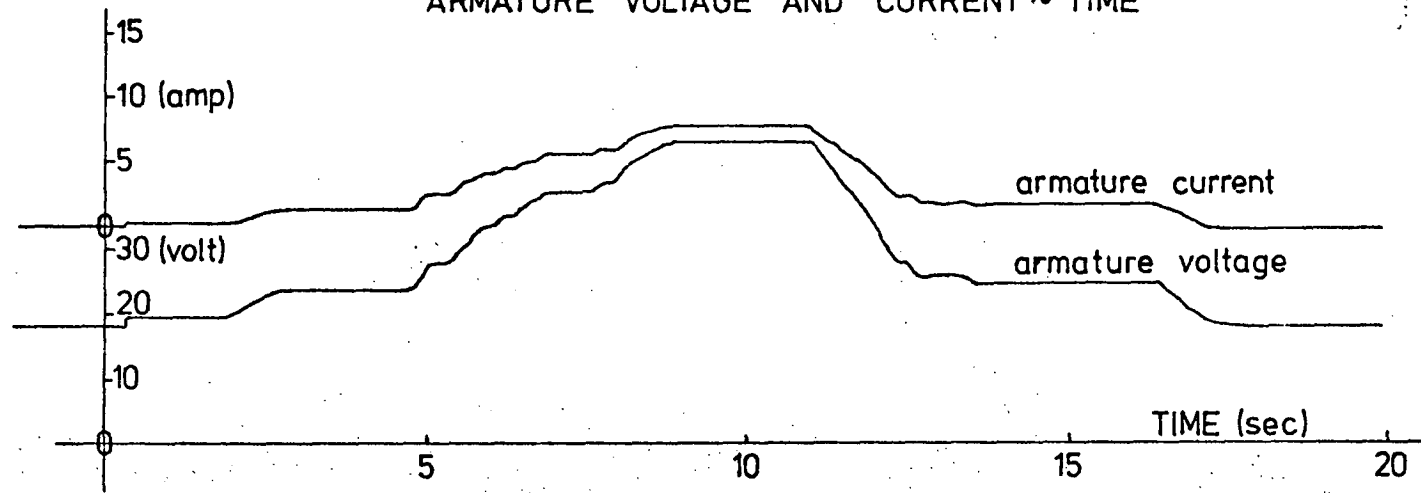
FIG 11-9
SECOND LIQUID HELIUM RUN
MOTOR TRANSIENT TEST
WITHOUT COMPENSATING WINDING
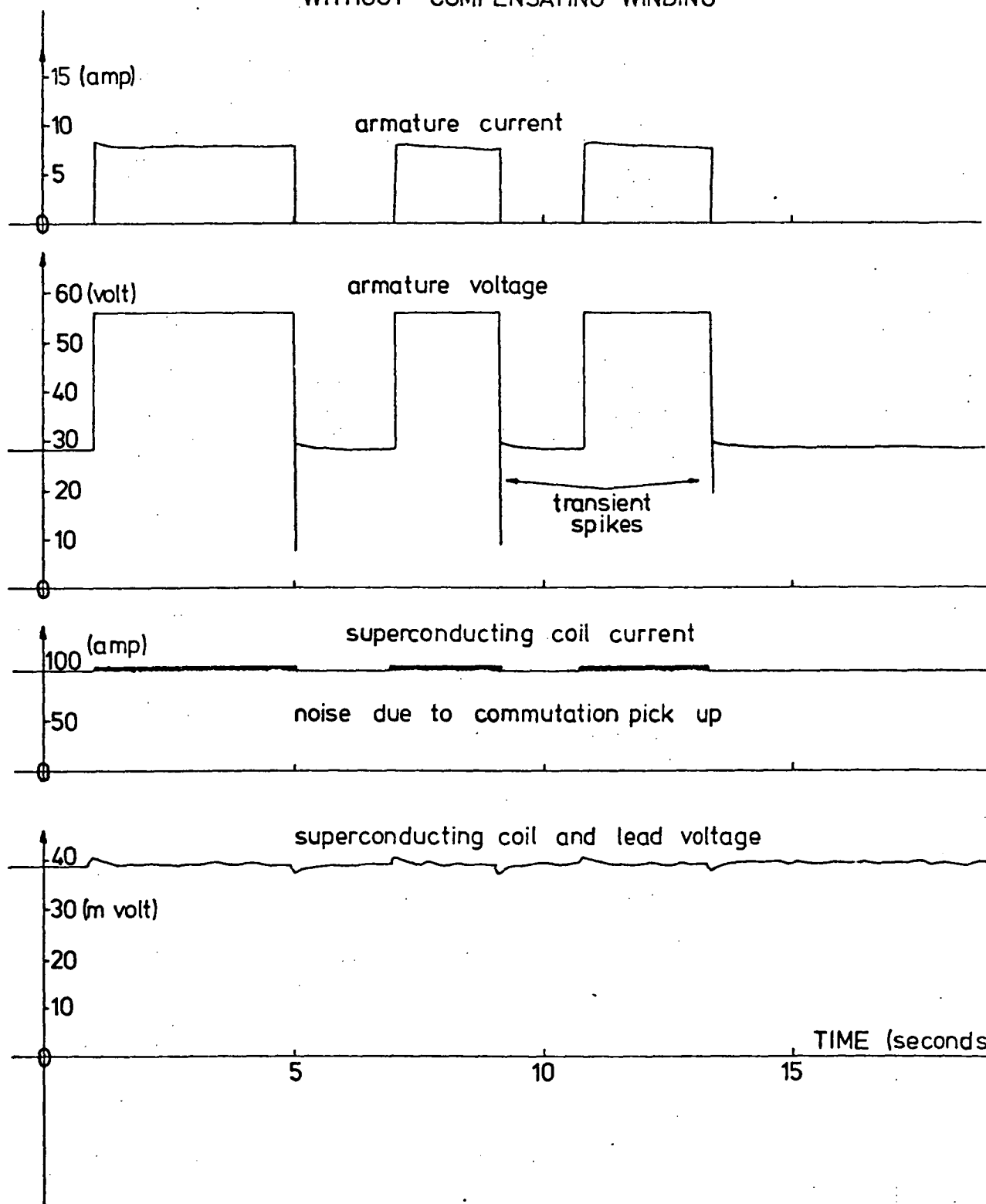
compensating winding acted as shorted turns, hence as a shield against changing fluxes which would have had an influence on the coil voltage transient time constants. The magnitudes of the induced transient voltages were greater than those produced with the compensating winding connected, but there was still no loss of superconductivity.

The slopes on the armature current trace were caused by the generated e.m.f. increasing as the machine speed increased. The slopes of the armature voltage open circuit values were caused by the machine speed decreasing once the armature supply was removed.

These tests indicated that with the configuration of the initial machine adopted (i.e. iron pole faces), a compensating winding was not necessary to ensure adequate shielding against weak armature reaction fluxes of magnitudes upto fifteen gauss and with slow rates of change of less than six gauss per second. The peak flux density at the field coil was approximately one quarter the critical value at the operating temperature of 4.2K.

11-4-9 Generating Tests with Compensating Winding

Similar tests to those carried out with the machine motoring were repeated but with the machine generating. With the compensating winding in circuit, the maximum armature current was limited to below 5 amperes because of the resistances in the armature and compensating windings and the low generated voltage of the machine. The open circuit voltage at a speed of 2000 r.p.m. and 100 ampere field current was only 17.5 volts; hence the need for the extra 26 volt assisting voltage to provide the rated armature current.

Neither slowly increasing the armature current (figure 11-10) nor the sudden application of a resistive load (figure 11-11) caused disruption to the supercurrent. The sudden loading did, however, produce an almost imperceptible transient voltage on the super conducting coil voltage

FIG 11-10
SECOND LIQUID HELIUM RUN
FIRST MACHINE GENERATING CYCLE
ARMATURE VOLTAGE AND CURRENT~TIME
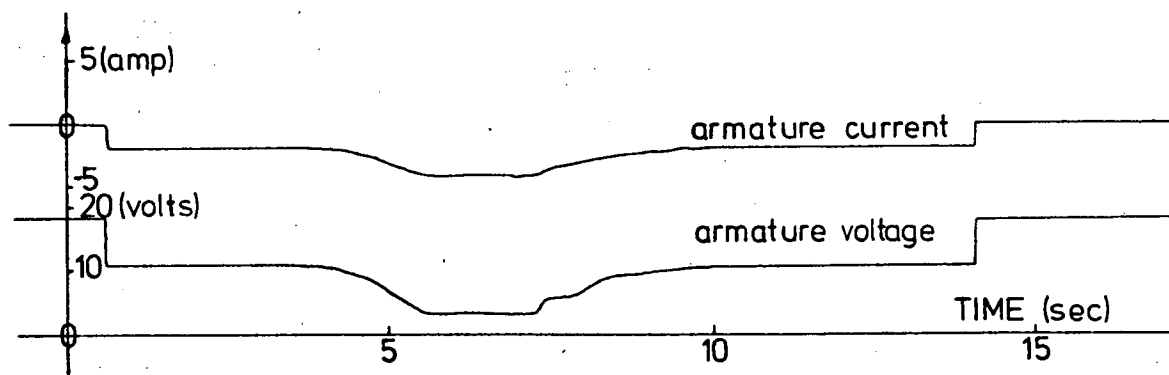
FIG 11-11
SECOND LIQUID HELIUM RUN
GENERATOR TRANSIENT TEST
WITH COMPENSATING WINDING
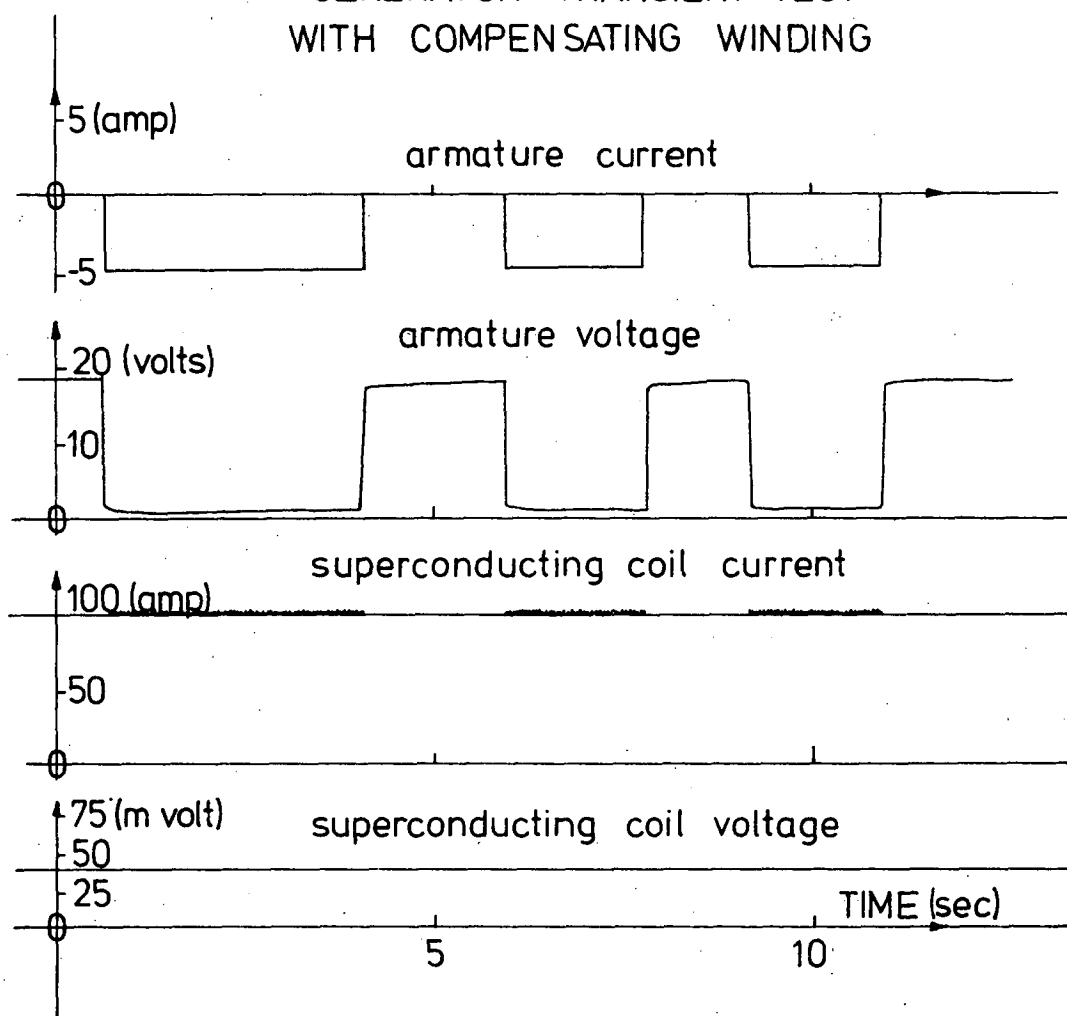
which was caused by the changing armature reaction fluxes.

11-4-10 Generating Tests without Compensating Winding

With the compensating winding short circuited, repetition of the machine generation tests resulted in similar loading characteristics and transient values as those obtained in the previously discussed tests - figures 11-12 and 11-13. The armature voltage was negative under the heavier armature currents as a result of the 26 volt assisting voltage connected in series with the armature.

The sudden application and removal of armature load resistances resulted in armature and superconducting coil transients similar to those obtained during the motor transient tests without the compensating winding. These transient voltages (armature voltage spikes produced on the removal of armature current and induced voltages in the superconducting coil - figure 11-13) were not as pronounced when the compensating winding was in circuit thus indicating the correct operation of that winding. As with the motoring transient tests, the superconducting coil voltage transients contained two time constants.

As in the previous tests, there were no changes in the supercurrent. Commutation noise which appeared on the supercurrent trace during loading was caused by pick-up by the recording instrument. This was later verified by short-circuiting the pick-up terminals where they were connected to the superconducting field coil and noting that the same noise patterns ensued.

11-4 -11 Transient Motoring Test with Compensating Winding
Reverse Connected

To increase the armature reaction fluxes and possibly cause a quench in the superconducting field coil, the compensating winding was reverse connected so that the armature reaction fluxes were reinforced by the

FIG 11 -12
SECOND LIQUID HELIUM RUN
GENERATOR LOAD CYCLE
WITHOUT COMPENSATING WINDING
ARATURE VOLTAGE AND CURRENT ~ TIME
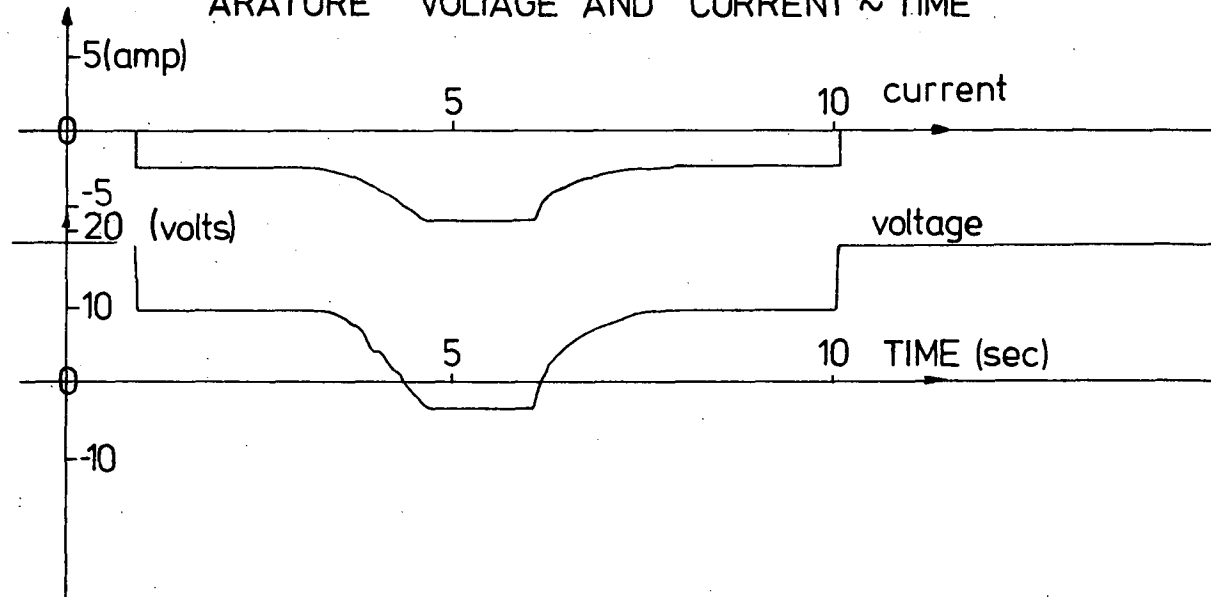
FIG 11-13
SECOND LIQUID HELIUM RUN
GENERATOR TRANSIENT TEST
WITHOUT COMPENSATING WINDING
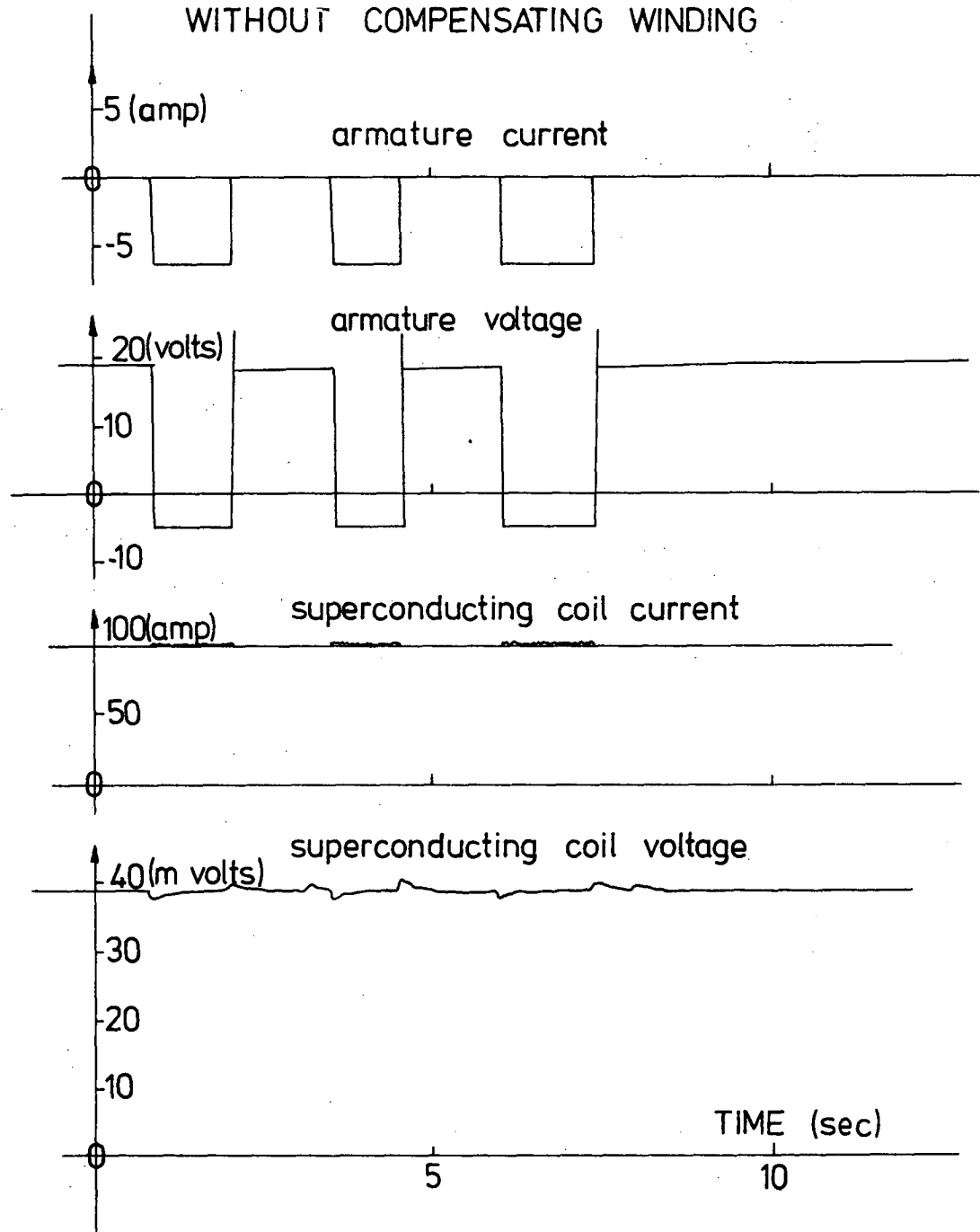
compensating winding magnetic fluxes. The sudden application of the armature supply, with the machine rotating at 2000 r.p.m., had no detectable influence on the supercurrent, but transient voltages were induced in the superconducting field coil and the armature - figure 11-14. The magnitudes and shapes of the induced voltages were much the same as those induced during the transient loadings without the compensating winding. However, the armature currents in those tests were greater than the currents with the compensating winding reverse connected.

11-4-12   Loss of Normal Field Excitation

In a further attempt to initiate a quench in the superconducting field coil, the current supply to the normal field coil was suddenly disconnected and reconnected with and without armature current. The tests failed to produce any detectable change in the supercurrent, but did produce superconducting coil transient voltages greater than those previously obtained - figure 11-15.

The transients contained two time constants: a long time constant, which was the same as that obtained during the armature transient tests, and a short time constant. The short time constant was different, depending on whether the normal field coil was being energised or de-energised; and these were different from the short time constant obtained during the armature loading transients.

On energising the normal coil, the short time constant was the same as that of the normal field coil, but rapid de-energisation of the normal field coil produced an even shorter time constant which was dependent on how fast the knife switch was opened. As the normal field current was reduced more quickly than it was increased, the peak transient voltage for de-energisation was greater than the peak voltage obtained during coil energisation. The peak induced voltages corresponded to a rate of change in the flux density at the superconducting coil of 130 gauss per

FIG 11-14
SECOND LIQUID HELIUM RUN
MOTOR TRANSIENT TEST
COMPENSATING WINDING REVERSE CONNECTED

armature current

armature voltage

superconducting coil current

superconducting coil voltage

TIME (seconds)
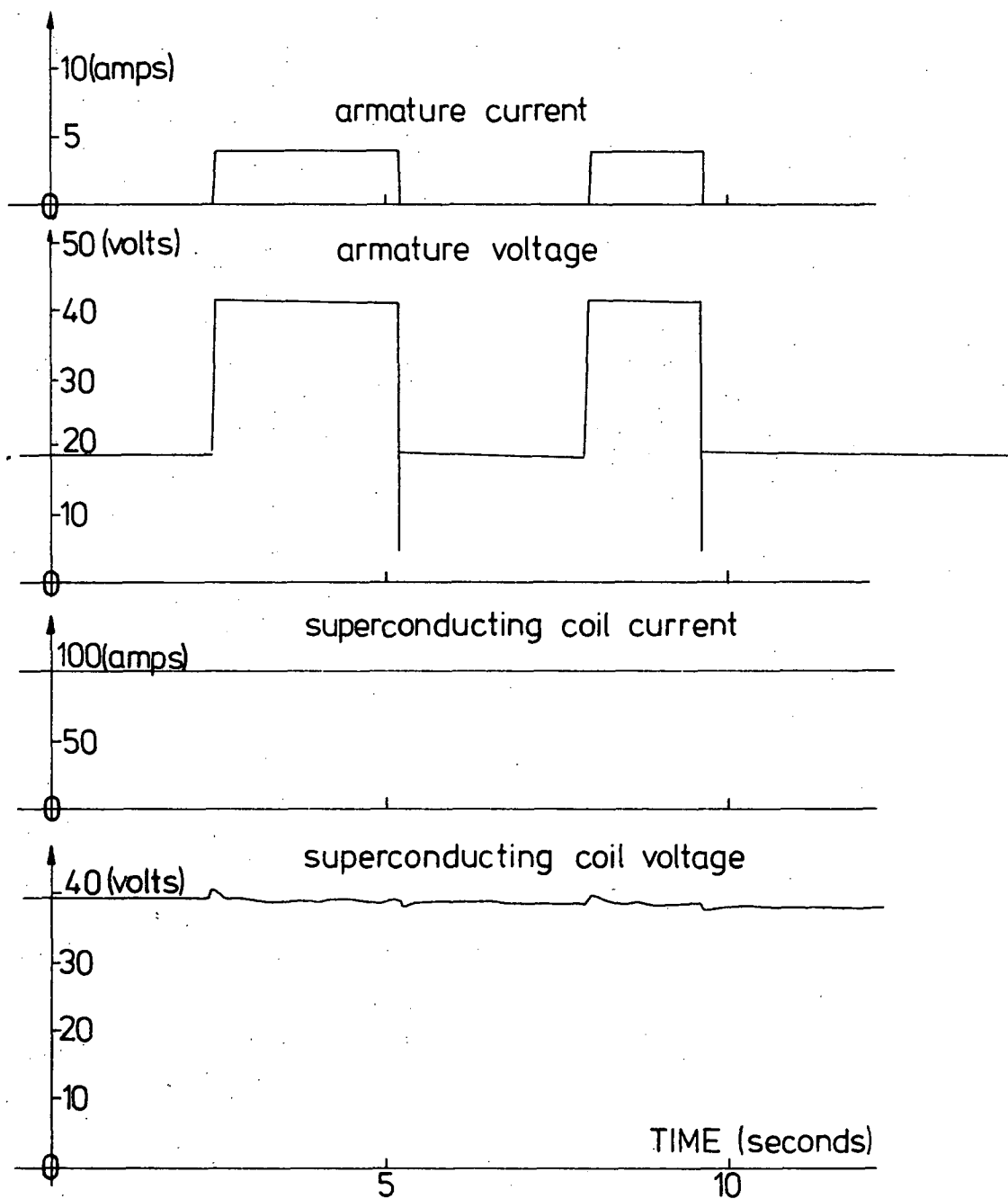
FIG 11-15
SECOND LIQUID HELIUM RUN
NORMAL FIELD COIL TRANSIENT
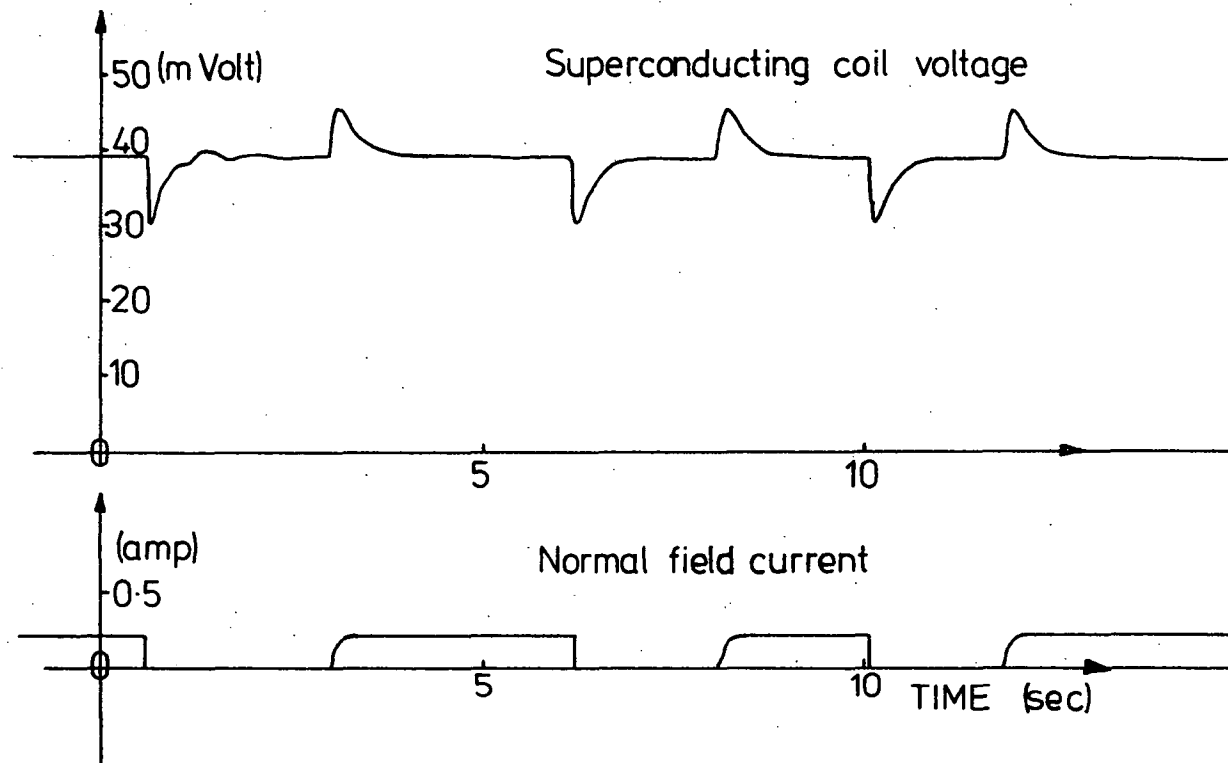
second. The duration of the induced transient was in excess of one second.

11-4-13   Motor Test

The previous motor tests were conducted with the machine driven at 2000 r.p.m. and allowing the speed to increase to 2200 r.p.m. when the superconducting machine was energised. For the following tests the supply to the load machine was disconnected; hence the superconducting motor provided the entire motive power. For the remainder of the tests, the compensating winding was out of circuit.

The voltage supply to the test machine, which was set to give a final armature current of near 10 amperes and a machine speed of 950 r.p.m., was suddenly applied to the stationary armature so that the influence of commutation on the superconducting coil could be investigated as the machine accelerated. The resulting trace (figure 11-16) indicated a double time constant field coil voltage transient and also indicated the induced commutation voltage which increased in frequency as the speed of the machine increased from the stationary start. The induced effects did not result in any operational difficulties with the superconducting coil.

11-4-14   Commutation

The absence of any sparking at the brushes during previous machine tests (Chapter 8) indicated that the commutation of the armature coil currents would not be a problem. This was found to be the case for all of the machine load cycles and armature transients performed as indicated by the absence of any serious sparking between the high copper content brushes and the commutator.

Because of the lack of difficulty experienced with commutation, the effectiveness or otherwise of the compensating winding to improve commutation was not established.

FIG 11-16
SECOND LIQUID HELIUM RUN
SUPERCONDUCTING MOTOR TRANSIENT
COMPENSATING WINDING SHORT CIRCUITED
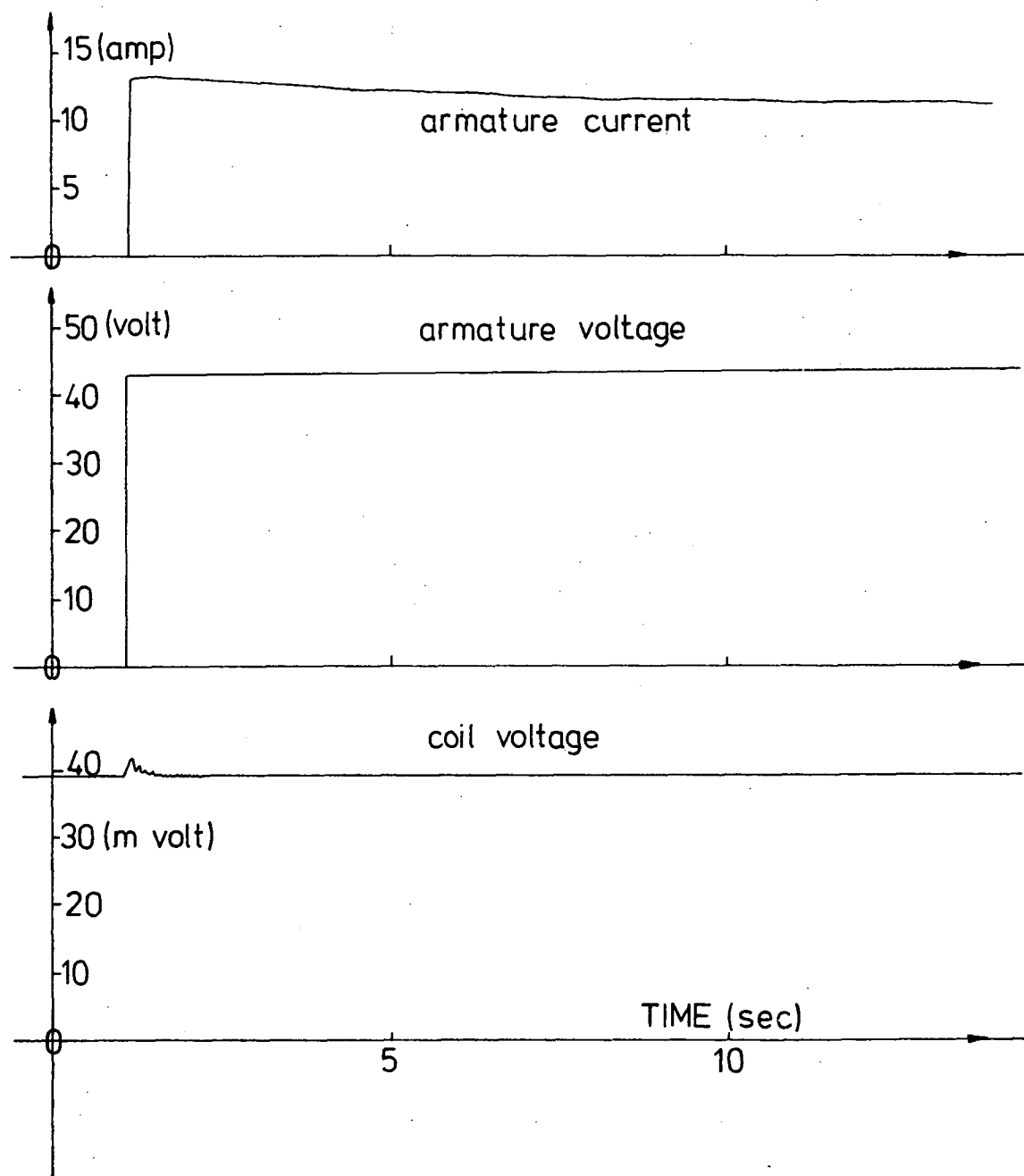
11-4-15 <u>Performance of the Cryogenic Components</u>

During the operational period of the superconducting coil, it was necessary to maintain a continuous flow of liquid helium into the cryostat. From the flow rate of the helium boil-off gases, the consumption of liquid helium by the entire system - that is, the dewar, the transfer tube, the current leads and the cryostat - was calculated to be 40 cc per minute. The rate of use of liquid corresponded to a total heat inleak to the liquid helium of 1.7 watts. This was one watt above that estimated for the leads alone.

The higher loss of liquid helium above that which can be attributed to the cryogenic leads improved the performance of the leads because the extra cooling gas reduced the lead temperature. This resulted in the lower lead voltage drops than predicted (figure 11-17) and also the ability of the leads to supply in excess of 30% more current to the coil than the designed optimum value of 95 amperes.

Once the machine tests were completed, the superconducting coil was de-energised and the liquid helium transfer tube was removed from the cryostat. The rate of loss of the cryostat's charge of liquid helium was 3 cc per minute, which corresponded to a heat inleak of 0.128 watts. The estimated heat inleak through the 100 ampere leads with no current was 0.11 watts, a calculation which agrees favourably with the observed total heat inleak to the cryostat.

The warm-up characteristics of the coil and cryostat after the charge of liquid helium was exhausted are shown in figure 11-18. The time rate of rise of the temperature was largely determined by the heat conducted to the cold region by the current leads. Without the cooling effect of the counterflow boil-off gases, the heat conducted by the leads to a region at 80K would have been at a rate of 0.5 watts. The time required to raise

FIG 11-17
LEAD PERFORMANCE
LEAD VOLTAGE ~ EXCITATION CURRENT

estimated voltage
drop with 95 amp
was 0.122 volts

design current

LEAD VOLTAGE DROP (mVolts)

EXCITATION CURRENT (amp)

FIG 11-18
SECOND LIQUID HELIUM RUN
COIL AND CRYOSTAT WARM UP
COIL RESISTANCE ~ TIME
TEMPERATURE ~ TIME
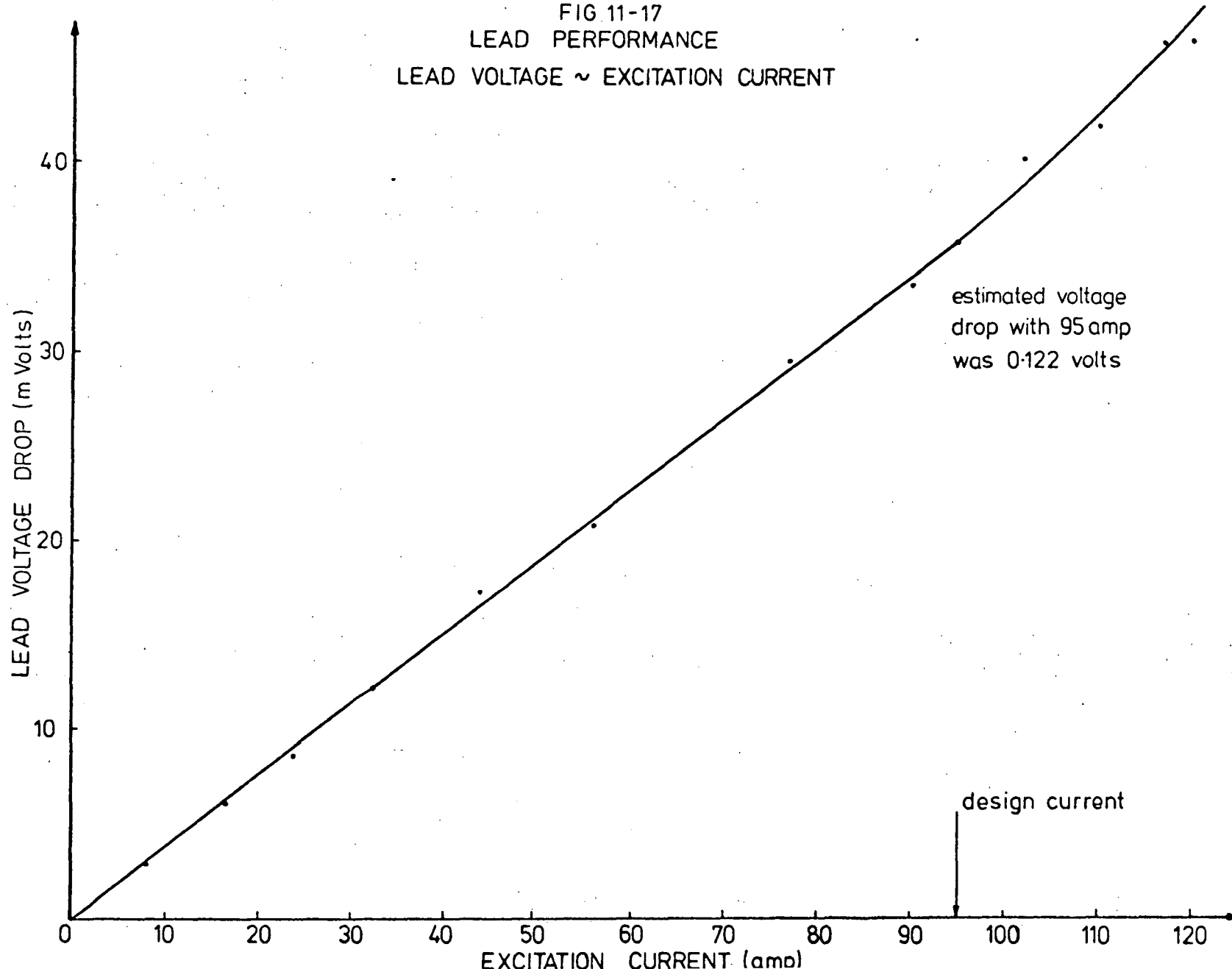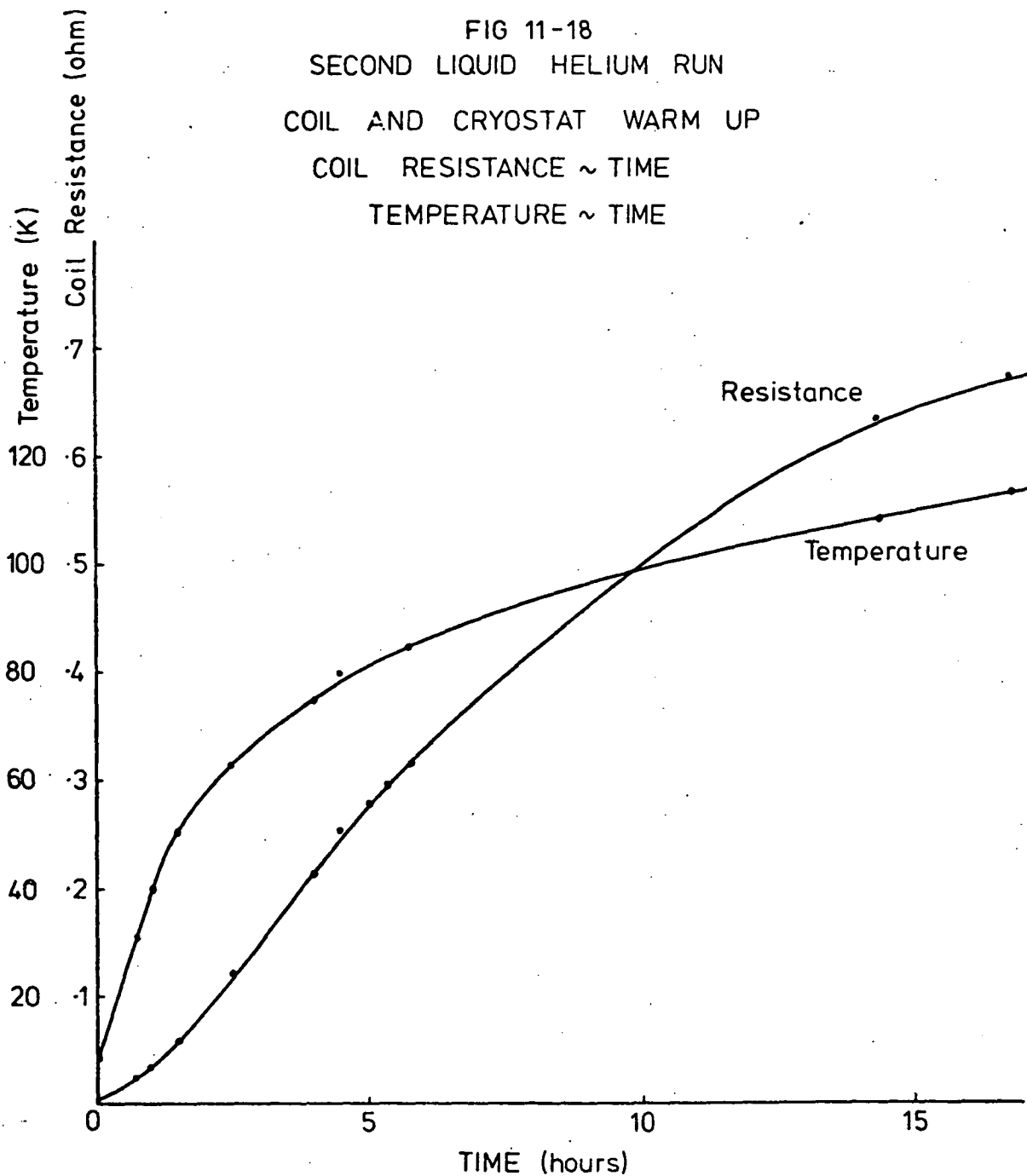
the coil and cryostat temperature to 80K from 4.2K was thus estimated at 5.3 hours, which compares with the measured time, thus confirming the assumption that the leads were the major source of heat inleak and that the insulation chosen was adequate and need not be improved upon for future experiments. During the course of the experiments, only 14 of the 26 litres of liquid helium supplied were used. The surplus enabled another test run from the single dewar of helium.

11-5 Third Liquid Helium Run

In the second helium run the superconducting coil was energised from a bank of batteries which ensured a ripple-free current. The purpose of the third run was to investigate the possibility of energising the super-conducting field coil from a 270 ampere D.C. generator.

The cooldown time for the third run was an hour longer than that for the second run because, during the weekend separating the tests, the cryostat had returned to room temperature. This result indicated the necessity for careful pre-cooling with liquid nitrogen so that a minimum of liquid helium is used for cooldown to 4.2K.

11-5-1 Superconducting Coil Operation

The output of the D.C. supply generator was controlled by manually varying the field current of the generator. The water resistor was series connected in the superconducting coil circuit, thus preventing any diffi-culties associated with the operation of a generator under virtually short circuit conditions.

The superconducting field coil was successfully energised several times to a maximum current of 120 amperes at a rate of rise of excitation current in excess of 3 amperes per second. This rate of rise of field current resulted in a rate of change of flux density at the superconductor

of 300 gauss per second. Higher rates of increase were not possible because of limitations in the supply generator. Difficulty with recording the variables was experienced because of commutation noise from the generator, but this was later overcome by employing differential amplifier filters with low upper cut-off frequencies.

The coil voltage was dominated by a 15 Hz alternating voltage of near 1 volt peak to peak which corresponded to the speed of rotation of the field current supply generator. The inductance of the superconducting coil was near 5 mH at a frequency of 15 Hz; thus the 15 Hz component of current would have been less than 1.1 ampere peak to peak.

This test indicated that the coil could be successfully energised from a rotating machine and that field coil excitation rates far in excess of those used initially could be employed. The commutation ripple of the supply generator and the ripple due to its rotational unbalance proved not to have a detrimental influence upon the performance of the super-conducting field coil.

11-6   Comments

The second and third helium runs answered the questions which were posed in section 11-4. These answers were vital for the future progress in research in the field of application of superconductivity at the University of Tasmania.

The successful operation of the machine and the comparative ease, when compared with the problems previously encountered, with which the super-conducting state and the required coil excitation current were achieved indicated that further, more involved experiments could be conducted from the available 30 litre supply of liquid helium.

The faultless operation of the superconducting coil throughout the

experiment nullified the necessity for a compensating winding with the machine configuration adopted. Earlier experiments (Chapter 8) indicated that the field pole face acted as an excellent shield against armature reaction fluxes; hence the absence of large transient effects on the performance of the coil was expected.

Loss of excitation current in the normal field pole resulted only in a transient voltage being induced into the superconducting coil. This raised the question as to what extent the superconducting coil can withstand transient flux changes or any other external disturbances, such as vibrations, before a quench would be initiated.

An important point which affects the faultless operation of the superconductor was that the conservative maximum excitation current of 120 amperes was well below the estimated coil quench current of 460 amperes. If the field coil was energised to just below the critical current, which would result in better usage of the superconducting property, then the ability of the coil to resist the transients induced during the aforementioned tests would be suspect. Under these conditions, the compensating winding could produce the added flux reductions required to protect the superconducting coil and this was later investigated.

11-7   Conclusion

An aim of the initial machine was achieved when the superconducting state was obtained and maintained without difficulty. This showed that satisfactory techniques for the design of the cryostat and cryogenic leads had been produced.

The inability to produce a quench as a result of flux changes at the superconductor indicated that the project should progress to a second stage machine. This machine should have a larger superconducting field coil

operating at a greater current and exposed to the full effects of armature reaction fluxes.

CHAPTER 12.

FOURTH HELIUM RUN

12-1   Introduction

In this chapter modifications to the successful machine are des-
cribed which subjected the superconducting field coil to more stringent
operating conditions. The superconducting coil was operated more closely
to its critical flux density and it was subjected to the full effects
of the armature reaction fluxes. The results of a fourth successful helium
run which tested the machine with the modifications are also presented.

The success of the fourth helium run indicated the format of a
prototype machine and this permitted a quantitative comparison to be
made between the results obtained during the experiment and those
estimated for the prototype - section 12-10.

12-2   Cryostat Modification and Tests

The cryostat was re-designed so that it could accommodate a larger
superconducting coil and leads which were capable of supplying an excita-
tion current of 300 amperes - figure 12-1. The top section of the cryo-
stat was re-designed to facilitate its construction and operation. A
larger chamber for the radiation shield coolant was provided so that
intervals between liquid nitrogen refills were increased to several hours.

Within fifty hours of continuous pumping the pressure within the
cryostat, as indicated by the vacuum gauge, was less than 10^{-6} torr,
this indicating vacuum tightness.

After a twenty-four hour period of cooling with liquid nitrogen,
the heat inleak performance of the cryostat within the 300 ampere leads

FIG 12-1
MODIFIED CRYOSTAT
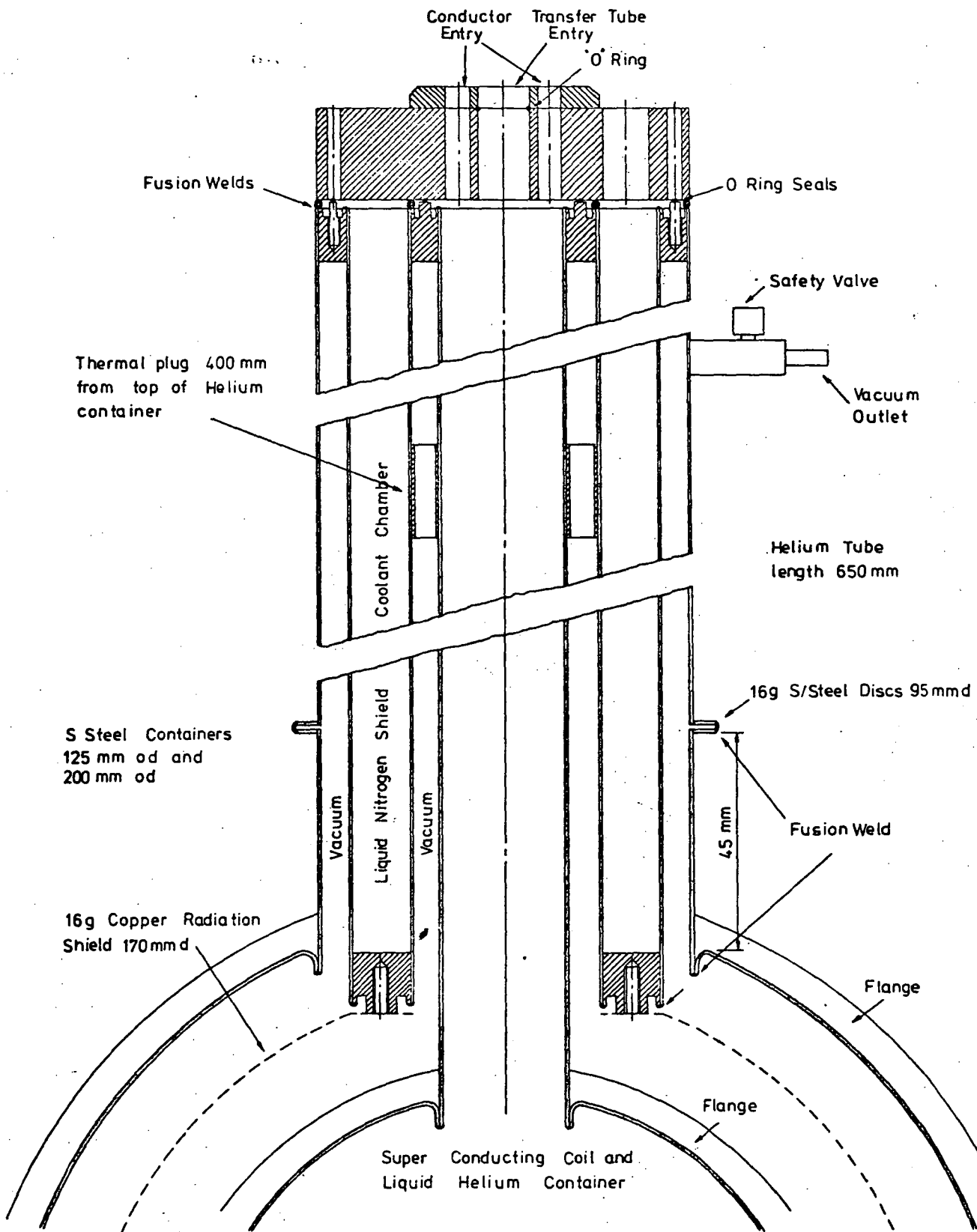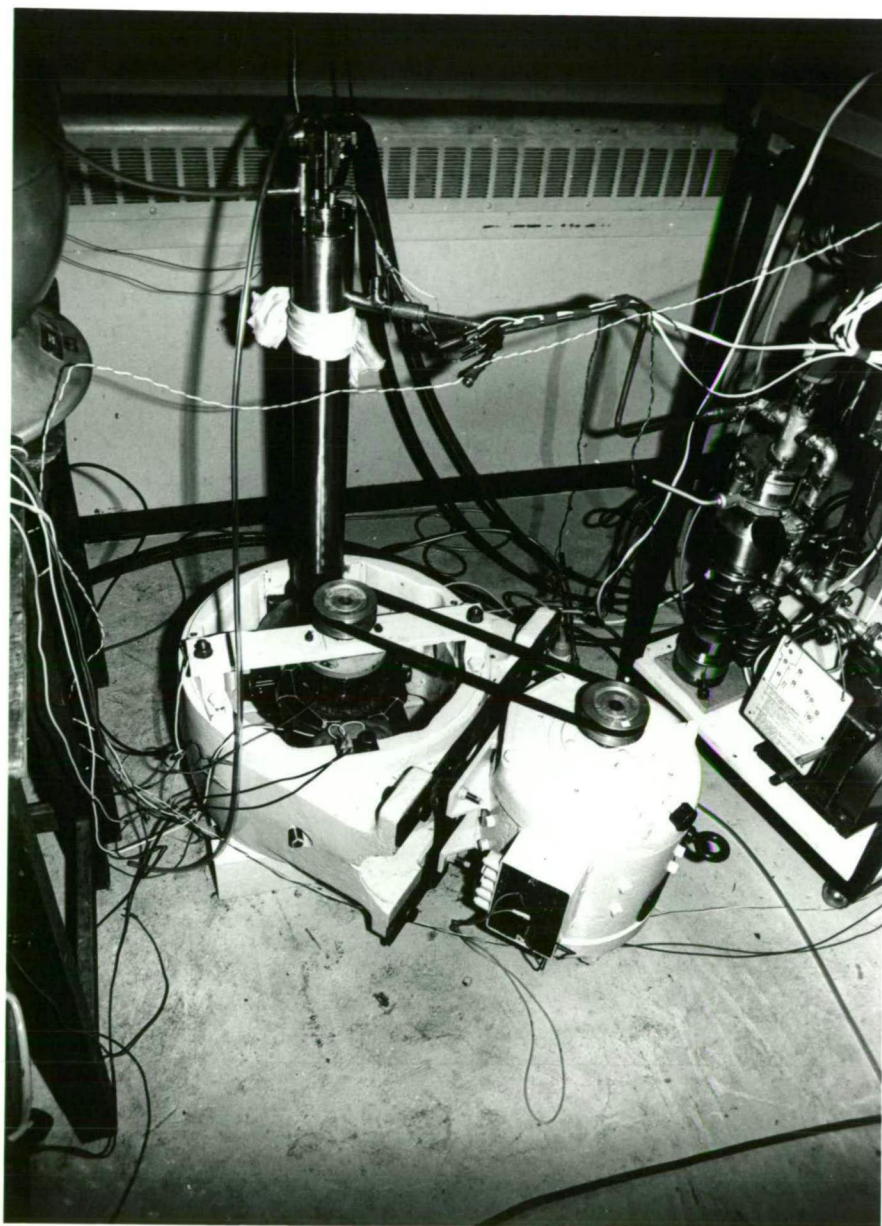
FIGURE 12-2

INITIAL MACHINE

AFTER SECOND MODIFICATION

in position and not carrying current was measured. With the radiation shield and the field coil cooled with liquid nitrogen, the total heat inleak to the field coil chamber was measured at 1.1 watt. Without the radiation shield cooled, the heat inleak was 2.05 watt. The calculated heat inleak due to the leads and without any other sources of heat inleak was 2 watt. This compared favourably with the measured value without the shield cooled. The reason for the marked decrease in the heat inleak, when the shield chamber was filled with liquid nitrogen, was that the heat plug, which was situated approximately 450 mm from the bottom of the leads, would have intercepted much of the lead heat inleak to the inner coil chamber by producing a temperature of near 77K near the room temperature extremity of the leads.

These tests indicated that the cryostat was adequately insulated and that it was ready for tests with liquid helium.

12-3   Coil Modifications

The number of turns on the superconducting field coil was increased from 400 to 800. This total required 178 metres of wire. At an excitation current of 300 amperes, the maximum flux density with the coil in free space was estimated at 4.14 tesla whereas the critical flux density is 6.5 tesla at 300 amperes. The free space quench current was 390 amperes; thus an excitation current of 300 amperes provided a small margin for the increase in flux density due to the low reluctance of the iron stator frame of the machine and the corresponding decrease in the critical current of the coil. The margin was small enough so that there would be the possibility of operating the superconductor up to its limits.

12-4   Machine Modifications

The field pole face which shielded the superconducting field coil

from armature reaction fluxes (in the second and third helium runs) was removed so that the new field coil could be subjected to the full effects of the armature reaction fluxes. The m.m.f. of the normal field pole was increased from 2000 ampere-turns to 4500 ampere-turns which, when combined with the superconducting field winding m.m.f., produced a field pole flux of 2.25 milliweber. The armature and compensating windings used in the previous tests were retained.

12-5 Coil Cooldown and Energising

As with the previous helium runs, the radiation shield of the cryostat was pre-cooled with liquid nitrogen for forty-eight hours. Before the transfer of helium was commenced, the coil was pre-cooled with sufficient liquid nitrogen to a temperature of 77K. Excess liquid nitrogen was removed by reducing the pressure within the coil chamber.

A dewar pressure of 60 mm of mercury was required to commence the transfer of liquid helium, but a lower pressure of 25 mm of mercury was adequate to maintain the flow of helium to the cryostat. The super-conducting state was achieved after only forty minutes of helium transfer and the coil was successfully energised with a current of 160 amperes.

The low value of current was caused by an unexplained increase in the resistance of the water resistor since the commissioning tests had been completed. In an attempt to reduce the resistance of the water resistor, a momentary fault occurred within the water resistor and the coil underwent a quench as indicated by a dramatic increase in the rate of helium boil-off. Quick action to open the supply switches de-energised the coil without any damage being caused. The temperature at the top of the helium chamber rose to above 40K as a consequence of the quench, but the superconducting state was regained after less than ten minutes of further helium transfer. This experience was invaluable as it indicated

that the system could withstand a quench and that the manually operated
supply switches were adequate for breaking the current before any
damage could occur, provided that the operators were alert. If the
current is not broken quickly the field coil would burn out.

A maximum excitation current of 215 amperes was achieved instead of
the intended 300 amperes. This resulted from the increase in the resist-
ance of the water resistor, but the effects of the iron stator upon the
maximum flux density within the field coil reduced the critical current
substantially; hence an excitation current of 300 amperes was not
possible if the superconducting state was to be maintained.

12-6   Coil Quenches

During the two afternoons of the fourth helium run, the coil under-
went a total of five quenches which were all successfully cleared without
any damage occurring to the coil or the cryostat.

Three of the quenches appeared to be as a result of training as they
occurred when the current was slowly increasing. The quench currents
were 182 amperes, 196 amperes, and 211 amperes for the successive quenches.
Between the occurrence of these particular quenches the field coil was
subjected to the effects of the armature reaction fluxes and attraction
forces to the iron stator. During these periods there were no transitions
within the superconducting coil to the normal state.

Measurements of the flux density due to the superconduting coil,
between the cryostat and the iron stator and between the cryostat and
the compensating winding, revealed values higher than those calculated
for equivalent distances from the coil, with the coil in free space. For
example, at the iron stator the flux density was measured at 0.38 tesla
at an excitation current of one-hundred amperes, whereas the calculated

value was only 0.23 tesla for the iron free case. At the compensating winding the increase was not as marked; for example, the measured flux density was 0.2 tesla, whilst the calculated value was 0.18 tesla at an excitation current of one-hundred amperes for the iron free case. If the increase in flux density at the stator is applied to the maximum flux density at the field coil the critical current becomes 290 amperes.

As discussed in section 12-5, one quench was the result of a fault within the water resistor which resulted in a high rate of increase of current. The fifth quench resulted from a test which allowed the temperature, as indicated by the carbon resistor thermometers, in the region of the transition from the supply leads to the superconductor to exceed the critical temperature of the niobium-titanium superconductor. This was achieved by stopping the transfer of helium and allowing the helium level to fall in the coil chamber.

Although coil quenches did occur, it should be noted that they did not occur as a result of the operation of the armature which was subjected to many normal and abnormal modes of operation during the successful tests.

12-7 Machine Tests

The machine was loaded as a generator during the test. The load was a series of variable resistors which allowed both gradual and rapid changes in the armature currents.

Difficulty was experienced in monitoring the voltage across the superconducting coil terminals as a mains induced voltage in the supply cables in excess of two-hundred millivolts r.m.s. occurred. This was a result of the long cable run required from the battery room to the cryogenics laboratory. Filters were used with some success, but they also filtered out the transient voltages which had frequency components near to

the mains frequency of 50 Hertz.

To overcome this problem the tests were synthesized; that is, the transients were induced with the coil carrying a supercurrent and any apparent effects upon the superconducting coil noted, and then repeated with the superconducting coil de-energised and disconnected from the supply so that the armature induced transient voltages could be recorded.

12-7-1   Compensating Winding in Circuit

Flux plots with the compensating winding and the armature energised indicated that equal currents in both windings resulted in cancellation of the armature reaction fluxes - figure 12-3.

At a speed of 2000 r.p.m. and a supercurrent of 200 amperes, the loads on the armature were increased slowly to full load without any apparent fluctuations in the operation of the superconducting coil. The rate of the application of load was increased until finally the load was both suddenly applied and suddenly removed repeatedly; once again there were no apparent effects upon the performance of the superconducting field coil.

Synthetic transient tests revealed that a voltage spike of approximately 50 mV was induced in the superconducting coil when an armature load, which corresponded to a final current of six amperes, was suddenly applied to the generator. The duration of the transient was approximately 40 msec and an average increase in the flux density through the bore of the coil of 5 gauss occurred. Thus the coil withstood a rate of change of flux density of near 0.06 tesla/second. With the compensating winding out of circuit, the magnitude of the voltage spike increased to 59 mV. Thus it was apparent that the compensating winding had little effect upon the armature induced transient voltages which was to be expected because the component of the compensating winding flux density which induces

FIG 12-3
MODIFIED MACHINE ARMATURE FLUX DISTRIBUTION
AT SUPERCONDUCTING FIELD COIL
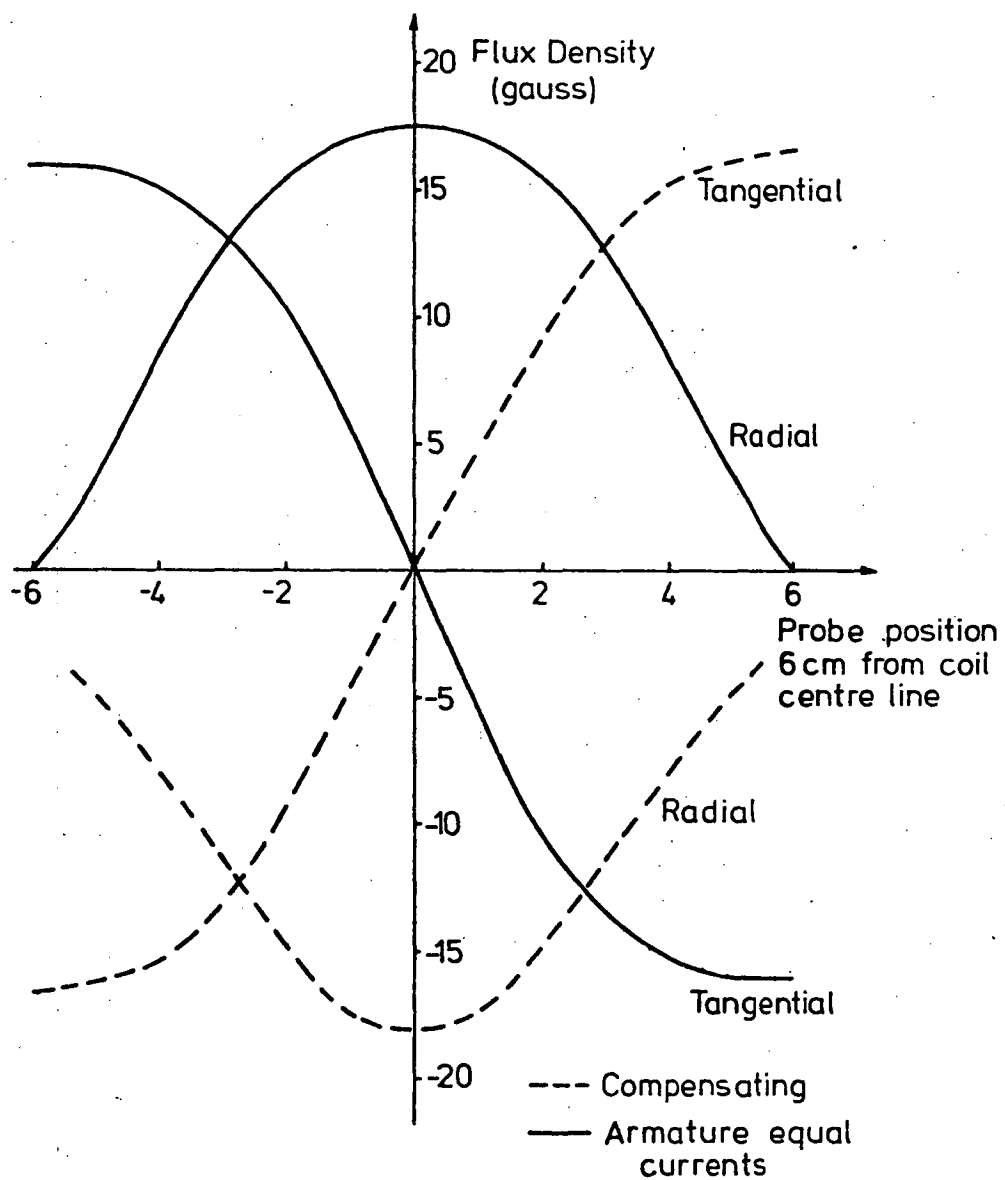
voltages in the field coil passes through a zero at the field coil.

The component of the armature reaction flux density which induces voltages in the field coil is the radial component. As the radial component of the armature flux density passes through a zero in the region of the field coil, there should not be an armature induced voltage in the field coils. This would not be the case if there were any slight imperfections in the symmetry of the armature; such imperfections would occur if a brush was incorrectly positioned or during the time the brushes were commutating current in a coil.

To test this reasoning, a 50 Hz, 6 ampere alternating current was applied to the stationary armature and then to the compensating winding. The voltage induced in the field coil by the compensating winding flux was found to be considerably less than that induced by the armature. The magnitude of the voltage induced by the armature flux was also found to be dependent upon the relative positions of the brush and the commutator segments.

12-7-2 Without the Compensating Winding

The tests conducted in the previous section were repeated but with the compensating winding out of circuit. As with the corresponding test on the machine prior to the modifications, there were no apparent fluctuations from the superconducting state even under transient loading of the armature. Armature loads, which corresponded to near twice full armature current and which produced rates of change in flux density of 0.1 tesla/second at the superconducting coil when suddenly applied, had little detectable effect upon the superconductor.

Under steady armature load conditions a voltage was induced into the superconducting coil which was a result of the commutation of the armature coil currents. The magnitude of the voltage was approximately 5 mV at

an armature speed of 2000 r.p.m. and an armature current of 6 amperes
and corresponded to a peak rate of change of flux density of near 0.006
tesla/second at the superconducting coil.

12-7-3 Normal Coil Transients

In a further attempt to induce a quench in the superconducting field
coil, the excitation current of the normal field coil was repeatedly switch-
ed on and off. With an initial normal current of one ampere, a voltage
spike of 0.64 volt was induced in the superconducting coil when the normal
field current was suddenly broken. The duration of the entire transient
spike was 0.09 seconds. To induce a voltage of 0.64 volt in the super-
conducting coil required a rate of change of flux linking the 800 turn coil
of 0.8 milli-weber per second. This corresponded to a rate of change of
the average flux density in the bore of the coil of 0.39 tesla/second.
The significance of these figures, as regards larger machines, is mention-
ed in the discussion.

However, this test failed to initiate a quench in the superconduct-
ing coil even after many attempts, in quick succession, to do so.

12-8 Cryostat and Lead Performances

The radial positioning of the superconducting field coil relied upon
the cantilever support of the inner chimney tube which was supported at
the top of the cryostat and by the heat plug. Deflection of the coil
chamber due to attractive forces between the coil and the iron stator
compressed the insulation. The insulation was not packed tightly hence
it did not have the capability of assisting in the support of the coil
container.   However, there were no apparent excessive losses of helium
during the experiment (except as a consequence of the quenches); hence
the slight compression of the insulation did not result in a significant
reduction in the insulating properties of the superinsulation.

The cryostat withstood the internal overpressures which arose during the coil quenches without any losses in vacuum. The boil-off passages around the current lead heat exchanger fins proved not to be a constriction to the helium boil-off gas flow, as the quench boil-off gases escaped within five seconds. The rapid escape of the helium gas was the reason why loss of the insulating vacuum did not occur after a coil quench due to helium intrusion into the vacuum space as a result of possible over-pressure within the coil chamber and opening of the indium seals.

With the transfer tube removed from the cryostat, the coil de-energised and completely immersed in liquid helium, the heat inleak was measured at 0.309 watt, which was 0.015 watt less than the estimated value for the leads with zero current flow. This result indicated that the lead design adopted was well suited to the conditions within the cyrostat chimney section and that future leads using the same construction could be produced with known heat inleaks.

The rate of helium boil-off decreased as the level of the liquid fell within the cryostat. The cryostat maintained the charge of helium for just over one hour, a fact which further proved the general design philosophy of the cryostat and its insulation.

12-9   Importance of the Superconducting State

The combined resistance of the leads and the coil with the coil superconducting was less than 2 milli-ohms, but after the transition to normal conduction the total resistance was 53.7 milli-ohms at a temperature of 10K. The room temperature resistance of the coil was 6.03 ohm; thus a reduction in the conductor resistance between room temperature and 10K by a factor of 112 occurred. However, with a coil temperature of 10K and an excitation current of 300 amperes, the total heat loss to the coolant would total 4.84 kW. This indicates the

necessity for the final transition to superconduction before cryogenic cooling of coils to temperatures below 10K and operation as field coils becomes practically and economically possible.

12-10   Discussion

As a result of the unresolved malfunction in the current supply to the superconductor, the maximum excitation current achieved was below that initially aimed for. However, from the occurrence of several quenches, it was apparent that the coil was operating close to its limits with an excitation current of only 215 amperes.

Despite this, the effects on the superconducting coil of the loading of the armature, both with and without the compensating winding in circuit were minimal; that is, there were no apparent fluctuations from the superconducting state in the coil during both normal and abnormal loading cycles of the armature.

The sudden removal of the excitation current of the normal field coil produced little effect upon the excitation current of the superconducting coil even though rates of change of flux density at the coil in excess of 0.39 tesla per second occurred during the disconnection. Rates of change in flux density of this magnitude for the supercurrents would result in field charging times of less than fifteen seconds. This would be too slow for many industrial applications; however, rapid armature current changes could be possible without exceeding the acceptable level of the rate of change of flux density for a well cooled superconducting field system. For example, the superconducting machine with the armature type field winding discussed in Chapter 13 has a peak armature reaction flux density at the field winding on full load of 0.037 tesla. To exceed the rates of change of flux density achieved during the experiments five complete armature current reversals per second would be required.

Throughout the tests it was apparent that commutation proceeded without difficulties for all of the armature loads applied. One brush sparked marginally, but this was found to be a result of the brush not being correctly seated on the commutator. Sparking was almost non-existent at the second brush at all armature speeds and loads used during testing. The compensating winding did not have an appreciable effect upon the commutation at the properly seated brush; however, a reduction in the sparking occurred at the other brush when the compensating winding was in circuit.

12-11 Conclusion

Although the tests did not indicate the limiting conditions for a quench to be initiated from armature loading, they showed that a compensating winding and a protective field pole face were not necessary for the successful operation of a superconducting field system in a large heteropolar D.C. machine. It was thus apparent that a compensating winding would only be included to protect the field system from the load torque of the machine and, to some extent, to induce a commutating voltage into coils undergoing commutation.

The format of the prototype machine selected completely eliminates iron from the magnetic circuit as the preceding experiments revealed that iron was not required to shield the superconductor from armature reaction fluxes. The compensating winding is not required for shielding and has been excluded from the model machine discussed in Chapter 14, but has been included in the design of the prototype machine discussed in Chapter 13.

CHAPTER 13.

MACHINE COMPARISONS

13-1   Introduction

To give an indication as to the competitiveness of the superconducting heteropolar machine it was necessary to produce the following designs of a conventional heteropolar machine, a superconducting heteropolar machine, and a superconducting homopolar machine.

The rating of the machines was chosen at 10MW at a speed of 200 r.p.m. The rating was determined on the basis of the limitations of the conventional type D.C. machines but large enough to make the superconducting machines economically attractive.

The final comparisons were based upon the overall dimensions and the weights of the machines with all ancilliary equipment, such as the cryogenerators for the superconducting machines, being neglected.

13-2   Conventional Heteropolar Machine Design

The following design followed clsely the methods suggested in the book by CLAYTON and HANCOCK (13-1). The D^2L relationship and, as in the case of large machines, the voltage between commutator segments were the limits to the design (13-2 to 13-6).

13-2-1   Armature

The output of a D.C. machine is given by equation 13-1

$$P = \pi^2 n \bar{B} q D^2 L \qquad (13-1)$$

The voltage between commutator segments, or the volts per bar, for single turn coils is given by equation 13-2. Single turn coils are essential in large rated machines so that the volts per bar can be

maintained within the desired limits.

$$V_b = 2\pi\ n\ B_{MAX}\ D\ L\ p/a \qquad (13-2)$$

P = output power (watts)

n = speed (rev/second)

$\bar{B}$ = average pole flux density at the armature winding (tesla)

B_{MAX} = maximum pole flux density at the armature winding (tesla)

q = armature specific electric loading (ampere/metre)

D = armature diameter (metre)

L = armature length (metre)

p/a = ratio of poles to parallel paths

For large machines a representative value of $\pi^2\ \bar{B}\ q$, or the output coefficient, is $3.6 * 10^5$ watts-sec/m^3; hence for a 10MW, 200 r.p.m. machine

$$D^2L = \frac{10 * 10^6 * 60}{200 * 3.6 * 10^5}\ m^3$$

$$D^2L = 8.3\ m^3$$

If the voltage between bars is 15 volts, as indicated in the references, then:

$$D\ L \le \frac{15 * \,^a/p * 60}{2 * \pi * 200 * 1.2}$$

$$D\ L \le 0.60\ \,^a/p\ m^2$$

Simple Lap Winding

For a simple lap winding $a/p = 1.0$ and solving the equations for D and L revealed

$$D \ge 13.8\ \text{metres}$$

$$L = 0.043\ \text{metres}.$$

These dimensions are unacceptable. A technique by which the diameter can be reduced is to reduce the maximum flux density. For example,

if B_{MAX} = 0.4 tesla D L $\leq$ 1.8 for a simple lap winding.

$$D \geq 4.61 \text{ metres}$$

$$L \leq 0.40 \text{ metres}$$

With B_{MAX} = 0.4 tesla the required value of the armature specific electric loading is near 100,000 amp/metre which for conventional machines is considered to be almost unobtainable. Thus at first it appears that a 10MW, 200 r.p.m. machine would be extremely large unless a technique by which the maximum allowable value of the volts per bar can be increased or the actual volts per bar reduced within the machine. The volts per bar can apparently be greatly increased by suitably ventilating the commutator - (13-7). The volts per bar can be reduced within the machine by adopting a duplex lap winding.

Duplex Lap Winding

For the duplex lap winding the ratio P/a = 0.5; hence, for the same pole flux and machine speed the volts per bar is half that for a simple lap winding.

Using the firstly obtained equations for D^2L and D L the following results were obtained:

$$D^2L = 8.3 \text{ m}^3$$

$$D L \leq 1.2 \text{ m}^2$$

$$\therefore D \geq 6.9 \text{ metres}$$

$$L \leq 0.173 \text{ metres.}$$

These limiting values were considered to be unacceptable hence the following approach to the design was taken.

If the ratio D/L $\leq$ 7 then from the D^2L relationship and an output coefficient of 3600 Joule/m^3:

$$D^2 \frac{D}{7} \leq 8.3 \ m^3$$

$$\text{or} \quad D \leq 3.87 \ \text{metres}$$

$$L \geq 0.553 \ \text{metres}$$

$$D \ L = 2.14 \ m^2$$

From the value of D L the associated value of B_{MAX} calculated from equation 13-2

$$B_{MAX} \leq \frac{V_b}{2 \pi n \ P/a \ D \ L}$$

$$= \frac{V_b}{2 * \pi * \frac{200}{60} * 0.5 * 2.14}$$

$$B_{MAX} \leq 0.0446 \ V_b :$$

V_b	B_{MAX}
15 volts	0.67 tesla
17 volts	0.759 tesla
20 volts	0.892 tesla

With V_b limited to 15 volts and with the assumption that $\bar{B} = 0.7 \ B_{MAX}$ the value of the armature specific electric loading was calculated from the Esson coefficient (output coefficient).

$$q = \frac{3.6 * 10^5}{\pi^2 * 0.7 * 0.67} \ \text{ampere/metre}$$

$$q = 77,800 \ \text{ampere/metre.}$$

This value of q was considered to be too high; hence, to obtain the desired dimensions V_b was increased to 20 volts and the corresponding value of q was 58,400 ampere/metre.

The values of D and L selected are 3900mm and 550mm respectively.

13-2-2   Number of Field Poles

A high terminal voltage for D.C. machines of 2000 volts was

selected which required an armature current of 5,000 amperes. A limit of 500 ampere per brush arm fixed the number of poles at 20.

13-2-3 Armature Conductors

With a limit of 20 volts for the maximum value of the volts per bar, the corresponding average generated voltage per conductor is 14 volts. Thus the number of series conductors required to obtain the terminal voltage of 2000 volts is 143, say 140; thus the total number of armature conductors is:

$$Z_c = 140 * 40 \text{ (for a duplex winding)}$$
$$Z_c = 5,600.$$

The current within the armature conductors for a duplex lap winding is one quarter the brush current, hence:

$$I_c = \frac{500}{4} \text{ amperes}$$
$$I_c = 125 \text{ amperes}$$

With a high current density of 4.5 ampere/mm^2 the required cross sectional area of the armature conductor is:

$$A_c = \frac{125}{4.5} \text{ mm}^2$$
$$A_c = 27.8 \text{ mm}^2$$

The length of the armature coils was estimated with the assumptions that a 50mm overhang occurred at each end of the armature core and that the coils were bent at 30° to the armature.

$$\text{pole pitch} = \frac{3900 * \pi}{20} \text{ mm}$$
$$= 613 \text{mm}$$
$$\therefore \quad L_c = [(550 + 100) + \frac{613}{\sin 60°}] * 2 \text{ mm}$$
$$= 2716 \text{mm}$$
$$\therefore \text{ total conductor length} = 2800 * 2716 * 10^{-6} \text{ km}$$
$$= 7.6 \text{ km}$$
$$\therefore \text{ conductor weight} = 7.6 * 27.8 * 8.9 * 10^{-3} \text{ tonnes}$$
$$= 1.88 \text{ tonnes.}$$

The total series resistance is thus:

$$R_s = 1.7 * 10^{-8} * \frac{7.6 * 10^3}{27.8 * 10^{-6}} \ \Omega$$

$$R_s = 4.65\Omega$$

The armature resistance is:

$$R_a = R_s/(N^o \text{ parallel paths})^2 \quad (N^o \text{ parallel paths} = 2 \times N^o$$

poles for a duplex lap winding)

$$= \frac{4.65}{40 * 40}$$

$$= 2.9m\Omega \text{ cold or } 3.5m\Omega \text{ hot.}$$

$$I^2R \text{ loss} = 5,000^2 * 3.5 * 10^{-3} \text{ watts}$$

$$= 88KW.$$

Adding on the eddy current loss the total losses in the copper are 110 KW or 1.1% efficiency drop.

13-2-4 Slot Design

The frequency of the flux reversals within the conductors for the machine is 33Hz. The depth of individual conductors should be therefore limited to below 19mm, preferably near 15mm.

The number of slots must be an integer multiple of the number of pole pairs so that equalising connections are possible. With ten conductors per slot then 560 slots are required which enables equalising connections. Thus the available width per slot and the corresponding armature tooth is 21.9mm.

The tables below list the allowances made for the materials that are contained within each slot and hence the slot dimensions. To maintain the conductor depths below 15mm it was decided that each coil would consist of two parallel conductors 10mm deep by 1.4mm wide. This method would add to the cost of the machine because of the added complication in forming the coils and making the end connections.

```
Slot Width

conductors 5 * 1.4mm        7mm
mica wrap 10 * 0.3mm        3mm

tape and lining            0.8mm
slack allowance            0.6mm
                           ‾‾‾‾‾‾
                           11.4mm
```

```
Slot Depth

conductor 4 * 10mm          40mm
mica wrap                   4mm
tape and lining            0.8mm
bakelized fabric wedge      5mm
micanite layer separator   0.5mm
slack allowance             3mm
                           ‾‾‾‾‾‾
                           53.3mm
```

13-2-5 Armature Core

The allowable flux density in the armature core should not exceed 1.25 tesla. A value of 1.1. tesla was selected because of the flux reversal frequency of 33Hz. The path in the core has to carry one half of the useful pole flux, i.e. 0.105 weber.

$$\text{core thickness} = \frac{\text{flux}}{(\text{flux density}) * (\text{core length})}$$

$$= \frac{0.105}{1.1 * 0.55} \text{ metres}$$

$$= 174\text{mm}.$$

$$\therefore \text{ inner diameter of core} = 3900 - 2 * 53.3 - 2 * 174\text{mm}$$

$$= 3445\text{mm}.$$

$$\therefore \text{ armature iron mass} = (\text{core volume} + \text{teeth volume}) * \text{density}$$

$$\text{core volume} = \pi * (3445+174) * 174 * 550 * 10^{-9} \text{ m}^3$$

$$= 1.088 \text{ m}^3.$$

$$\text{teeth volume} = 560 * 550 * 53.3 * 10.5 * 10^{-9} \text{ m}^3$$

$$= 0.172 \text{ m}^3.$$

$$\therefore \text{ armature iron mass} = 7.8 * (1.088 + 0.172) \text{ tonnes}$$

$$= 9.83 \text{ tonnes.}$$

13-2-6 Commutator

For this design an estimate of the commutator diameter was necessary to ensure that it is compatible with other dimensions.

With an allowance of 4mm for each commutator bar then:

$$\text{Commutator diameter} = \frac{N^o \text{ bars } * \text{ width}}{\pi}$$

$$= \frac{2800 * 0.004}{\pi} \text{ metres}$$

$$= 3.56 \text{ metres.}$$

This diameter allowed sufficient space for the brush gear; hence it was acceptable.

13-2-7 Field Poles

The field pole flux on load was chosen as 20% higher than the effective field pole flux because of armature reaction fluxes and leakage fluxes. A working flux density of 1.5 tesla resulted in a pole area of:

$$\text{pole area} = \frac{\text{pole flux}}{\text{flux density}}$$

$$= \frac{1.2 * 0.21}{1.5} \text{ m}^2$$

$$= 0.168 \text{ m}^2$$

$$\text{allowance for laminations pole area} = \frac{0.168}{0.75} \text{ m}^2$$

$$= 0.177 \text{ m}^2$$

$$\therefore \text{limb breadth} = \frac{0.177}{0.55 - 0.015} \text{ metre}$$

(armature length 550mm)

$$= 331\text{mm}$$

(spacing allowance 15mm)

The space available for each pole limb is 613mm hence there is adequate space for the limb, windings and interpoles.

Pole Length

The design of the field windings was based upon the permissible heat loss per unit surface area of the field coils and that the field ampere turns was 25% higher than the armature ampere-turns. To obtain the required field flux physical adjustments to the airgap between the pole shoes and the armature surface are necessary.

$$\text{armature ampere turns per pole} = \frac{(\text{conductor current}) \ast (N^o \text{ coils})}{\text{number of poles}}$$

$$= \frac{125 \ast 2800}{20} \text{ ampere-turns}$$

$$= 17,500 \text{ ampere-turns}$$

$$\therefore \text{field pole ampere turns} = 1.25 \ast 17,500 \text{ ampere-turns}$$

$$\therefore Z_p = 21,900 \text{ ampere-turns.}$$

The following derivation related the permissible heat loss per unit surface area of the field windings to the required field pole MMF and the field coil dimensions.

ℓ = average length of turns (metre)

h = height of winding (metre)

d = depth of winding (metre)

σ = winding space factor

α = current density (amp/metre^2)

P = heat loss per unit area (watt/m^2)

ρ = conductivity of wire (ohm-m)

Z_p = field pole MMF (ampere-turns)

$$\text{coil surface area} = 2 \ell h$$

$$\text{total conductor area} = \sigma d h$$

$$\text{field pole ampere turns} = \sigma d h \alpha = Z_p$$

$$\text{power loss} = Z_p^2 * \frac{(\text{turn length}) * \rho}{(\text{total copper area})}$$

$$= (\sigma d h \alpha)^2 * \frac{\ell \rho}{\sigma d h}$$

$$= \alpha^2 \sigma \ell d h \rho$$

$$\therefore \text{coil surface area} = \frac{\text{power loss}}{P}$$

$$\therefore 2 \ell h = \frac{\alpha^2 \sigma \ell d h \rho}{P}$$

$$\text{or} \quad \alpha = \left(\frac{2P}{\sigma d \rho}\right)^{\frac{1}{2}} = \frac{Z_p}{\sigma d h}$$

$$\therefore \quad h = Z / \sqrt{2P \sigma d/\rho}$$

With representative values of P, σ and ρ, h can be calculated in terms of d.

$$P = 660 \text{ watt/m}^2$$

$$\sigma = 0.65$$

$$\rho = 2 * 10^{-8} \text{ ohm-metre}$$

$$\therefore \quad h = \frac{21900}{\sqrt{\frac{2 * 660 * 0.65}{2 * 10^{-8}}}} * \frac{1}{d^{\frac{1}{2}}}$$

$$\therefore \quad h = \frac{0.106}{d^{\frac{1}{2}}}$$

The values of d and h which could be easily accommodated in the space available are d = 60mm and h = 430mm.

The total mass of the field copper was estimated at 5.67 tonnes and the mass of the field pole limbs was 11.8 tonnes.

13-2-8 Yoke

The full load flux density was limited to 1.2 tesla and the full

load yoke flux was one half the full load pole flux or 0.126 weber (section 13-2-8).

$$\therefore \text{ yoke area } = \frac{\text{flux}}{\text{flux density}}$$

$$= \frac{0.126}{1.2} \text{ m}^2$$

$$= 0.105 \text{ m}^2$$

For a yoke length of 800mm the required yoke thickness is 130mm and the weight of the yoke was estimated at 12.1 tonnes.

13-2-9   Machine Mass

Copper

armature	2.6	tonnes
field	5.67	tonnes

Iron

armature core	8.49	tonnes
armature teeth	1.34	tonnes
yoke	12.1	tonnes
pole limbs	11.8	tonnes
Total	42	tonnes

With an allowance for the shaft, end bells, bearings and interpoles the machine weight would approach 47 tonnes thus giving the machine a specific weight ratio of 4.7 tonnes/MW.

13-2-10   Efficiency

Only the electrical losses were considered and they were:

armature copper loss	120KW
field copper loss	22KW
armature iron loss (3 watt/kg)	25KW
brush contact loss	10KW
	177KW or 1.7% efficiency drop.

13-3   Superconducting Homopolar Machine Design

13-3-1   Armature

The two forms of the homopolar machine are the segmented disc type - figure 13-1 and the drum type - figure 13-2. The disc type armature was chosen because of its greater simplicity. The limitations of the homopolar machine are the current collection problems and the stage voltage of the armature segments. To obtain a convenient terminal voltage, thus decreasing the armature current, and to maintain an acceptable voltage between segments, the series parallel connection developed by IRD (13-8) was chosen for the armature configuration - figure 13-1.

If the maximum stage voltage allowed is 25 volts then the machine flux is given by

$$\phi = \text{stage voltage/speed}$$
$$= 25 * 60/200 \text{ weber}$$
$$\phi = 7.5 \text{ weber.}$$

For a terminal voltage of 500 volts, 40 segments per side of a double sided armature using the series parallel connection are required. A rating of 10MW at 500 volts requires an armature current of 20,000 amperes; thus the brush current, which equals the armature conductor current, is 10,000 amperes.

The rating of a homopolar machine can be expressed by the following design equation:

$$P/N = c \bar{q} \phi D \qquad (13\text{-}3)$$

P = power (watts)

N = speed (r.p.s.)

$\bar{q}$ = total slip ring current per metre of circumference per slip ring (amp/metre).
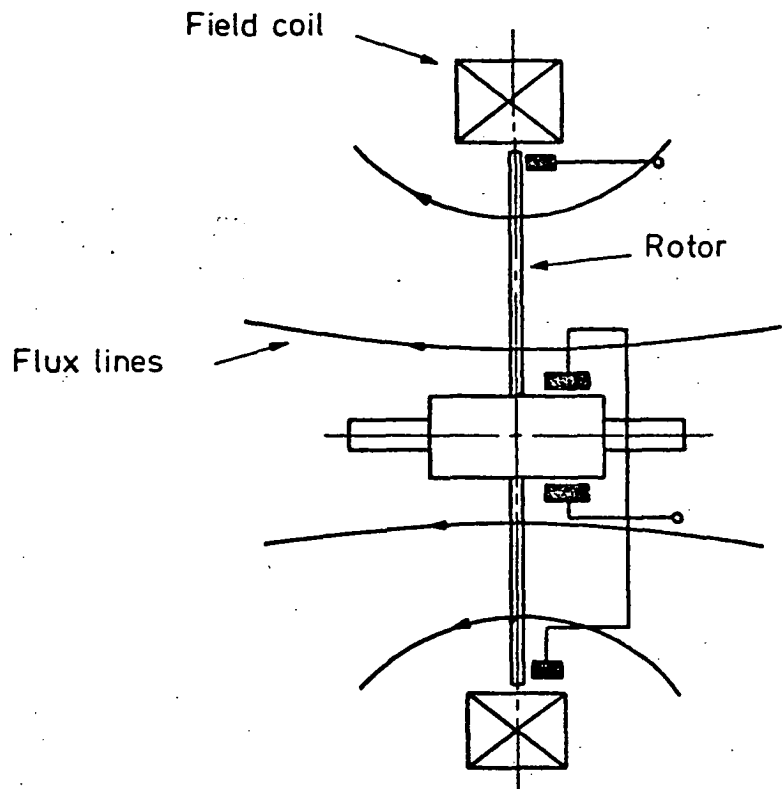
DISC TYPE HOMOPOLAR MACHINE
FIG 13-1
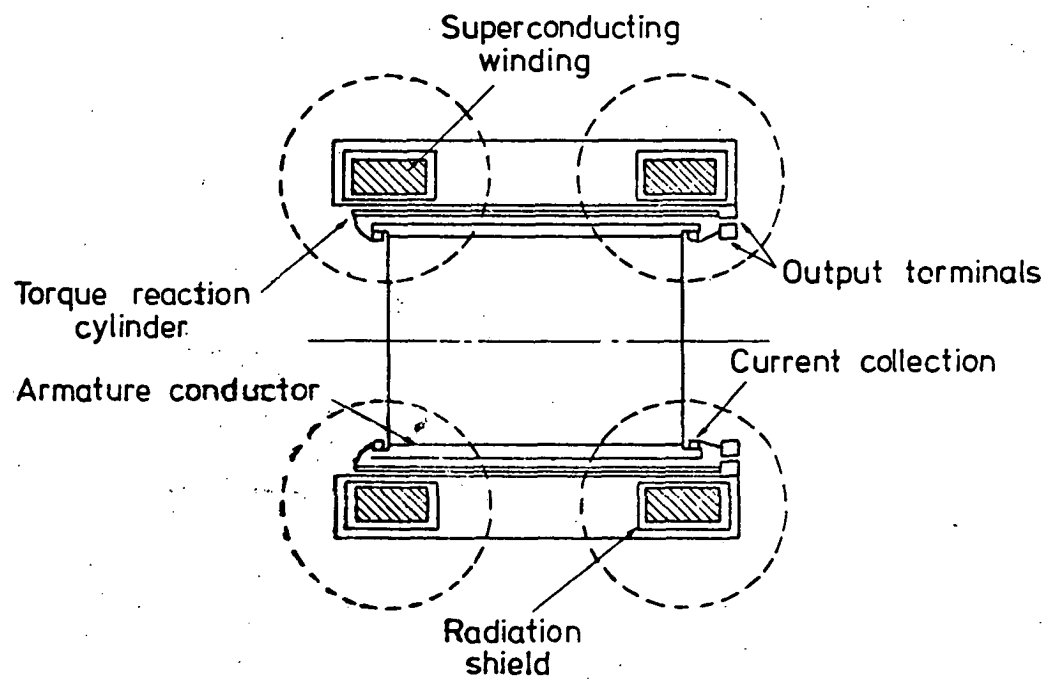
DRUM TYPE HOMOPOLAR MACHINE
FIG 13-2

D = outer brush gear contact diameter (metre)

C = 2π for double sided armature.

A realistic value of $\bar{q}$ was obtained from the following considerations:

For the Fawley machine high copper content carbon brushes were used. From dimensions given in reference 13-9, $\bar{q}$ was estimated at near 8000 ampere/metre. In reference 13-8 it is stated that 8000 HP could be developed within the same frame size. This would require that:

$$\bar{q} = 8,000 * \frac{8,000}{3,250} \text{ ampere/metre} \quad \text{(Fawley machine rating 3250 HP)}$$

$$= 20,000 \text{ ampere/metre}$$

With $\bar{q}$ = 20,000 ampere/metre the actual value of q under the brushes would be a little greater than 40,000 ampere/metre for the disc type homopolar machine.

If instead of using high copper content carbon brushes liquid metal brushes are used then $\bar{q}$ could be as high as 50,000 ampere/metre (13-8 to 13-10). The other alternative is the carbon fibre brushes developed by the IRD which suggest that $\bar{q}$ could be in the vicinity of 30,000 ampere/metre (13-11).

The carbon fibre brushes were selected because they did not involve any hazardous materials as is the case with some liquid metal brushes nor is there any need for special ancilliary equipment which maintained and cleaned the liquid metal.

Thus with carbon fibre brushes the values of $\bar{q}$ and D chosen were

$\bar{q}$ = 29,000 ampere/metre

D = 2.2 metres.

The slip ring speed is thus 23 m/sec.

At this point it should be noted that 2.2 metres is approximately the same diameter as the Fawley armature which produced 2.42MW at 200 r.p.m.

The above design therefore requires over four times the output from the same armature as the Fawley motor. The Fawley motor however employed conventional brushes capable of a current density of 300 kA/m^2 at a slip ring speed of 40m/sec whereas the carbon fibre brushes are capable of 930 kA/m^2 at 40m/sec or over three times the current density of the conventional brush (13-9). For four times the power with only three times the brush current density the above design probably favours the cause of the homopolar machine in the final comparisons

The current collection at the inner diameter is achieved with a commutator with only 40 segments and the restrictions on $\bar{q}$ for the outer diameter are not applicable. However, the length of the commutators cannot be too large.

13-3-2 Shaft Design

The design of the shaft was based upon the theory given in TIMOSHENKO and GOODIER's book *Theory of Elasticity* (13-12).

The shear stress σ_I at radius r in a shaft of radius α subject to a load torque T is given by equation 13-4.

$$\sigma_I = \frac{2Tr}{\pi \alpha^4} \tag{13-4}$$

The maximum shear stress occurs at $r = \alpha$

$$\sigma_{IMAX} = \frac{2T}{\pi \alpha^3} \tag{13-5}$$

If the maximum permissible sheer stress in the shaft is limited to 69MPa(10,000 psi) then the shaft diameter is given by equation 13-6.

$$d_s = 2 * (\frac{2 * P}{\pi * N * \sigma_{IMAX}})^{1/3} \tag{13-6}$$

P = machine rating (watt)

N = machine speed (radian/second)

$$\therefore d_s = 2 * (\frac{2 * 10^7 * 60}{\pi * 200 * 2 * \pi * 69 * 10^6})^{1/3} * 1000mm$$
$$d_s = 328mm.$$

Choose the shaft diameter as 330mm.

The weight of the shaft was thus 0.667 tonne/metre.

13-3-3 Brushes and Commutators

Outer Brushes

The diameter of the armature and the need for 40 segments per side provided less than 170mm of the armature circumference per brush. At the surface speed of 23 metre/sec. current densities near 930kA/m^2 are possible. To allow a small margin of safety the required brush length at a current density of 800kA/m^2 and a brush current of 10,000 amperes is given by:

$$\ell_b = \frac{10,000}{800} * \frac{1,000}{170} \text{ mm}$$

$$\ell_b = 73.5\text{mm.}$$

Thus the outer diameter brush size required is approximately 165mm x 75mm.

Inner Brushes

If the active length of the commutators is limited to near 400mm and a brush current density of 0.8 amp/mm^2 is used then the required diameter of the commutators is:

$$\text{Brush width} = \frac{10,000}{0.8 * 400} \text{ mm}$$

$$= 31.3\text{mm.}$$

To eliminate the possibility of the brushes short circuiting the armature each brush was assumed to be 95% the width of a commutator bar and that a spacing of 3mm between each commutator bar was necessary. Thus the inner commutator circumference required is:

$$C_c = (\frac{31.3}{0.95} + 3) * 40\text{mm}$$

$$= 1440\text{mm.}$$

Thus the minimum commutator diameter is 458mm.

The actual length of the commutators would be near 500mm which allows for ten separate brushes, which make up the required brush area, with a spacing of 10mm between brushes.

The required depth of each commutator bar was estimated as follows.

With good current sharing between brushes the current distribution along the length of each bar would be as in figure 13-3. The best design for the commutator bars when considering the actual current density would produce tapered bars but it is considered that constant cross sectional area bars are the best choice using $1/\sqrt{3}$ * (RMS armature conductor current) as the design current. The fact of $1/\sqrt{3}$ leads to the same I^2R losses in the commutator bar as the assumed current distribution. The RMS conductor current was calculated using the estimated dimensions of the brushes and commutator segments and the resulting conductor current waveform - figure 13-4.

Thus the design current $= \dfrac{5960}{\sqrt{3}}$ ampere

$\qquad\qquad\qquad\qquad = 3,440$ ampere.

With a current density of 4 amp/mm^2 the bar cross sectional area is 860mm^2 and the bar depth required to achieve the cross sectional area is 26mm.

These dimensions result in a commutator inner diameter of near 400mm which gives adequate clearance between the shaft and the commutators.

The total weight of the copper in both of the commutators is given by:

$$W_c = 80 * 860 * 500 * 8.9 * 10^{-9} \text{ tonnes}$$

$$= 0.306 \text{ tonnes}.$$

13-3-4   Armature Conductors

The RMS value of the armature conductor current as obtained from
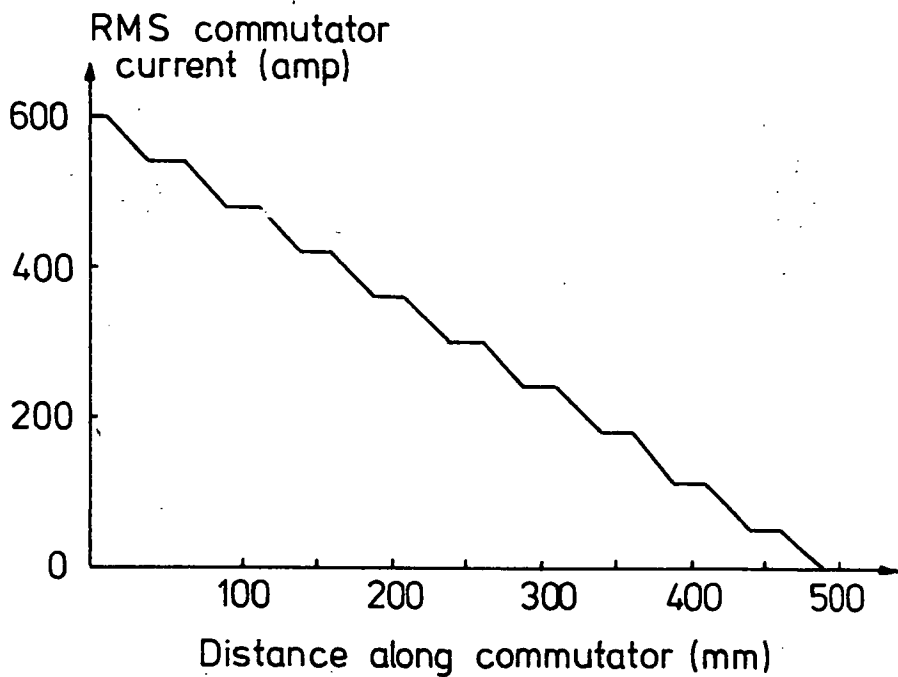
HOMOPOLAR MACHINE COMMUTATOR BAR CURRENT DENSITY
DISTRIBUTION
FIG 13-3
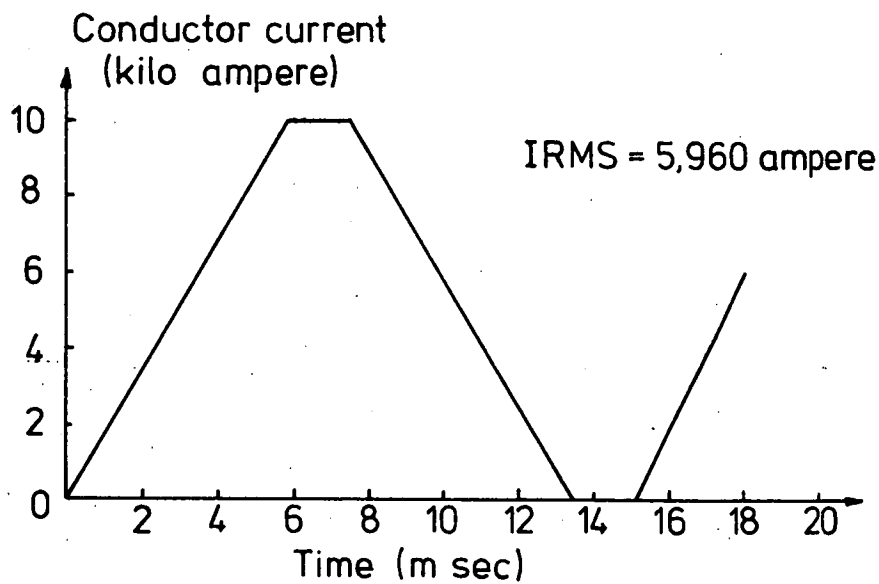
IRMS = 5,960 ampere

HOMOPOLAR MACHINE CONDUCTOR CURRENT WAVEFORM
FIG 13-4

figure 13-4 is 5,960 ampere. The maximum width available for each conductor (assuming zero spacing between bars) ranges from 36.1mm at the commutator to 173mm at the outer armature diameter.

To maintain a constant conductor current density would require bars of constant cross sectional area which necessitates either varying the conductor thickness or varying the spacing between bars or both. For ease of manufacture constant thickness and constant spacing between bars is desirable, hence the current density is not constant.

In large conventional DC machines current densities are normally limited to 4.5 amp/mm^2 but with the freely ventilated armature conductors of the homopolar machine and the possibility of forced cooling greater current densities are possible. The shape of the conductors results in a 5-fold reduction in current density from the inner to the outer radii. The heat generated in the region of the greatest current density is conducted to and dissipated from the region of lower current density. With a current density of 7.5 amp/mm^2 at the inner radius the average current density is 3.1 amp/mm^2 which is a representative value for force cooled heavy current conductors.

At a current density of 7.5 amp/mm^2 at the inner radius and allow a spacing of 5mm between conductors.

$$\text{Conductor depth} = \frac{5960}{7.5 * 31.1} \text{ mm}$$

$$= 25.6\text{mm}$$

$$\text{Approximate weight of copper} = 2 * \pi * 25.6 \, (1100^2 - 230^2)$$
$$* \, 8.9 * 10^{-9} \text{ tonnes}$$
$$= 1.66 \text{ tonnes.}$$

$$\text{Resistance of each conductor} \simeq \frac{1440}{31.1} * \frac{1.7 * 10^{-6}}{2 * \pi * 2.56} \, \ell n \, \frac{1.1}{0.23} \, \Omega$$
$$= 7.7\mu\Omega$$

$$\text{Total armature } I^2R \text{ loss} = 5,960^2 * 80 * 7.7 * 10^{-6} \text{ watt}$$
$$= 22\text{KW or } 0.22\% \text{ efficiency loss.}$$

13-3-5 Superconducting Field Coil

The superconducting field coil is required to produce a flux of 7.5 weber between the radii of 230mm and 1100mm. The restrictions on the design are that it should use as little superconductor as possible, have the minimum volume possible, and that the maximum flux density within the coil does not exceed the critical flux density.

The superconducting wire chosen for the coil was the IMPERIAL METAL INDUSTRIES multifilamentry niobium titanium wire NIOMAX FM c361/142 - Appendix H.

The inner diameter of the superconducting field coil was estimated as below.

Armature outside radius	1100mm
Clearance from armature to cryostat	5mm
Cryostat outer section metal thickness	10mm
Insulation path to radiation shield	35mm
Radiation shield thickness	3mm
Insulation path of helium chamber	35mm
Cryostat helium chamber metal	10mm
Helium flow passage between coil and the cryostat.	10mm
Total	1208mm

Thus the coil inside diameter was chosen at 2420 mm.

The insulation allowance exceeds that necessary from insulation considerations only to simplify construction through increased tolerances. Metal thicknesses are confirmed in section 13-3-8.

First Design

The design of the coil was based upon obtaining the minimum coil volume which produced the required central flux density - Appendix J.

For the superconductor chosen a wire current density of 300 amp/mm^2 or an excitation current of 475 ampere were considered to be satisfactory values. This decision took into account the characteristics of the wire and the flux densities expected in the field coil. If a packing factor of 0.67 is achieved within the coil then the coil current density would be 200 amp/mm^2.

As a guess, until further experience with coil design is obtained, the ratio of the average flux density within the active region to the central flux density was taken as 1.1. The average flux density $\bar{B}$, and hence the central flux density B_0 were obtained from the following

$$\bar{B} = 7.5/\pi(1.1^2 - 0.23^2) \text{tesla}$$
$$= 2.063 \text{ tesla}$$
$$\therefore \ B_0 = 2.063/1.1 \text{ tesla}$$
$$= 1.88 \text{ tesla}.$$

The technique discussed in Appendix J was used to determine the optimum coil with $B_0 = 1.88$ tesla, $J = 200$ amp/mm^2, and $R_0 = 1.21$ metres. The results of this search are tabulated below.

Volume	$2A/R_0$	$2B/R_0$	$\dfrac{B_0 R_0}{\mu_0 I}$	Comments on final Column
0.02	0.01722	0.1833	1.96	too large
0.10	0.0496	0.3131	0.398	too small
0.085	0.04475	0.296	0.467	too small
0.0813	0.044	0.2876	0.488	just too large
0.08185	0.0442	0.288	0.486	final answer

With $2A/R_0 = 0.0442$, $2B/R_0 = 0.288$ and $B_0 = 1.88$ tesla, the maximum flux density within the coil was estimated as 7.2 tesla - Appendix I. The quench flux density is 7.4 tesla, so the coil is only just safe if the wire performs up to its short sample characteristic.

Second Design

The next step is to use the first design to obtain a better estimate of the flux density distribution for the final coil. The flux density across the bore was calculated (Appendix I) hence the useful flux was calculated. From this a better value of the ratio (average flux density in active region)/(central flux density) was obtained and a second coil with the new central flux density was designed.

The ratio of $\bar{B}/B_0$ was given by equation 13-7.

$$\bar{B}/B_0 = \frac{2 R_0^2}{\beta(o)(R_2^2 - R_1^2)} \int_{R_1/R_0}^{R_2/R_0} \beta(r) \, r \, dr \qquad (13\text{-}7)$$

R_2 = outer active radius

R_1 = inner active radius

$$\beta(r) = \frac{B(r) R_0}{\mu_0 I} \qquad I = \text{coil ampere-turns}$$

r = non dimensional radius.

The flux density distribution of the first coil (figure 13-5) indicated that the ratio $\bar{B}/B_0 = 1.64$. This value is much greater than the assumed value of 1.1 hence a second design is necessary with $\bar{B}/B_0 = 1.64$.

The second design has the same current density and inner radius but the central flux density required is only 1.26 tesla.

Repeating the search process results in the following

Volume	$2A/R_0$	$2B/R_0$	$\dfrac{B_0 R_0}{\mu_0 I}$	Comments on Final Column
0.0442	0.08185	0.288	0.325	too small
0.05	0.0316	0.248	0.529	too large
0.054	0.0334	0.253	0.49	just too large
0.05433	0.0336	0.2531	0.4872	final result
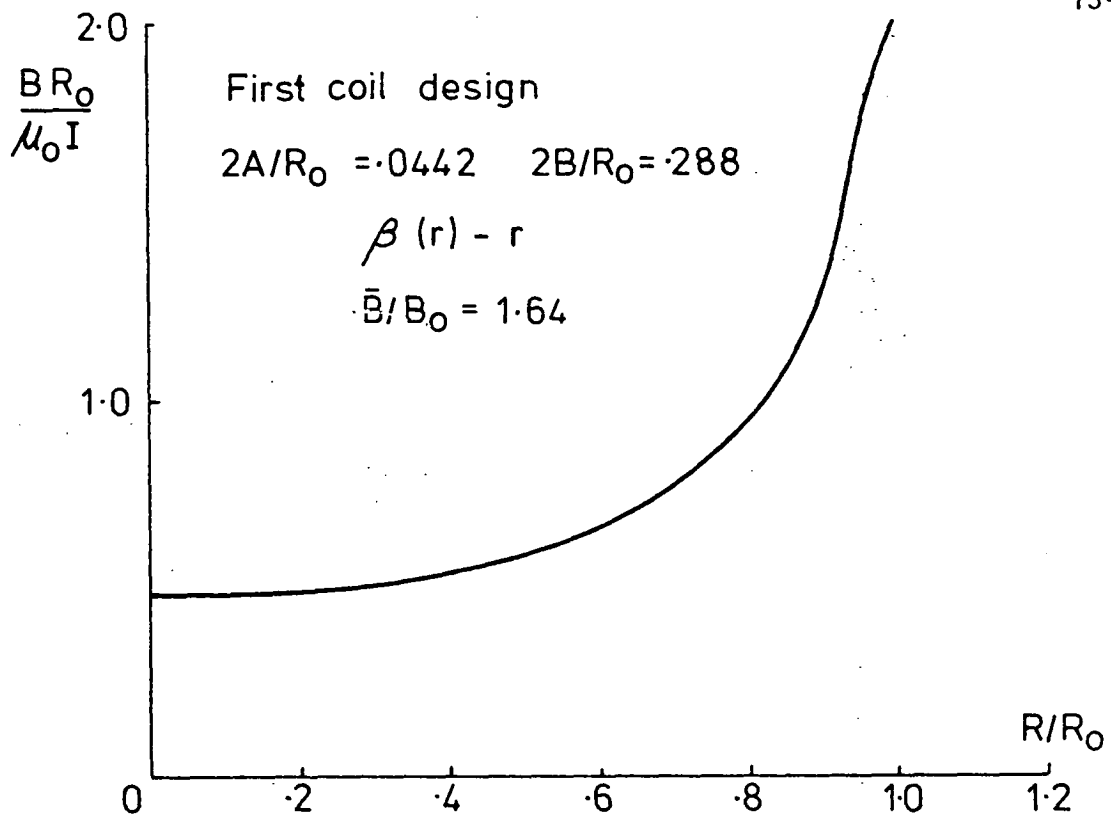
First coil design

$2A/R_0 = \cdot 0442 \quad 2B/R_0 = \cdot 288$

$\beta (r) - r$

$\bar{B}/B_0 = 1 \cdot 64$

COIL CENTRAL PLAIN FLUX DENSITY 10 MW HOMOPOLAR MACHINE

FIG 13-5

Second coil design

$2A/R_0 = \cdot 0336 \quad 2B/R_0 = \cdot 2531$

$\beta (r) - r$
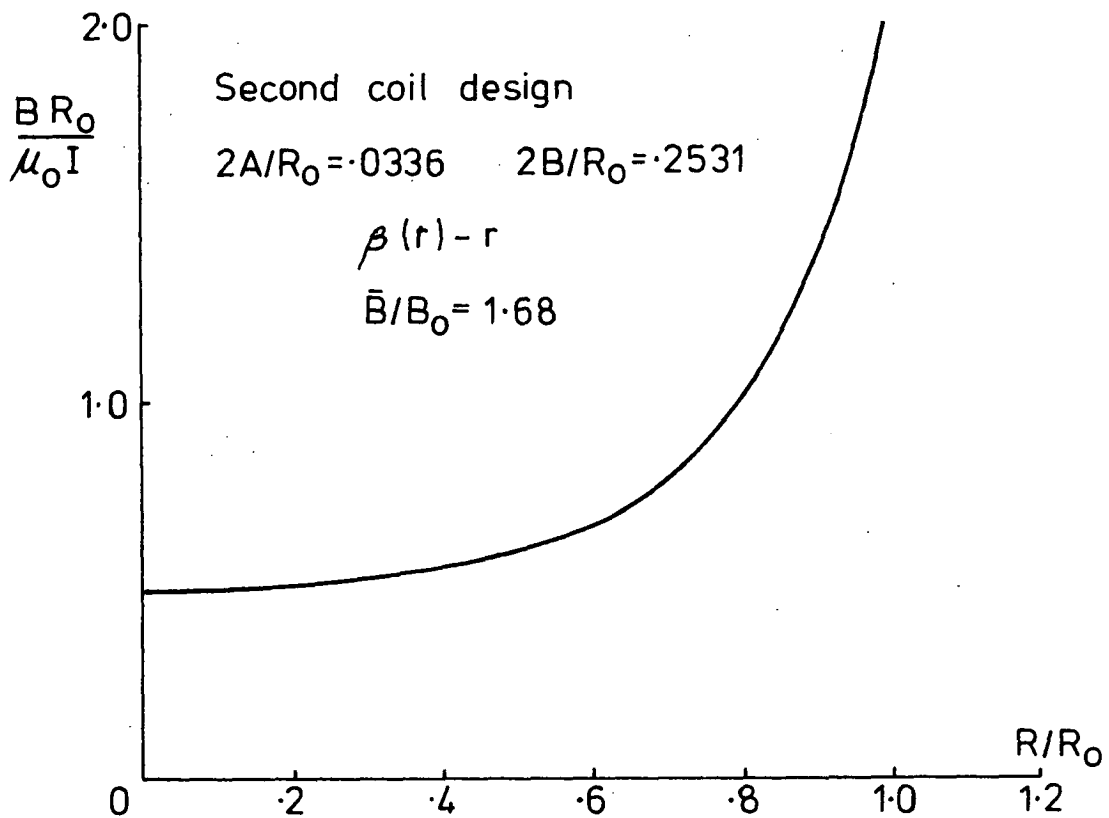
$\bar{B}/B_0 = 1 \cdot 68$

COIL CENTRAL PLAIN FLUX DENSITY 10 MW HOMOPOLAR MACHINE

FIG 13-6

The calculated flux density distribution of the second coil (figure 13-6) indicated that $\bar{B}/B_0 = 1.68$ which compared favourably with the estimated value of 1.64.

This design was considered to be adequate and its characteristics are tabulated below. The coil thickness is only 40.6mm hence adequate cooling would be achieved without having to resort to pancake coil construction.

HOMOPOLAR MACHINE

FIELD COIL CHARACTERISTICS

Inner radius	1210mm
Outer radius	1251mm
axial length	306mm
average current density	200 amp/mm^2
conductor current density	300 amp/mm^2
conductor current	475 amp
active flux	7.7 weber
central flux density	1.26 tesla
maximum flux density	5.2 tesla
quench flux density	7.4 tesla
ampere turns	$2.5 * 10^6$ ampere
number of turns	5263
conductor length	40.5 Km
conductor weight	0.515 tonnes
inductance (13-13)	121 Henry
stored energy	13.7 M Joule

It is of interest to compare this coil design with that of the Fawley coil which has 5 tonnes of conductor yet supplies the same flux. This indicates the progress made in superconductor technology since the design of the Fawley machine.

13-3-6 Armature Strength Disc

The copper conductors have to be supported by a stainless steel strength disc which has to withstand the hoop and radial stresses due to rotation as well as transmit the load torque of the machine to the shaft.

The solution to the design of the strength disc is discussed in Appendix K and the results are tabulated below. The inner radius of the strength disc is greater than the radius of the shaft so that adequate space is available for attaching the disc to the shaft.

Total copper thickness	51.2mm
Machine shaft radius	165mm
Selected disc radius	175mm
maximum speed	250 r.p.m.
strength disc thickness	40mm
principal stresses	69MPa and -56MPa
Maximum shear stress	62.4MPa
Shear due to load torque	62MPa
Strength disc weight	1.15 tonne

It is of interest to note that the shear stress due to the machine torque was 62MPa hence the stresses caused by rotation are negligible in comparison with the load torque stresses.

The above design took into account shear stress due to the normal load torque and neglected the possibility of fault currents which can produce shear forces at least five times greater than the full load torque shear stress. There is however a factor of safety of over two applied to the maximum allowable shear stress so twice full load torques would be acceptable. If the design included the possibility of fault currents the disc would need to be at least 100mm thick and its weight would approach 3 tonnes or a very high percentage of the total machine weight.

13-3-7 Torque Reaction Conductors

The very high current carrying torque reaction conductors are
stationary bars which can be easily cooled. To ensure appropriate conductor
proportions a current density of 3 amp/mm^2 is necessary. The torque
reaction bars require suitable support because they experience the entire
machine torque when considered as a group. The framework which supports
the two sets of torque reaction conductors has also to support the brush
gear and the cryostat.

The current in the torque reaction conductors is constant and for the
series parallel armature connection under consideration it equals one half
of the full armature current, i.e. 10,000 ampere.

Thus the torque reaction conductor area required is 3330mm^2. The
length of the return conductors is less than the active length of the
armature because of the brush gear. With a length of 0.67 metres the total
weight of the torque reaction conductors is 0.8 tonnes.

The total series resistance of these conductors is 0.137mΩ hence the
I^{2}R loss is 14 KW or 0.14% efficiency drop in the machine.

13-3-8 Cryostat

The cryostat consisted of an outer, room temperature stainless
steel section which had to withstand a pressure differential of 0.1MPa
and the full machine torque if the design is such that the torque reaction
conductor support is in turn supported by the cryostat; a radiation shield
which is not subject to any loading hence it is designed on thermal consid-
eration only; and an inner liquid helium and coil container which has to
withstand the extreme cold as well as a pressure of up to 0.8MPa. The
high pressure was required because of the helium compressor considerations
and a safety margin for the release valves to operate.

A structural design program produced by Dr. R. Rish, Senior Lecturer at the University of Tasmania was used to calculate the thickness of the cryostat sections. For the helium chamber British Standard BS 1515 was followed which allowed a maximum stress of 148MPa at the cryogenic temperatures for the stainless steel AISI 304L.

Cryostat Dimensions

Inner Can

The coil dimensions were:

Inside diameter	2420mm
outside diameter	2502mm
length	306mm

From section 13-3-5 the mean inner diameter of the can is 2386mm.

A clearance of 40mm from the coil to outer diameter of the helium chamber required a mean diameter of 2592mm (10mm for the metal thickness). The length of the chamber was determined as 356mm after allowing 20mm clearance from the end of the coil to the cryostat wall and 10mm for the metal thickness.

From the design program the following results were obtained for the above dimensions

Metal Thickness	Maximum Stress
10mm	156MPa
10.5mm	150MPa

A thickness of 10.5mm was selected which resulted in a weight of 0.53 tonnes for the inner section.

Outer Can

The design of this section assumed that a framework supported the cryostat and that the framework also transmitted the machine torque

to the foundations. This meant that the cryostat outer section had only to withstand the pressure differential of 0.1MPa.

The dimensions of the outer section were determined as follows.

From section 13-3-5 inner diameter is 2210mm and the outer diameter is 2758mm. The length of the outer cryostat was determined by the overall length of the armature of the machine because this method resulted in an easy design for the bearing and cryostat supports.

$$\text{Length} = 500 * 2 + 40 + 2 * 25.6 + 50\text{mm}$$
$$= 1145\text{mm}$$

The following results were obtained from the design program.

Metal Thickness	Maximum Stress
5mm	158MPa
5.5mm	132MPa
6mm	111MPa

A thickness of 5.5mm was selected which resulted in a weight of 0.96 tonnes.

Radiation Shield

If a copper radiation shield is used extreme speed in construction and evacuation of the cryostat would be necessary to avoid tarnishing of the surfaces. For this reason a stainless steel shield was selected of 1mm thickness. The weight of the shield is approximately one tenth that of the inner section of the cryostat or 56Kg.

13-3-9 Efficiency

The efficiency calculated considers only the electrical losses within the machine and neglects the power consumed by the helium

refrigerator, which for a requirement of 100 watts of cooling at 4.2K could consume near 75 KW or 0.75% drop in efficiency.

The I^2R losses were calculated in sections 13-3-4 and 13-3-7 as 36 KW or 0.36% efficiency drop. The major loss in the machine was the brush contact loss. If an average contact voltage for the positive and negative brushes of 0.2 volts occurs (13-11) then the total contact loss would be 160 KW or 1.6% drop in efficiency. Thus the overall electrical efficiency of the machine would be near 98.0%.

13-3-10   Overall Machine Mass

Armature

conductors	1.66	tonnes
strength disc	1.15	tonnes
commutators	0.31	tonnes
	3.12	tonnes

Cryostat

outer section	0.96	tonnes
radiation shield	0.06	tonnes
inner section	0.53	tonnes
	1.55	tonnes

Other

superconductor	0.515	tonnes
torque reaction conductors	0.80	tonnes
2000mm long shaft	1.33	tonnes
brush gear	0.2	tonnes
bearings	0.1	tonnes
framework	0.3	tonnes
	3.245	tonnes

Total machine weight is therefore approximately 7.915 tonnes or near 1/6th that of the conventional heteropolar machine.

13-4   Superconducting Heteropolar Machine

13-4-1 Armature

The design of the armature followed the basic D^2L relationship and the average voltage between commutator segments was limited to near 15 volts.

The design of the conventional machine produced a slot width to iron tooth width ratio of near unity; hence, in the superconducting machine, some of the armature surface normally occupied by iron can be occupied by the armature conductors. The entire surface cannot be easily utilised because the coil end connections require at least 40 percent more circumferential space than the armature bars occupy, thus there is approximately 40% more space per metre of circumference available for conductors. The radial depth of the conductors can be increased provided they are stranded and properly transposed to reduce eddy current losses generated by the difference in the magnitude of the field flux density at the different radii. The space that is not occupied by the conductors allows improved cooling and hence higher conductor current densities. An armature specific electric loading greater than the 60,000 ampere/metre used in the conventional machine is possible. Considering that there is 40% more of the armature surface available for conductors and better cooling is possible a value of 90,000 ampere/metre was selected. A generated voltage of 2000 volts was selected; hence the required armature current is 5000 ampere.

$$D^2L = \frac{P}{n\pi^2 q \bar{B}}$$

$$= \frac{10^7 * 60}{200 * \pi^2 * 90,000} * \frac{1}{\bar{B}} \quad \text{metre}^3$$

$$D^2L = 3.38/ \bar{B} \text{ metre}^3$$

$$DL \leq \frac{V_b \; a/p}{2*\pi*200/60} * \frac{1}{\bar{B}_{max}}$$

$$= \frac{V_b * 2 * 60}{2 * \pi * 200} * \frac{1}{\bar{B}_{max}} \qquad m^2 \text{ for a duplex lap winding}$$

$$DL \leq 0.0955 * \frac{V_b}{\bar{B}_{max}}$$

$$\therefore \quad D \geq \frac{3.38}{0.0955} * \frac{\bar{B}_{max}}{\bar{B} * V_b} \quad \text{metres}$$

$$D \geq 35.4 \; \frac{\bar{B}_{max}}{\bar{B} * V_b} \quad \text{metres}$$

$$L \leq 0.0027 \; V_b^2 * \bar{B} / \bar{B}_{max}^2 \quad \text{metres}$$

$\bar{B}$ is the average over the entire pole

$\bar{B}_{max}$ is the maximum average over any axial direction

B_{max} is the maximum point flux density

At this stage it is necessary to distinguish between two forms of field system.

(a) A field system consisting of circular coils with a rectangular cross-section; coil type field - figure 13-7.

(b) A field system consisting of pancake windings which occupy the entire area shadowing the armature; armature type field (Appendix L).

(a) <u>Coil Type Field</u>

An initial assumption that $\bar{B}/\bar{B}_{max} = 0.73$ for a coil type field indicated that D > 2.44 metres and L < $0.781/\bar{B}_{max}$ metres for an average bar voltage of 14.5 volts or V_b = 19.9 volts.

(b) <u>Armature Type Field</u>

An initial assumption that $\bar{B}/\bar{B}_{max} = 0.55$ for an armature type field indicated that D > 2.44 metres and L < $1.035/\bar{B}_{max}$ metres for an average bar voltage of 14.5 volts or V_b = 26.4 volts.

13-4-2   Number of Field Poles and the Commutator

The factors which influence the number of poles and the design of the commutator are the maximum current that can be successfully collected from the commutator, the average value of the voltage between bars, and a commutator diameter that is compatible with the armature diameter.

With an average bar voltage of 14.5 volts and a terminal voltage of 2000 volts, 138 bars per pole are required. A minimum bar plus insulation width of 4mm results in the relationship below between the commutator, D_c, and the number of poles, p.

$$D_c = \frac{138 * 0.004}{\pi} * p \quad \text{metres}$$
$$= 0.176 * p \quad \text{metres}$$

With p = 16, D_c = 2.8 metres which, although greater than the diameters of the armatures, was considered to be the correct choice because with p = 18, the commutator diameter would be too large and with p = 14, the current per brush arm would be unacceptably high.

To ensure that equalising connections can be made, the number of commutator bars per pole selected was 144. The resulting commutator diameter was thus 2.93 metres; the current per brush arm required is 625 ampere, and the commutator peripheral speed is 30.7 m/sec.

With a brush current density of 0.062 amp/mm^2, the required brush area per arm is 10,000 mm^2. A brush width of 16mm required a brush length of 625mm. With 15 brushes per arm, each with a length of 40mm and a spacing of 5mm between brushes, the commutator length required is 670mm. A bar depth of 10mm resulted in a commutator weight of 0.41 tonnes.

13-4-3   Armature Conductors

For a duplex lap winding and a current per brush arm of 625 ampere,

the conductor current is 156 ampere. The possibility of improved armature cooling permitted a current density of 5 amp/mm^2; hence, the cross-sectional area of the conductors required is 31 mm^2.

The number of armature conductors required for a 16 pole, 144 commutator bars per pole machine is 4608; hence the total armature copper area required is 0.143 m^2. An increase of 40% in the actual copper area to allow for the insulation and the extra space required by the end connections resulted in an armature cross-sectional area of 0.200 m^2. The mean diameter of the armature winding was estimated at 2.43 metres; hence, the depth of winding is:

$$\text{armature winding depth} = \frac{\text{cross-sectional area}}{\pi * \text{mean diameter}}$$

$$= \frac{0.20}{\pi * 2.43} \text{ metres}$$

$$= 26\text{mm}.$$

It is necessary to estimate the armature winding radial depth at this stage so that the design of the field systems can proceed. The remaining armature characteristics, copper weight, and resistance cannot be estimated until the length of the armature is selected.

13-4-4   Field System Design

(a) Coil Type Field

The shape of the coils was selected to be circular rather than rectangular on the basis that a successful design technique had been developed for circular coils. The stresses in circular coils could be better allowed for than those in rectangular coils as stress concentration can occur in the corners. The inner diameter of the helium chamber - figure 13-7 - was estimated as follows for a peak and average bar voltage of 19.9 volts and 14.5 volts respectively.
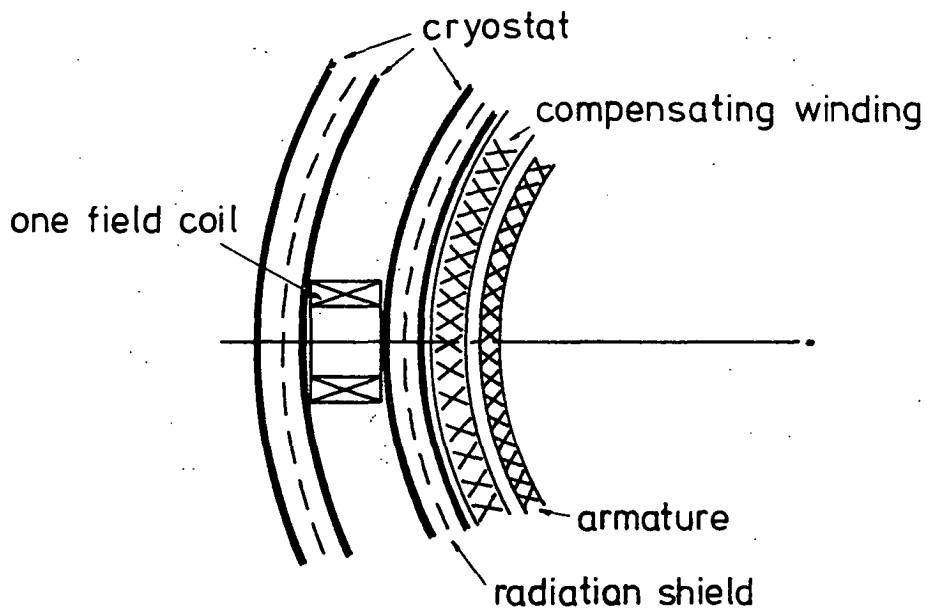
MACHINE LAYOUT
FIG 13-7

mean armature diameter	2427mm
armature outer diameter	2440mm
rotational clearance	5mm
compensating winding thickness	45mm
cryostat metal thickness	20mm
cryostat insulation paths	40mm

inner diameter of helium
    chamber $= 2440 + 2(5+45+20+40)$ mm

$\qquad = 2660$ mm

space available for each
    field coil $= \dfrac{\pi \times 2660}{16}$ mm

$\qquad = 522$ mm.

With an armature length of 520mm, the peak flux density required at the armature is 2.0 tesla - section 13-4-1. The design of the field coils necessitated a knowledge of the coil bore flux density. This was obtained by guessing an angle of 120° subtended from the bore of the coil to the mean armature diameter; hence, the bore flux density was approximately:

$$B_0 = 2.0/\sin^3 120/2 \text{ tesla}$$

$$= 3.08 \text{ tesla.}$$

A mean current density of 200 amp/mm^2 was selected and the coil design followed the procedure described in Appendix J.

Estimated coil inner radius 240mm

$$\frac{B_0 R_0}{\mu_0 I} = \frac{B_0}{\mu_0 R_0 J} \times \frac{1}{\frac{2A}{R_0} \times \frac{2B}{R_0}}$$

$$= \frac{3.08}{4 \times \pi \times 10^{-7} \times 0.24 \times 200 \times 10^6} \left(\frac{2A}{R_0} \times \frac{2B}{R_0}\right)^{-1}$$

$$= 0.0511 \times \left(\frac{2A}{R_0} \times \frac{2B}{R_0}\right)^{-1}$$

Volume $\frac{}{R_o^3}$	$\frac{2A}{R_o}$	$\frac{2B}{R_o}$	$\frac{B_o R_o}{\mu_o I}$	
			from Appendix J	calculated
0.5	0.142	0.523	0.454	0.688
0.7	0.179	0.571	0.445	0.57
0.8	0.195	0.595	0.44	0.44

Estimated coil outside diameter = 2 * 240 * 1.195mm

= 574mm (too large)

Estimated coil axial length = 240 * 0.595mm

= 143mm

From the results in Appendix I :

bore flux density = 3.08 tesla

peak armature flux density = 1.75 tesla (2.0 tesla required)

For the second coil design, a bore flux density of 3.08 * 2.0/1.75 = 3.52 tesla and a bore radius of 240 * 510/574 = 213mm were selected.

$$\frac{B_o R_o}{\mu_o I} = \frac{3.52}{4 * \pi * 10^{-7} * 0.213 * 200 * 10^6} * (\frac{2A}{R_o} * \frac{2B}{R_o})^{-1}$$

$$= 0.06575 * (\frac{2A}{R_o} * \frac{2B}{R_o})^{-1}$$

Volume $\frac{}{R_o^3}$	$\frac{2A}{R_o}$	$\frac{2B}{R_o}$	$\frac{B_o R_o}{\mu_o I}$	
			From Appendix J	calculated
0.8	0.195	0.595	0.440	0.567
0.9	0.209	0.621	0.437	0.507
1.00	0.223	0.642	0.433	0.459
1.06	0.231	0.655	0.431	0.435

Second coil outside diameter = 2 * 213 * 1.231mm

= 524mm (too large)

Second coil axial length   = 218 * 0.642mm

= 140mm

From the results of Appendix I:

bore flux density = 3.49 tesla

peak armature flux density = 1.8 tesla (2.0 tesla required)

For the third coil design, a bore flux density of 3.49 * 2.0/1.8 = 3.88 tesla and a bore radius of 200mm were selected.

$$\frac{B_o R_o}{\mu_o I} = \frac{3.88}{4*\pi*10^{-7}*0.2*200*10^6} * (\frac{2A}{R_o} * \frac{2B}{R_o})^{-1}$$

$$= 0.07712 * (\frac{2A}{R_o} * \frac{2B}{R_o})^{-1}$$

$\frac{Volume}{R_o^3}$	$\frac{2A}{R_o}$	$\frac{2B}{R_o}$	$\frac{B_o R_o}{\mu_o I}$	
			From Appendix J	calculated
1.06	0.231	0.655	0.431	0.510
1.25	0.257	0.686	0.426	0.437
1.30	0.263	0.695	0.425	0.422

Third coil outside diameter = 2 * 200 * 1.263mm

= 505mm

Third coil axial length = 200 * 0.695mm

= 139mm

From the results of Appendix I :

bore flux density = 3.9 tesla

peak armature flux density - 1.92 tesla (2.0 tesla required)

For the fourth coil design, a bore flux density of 4.07 tesla and inner radius of 300mm were selected.

$$\frac{B_o R_o}{\mu_o I} = \frac{4.07}{4*\pi*10^{-7}*0.20*200*10^6} * (\frac{2A}{R_o} * \frac{2B}{R_o})^{-1}$$

$$= 0.08097 * (\frac{2A}{R_o} * \frac{2B}{R_o})^{-1}$$

Volume $\dfrac{\text{Volume}}{R_o^3}$	$\dfrac{2A}{R_o}$	$\dfrac{2B}{R_o}$	$\dfrac{B_o R_o}{\mu_o I}$	
			from Appendix J	calculated
1.30	0.263	0.695	0.431	0.443
1.36	0.27	0.706	0.423	0.424

Fourth coil outside diameter = 2 * 200 * 1.27mm

= 508mm

Fourth coil axial length = 200 * 0.706mm

= 141mm

From the results of Appendix I:

bore flux density = 4.05 tesla

peak armature flux density = 2.00 tesla.

For the fourth coil design and allowing for the effects from other field coils, the following flux densities at the armature were estimated:

Peak point flux density = $0.2317 * 4 * \pi * 10^{-7} * 200 * 10^6 * 0.27 * 0.706 * 0.2$ tesla

= 2.22 tesla

Maximum average flux density = 0.18065 * 2.22/0.2317 tesla

= 1.73 tesla

Pole average flux density = 0.125 * 2.22/02317 tesla

= 1.2 tesla

$\therefore$ Peak bar voltage = $1.73 * \dfrac{200 * 2 * \pi}{60} * \dfrac{2.44}{2} * 0.52$ volts

= 23 volts

$\therefore$ Average bar voltage = 1.2 * 23/1.73 volts

= 15.9 volts

$\therefore$ Terminal voltage = 15.9 * 144 volts

= 2300 volts.

The armature specific electric loading with 144 commutator bars per

pole and a terminal voltage of 2300 volts would be 81,700 ampere/metre
which is less than the assumed design value of 90,000 ampere/metre.
A terminal voltage of 2090 volts would require an armature specific
electric loading of 90,000 ampere/metre to achieve the 10MW rating for
the dimensions previously estimated. The average and peak bar voltages
become 14.5 volts and 20.9 volts respectively. The field excitation
average current density can also be reduced to 182 ampere/mm^2.

The assumed value for the ratio $\bar{B}/\bar{B}_{max}$ of 0.73 was five percent
greater than 0.694 estimated for the above coil design. To retain the
designs for the coils and the armature, a corresponding increase of five
percent in the maximum bar voltage to 20.9 volts was required to satisfy
the basic design equations.

The characteristics for this field system are:

coil average current density	182 ampere/mm^2
coil conductor current density	273 ampere/mm^2
excitation current	430 ampere
critical flux density	7.3 tesla
maximum coil self flux density	6.77 tesla
armature peak field flux density	2.02 tesla
armature average field flux density	1.09 tesla
field coil inside diameter	400 mm
field coil thickness	54 mm
field coil length	141.2 mm
number of turns per coil	3227
coil ampere turns	$1.388 * 10^6$
total conductor length	73.6 km
total conductor mass	0.929 tonnes
coil self inductance (13-13)	5.21 henry

It was apparent from the above data that the safety margin between
the coil self peak flux density and the guaranteed critical flux density

of the superconductor used is insufficient. This is further aggravated by the contribution of a further 0.5 tesla from adjacent coils to the peak flux density within a field coil.

This situation was alleviated by reducing the peak armature flux density from 2.02 tesla to 1.5 tesla, and reducing the peak bar voltage to 18 volts. The required armature outside diameter becomes 2680mm and the armature active length required is 570mm. These values were selected as the circumferential space available for each coil at the inner diameter of the helium chamber equals the active length of the armature.

$$\text{Helium chamber inside diameter} = 2680 + 220\text{mm}$$
$$= 2900\text{mm}$$
$$\text{Space available for each field coil} = \pi * 2900/16\text{mm}$$
$$= 570\text{mm}$$

The design of the field coils drew upon the result from the previous design that has the coil flux density at twice the armature peak flux density.

A mean current density of 200 ampere/mm^2 was retained and the coil design followed the procedure described in Appendix J.

Estimated coil inner radius = 220mm

$$\frac{B_o R_o}{\mu_o I} = \frac{2 * 1.5}{4*\pi*10^{-7}*200*10^6*0.22} * (\frac{2A}{R_o} * \frac{2B}{R_o})^{-1}$$
$$= 0.0543 * (\frac{2A}{R_o} * \frac{2B}{R_o})^{-1}$$

Volume $\frac{}{R_o^3}$	$\frac{2A}{R_o}$	$\frac{2B}{R_o}$	$\frac{B_o R_o}{\mu_o I}$	
			from Appendix J	calculated
0.8	0.195	0.595	0.440	0.468
0.85	0.2	0.615	0.439	0.442
0.855	0.202	0.612	0.438	0.439

Coil outside diameter = 2 * 220 * 1.202mm

= 529mm

Coil axial length = 0.612 * 220mm

= 135mm

From the results of Appendix I:

coil bore flux density = 3 tesla

peak armature flux density = 1.54 tesla

The space available for each coil is 570mm; hence, the coil inner radius was increased to 235mm.

$$\frac{B_o R_o}{\mu_o I} = \frac{3 * 1.5/1.54}{4 * \pi * 10^{-7} * 200 * 10^6 * 0.235} * (\frac{2A}{R_o} * \frac{2B}{R_o})^{-1}$$

$$= 0.04947 * (\frac{2A}{R_o} * \frac{2B}{R_o})^{-1}$$

$\frac{Volume}{R_o^3}$	$\frac{2A}{R_o}$	$\frac{2B}{R_o}$	$\frac{B_o R_o}{\mu_o I}$	
			from Appendix J	calculated
0.855	0.202	0.612	0.438	0.400
0.80	0.195	0.595	0.439	0.426
0.75	0.185	0.591	0.442	0.453
0.77	0.189	0.592	0.442	0.442

Coil outside diameter = 2 * 235 * 1.189mm

= 559mm

This provides 5mm clearance on the radius.

Coil axial length = 0.592 * 235mm

= 139mm

From the results of Appendix I :

coil bore flux density = 2.92 tesla

peak flux density at the armature = 1.57 tesla.

With the influence of adjacent coils taken into account, the following field flux parameters at the armature were obtained. The coil mean current density used was 200 ampere/mm^2 - figures 13-8 and 13-9.

        peak point flux average   = 1.75 tesla

        peak average flux density = 1.4   tesla

        pole average flux density = 1.0   tesla

From these values, the bar voltages were obtained.

        peak bar voltage   = 22.3 volts

        average bar voltage   = 15.9 volts

With these values, the terminal voltage would be 2275 volts, or 275 volts higher than the design value. To overcome this, a reduction in the field coil average current density to 175 ampere/mm^2 was necessary. A better approach would have been to maintain the average current density and redesign the coils again. Retention of the design gave the following field parameters.

        coil average current density   = 175 ampere/mm^2

        coil conductor current density   = 264 ampere/mm^2

        excitation current   = 418 ampere

        critical flux density guaranteed   = 7.4 tesla

        critical flux density typical   = 7.7 tesla

        maximum flux density at field coil   = 6.5 tesla

        armature peak field flux density   = 1.53 tesla

        armature average field flux density   = 0.873 tesla

        armature peak average field flux density = 1.222 tesla

        field coil inside diameter   = 470 mm

        field coil thickness   = 44.4 mm

        field coil length   = 139.1 mm

        number of turns per coil   = 2586

        coil ampere turns   = 1.081 * 10^6

COIL TYPE FIELD FLUX
DENSITY DISTRIBUTION
FROM A SINGLE COIL
FIG 13-8

$2A/R_0 = 0.189$
$2B/R_0 = 0.592$
$b/R_0 = 0.82$
$BMAX\, R_0/\mu_0 I = 0.91$
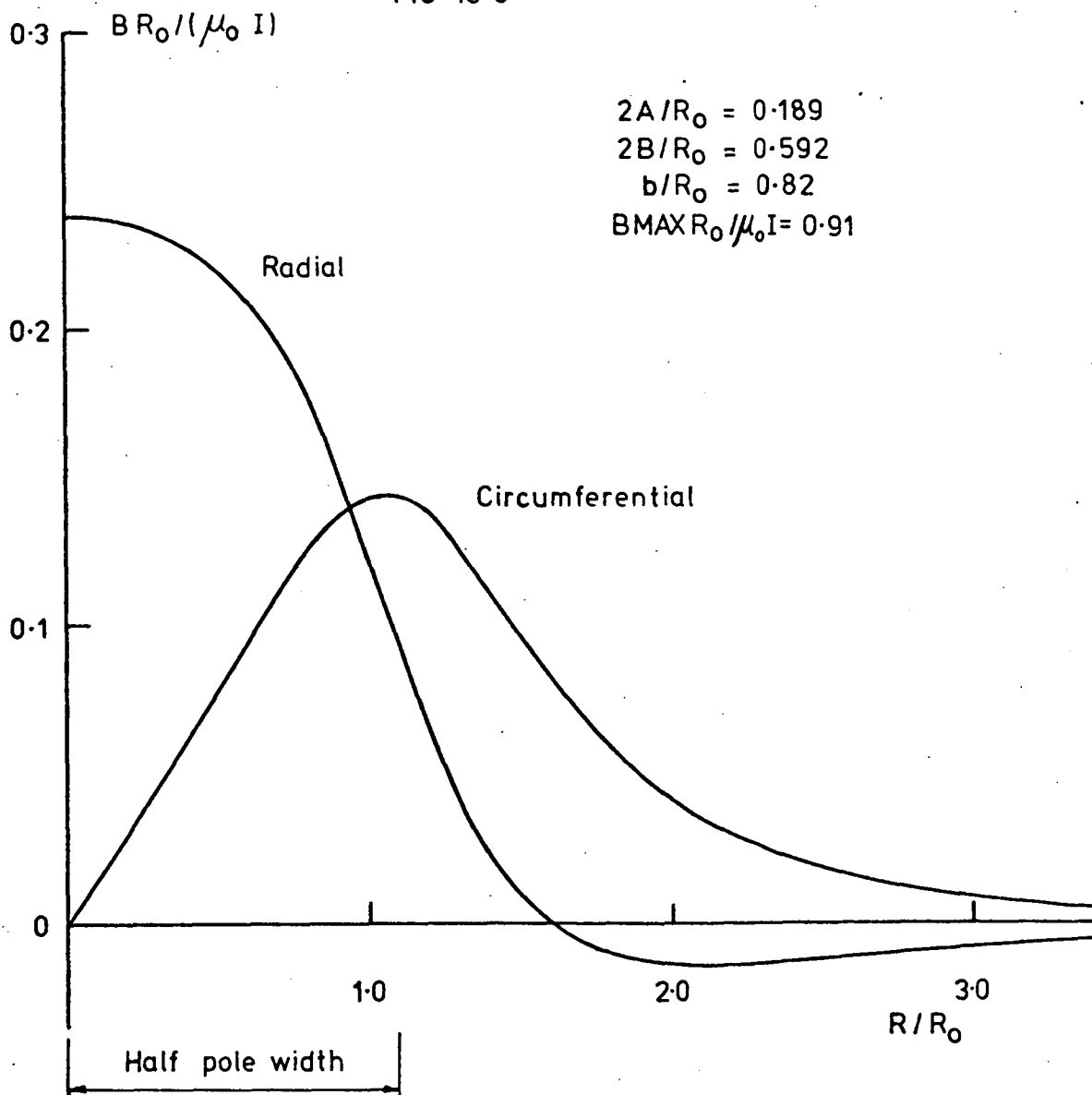
COIL TYPE FIELD FLUX
DENSITY DISTRIBUTION

Through the pole centre
FIG 13-9
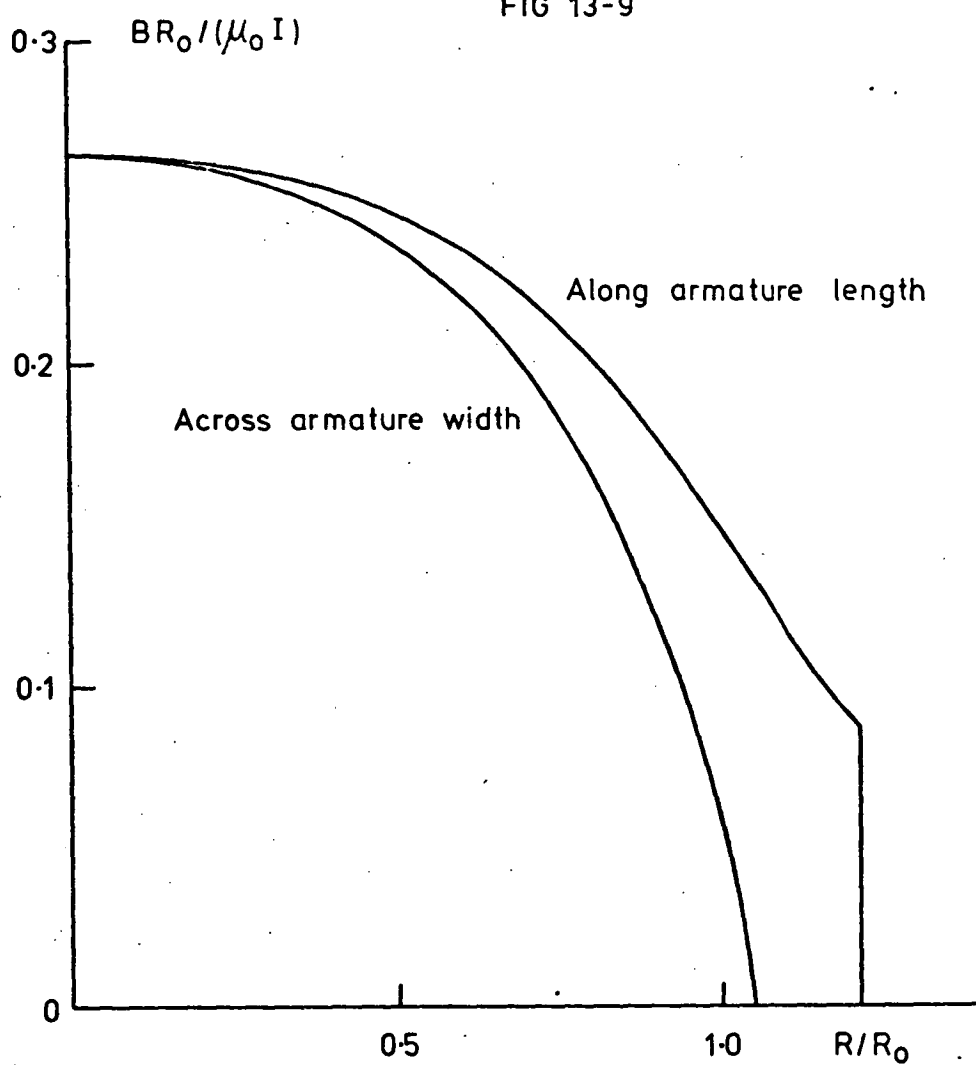
total conductor length	= 66.9 km
total conductor mass	= 0.844 tonnes
coil self inductance, reference (13-13)	= 2.2 henry
adjacent coil mutual inductance	= 0.22 henry
peak bar voltage	= 19.5 volts
average bar voltage	= 13.9 volts

The total inductance of the field system would be greater than sixteen times the self inductance of each coil because of the additive flux linkages of adjacent coils. An estimate of the total inductance was obtained from the mutual inductance of adjacent coils and assuming that the total flux linkage of a given coil is due to itself and the two adjacent coils only. With mutual inductance M, and self inductance L, the total flux linkage of a coil would be $I(L + 2M)$; hence, the total inductance of the field system is given by equation 13-8.

$$L_T = P(L + 2M) \qquad (13-8)$$

P = number of poles

L_T = total field inductance

The mutual and coil self inductances were calculated using reference 13-10 as 0.22 and 4.2 henry respectively, this resulted in a total inductance of 74.2 henry, which represents a stored energy of 6.5 MJoule in the magnetic field of the field system at the design excitation current. This result gives an indication of the complexity of field protective equipment required to dissipate inductively stored energy in the event of a field system quench.

Another point arising from the designs is that a reduction in field flux density increases the size of the machine, but reduces the quantity of superconductor required. With increased size, the efficiency of the machine is reduced; hence, an economical design between running costs

and capital costs could be determined.

(b) Armature Type Field Winding

An amarature type field was considered because the coil type field winding added considerably to the overall diameter of the machine. A large cryostat is thus required, which is inefficient in terms of the field coil volume when compared with the total volume of the helium chamber. The support of the armature type winding is easier because it is a compact unit rather than a set of individual coils as with the coil type field system.

The number of poles was selected as sixteen, the same number as the coil type system. The required inside diameter of the field system was estimated from the estimated armature diameter - section 13-4-1b - of 2440mm.

armature outside diameter	- 2440 mm
rotational clearance	- 5 mm
compensating winding thickness	- 45 mm
cryostat metal thickness	- 20 mm
cryostat insulation paths	- 40 mm
inner diameter of field system	- 2660 mm

For a maximum average flux density at the armature of 2 tesla, which for the armature type field is the same as the peak flux density, an active armature length of 520mm is required - section 13-4-1.

The design of the armature type field system assumed an infinitely long armature core and based on the results of Appendix L, the design procedure is as follows.

P = number of poles

R = armature conductor mean radius (metres)

R_o = field system inner radius (metres)

$2A$ = field system thickness (metres)

$R_0 + 2A$ = field system outer radius (metres)

$\bar{B}_{max}$ = maximum average radial component of flux density at the armature (tesla)

$\bar{J}$ = average current density (ampere/m^2)

R = $(2440 - 26)/2 = 1207mm$

R_0 = $1330mm$

R/R_0 = 0.9075

An initial value for $2A/R_0 = 0.01$ was selected and, for a sixteen pole system at $R/R_0 = 0.9075$ - Appendix L.

$$\frac{\bar{B}_{max}}{\mu_0 R_0 \bar{J}} = 0.00335$$

hence $\bar{J}$ = $\dfrac{2}{4*\pi*10^{-7}*1.33*0.00335}$ ampere/m^2

= 357 ampere/mm^2

With an average current density of 342 ampere/mm^2, the conductor current density would be 513 ampere/mm^2 with a corresponding guaranteed critical flux density of 3.8 tesla. The maximum flux density at the field winding was calculated to be 8.9 tesla or well above the quench flux density. This unacceptable situation can be corrected by two methods:

(a) increase the field winding thickness, thus reducing the required conductor current density and increasing the guaranteed critical flux density, or

(b) reduce the required maximum flux density at the armature by increasing the active length of the armature.

The first alternative requires an excessive quantity of superconductor; hence, a reduction in the required maximum flux density was necessary.

A maximum average flux density at the armature of 1.1 tesla, instead of 2 tesla, was next assumed. For a 144 commutator bar per pole machine,

an average bar voltage of 13.9 volts is required. With the assumption that the ratio $\bar{B}/\bar{B}_{max}$ = 0.55; the maximum bar voltage is 25.3 volts. From the basic design equation in section 13-4-1, the design data below was derived.

$$P = 16 \text{ poles}$$
$$R = 1270\text{mm}$$
$$L = 860\text{mm}$$
$$R_0 = 1380\text{mm}$$
$$\bar{B}_{max} = 1.1 \text{ tesla}$$
$$R/R_0 = 0.9203.$$

An initial guess value of five layers of field conductor per coil, an assumed packing factor of two-thirds, and a conductor diameter of 1.42mm resulted in an initial value for $2A/R_0$ of:

$$2A/R_0 = 1.42 * 5 * (\frac{3 * \Pi}{8})^{\frac{1}{2}}/1380$$
$$= 0.00558$$

From the results of Appendix L, the required average current density is 296 ampere/mm^2. To reduce this current density to near 200 ampere/mm^2, eight layers of conductor per pole are required.

$$2A/R_0 = 1.42 * 8 * (\frac{3 * \Pi}{8})^{\frac{1}{2}}/1380$$
$$= 0.008935$$

The required average current density to provide a peak flux density of 1.1 tesla at the armature was estimated at 187 ampere/mm^2. The maximum flux density at the field winding was estimated as 4.64 tesla or well below the guaranteed quench value of 7.2 tesla. With seven layers of conductor, the required average current density is 213 ampere/mm^2, and the maximum flux density at the field winding is 4.8 tesla or well below the guaranteed quench value of 6.6 tesla. For these field windings, $\bar{B}/\bar{B}_{max}$ = 0.56 instead of the assumed value of 0.55. The length of

conductor required for the seven layer winding is approximately 50.7 km.

The large safety margin between the quench and the maximum flux density, over correction, enabled an increased maximum average flux density of 1.45 tesla. The higher value of $\bar{B}/\bar{B}_{max} = 0.56$ resulted in the design below.

$$P = 16 \text{ poles}$$
$$V_b = 13.9/0.56 = 24.8 \text{ volts}$$
$$R = 1270\text{mm (as before)}$$
$$L = 640\text{mm}$$
$$R_o = 1380\text{mm (as before)}$$
$$\bar{B}_{max} = 1.45 \text{ tesla}$$
$$R/R_o = 0.9203 \text{ (as before)}$$

A winding with ten layers required an average current density of 200 ampere/mm^2. The maximum flux density at this winding is 5.9 tesla, which is sufficiently below the guaranteed quench flux density of 6.9 tesla. The radial component of the field flux density at the armature - figure 13-10 - indicated that the ratio $\bar{B}/\bar{B}_{max} = 0.56$ which compares well with the assumed value above.

A summary of the characteristics of this armature type field is given below.

field system average current density	= 200 ampere/mm^2
field conductor current density	= 300 ampere/mm^2
field system excitation current	= 475 ampere
peak field flux density at the armature	= 1.45 tesla
average field flux density at the armature	= 0.831 tesla
peak field flux density at the field	= 5.9 tesla
guaranteed quench flux density at 475 ampere	= 6.9 tesla
field system inside diameter	= 2760 mm
field system outside diameter	= 2790 mm

ARMATURE TYPE FIELD SYSTEM
FIELD FLUX DENSITY DISTRIBUTION
FIG 13-10

$$\frac{BRAD}{(\mu_0 * R_0 * \bar{J})}$$

$2A/R_0 = \cdot01117$

$R/R_0 = \cdot9203$

$\bar{B}/Bpeak = \cdot561$

$Bpeak = 1\cdot45$ tesla

ANGLE
ELECTRICAL
DEGREES

0·004

0·003

0·002

0·001

-90   -60   -30   0   30   60   90
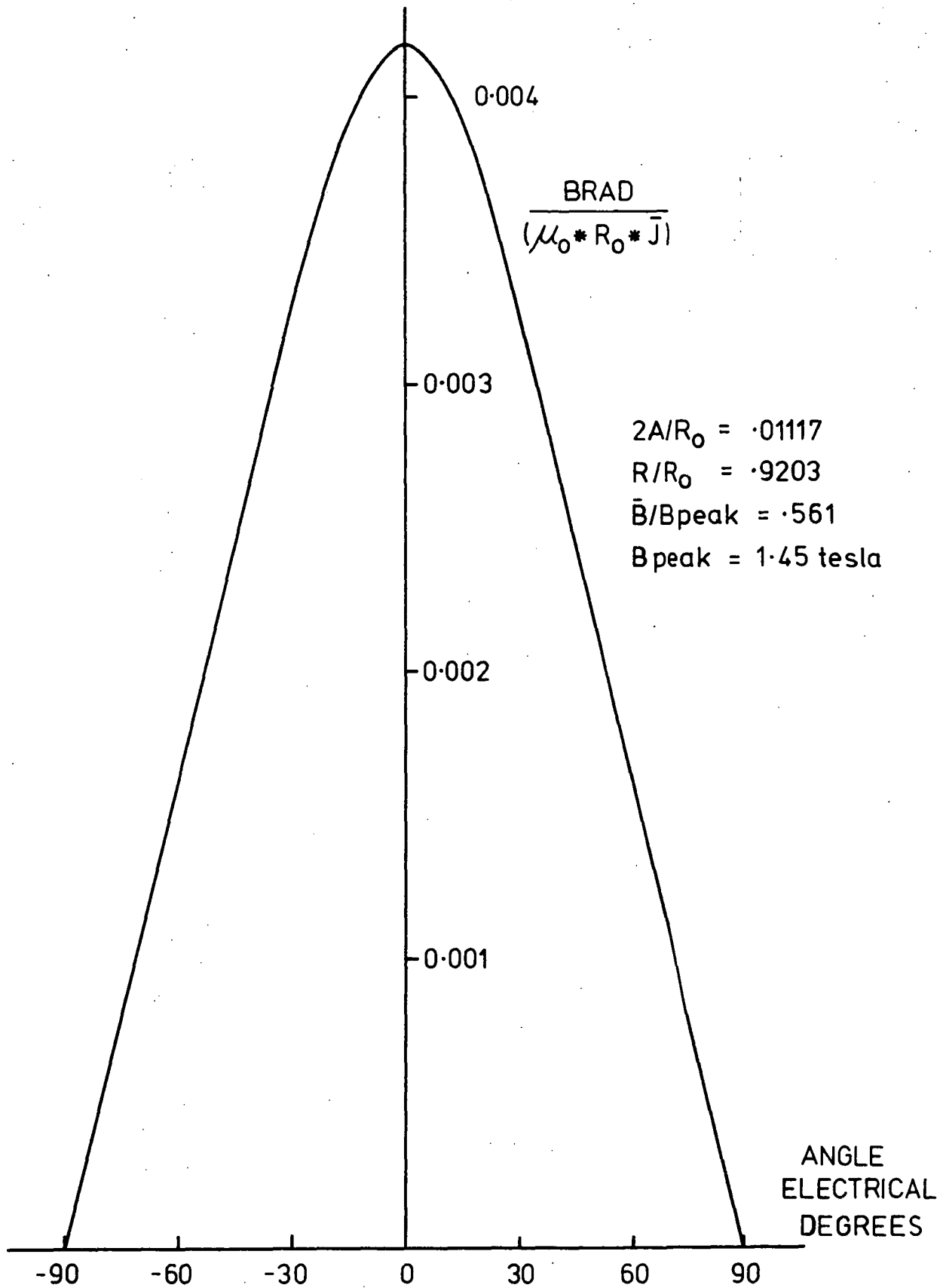
field ampere turns per coil = 836,000

number of layers per coil = 10

number of turns per coil = 1,760

active field coil length = 640 mm

overall length of each coil = 1170 mm

circumferential width of each coil = 542 mm

total length of superconductor = 58.4 km

total mass of superconductor = 0.72 tonnes

peak bar voltage = 24.8 volts

average bar voltage = 13.9 volts

As with the coil type field system, high field flux densities have reduced the size of the machine but have increased the quantity of super- conductor required. Thus the same economic design approach, for example, minimising the total annual operating and capital charges, can be employed.

13-4-5 Cryostat

As with the design of the homopolar machine, the design of the cryostat was obtained with the aid of the program developed by Dr. R. Rish. The helium chamber was designed to withstand an internal pressure of 0.8 MPa and the design pressure for the room temperature section was 0.1 MPa.

(a) Coil Type Field System

The dimensions of the cryostat required to house the coil type field system are:

Helium Chamber

section inside diameter = 2680 + 2 * (5 + 45 + 10 + 40) mm

= 2880mm

section outside diameter = 2900 + 2 * (139.1 + 10 + 10) mm

≑ 3220mm

section length = 470 + 2 * (44.4 + 20) mm

≑ 600mm

required metal thickness = 17mm

Room temperature section

inside diameter = 2680 + 2 * (5 + 45) mm

= 2780mm

outside diameter = 3220 + 2 * (40 + 10) mm

= 3320mm

length = 600 + 2 * (40 + 10) mm

= 700mm

required metal thickness = 5mm

The total weight of the cryostat, including the radiation shield, was estimated at 2.83 tonnes. The volume of the helium chamber is 980 litres of which 160 litres is occupied by the field coils, hence, a helium charge of 820 litres is required.

(b) Armature Type Field System

The dimensions of the cryostat required to house the armature type field system are:

Helium Chamber

section inside diameter = 2540 + 2 * (5 + 45 + 10 + 40) mm

= 2740mm

section outside diameter = 2760 + 2 * (15 + 20 + 10) mm

= 2850mm

section length = 1170 + 2 * (10 + 10)mm

≑ 1210mm

required metal thickness = 10mm

Room temperature section

inside diameter = 2540 + 2 * (5 + 45) mm

= 2640mm

outside diameter   = 2850 + 2 * (40 + 10) mm

                     = 2950mm

length   = 1210 + 2 * (40 + 10) mm

                     = 1310mm

required metal
         thickness   = 3mm

The total weight of the cryostat, including the radiation shield, was estimated at 2.74 tonnes. The volume of the helium chamber is 584 litres of which 141 litres is occupied by the field winding. A helium charge of 443 litres is consequently required.

13-4-6 Armature Winding

(a) Coil Type Field

The design data for the armature required with the coil type field is given below.

machine rating	= 10 MW
rated voltage	= 2 kV
rated current	= 5 kA
number of poles	= 16
commutator bars per pole	= 144
conductor current density	= 5 ampere/mm^2
armature active length	= 570 mm
armature outside diameter	= 2680 mm

For a duplex lap winding, the conductor current is 156 ampere; hence, a conductor area of 31mm^2 is required. With an end winding angle of 45° and an allowance for insulation, an armature surface occupancy of 65 percent by the conductor copper is expected. The allowable conductor width is hence 2.4mm and the depth is 12.9mm. The overall winding depth would be near 30mm when insulation and stranding is allowed for.

The length of each turn was estimated at 2.65 metres which resulted in a total conductor length of 6.1 km and a mass of 1.68 tonnes. The total series resistance of the conductor would be 3.35Ω; hence, the armature resistance would be 3.27mΩ. The armature loss would be 82 kW or a drop in efficiency of 0.82%.

(b) Armature Type Field

The design data is the same as for the coil system, but the armature outside diameter is 2540mm and the active length is 630mm. The allowable conductor width is 2.25mm for an armature surface occupancy of 65 percent. To obtain the necessary conductor area of 31mm^2 a conductor depth of 13.8mm is required.

The length of each turn was estimated at 2.7 metres which resulted in a total conductor length of 6.22 km and a mass of 1.71 tonnes. The total series resistance of the conductor would be 3.42Ω; hence, the armature resistance would be 3.34mΩ. The armature loss would be 83.4 kW or a drop in efficiency of 0.83%.

13-4-7 Compensating Winding

The principle of the compensating winding is twofold:
(a) to shield the superconducting field winding from the armature reaction fluxes.
(b) to transmit the machine torque to the foundations.

The form of the compensating winding considered was an armature type winding which carries the full armature current. A sixteen pole wave winding was proposed as it does not involve potentially difficult end connections.

Along the geometric neutral axis, the magnitude of the maximum armature reaction flux density at the field system was estimated at 0.034 tesla

for both the field systems under consideration. This is considerably less than the peak self flux densities of the field systems, which is near six tesla; hence the possibility of a field quench as a result of armature reaction is remote.

The designs of the compensating windings were based on the balancing of the machine torques. With the proper aligning of the armature and compensating windings there is no interaction between them; hence torque balancing is through interactions with the field system, which cancel.

The specific electric loading of the compensating winding required to produce torque cancellation at full load is given by equation 13-9.

$$q_c = \frac{2}{\pi} * \frac{T}{D_c^2 L_c \bar{B}_c} \qquad (13-9)$$

q_c = compensating winding specific electric loading (ampere/m)

T = machine full load torque (Newton-metre)

D_c = compensating winding diameter (metre)

L_c = compensating winding active length (metre)

$\bar{B}_c$ = average pole field flux density at the compensating winding (tesla)

(a) Coil Type Field Compensation

$$\text{Full load torque} = 10 * 10^6 / \frac{200 * 2 * \pi}{60} \quad \text{N-m}$$
$$= 477 \text{ kN-m}$$

From an analysis of the coil type field flux density distribution in the region of the compensating winding, the average flux density was estimated as 1.13 tesla - figure 13-11.

The length of the compensating winding was selected to be the same as that of the armature which is 570mm. The diameter of the compensating winding was estimated to be 2730mm.

COIL TYPE FIELD FLUX
DENSITY AT THE
COMPENSATING WINDING
SINGLE COIL
FIG 13-11

$2A/R_0 = 0.189$

$2B/R_0 = 0.592$

$b/R_0 = 0.65$

$R_0 = 235\,mm$

$\bar{J} = 175\,amp/mm^2$

$I = 2A*2B*\bar{J}$

$\bar{B} = 1.13\,tesla$
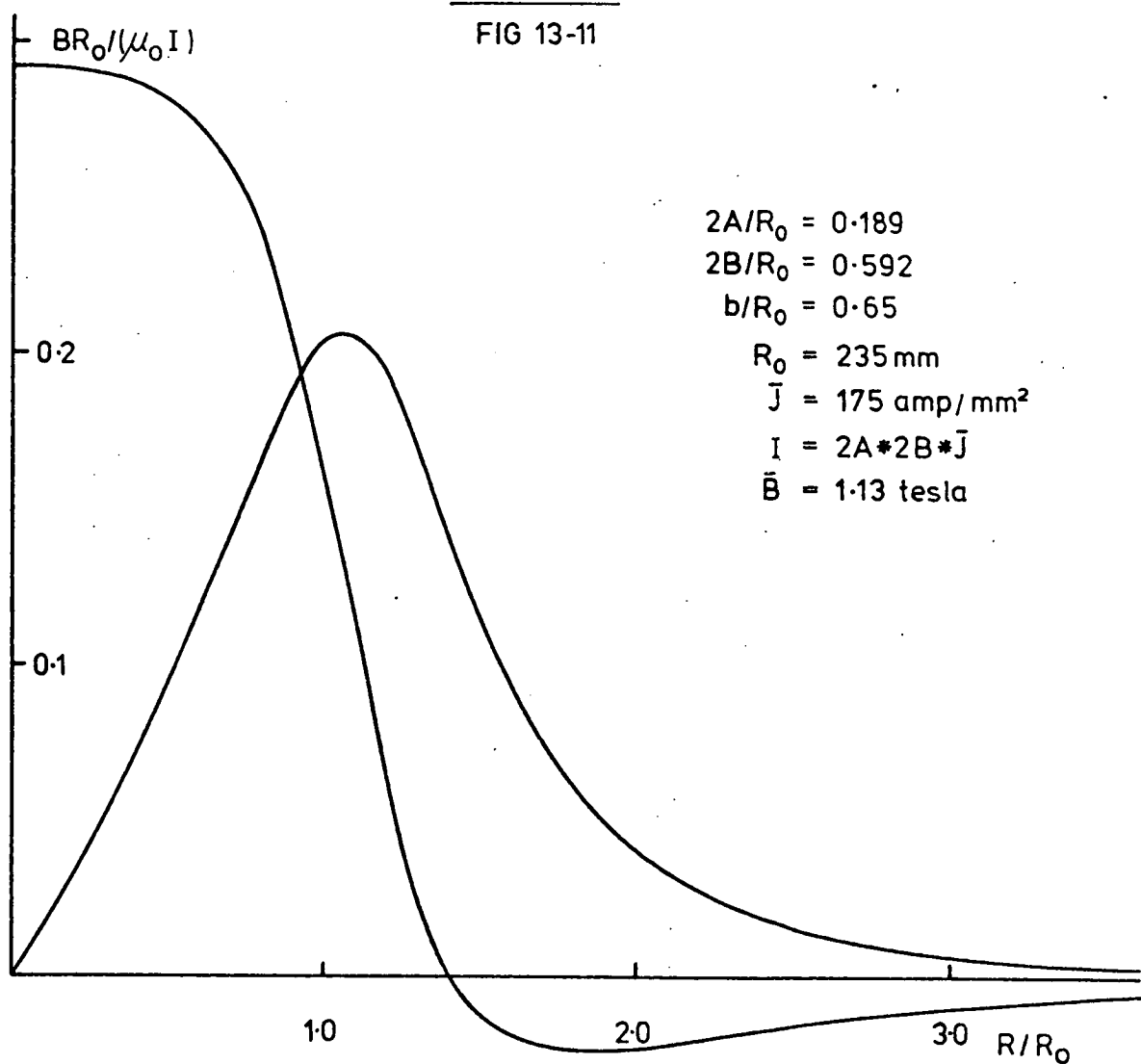
$$q_c = \frac{2}{\pi} * \frac{477 * 10^3}{2.73 * 2.73 * 0.57 * 1.13} \text{ ampere/m}$$
$$= 63{,}260 \text{ ampere/m}.$$

The required depth of the compensating winding with a conductor current density of 5 ampere/mm^2 and an allowance of fifty percent increase in area for spacing and insulation is 19mm. The available space of 45mm was considered to be adequate for the winding and the support structure. The mass of the conductor was estimated at 1.29 tonnes.

The maximum resultant armature and compensating winding magnetic field in the region of the field coils was estimated to be 0.0023 tesla at full load.

The compensating winding carried the full armature current. Thus, for a wave winding, the conductor current would be 2,500 ampere at full load. The winding resistance was estimated at 2.44mΩ and the corresponding power loss is 61 kW or 0.61 percent drop in efficiency.

(b) Armature Type Field Compensation

From an analysis of the armature type field flux density distribution in the region of the compensating winding, the average flux density was estimated as 0.963 tesla - figure 13-12.

The length of the compensating winding was selected to be the same as that of the armature which is 640mm. The estimated diameter is 2590mm. The required specific electric loading to develop full load torque is 73,450 ampere/metre.

The required winding depth is 22mm and the estimated mass of the copper in the winding is 1.45 tonnes. The calculated resistance of the compensating winding is 27.5mΩ and the power loss at full load would be 68.9 kW or 0.69 percent drop in efficiency.

The maximum resultant armature and compensating winding magnetic

ARMATURE TYPE FIELD SYSTEM
FIELD FLUX DENSITY AT THE COMPENSATING WINDING
FIG 13-12

$$\frac{BRAD}{(\mu_0 * R_0 * \bar{J})}$$

$2A/R_0 = \cdot01117$

$R/R_0 = \cdot94$

$\bar{B}/B_{peak} = \cdot547$

$B\ peak = 1\cdot76\ tesla$

ANGLE ELECTRICAL DEGREES
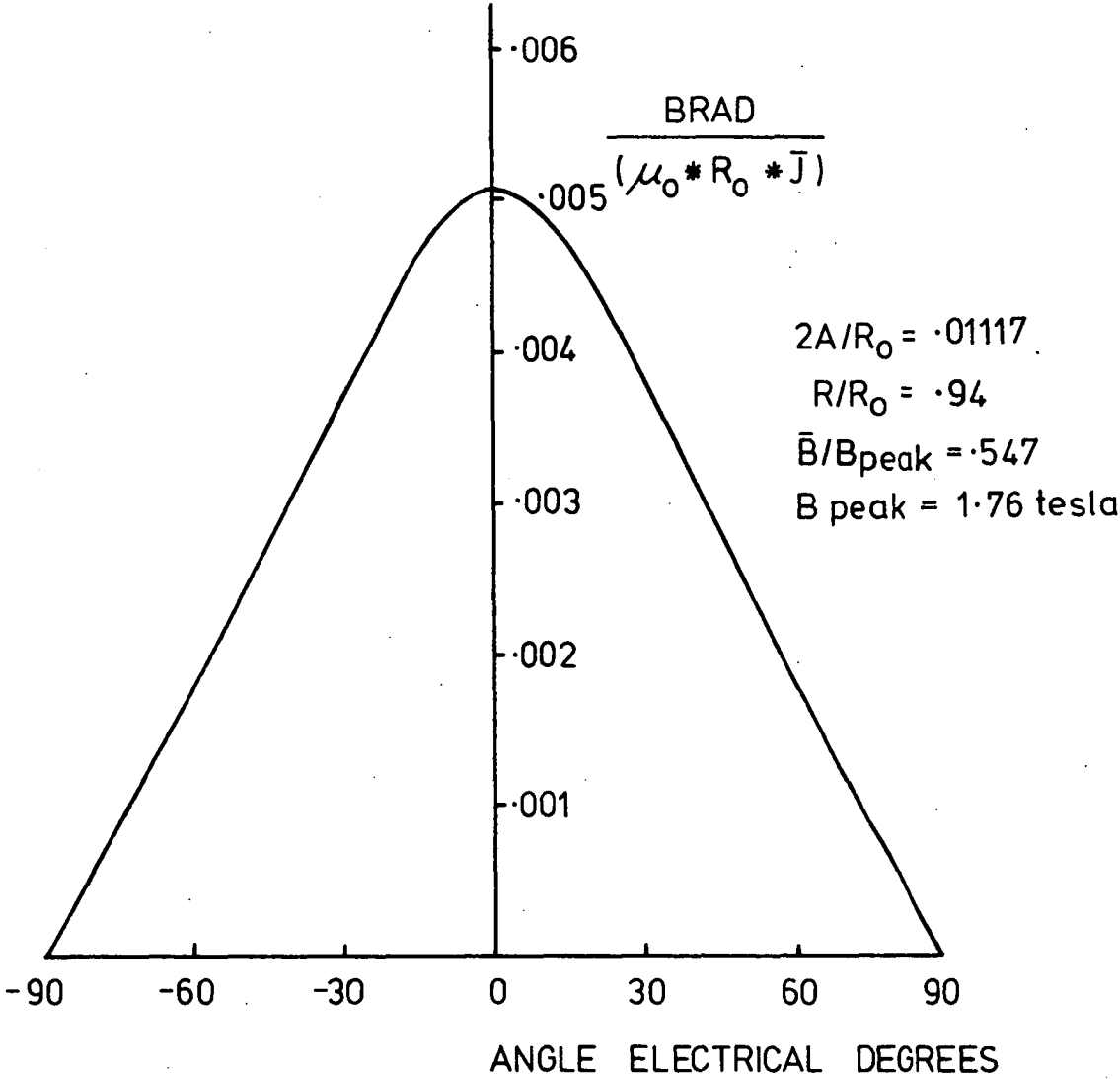
field in the region of the field winding would be near 0.0016 tesla at full load.

13-4-8 Conductor Support

The conductors of the armature and compensating windings require a technique by which they can be supported against forces due to load torque and rotation (for the armature).

To gauge the requirements of the support structures, the following parameters for the machine with the armature type field were considered.

rated output	10 MW
rated speed	200 rpm
armature diameter	2450 mm
armature length	640 mm
conductor area	31 mm^2

The centrifugal force experienced by the support structure due to the rotation of the armature amounts to 154 N/m/conductor, which is equivalent to a pressure of 0.089 MPa over the surface of the armature. If the rotational forces were constrained with a steel cylinder, the metal thickness required would be 0.8mm and the mass of the cylinder would be only 30.5 kg. This technique is undesirable because eddy current losses will occur and the cylinder will require insulation to withstand the full terminal voltage. However, the foregoing indicates that rotational forces can be contained without a large increase in the overall mass of the machine. An alternative support technique using epoxy resins and/or carbon-fibres is possible.

The circumferential force required to balance the load torque is 0.376 MN. To prevent conductor movement, steel armature "teeth" with a combined thickness of only 8mm are sufficient. If ninety-six conductors were supported per "tooth", then the individual thickness

would be 0.17mm. As the thicknesses required are small, an alternative technique using epoxy materials is possible.

The problem of maintaining a cylindrical armature and transferring the load torque to the shaft can be solved with suitably spaced spider arms.

13-4-9 Machine Efficiency

The armature conductor losses amount to a drop in efficiency of 1.43 and 1.52 percent for the coil and armature type fields respectively. Brush contact losses and friction losses both resulted in drops in efficiency of 0.1 percent. This compares with 1.6% loss in the homopolar machine. Windage and bearing loss would result in a decrease in efficiency of near 0.05 percent   (13-4). The machine efficiency, excluding refrigeration requirements, would be near 98.25 percent.

13-4-10 Machine Size and Mass

(a) Coil Type Field

armature outside diameter	2680 mm
armature overall length	1090 mm
armature plus commutator length	1760 mm
cryostat outside diameter	3320 mm
cryostat length	700 mm
armature copper mass	1.68 tonnes
compensating winding copper mass	1.29 tonnes
cryostat mass	2.83 tonnes
commutator mass	0.41 tonnes
superconductor mass	0.84 tonnes
shaft, bearings, brush gear mass	1.6 tonnes
Total mass	8.65 tonnes

(b) <u>Armature Type Field</u>

armature outside diameter	2540 mm
armature overall length	1130 mm
armature plus commutator length	1800 mm
cryostat outside diameter	2950 mm
cryostat length	1310 mm
armature copper mass	1.71 tonnes
compensating winding copper mass	1.45 tonnes
cryostat mass	2.74 tonnes
commutator mass	0.41 tonnes
superconductor mass	0.72 tonnes
Shaft, bearings, brush gear mass	1.6 tonnes
Total mass	8.63 tonnes

13-4-11 Commutation

When investigating the commutation of an armature coil, the following points require consideration:

1. The total induced voltage of the coil which consists of dynamic and static voltages. The dynamic voltages result from the movement of the coils through a stationary flux and the static voltages arise from changing currents (self and mutual inductances).

2. The effect of the brush contact resistance.

3. What actually causes the current to reverse in the coil undergoing commutation.

4. What is the cause of sparking and what energy is associated with sparking. The energy is required to indicate the severity or otherwise of the sparking.

The answers to some of the above questions were obtained by

considering the simple equivalent circuit of a coil undergoing commutation - figure 13-13. The resistances R_{bt} and R_{bl} represent the brush contact resistances to the trailing and leading commutator bars respectively. During commutation, R_{bl} changes from open circuit to a low value, whereas R_{bt} changes from a low value to open circuit. In non-interpole machines, changes in R_{bl} and R_{bt} cause the reversal of current. In interpole machines, the reversal is achieved by the combination of the interpole dynamic voltage and the brush resistance changes.

Sparking occurs if, when R_{bt} becomes open circuit, the coil current, I_c, does not equal the armature conductor current, I. If the coil current is less than the conductor current when the brush leaves the trailing commutator bar, then the coil current has to suddenly increase. The required energy to achieve this is supplied from the external, constant current circuitry. If the coil current exceeds the required value, then the energy has to be dissipated from the coil undergoing commutation. The magnitude of the spark energy was estimated as follows:

Summing voltages around the loop resulted in equation 13-10.

$$E_s + E_d + I_c(R_c + R_{bl}) = (I - I_c)R_{bt} = 0 \qquad (13\text{-}10)$$

$$\text{where} \quad E_s = L\frac{dI_c}{dt} + \sum_i M_i \frac{dI_i}{dt}$$

and E_d = constant during commutation.

The summation term was included to account for the mutual effect of coils undergoing commutation simultaneously.

With the assumptions that coils which are completing commutation do so together and that their currents are the same, and that the rate of change of current during sparking is large in comparison with that of any other coils which are in the process of commutation, then:
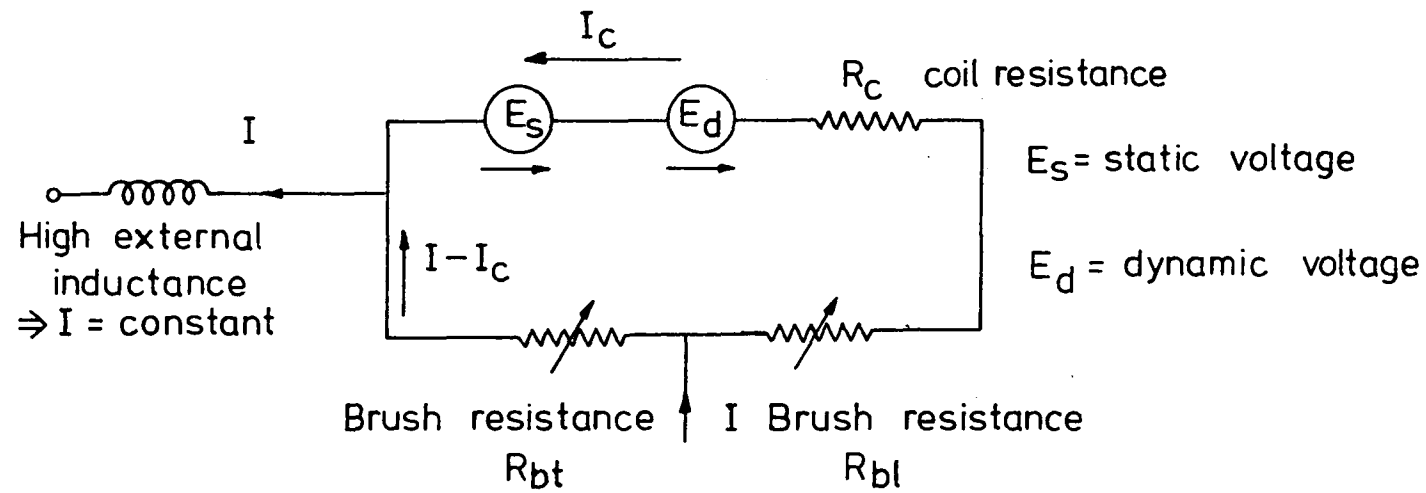
EQUIVALENT CIRCUIT OF A COIL UNDERGOING COMMUTATION

FIG 13 - 13

$$E_s = (L + \Sigma M) \frac{dI_c}{dt}$$

$$= L_{eff} \frac{dI_c}{dt} \quad \text{where} \quad L_{eff} = L + \Sigma M.$$

Neglecting all resistive voltage drops, then the spark voltage is equal to $E_s + E_d$ and the instantaneous spark power is given by equation 13-11.

$$P_{sp} = (E_s + E_d)(I - I_c) \tag{13-11}$$

Integration of equation 13-11 over the spark duration gives the spark energy, equation 13-12.

$$E_{sp} = \int_0^{tsp} (E_s + E_d)(I - I_c)\, dt \tag{13-12}$$

$$= \frac{L_{eff}}{2} (I - I_{c0})^2 + E_d \int_0^{tsp} (I - I_c)\, dt \tag{13-13}$$

The second term cannot be evaluated unless the actual spark current is known. An upper limit was obtained by assuming that the spark current remained at the pre-commutation conductor current.

The armature coil self inductances and the total mutual inductance from two coils which are identically positioned electrically and commutated by adjacent brush sets are given in the table below. The full load armature reaction flux density and the compensating winding flux density along the geometric neutral axis at the armature conductors are given in the table below.

The calculation of the spark energy assumed no reversal of the coil current until the onset of sparking. For this reason, the estimate could be an order of magnitude or more above the actual value. The energy involved is apparently small; hence, little or no damage may occur to the commutator. This spark energy represents an average total power loss

Item	coil type field		armature type field	
coil self inductance	2.32	μh	2.32	μh
total mutual inductance	0.72	μh	0.75	μh
armature reaction flux density	0.14	tesla	0.146	tesla
compensating winding flux density	0.063	tesla	0.071	tesla
dynamic voltage (E_d)	2.43	volts	2.53	volts
L_{eff}	3.04	μh	3.07	μh
I_{c0}(no reversal)	-156	ampere	-156	ampere
tsp	50	μSec	50	μSec
spark energy	0.186	joule	0.188	joule

of near 23 kW. The spark voltage for the worst case condition and a short spark duration of ten microseconds was estimated at near 95 volts.

13-5 Commutation Improvements

The major reasons why the heteropolar machine ratings have been limited to near 15 MW are the problems associated with current collection and commutation. The problems include:

(a) the low voltage limit between commutator bars;

(b) the need for complete and consistent current reversals;

(c) the maintenance of an electrical contact between a stationary and a rotating surface.

This thesis shows the feasibility of the use of superconducting wire in the field systems of heteropolar D.C. machines; hence, commutation and current collection have not been extensively investigated. However, the study would not be complete without showing that there is a strong possibility of overcoming the commutation and current collection problems.

In the previous section, natural commutation was considered. The

following sections cover methods by which current collection and commutation can be assisted.

13-5-1 Current Per Brush Arm

The problems of commutation and current collection can be substantially reduced if the magnitude of the current per brush arm can be decreased.

A reduction in brush arm current can be obtained by either increasing the number of poles in a machine or by increasing the voltage per commutator bar limit. Increasing the number of poles cannot be seriously considered because the time available for commutation is proportionately reduced, which vitiates the reduction in the brush current. Increasing the number of poles also has the disadvantage of increasing the required diameter of the commutator for a predetermined terminal voltage.

In conventional machines, the average bar voltage is limited to near twenty volts. This is a severe restriction to the acceptable dimensions of a machine. If bar voltages above this value are used, then there is the possibility that damaging flashover can occur at the commutator. The flashover can be severe in that the machine may have to be shut down as a result of overcurrents, or the erosion of the brush housings and brush arms may be excessive or, more rarely, the commutator becomes badly damaged.

References suggest that the main reasons for the low value of the acceptable volts per bar limit are the presence of ionised air, which results from the brush sparking, and carbon dust which accumulates from the brushes as they wear. The elimination of these could substantially increase the volts per bar limit. A technique by which their removal can be achieved is described by Brüderlink (13-7). A slotted and force ventilated commutator is suggested which enables the removal of the

ionised gases and the carbon dust particles.

13-5-2 Coil Inductances

The elimination of iron in the magnetic circuits of superconducting machines results in a reduction in the reactance voltages induced into coils undergoing commutation. The smaller coil sizes possible with the use of superconductors also reduces the reactance voltages. Reduced reactance voltages and coil inductances are conducive to improved commutation.

Another technique by which the effective coil inductance can be reduced makes use of the transformer effect a short circuited secondary has on coil inductances. Damper windings were investigated by Trettin in the 1930's and were intended to be the sole means of controlling commutation. However, it is an historical fact that damper windings have not come into widespread use.

Unlike the damper windings, which are intended to have an effect throughout the commutation period, Taylor (13-14) describes a method by which the severity of sparking can be reduced by the use of flux traps which have an effect only at frequencies associated with sparking. The function of controlling commutation is left to the interpoles and the brushes.

13-5-3 Environment

It has been known for many years that correct atmospheric conditions and suitable materials are vital for successful commutation and long brush life.

Materials research in the past has resulted in superior commutator materials (13-15), and investigations have shown that the presence or absence of some compounds or elements does affect commutation (13-16).

For example, low humidity substantially reduces the life of a brush; minute traces of hydrogen sulphide can cause poor commutation; and chlorine gas can dramatically improve commutation.

The surface condition of the commutator bars is paramount for successful commutation. The formation of the correct surface film, which assists commutation, can only take place under suitable atmospheric conditions. Small concentrations of some elements and compounds result in the formation of incorrect surface films; thus poor commutation can result. Work on this aspect of commutation (13-17 to 13-24) has led to a better understanding of the influence of prevailing conditions upon commutation and has resulted in improved commutation.

13-5-4 Brushes

Probably the most important components which determine the successful operation or otherwise of D.C. commutating machines are the brushes. The role played by the brushes in D.C. machinery is three-fold in that they are required to transfer energy to or from rotating surfaces, to reduce coil short circuit currents during commutation, and act as fast recovery circuit breakers and makers.

For the conventional form of brush to transfer current whilst incurring small losses and preventing large coil short circuit currents leads to opposing requirements in the contact and internal resistances of the brush. The needs for low brush losses and the ability to repeatedly make and break circuits lead to contradictions as to which brush material should be used. For low resistance, metals are required, but heating at point contacts tends to cause local melting, a fact which results in brush degradation and poor energy transfer conditions.

The carbon brush has proven to be a very satisfactory compromise, but further developments are required to improve their performance and

to ease their duty cycles.

The contact drop of carbon brushes and its influence on commutation has been the subject of many papers (13-22). Differing contact characteristics of the available types of carbon brush were used by Mayeur (13-23) to improve commutation by forming a single brush from two slices of differing types of carbon brush. Mayeur concludes that this technique improves commutation.

The solid carbon brush relies upon many small points of contact which operate at high current densities (13-26). The inflexibility of solid carbon brushes can combine with their contact characteristics to result in poor commutation and current transfer as a consequence of even slight commutator surface imperfections. Improved brush performance and ease of operation, in particular for homopolar machines, has been obtained from the use of brushes made from coated carbon-fibres (13-11). These brushes have many more points of contact than do conventional, solid brushes and are less subject to surface imperfections. The combination of conventional brushes and carbon-fibre brushes in parallel has been tested by Bates and Powell (13-27) on a conventional D.C. machine. Their tests indicated that the carbon-fibre brushes enabled considerably greater currents to be transferred and that they have great promise when applied to improvements in commutation.

13-5-5 Diode- and Thyristor-Assisted Commutation

With the advent of thyristors, methods of commutating machines electronically became feasible. The present form of commutator would appear to be a most effective means of changing the armature circuit connections and would almost function as a slip ring if it could be relieved of switching current. Switching can be arranged by circuits involving thyristors, without mechanical breakage of current. A paper by Andrews

(13-28) describes a system which utilises a segmented brush and thyristors in which the thyristors have the switching duty and the brush retains the duty of changing the armature connections. Tests with this system have indicated the possibility of improving electronically the commutation of a D.C. machine that has a conventional commutator.

Early investigations into the use of the diode-assisted and thyristor-assisted commutation in small D.C. machines were very successful. However, their application in larger machines resulted in special contact problems which resulted in severe burning of the commutator segments. This burning occurred immediately for diode-assisted commutation and after a period of running and the formation of surface films for thyristor-assisted commutation. Carbon-fibre brushes were found to prolong the period of successful operation, see Bates (13-29 to 13-32). Bates has since developed a 300 kW, 3000 r.p.m. D.C. machine using thyristor-assisted commutation. With the aid of thyristor suppression circuits, the machine has overcome the contact problems which were caused by the very high rates of rise of brush current (13-33). The system has two commutators and brush gear and these are of conventional construction. A paper describing the terminal characteristics of the machine suggests that equalising connections are unnecessary (13-34).

There are now available Toshiba 600 ampere, 1300 volt gate turn-off thyristors and ASEA 1650 ampere, 2000 volt ordinary thyristors which suggests a promising future for very large thyristor-assisted D.C. machines.

13-5-6 Voltage Injection

For successful commutation, most machines require an induced voltage in the coils undergoing commutation, which assists the current reversal. Even the thyristor-assisted machines described by Bates rely

on interpoles, which is the conventional method of inducing the necessary reversing voltage.

The superconducting machine could require an induced voltage as pure resistive commutation may not be adequate. As a consequence of the elimination of iron, interpoles are not feasible as they would require excessive space, reduce the machine efficiency, and induce a torque in the field system. With this in mind, an alternative method of inducing the voltage is required.

With the use of segmented brushes or part brushes and thyristors, a possible circuit for inducing the voltage is shown in figure 13-14. As the voltage source can be separate from the machine, electronic circuitry can be used with the advantage that optimum induced voltages could be provided for all machine speeds and loads.

31-5-7 Commutatorless Machines

Commutatorless D.C. motors have been used in applications ranging from steel rolling mills to wowless stereo phonograph turntables (13-35, 13-36). These machines have rotating field systems and stationary armatures. The armature is supplied from a D.C. source via a thyristor inverter. The machines would best be described as synchronous machines that are powered from a controlled variable frequency supply. The proven techniques used in turbo alternators with superconducting field windings could be used in commutatorless motors to advantage.

13-6 Discussion

The specific masses of the conventional heteropolar, the super-conducting heteropolar and homopolar machines were estimated as 4.7, 0.86 and 0.75 tonnes/MW respectively. The mass advantage of the super-conducting machines is apparently considerable, which indicates the

I
Commutator
+
Voltage
source
−

2 I
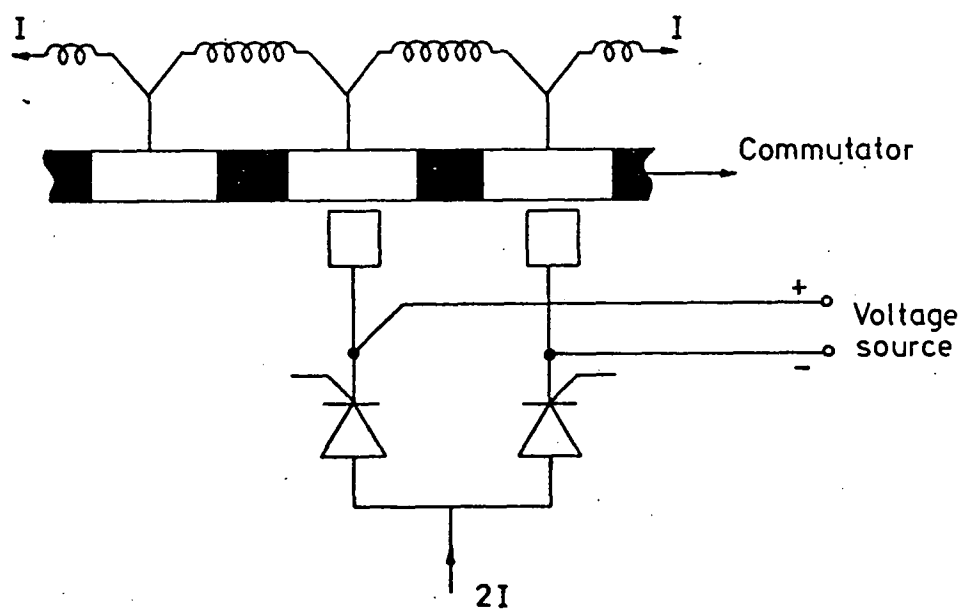
EXTERNAL SOURCE   VOLTAGE
INJECTION REPLACES INTERPOLES
FIG 13-14

necessity for their advancement.

Machine Type	Outside Diameter mm	Length mm	Mass tonnes
Conventional heteropolar	4000	2000	47
Superconducting heteropolar			
coil type field	3320	2000	8.6
armature type field	3000	2050	8.6
Superconducting homopolar	2760	1500	7.9

A difficult problem with the homopolar machine is the current sharing characteristics of the current collection system considered. This can be overcome with liquid metal systems, but these are generally restricted to drum-type machines, for example, the "field shaping drum machine" (13-37).

The dimensions of the heteropolar machines can be reduced if a greater volts per bar is used. If 40 volts were acceptable (13-7) then the armature diameter of the 10 MW, 200 r.p.m. machine with the same peak field flux density can be reduced to less than two metres and the length increased to two metres. Thyristors have been shown to be able to reduce the number of commutator bars in a machine by assisting commutation.

The production of the required field flux density with the smaller armature diameter could be very difficult with a niobium-titanium field conductor as a result of exceeding the quench flux density. It may be necessary to use the brittle, higher field superconductors. The difficulty of producing the field coils from the brittle superconductor would not be acute because the coils are not large; consequently a very large curing oven would not be required. The brittle conductors could permit higher flux densities at the armature, hence a further reduction in

machine dimensions.

From the previous comments and the possibilities of improving machine commutation, it is apparent that further research into the development of large superconducting D.C. heteropolar machines should be conducted.

CHAPTER 14.

MODEL MACHINE

14-1   Introduction

The success of the tests on the initial machines and the favourable results of Chapter 13 indicate that a model of a prototype machine should be designed, constructed and tested to confirm the conclusions of Chapter 13.   A field winding containing semicircular end sections and totally occupying a cylindrical surface, in a similar fashion to an armature winding, was selected - figure 14-1.

14-2   Machine Design

The model machine was designed with the intention of maximising its output and simulating the operation of a superconducting field winding in a prototype machine.

The limitation of the size of the machine was that it had to be possible to obtain the superconducting state and to have sufficient helium remaining from a thirty litre dewar for a period for testing of the machine.

14-2-1   Cryostat Helium Chamber

An estimate of helium consumption during initial filling of the machine cryostat was obtained as a function of the design parameters of the machine - equation 14-1.

$$V_c = (V_s + V_w + V_0)/(1 - \frac{Q_0}{qL})$$ (14-1)

V_c = volume of helium used during filling (litre)

V_s = volume of helium to cool the stainless steel (litre)

V_w = volume of helium to cool the superconductor (litre)

V_0 = helium capacity of the cryostat (litre)

FIG 14-1
ARMATURE TYPE FIELD SYSTEM
FIELD COIL
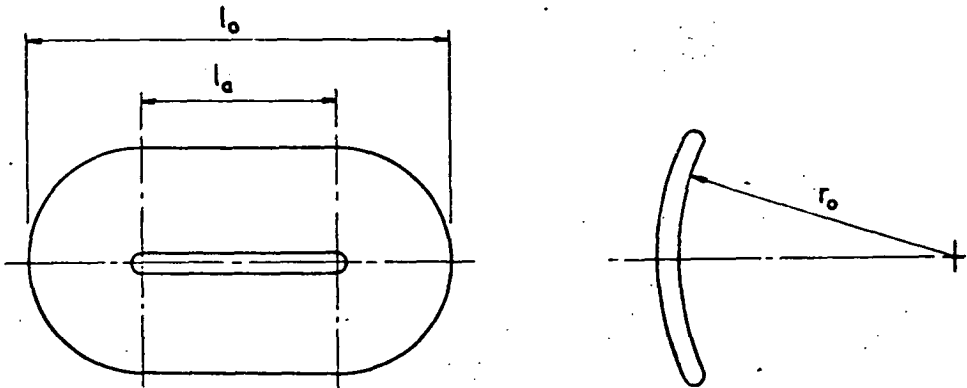
FIG 14-2
SECTION OF THE 430 AMPERE
CURRENT LEAD

TOTAL LENGTH = 650 mm

4×3·175 mm diameter copper rods

30·1mm

5mm

12·7mm

Teflon alignment
spacers

3·175 mm
2 holes

No 26 drill
4 holes

No 10 drill
2 holes

18 gauge copper fin
heat exchangers

28·0mm O.D.
12·7mm I.D.
20·4mm P.C.D.
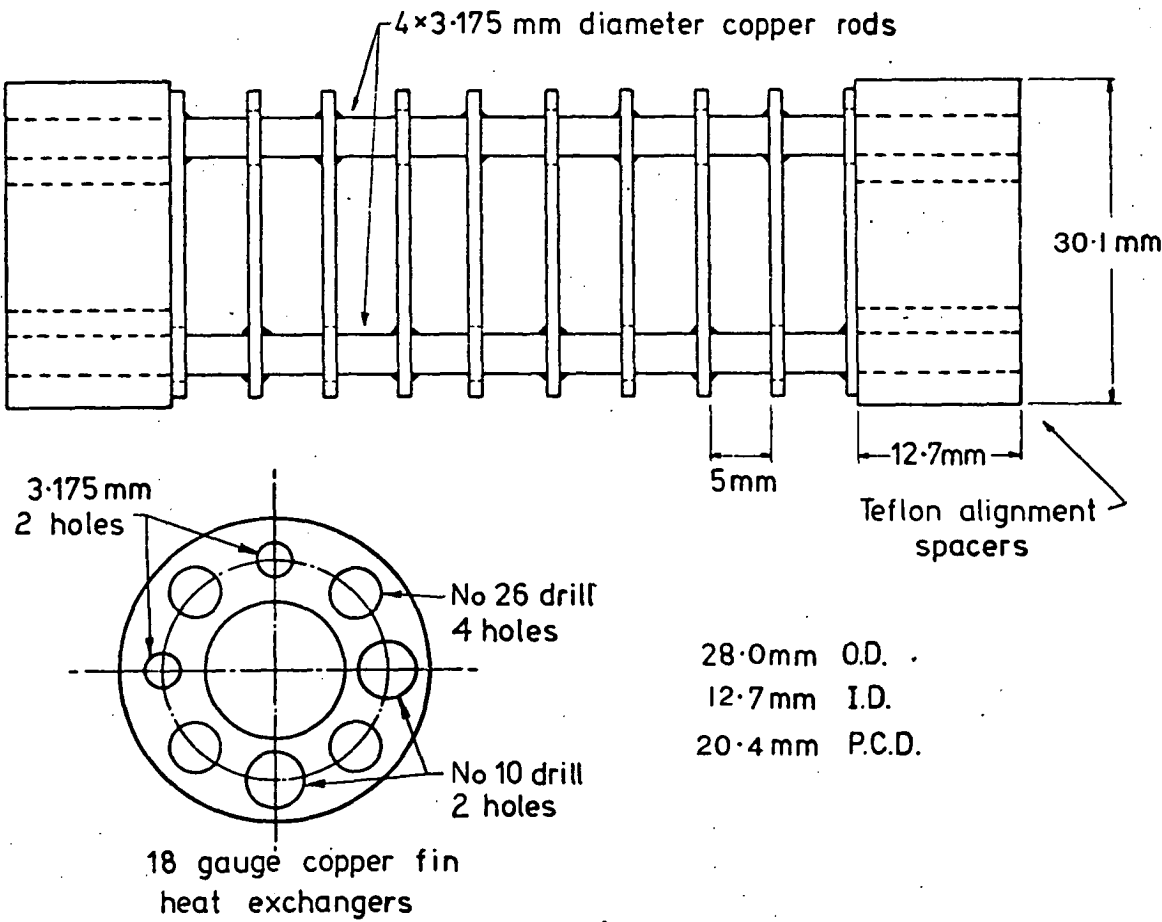
Q_0 = heat inleak to the cryostat during filling (watt)

q = rate of transfer of helium (litre/sec)

L = latent heat of vaporization (joule/litre)

The form of the field winding is indicated in figure 14-1. From this diagram the helium required to cool the field system was obtained - equation 14-2.

$$V_w = \Delta h_w L^{-1} n(2\ell_a p + \pi^2 r_0) \qquad (14-2)$$

Δh_w = enthalpy difference of the wire per unit length (joule/m)

n = number of turns per coil

p = number of field poles

ℓ_a = active length of the field (m)

r_0 = inner radius of the field system (m)

The volume to cool the stainless steel, V_s, and the volume to fill the helium chamber, V_0, were obtained from equations 14-3 and 14-4 respectively.

$$V_s = \Delta h_s L^{-1} t_s 2\pi(2r_0 t_c + (2r_0 + t_c)(\ell_a + \frac{2\pi r_0}{p})) \qquad (14-3)$$

$$V_0 = 2\pi r_0(\ell_a + \frac{2\pi r_0}{p})(t_c - t_w) * 1000 \qquad (14-4)$$

Δh_s = enthalpy difference of stainless steel per unit volume (joule/m^3)

t_s = thickness of stainless steel (m)

t_c = helium chamber thickness (m)

t_w = winding thickness (m)

The availability of suitable off-the-shelf stainless steel tubing of appropriate dimensions and the thirty litre limit on liquid helium allowed a maximum field winding inner diameter of 178mm. The number of field poles selected was four and the active length of the field was

initially assumed to be 100mm.

From Appendix B,

$$\Delta h_w = 31 \text{ J/m}$$

$$\Delta h_s = 26.1 * 10^6 \text{ J/m}^3$$

The availability of stainless steel tubing required that:

$$t_s = 1.625 \text{ mm}$$

$$t_c = 19 \text{ mm}.$$

The maximum width of each field coil is 140mm which permits sixty turns per field coil layer. The preceding data substituted into equations 14-2, 14-3, and 14-4 resulted in the following:

$$V_w = 1.2 * m \text{ litres}$$

$$V_s = 5.17 \text{ litres}$$

$$V_o = 134.1 (0.019 - 0.0011 * m) \text{ litres}$$

$$m = \text{number of layers per field coil}$$

$$\text{thickness of each layer} = 1.1 \text{ mm}.$$

14-2-2 Field System

The intention was to operate at 90 percent of the critical current of the selected winding. The critical current is related to the number of layers in the field system, and to a first approximation the flux per field pole is independent of the number of layers in the field winding. Consequently the number of layers per field coil was determined by maximising the period for operating the superconducting field system from 30 litres of liquid helium.

The period of operation available depends on the quantity of helium used for cooldown and the heat inleak during operation, as given in equation 14-5.

$$T = (30 - V_c) LQ^{-1}/3600 \tag{14-5}$$

Q = heat inleak during operation (watts)

T = time for operation (hours)

With the assumption that the heat inleak to the helium is via the current leads only, Q and Q_o are functions of the operating current only. With an operating current of 90 percent of the quench current, values of Q and Q_o can be evaluated using the results of Chapter 6. From the experience gained during the earlier experiments, a rate of transfer of helium during cooldown of 3 litres per hour was used in equation 14-1. A winding packing density of 0.65 was assumed, so that the volume of the field winding could be calculated.

The results of Table 14-1 indicate a flat optimum. A winding with five layers was selected in preference to four layers because of the lower operating current which reduced current supply difficulties.

The estimated operating times were more than sufficient to conduct the testing of the machine so the field system active length was increased from 100mm to 130mm.

14-2-3 Field Supply Lead

The design current for the leads was 445 amperes as given in Table 14-1. This figure allowed for the possibility of increasing the excitation current to near the quench current for short periods. The lead length used previously was retained, 650mm, and from the results in Chapter 6 a lead conductor area of 15.7mm^2 was required. The availability of 3.175mm diameter copper rod resulted in a lead design consisting of two rods per conductor and a conductor area of 15.8mm^2.

Copper fin heat exchangers similar to those used successfully on previous leads and soldered to alternate conductors at the same interval used previously were retained. Teflon spacers at 50mm intervals were

Number of layers per coil	Conductor quench current density		Operating current		Volume of helium used during cooldown		Time for operation	
	typical amp/mm^2	guaranteed amp/mm^2	typical amp	guaranteed amp	typical litre	guaranteed litre	typical hours	guaranteed hours
3	750	625	530	440	14.6	13.8	9.9	12.6
4	672	570	475	405	15.5	14.8	10.5	12.8
5	631	535	445	380	16.5	15.9	10.3	12.7
6	590	506	415	360	17.6	17.0	10.3	12.4
7	560	485	395	345	18.7	18.1	9.8	11.8

Operating Time Optimisation

TABLE 14-1

used to position the lead centrally within the chimney tubing of the cryostat - figure 14-2.

14-2-4 Cryostat

The remainder of the cryostat (figure 14-3) was designed around the need for adequate clearances for insulation purposes and the field coil container support.

As the field system had to be supported from the outer sections of the cryostat, chimney contraction could not be allowed for by appropriate positioning of the helium chamber (vide the previous cryostats). Contraction in the chimney was allowed for by the introduction of an "O" ring sealed contraction joint in the outer section of the chimney - figure 14-4.

14-2-5 Armature

The diameter of the armature was selected as 144mm so that it would rotate freely within the bore of the field system cryostat. The active length of the armature was chosen as 130mm which matched the active length determined for the field system. A machine terminal voltage in the region of 450 volts was required so that insulation stressing would be representative of the conditions in a larger prototype machine. The envisaged voltage rating and an average voltage between commutator bars of near 20 volts required a commutator with 90 segments. A commutator with 78 segments and with dimensions that were suited to the machine was available; consequently the number of armature coils was set at 78.

The armature design required that the largest rating be achieved whilst maintaining a high efficiency. The entire armature volume is available for conductors; however, at the smaller radii the conductor efficiencies become unacceptably low if a constant conductor current density is used in the armature conductors.

FIG 14-3A
MODEL MACHINE
CRYOSTAT
Section B-B

Container diameters
1 241 mm
2 216 mm
3 178 mm
4 152 mm

Thermal plug

Contraction joint

① ②

③ ④

Copper radiation shield

Thrust support 3mm teflon

Field winding

300 mm

A
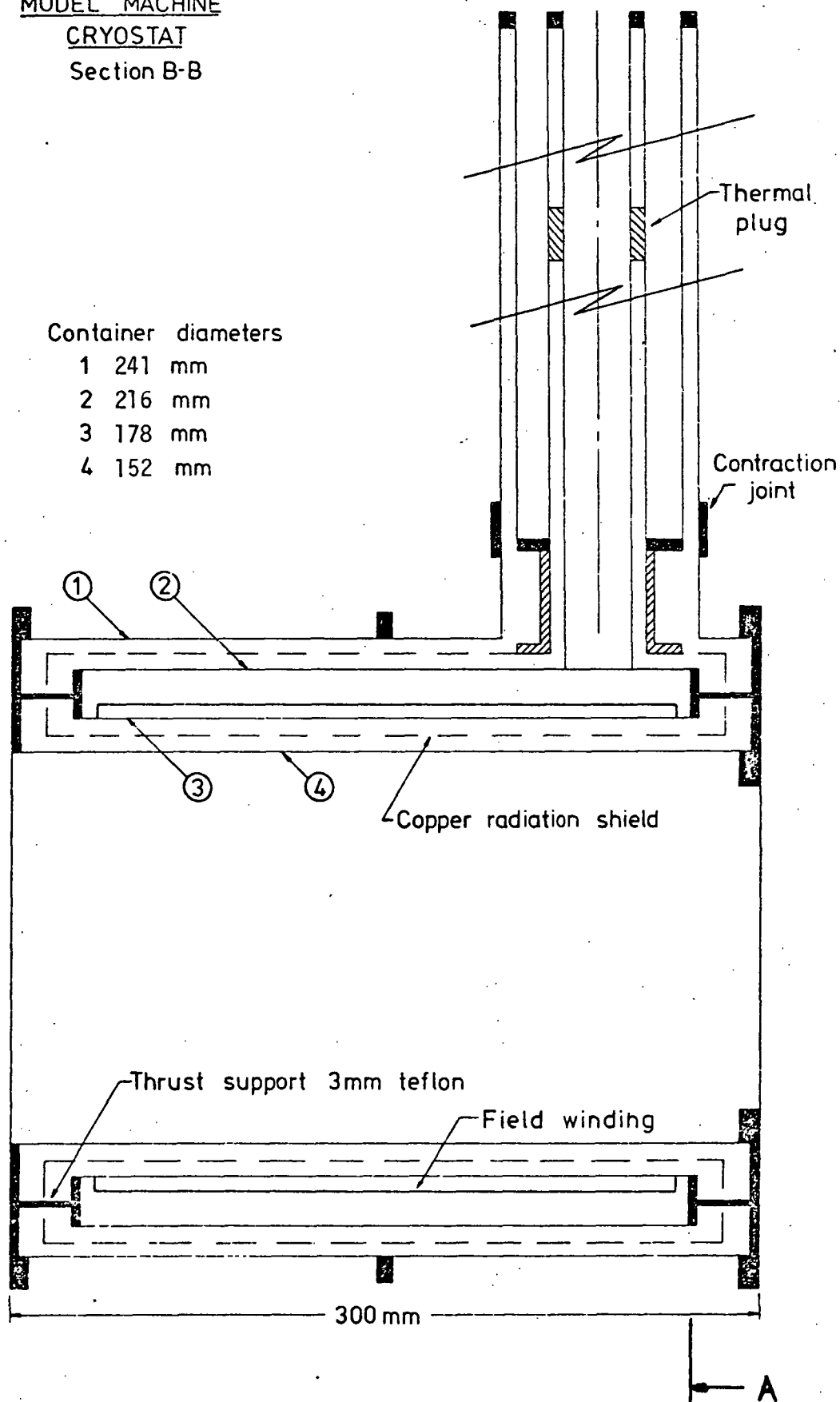
FIG 14-3B
MODEL MACHINE
CRYOSTAT
SECTION A-A
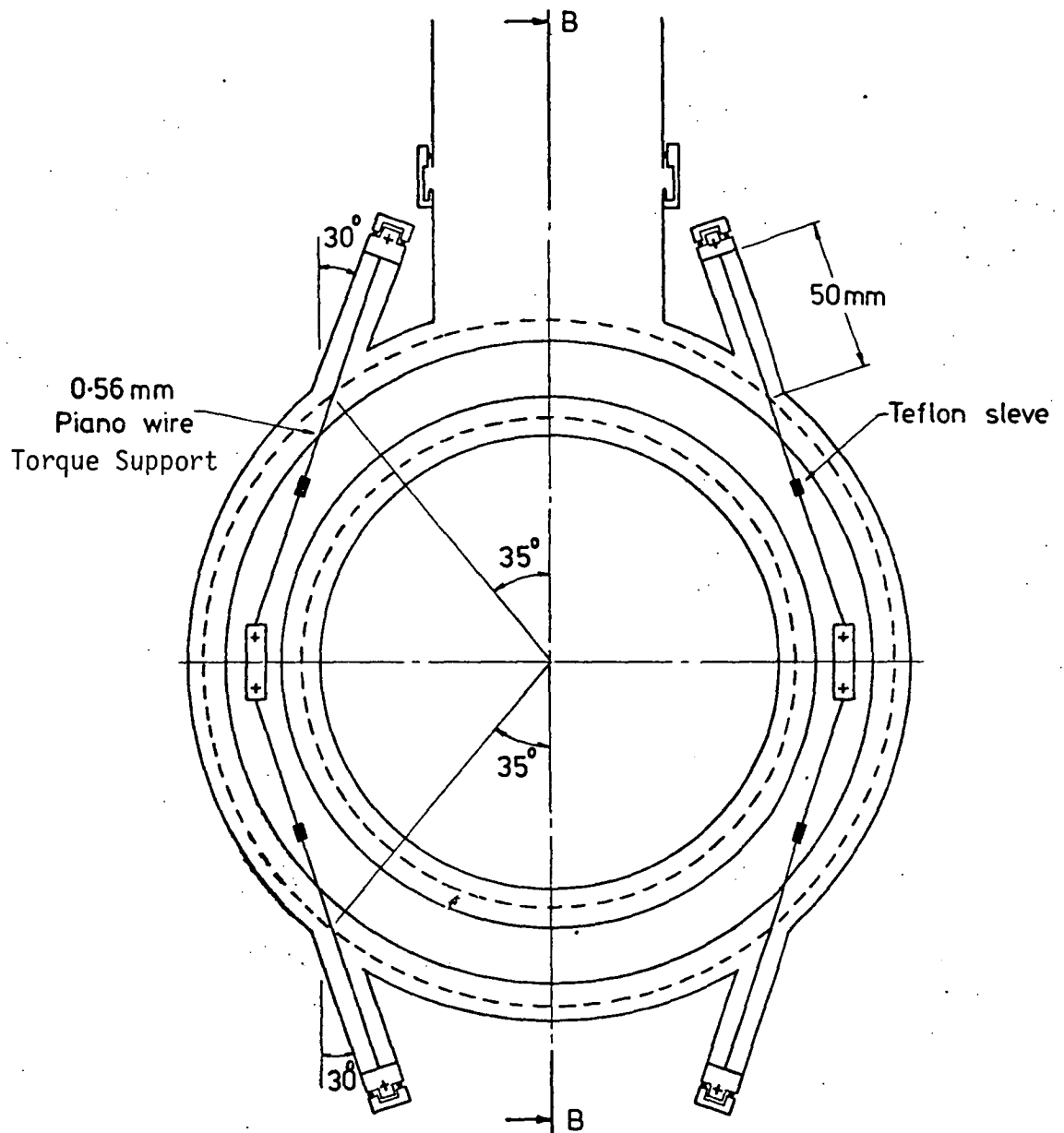
FIG 14-4
MODEL MACHINE CRYOSTAT
CONTRACTION JOINT

7·1mm

47·6mm

76·4mm

85·1mm

100·7mm
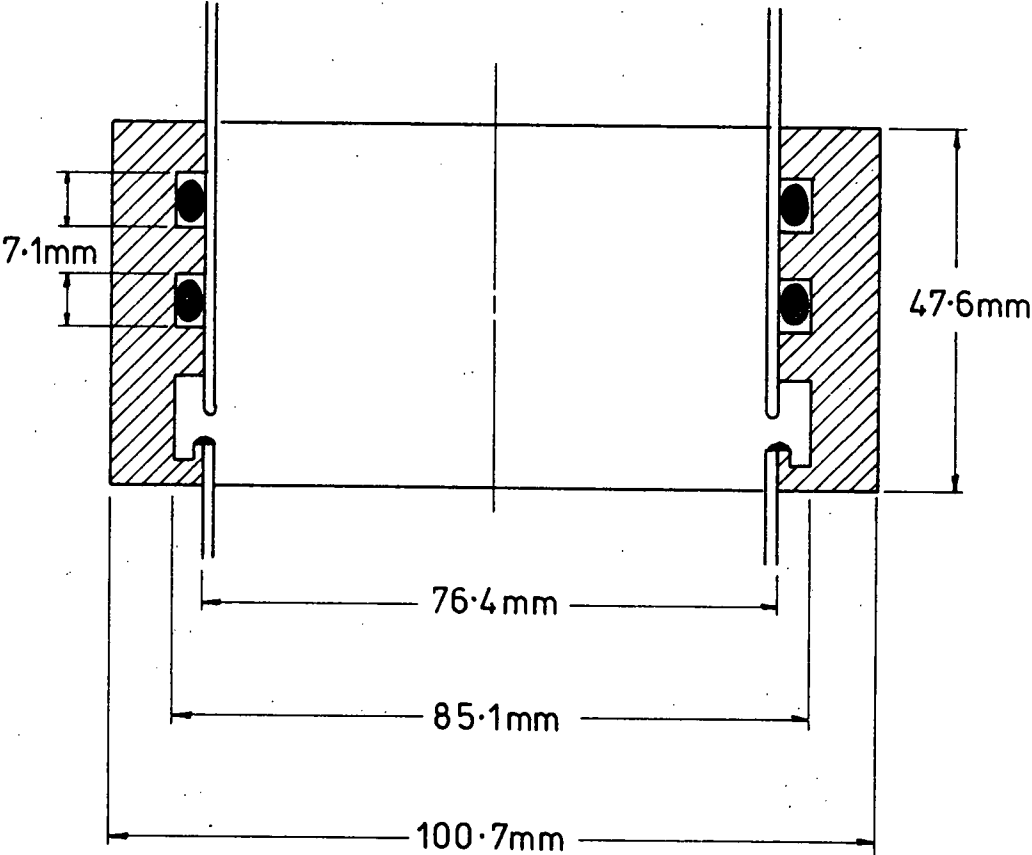
The minimum radius to be utilised whilst maintaining a conductor efficiency of greater than 90 percent was determined as given below.

$$\text{Conductor induced e.m.f.} \quad = \quad \bar{B}(r) r \omega \ell_a \qquad (14-6)$$

$$\text{Conductor IR drop} \quad = \quad \rho \ell_t J \qquad (14-7)$$

$$\text{Conductor efficiency} \quad = \quad 1 - \frac{\rho \ell_t J}{\bar{B}(r) r \omega \ell_a} \qquad (14-8)$$

$$\bar{B}(r) r \quad > \quad \frac{J \rho \ell_t}{\omega \ell_a} \quad * \quad \frac{1}{1 - \eta_c} \qquad (14-9)$$

$\bar{B}(r)$ = average flux density at radius r (tesla)

r = radius (m)

ω = speed (rad/sec)

ℓ_a = armature active length (m)

ρ = armature conductor resistivity (Ω-m)

J = armature conductor current density (ampere/m^2)

ℓ_t = total length of an armature conductor (m)

η_c = conductor efficiency.

Typical data is

ω = 1500 r.p.m. = 157 rad/sec

ρ = $2 * 10^{-8}$ Ω-m for copper at 65°C

ℓ_t / ℓ_a = 2

J = $3 * 10^6$ ampere/m^2

$$\bar{B}(r) r \quad > \quad \frac{3 * 10^6 * 2 * 10^{-8} * 2}{157 * (1 - 0.9)} \qquad \text{tesla-m}$$

$$B(r) r > 7.6 * 10^{-3} \quad \text{tesla-m.}$$

For the field winding selected and an excitation current of 430 ampere, the minimum armature radius had to be greater than 28mm.

After consideration of many armature coil shapes, the configuration given in figure 14-5 was selected because it was easily wound and the tops

FIG 14-5
ADOPTED ARMATURE
COIL FORMAT

45° 45°

A

A : Critical position for
winding to fit

45° 45°
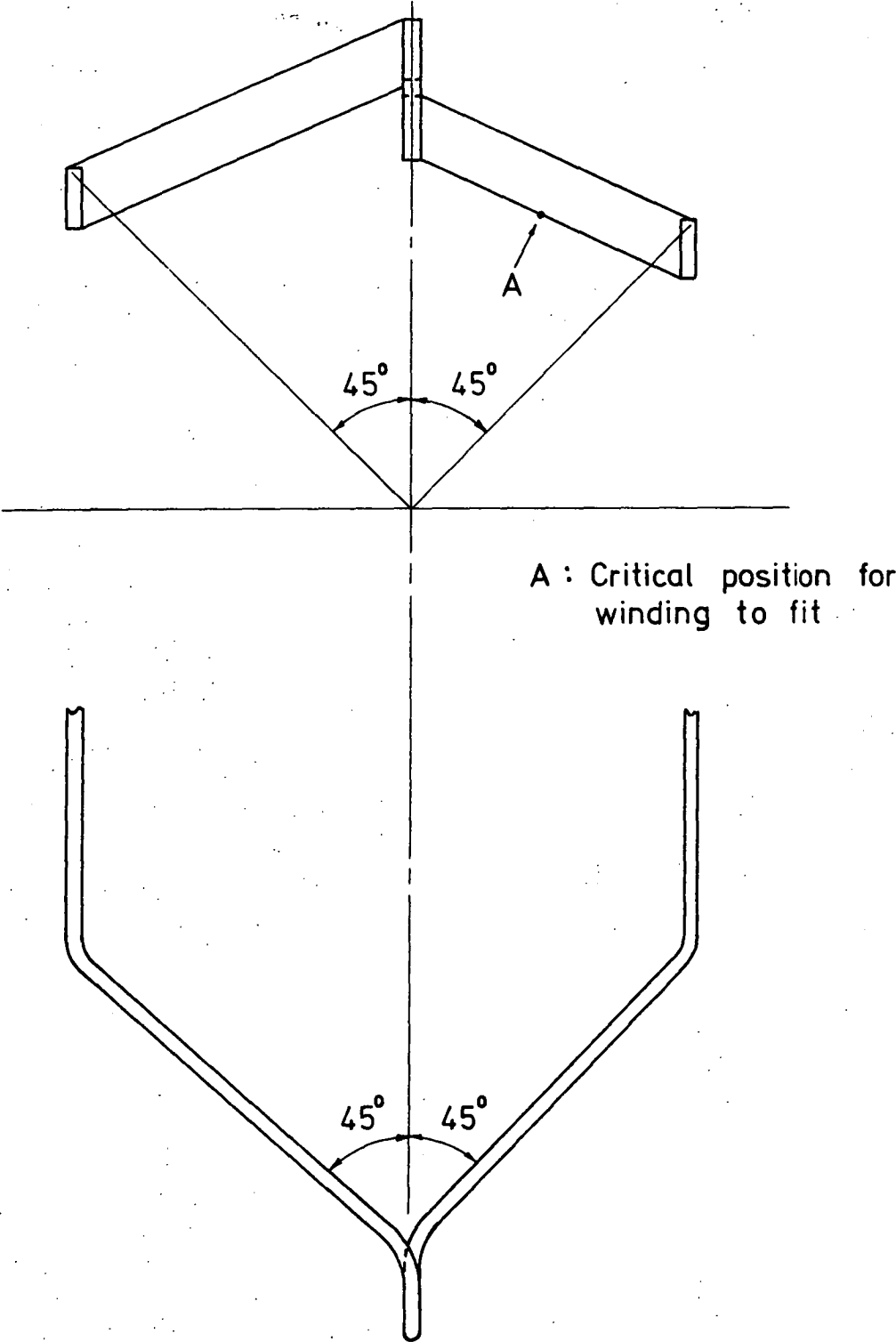
and bottoms of coils formed a fan which assisted cooling.

The largest wire size possible as determined by the space available for an armature winding with an inner active radius of 28mm, one turn per layer, and an end winding angle of 45° is 18 B and S. The maximum possible number of turns per coil is 19, consequently the machine output with this winding would be 10 ampere, 400 volts, 4 kW at 1500 r.p.m. This winding would have an armature surface occupancy of only 18.5 percent.

To improve the surface occupancy, hence the efficiency of the machine, a two turn per layer winding with an 18 B and S conductor was investigated. The minimum inner active radius possible is 47.5mm. A winding with the maximum turns per coil of 18 results in a machine with an output of 10 ampere, 500 volts, 5 kW at 1500 r.p.m. An armature surface occupancy of 37% resulted.

Further windings with two turns per coil layer but with larger wire sizes, 16 and 17 B and S, were investigated. The results are summarized below:

wire size (B and S)	16	17	18
inner active radius (mm)	58	52	47.5
number of turns per coil	8	14	18
armature current (ampere)	15.7	12.5	10
armature voltage at 1500 r.p.m. (volt)	260	417	500
output (kW)	4.1	5.2	5

The 17 B and S winding was selected because of the maximised output. The armature resistance was estimated to be 0.7 Ω for a winding temperature of 65°C. The armature copper loss represented a loss in efficiency of 2.1%.

14-2-6 Field System Support

The method adopted for the support of the helium chamber against

its own weight, machine torque reaction, and to prevent lateral movements of the helium chamber with respect to the outer room temperature section of the cryostat consists of tensioned high tensile steel wires which secure the helium chamber - figures 14-3B and 14-6. The chimney sections for the helium chamber suspension were required to reduce the heat conducted to the helium. The lengths of the chimneys were calculated on the basis of equalising the heat conducted via the wire supports to the nitrogen shield and to the helium.

Full load machine torque is 33.1 N-m which, at a radius of 190mm, required a balancing force of 350N. Inclined supports were selected because they resist lateral movement. A total of eight wires were used; however, only four provide support against load torque because the remainder would be in compression. With an angle of inclination of 30°, the tension in each support as a result of the load torque is 100 N.

Tests on high tensile steel wire led to the selection of a 0.56mm wire which had an ultimate tensile load of 580 N at room temperature. Teflon thrust support spacers with a diameter of 3mm were included between the ends of helium and room temperature sections of the cryostat - figure 14-3A. A photograph of the completed model is given in figure 14-6.

14-3 Initial Testing

14-3-1 Field Flux Densities

The dimensions of the field winding wound from the superconductor are given below.

outside diameter	=	193.7 mm
inside diameter	=	176.2 mm
active length	=	127 mm
overall length	=	254 mm
number of turns per coil	=	300.
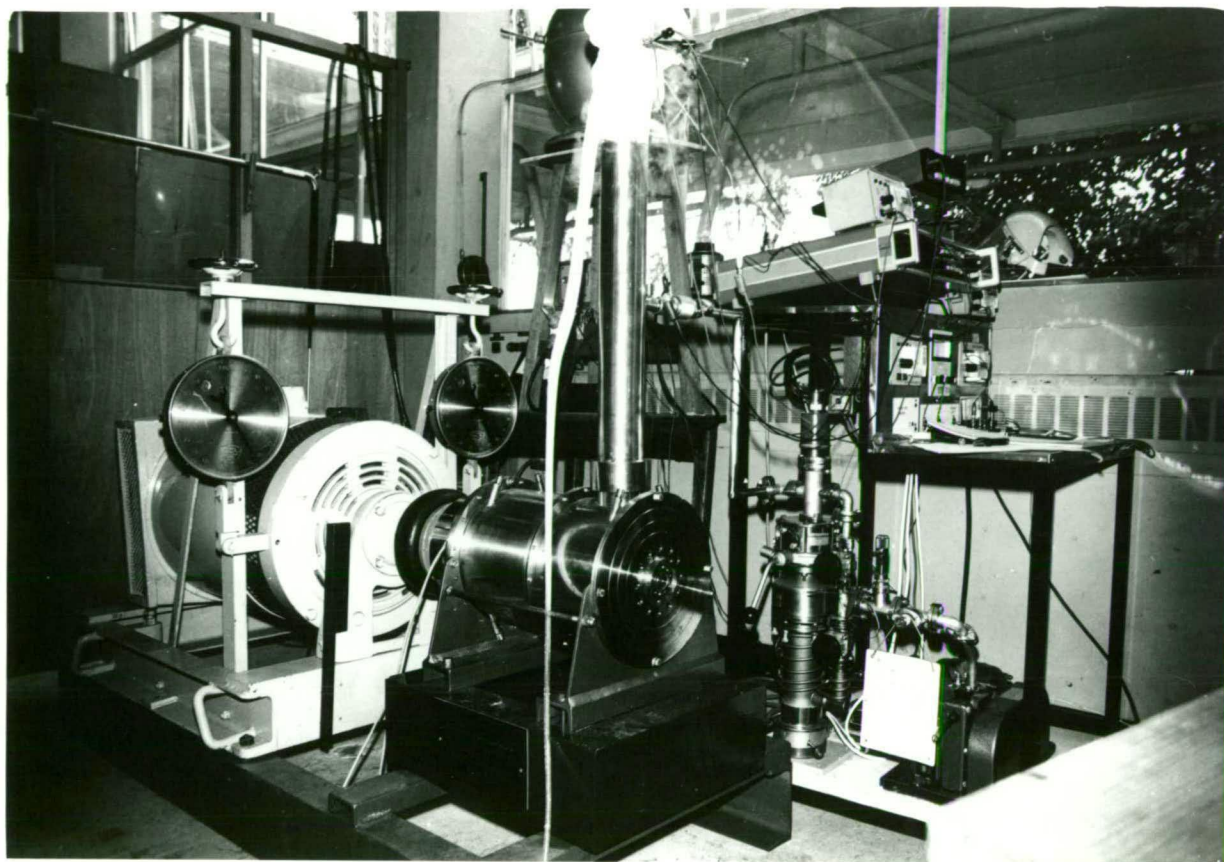
FIGURE 14-6

MODEL MACHINE

The achieved winding thickness, 8.75mm, represents an overall packing factor of only 37.1 percent. This figure is low when compared with the assumed value for design purposes of 65 percent. The lower packing achieved marginally reduces the field flux but reduces the helium charge by 0.55 litres. At an operating current of 430 ampere, the total winding average current density is 203 ampere/mm^2.

A comparison between measured and calculated values of the field flux density in the vicinity of the armature winding is given in figure 14-7. The measured values are greater than the calculated values; hence a greater machine output than that estimated will be possible. The opposite occurred for the peak flux density at the superconductor. The recalculated peak flux density was 2.9 tesla, whereas the measured value was 2.24 tesla. The guaranteed quench flux density is 3.3 tesla.

14-3-2   Open Circuit Voltage

The estimated open circuit voltage at 1500 r.p.m. and with a field current of 430 ampere was 417 volts. The increased field pole flux values of the previous section indicated that a terminal voltage 20 percent higher than that previously estimated (section 14-2-5) could be expected. Open circuit tests on the machine indicated that the terminal voltage is related to the field current and speed by equation 14-10.

$$V_{oc} = 8.42 * 10^{-4} * r.p.m. * I_f \qquad (14-10)$$

At rated speed, 1500 r.p.m., and rated field current, 430 ampere, the open circuit voltage would be 543 volts. This is 30% higher than the estimated value of 417 volts. Discrepancies in the field flux accounts for 20% and the further 8% increase is a result of induced voltages in the armature end turns. The rated machine output is thus 6.8 kW.

FIG 14-7

FIELD SYSTEM
RADIAL FLUX DENSITY

Current =1amp
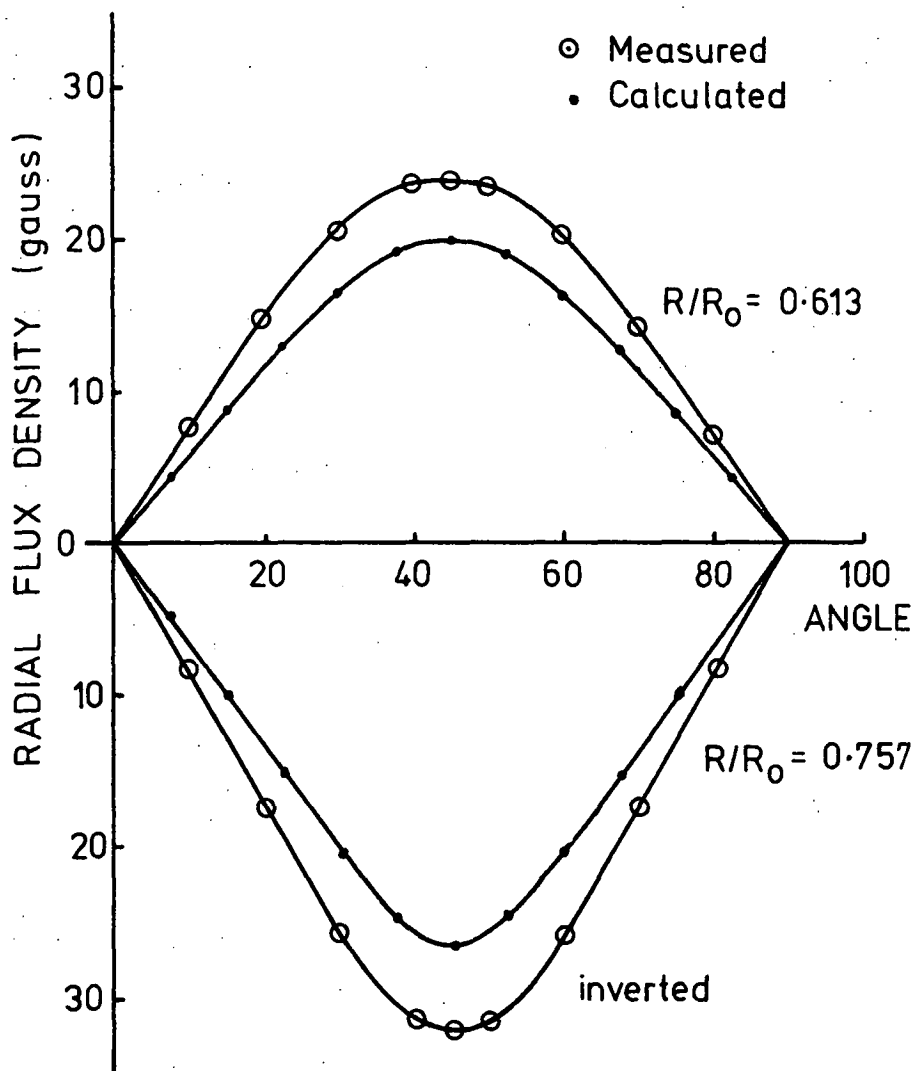
14-3-3 Armature Resistance

Tests on the armature revealed that adjacent bar to bar resistances were all near 0.145 ohm. The coil resistances were thus 0.147 ohm which corresponds to an armature resistance of 0.716 ohm at room temperature. At the operating temperature of 65°C, an armature resistance of 0.842 ohm results in an armature copper loss of 132 watts or a 1.9% drop in the output.

14-3-4 Liquid Nitrogen Tests

As a result of the physical size of the machine, the actual heat inleak to the helium chamber has to be no greater than that calculated for the design because, if it were greater, there would be a strong possibility that thirty litres of helium would not be sufficient to ensure that the superconducting state could be achieved.

The liquid nitrogen tests were required to show that the heat inleak can be attributed to the field supply leads as well as to test the contraction joint for satisfactory operation.

The lead heat inleak to nitrogen without field excitation was estimated at 2.9 watts. Measurement of rates of boil-off without shield cooling indicated a heat inleak of 2.8 watts. This proved that the heat inleak could be attributed to the leads and that the cryostat was suitably insulated.

With the radiation shield cooled, a heat inleak of only 1.1 watt was measured. This reduced value was expected in the light of tests on previous cryostats and the fact that the heat plug between the shield nitrogen chamber and the lead intercepts heat conducted by the leads.

No operational difficulties were encountered with the contraction joint. A contraction of approximately 2mm occurred which was accounted

for by the expected contraction over the 650mm length of the shield coolant chamber.

14-4 Model Machine Tests with Helium

Experiments to induce the superconducting state into the four pole, armature type field winding were attempted in March 1979, August 1979, February 1980, and September 1981.

The first experiment was conducted over two days. On the first day the method of helium transfer attempted duplicated the methods used during the previously successful experiments. Although liquid helium was successfully delivered into the cryostat, as indicated by temperature sensors within the chimney of the cryostat, the liquid helium did not distribute around the coil chamber, with the result that the cooling was not effective. This problem was not encountered during tests with liquid nitrogen. On the second day a nozzle was fitted to the outlet of the transfer tube. The nozzle directed the ingoing liquid helium along the length of the field coil chamber. The minimum resistance achieved represented a 270 fold reduction from the room temperature resistance. The copper matrix resistance reduction as specified by the manufacturer is 180 fold, thus approximately 30% of the field winding attained the superconducting state.

In the light of the apparent closeness of achieving a total transition to the superconducting state and the loss of helium during the first day of the experiment, another experiment was conducted after a delay resulting from difficulties encountered with short circuiting of the leads supplying the field coils. Difficulties with the transfer of helium were encountered as a result of ice that had formed in the helium dewar, probably during filling, and the problem with poor helium circulation recurred. The final resistance reduction of 9.6 fold from room temperature represents a coil temperature only slightly less than that produced by

liquid nitrogen which gives an 8 fold reduction.

In order that the problem of not obtaining helium circulation around the field coil could be investigated a perspex replica of the field coil chamber was constructed. Dyed water was used to indicate flow patterns.

Duplication of transfer techniques used during the successful experiments with helium revealed that instead of circulating around the coil chamber most of the entering dyed water, after leaving the transfer tube, promptly flowed out of the replica.

A nozzle fitted to the outlet of the transfer tube directed the ingoing water along the top of the coil chamber. With the nozzle in place the entering water circulated throughout the chamber before flowing from the replica. It was revealed that the location of the nozzle was critical otherwise circulation ceased and the flow became similar to patterns obtained without the nozzle.

It was realised that a tube taking the helium from the transfer tube to an extremity of the coil chamber would be preferable to the nozzle; however, to install such a distribution tube required the dismantling of the machine and in light of the near success of the first experiment it was thought not to be necessary.

The third helium test resulted in a 12.6 fold reduction in resistance, but at this point the vacuum in the insulation failed, as later discovered, the result of a faulty vacuum pump seal. The rate of cooldown obtained during the third experiment was less than that obtained during the first experiment. This suggested that the effectiveness of the nozzle had been reduced probably as a result of the relocation of the current leads when the short circuit was eliminated. The tests on the replica indicated that the position of the outlet of the nozzle was critical in that it had to be below the lowest extremity of the chimney. With the relocation of the leads

it was possible that the outlet became too close to the chimney extremity thus reducing the effectiveness of the nozzle.

In light of the poor cooling obtained since the first test it was decided to dismantle the machine and to install a pipe to transfer the helium to the extremity of the coil chamber. Another modification involved increasing the diameter of the inner chimney pipe so that greater clearances between the lead cooling fins and the conductors were possible. Another tube extending from the bottom of the coil chamber to the top of the cryostat chimney was installed so that excess pre-cooling liquid nitrogen could be withdrawn prior to the commencement of the helium transfer.

Tests on the replica were conducted to determine the orientation and location of the outlet of the distribution tube that resulted in the best utilisation of the coolant and did not produce regions of poor coolant flow. The location selected was at the bottom extremity from the chimney and the orientation such that the coolant spiralled around the coolant chamber.

Tests with liquid nitrogen on the rebuilt machine indicated the effectiveness of the distribution tube. These tests were initially charact-erised by the inability to transfer liquid nitrogen as a result of initial back pressure within the uninsulated distribution tube and the transfer tube. This problem was overcome by ensuring that the transfer tube was properly pre-cooled prior to insertion into the distribution tube.

The fourth test with helium was characterised by a rapid cooldown from the precooling temperature to a stage when the resistance had reduced 380 fold from the toom temperature resistance. This reduction in resistance indicated that approximately 53% of the field winding attained the super-conducting state. The rate of cooldown was 40% greater than that obtained during the first experiment even though the dewar pressure used to maintain

the transfer of helium was reduced by half. This clearly demonstrated the effectiveness of the coolant distribution tube.

At an average coil temperature of near 10K the reduction in temperature suddenly ceased without any apparent reason. With an increased rate of helium transfer further cooling was achieved. Temperature sensors situated at the base of and midway up the field coil registered 4.2K. A sensor situated at the top of the field winding registered a minimum temperature of 7.2K. These temperatures meant that the entire field winding should have become superconducting. The resistance of the field winding varied as a result of sections of the coils fluctuating between the normal and the superconducting states. Two hours after the initial cessation of the rapid cooldown the helium supply was exhausted.

Recordings of the rate of rise of the field winding temperature after the helium supply was exhausted indicated an average heat inleak of approximately 2.3 watts.

14-5 Possible Reasons for Not Achieving a Total Superconducting Field Winding

The sudden cessation in the reduction of the field winding temperature after an initial period of rapid cooldown suggests two possibilities:

1. the temperature had been reduced to the coolant temperature, which was greater than the transition temperature of the superconductor.
2. that a sudden increase in the heat inleak to the field coil chamber occurred.

The first possibility would have meant that the transfer tube was faulty. If this was the case then condensation formation on or frosting of the transfer tube would have been expected to occur, but this did not occur.

Estimates of the contributions to the total heat inleak from all sources were calculated so that possible sources of sudden increases in heat inleak could be identified.

The sources of heat inleak are:
1. radiation through the insulation,
2. gaseous conduction through the insulation,
3. conduction down the current leads,
4. conduction through the torque supports, and
5. conduction through the thrust supports.

14-5-1   Radiation

Radiation-heat transfer between two surfaces is given by the Stefan-Boltzmann equation.

$$Q = A_1 \, \sigma \, \epsilon \, (T_2^4 = T_1^4) \tag{14-1}$$

$$\epsilon = \epsilon_1 \, \epsilon_2 / (\epsilon_2 + \epsilon_1 \, (1 - \epsilon_2) \, A_1/A_2) \tag{14-2}$$

Q total radiant heat transfer   (watts)

A_1 inside (cold) surface area   (m^2)

A_2 outside (warm) surface area   (m^2)

σ Stefan-Boltzmann constant   ($5.7 * 10^{-8}$ watts-m^2-K^{-4})

ϵ_1 and ϵ_2 inside and outside surface emissivities

T_1 and T_2 inside and outside surface temperature   (K)

The insulation comprises layers of aluminium coated mylar with fibreglass spacing.   Thus the appropirate emissivities are those applicable to aluminium.   The calculation of radiant heat transfer through multilayer insulation is complicated by the temperature dependence of the emissivity; for example the total emissivity of aluminium at 300K is 0.03, at 77K is 0.018, and at 4K is 0.011.   An estimate of the heat transfer did not warrant an accurate calculation, consequently a conservative value of the

effective emissivity of 0.01 was used in equation 14-1.

The surface area of the helium chamber is $0.35m^2$ and there are 7 layers of insulation between room temperature and the radiation shield and 5 layers between the radiation shield and the helium chamber.

Thus the estimated radiant heat inleaks are:

1. radiation shield operating correctly

$$Q = 0.35 * 5.7 * 10^{-8} * 0.01 * (77^4 - 4.2^4)/6 \text{ watts}$$
$$= 0.0012 \text{ watts}$$

2. radiation shield operating incorrectly

$$Q = 0.35 * 5.7 * 10^{-8} * 0.01 * (300^4 - 4.2^4)/13 \text{ watts}$$
$$= 0.12 \text{ watts.}$$

14-5-2 Gaseous Conduction

Gaseous conduction heat transfer in vacuo between two surfaces is given by the Knudsen formula.

$$Q = 140 * A_1 \alpha * \frac{\gamma+1}{\gamma-1} * \frac{P}{\sqrt{M}} * (T_2 - T_1) \qquad (14-3)$$

$$\alpha = \alpha_1 \alpha_2 / (\alpha_2 + \alpha_1 (1 - \alpha_2) A_1/A_2) \qquad (14-4)$$

Q	total gaseous conduction heat transfer	(watts)
A_1	inside (cold) surface area	(m^2)
A_2	outside (warm) surface area	(m^2)
α_1 and α_2	inside and outside surface accommodation coefficients	
γ	specific heat ratio for the gas	(air 1.41)
M	molecular weight of the gas	(air 29)
P	gas pressure	(mm mercury)
T_1 and T_2	inside and outside surface temperature	(K)

The accommodation coefficient for air ranges from approximately 0.85 at

300K to 1 at 77K and below. The vacuum gauge indicated pressures of less than 10^{-5} mm of mercury. The location of the vacuum gauge sensor meant that the actual pressure within the insulation could be different from that indicated. Pressures of 10^{-5} and 10^{-4} mm of mercury were assumed as indicative and upper values.

The estimated gaseous conduction heat inleaks are:

1. radiation shield operating correctly

$$Q = 140 * 0.35 * 1 * \frac{2.41}{0.41} * \frac{77-4.2}{\sqrt{29}} * P/6 \quad \text{watts}$$
$$= 650 * P \quad \text{watts}$$

      indicative 0.0065 watts

      upper value 0.065   watts

2. radiation shield operating incorrectly

$$Q = 140 * 0.35 * 0.85 * \frac{2.41}{0.41} * \frac{300-4.2}{\sqrt{29}} * P/13 \quad \text{watts}$$
$$= 1000 * P \quad \text{watts}$$

      indicative 0.010   watts

      uper value 0.10   watts

14-5-3 Conduction Down the Current Leads

The lead heat inleak during cooldown was estimated using the results of Chapter 6 to be 0.45 watts. This assumes that the rate of helium loss corresponds to the lead heat inleak only and the lead copper is 99.95 per cent pure copper.

The following analysis indicated the influence of helium gas flows greater than that given by the lead only heat inleak. The differential equations describing the cooled leads are:

$$\frac{dQ(x)}{dx} = nC_p\frac{dT(x)}{dx} \tag{14-5}$$

$$Q(x) = -A \, K[T(x)] \, \frac{dT(x)}{dx} \qquad (14-6)$$

These equations lead to the following relationships:

$$\frac{Q(x)}{nC_p} - T(x) = \frac{Q_c}{nC_p} - T_c \qquad (14-7)$$

$$\int_{T_c}^{T_H} \frac{K[T]}{\dfrac{Q_c}{nC_p} - T_c + T} \, dT = \frac{nC_p \ell}{A} \qquad (14-8)$$

x	distance from warm end	(cm)
$T(x)$	temperature at x	(K)
T_H	warm end temperature	(K)
T_c	cold end temperature	(K)
$Q(x)$	lead heat conduction at x	(watts)
Q_c	lead heat inleak	(watts)
n	helium gas flow rate	$(gm\text{-}sec^{-1})$
C_p	helium gas specific heat	$(joule\text{-}gm^{-1}\text{-}K^{-1})$
ℓ	lead length	(cm)
A	lead cross sectional area	(cm^2)
$K[T]$	copper thermal conductivity	$(watts\text{-}cm^{-1}\text{-}K^{-1})$

As the helium gas flow rate is increased above that required to dissipate the lead heat inleak alone, inspection of equation 14-8 shows that two conditions can arise. The warm end temperature either remains unchanged or decreases.

Evaluation of the integral for various values of $\frac{Q_c}{nC_p} - T_c$ with the warm end temperature at 300K reveals that for increasing n, Q_c decreases. If the warm end temperature decreases, as is the case in reality, for the same n then to satisfy equation 14-8 the heat inleak has to be reduced below that

for a constant warm end temperature.

The conclusion to be drawn is that increasing the coolant flow decreases the lead heat inleak despite the average thermal conductivity of the lead increasing.

Another possibility is that the purity of the lead copper is greater than that assumed with a consequent increase in the thermal conductivity and heat inleak. For example, for 99.999 percent pure copper the lead alone heat inleak to a temperature of 4.2K was estimated to be 5.7 watts which corresponds to a helium loss of 7.9 litres of liquid per hour. The heat inleak through the leads to a temperature of 35K with a helium liquid flow of 3 litres per hour is very nearly zero. Thus there could have been a dramatic increase in the lead heat inleak as the temperature fell below 35K which could explain the initial rapid decrease in coil temperature and then the sudden cessation in the cooldown as experienced in the final experiment.

14-5-4   Conduction Through the Torque Supports

The heat conduction through the eight torque support wires was estimated to be 0.008 watts with the radiation shield operating correctly and 0.025 watts without the shield.

14-5-5   Conduction Through the Thrust Supports

The heat conduction through the four teflon thrust supports was estimated to be 0.054 watts with the radiation shield operating correctly and 0.3 watts without the shield.

14-5-6   Summary of Results

With leads of the assumed purity the estimated heat inleaks are:

HEAT INLEAKS
(watts)

	radiation shield operating correctly	radiation shield operating incorrectly
radiation	0.0012	0.12
gaseous conduction	0.065	0.10
leads	0.45	0.45
torque supports	0.008	0.025
thrust supports	0.054	0.3
TOTAL	0.5782	0.995

These heat inleaks correspond to liquid helium evaporation rates of 0.8 litres per hour and 1.3 litres per hour. With liquid helium transfer rates exceeding three litres per hour the above heat inleaks should have been readily dissipated.

14-6   Conclusion and Recommendation

Estimates of the total heat inleak during cooldown would indicate that without the almost total failure of the thermal insulation the most likely cause of the sudden increase in the heat inleak is a result of the possible use of high purity copper in the current leads.

It is suggested that the following procedure should now be adopted:

(a) A sample of the copper used in the leads should be tested for the degree of purity.   -

(b) The leads should be installed in one of the cryostats in which the superconducting state was successfully achieved and tested to determine whether or not they are the cause of the sudden increase in the heat inleak.

(c) With the leads removed from the cryostat of the model

machine cooldown tests to determine whether the super-
conducting state can be achieved would verify the cause
of the increased heat inleak.

These experiments would locate the source of the excessive heat inleak
if such does exist. They would also check the estimates of the heat inleaks
and show whether or not there is some other reason for the coils not
becoming superconducting.

The reasons why the tests suggested above were not carried out after
the earlier experiments did not behave as expected were:

(a) in each of the earlier experiments other factors which could
     have been the cause of the failures were found to be present
     and overshadowed any other possible causes of failure,

(b) it was felt that the experience gained with the earlier
     successful cryostats was properly translated into the
     design of the model machine cryostat,

(c) the cost of helium shipped from Sydney precluded piecemeal
     testing of the system at helium temperatures,

(d) the considerable time involved in dismantling and
     reconstructing the machine meant that this had to be
     kept to an absolute minimum.

Despite the fact that the superconducting state was not reached in
the model machine it is evident from the experiments carried out on the
model machine and those carried out on the earlier successful machines that
with further research on the lines suggested above,the machine, as it
stands with some minor modifications, could be built into a highly useful
machine.

Basic research could then be conducted at a relatively small cost,

on the model which would point the way for the development of very large
heteropolar direct current machines with superconducting field windings.
It is hoped that the Department of Electrical Engineering of the University
of Tasmania will be able to continue this research to the stage that the
superconducting operation is attained and other valuable research is
then carried out on the model machine.

REFERENCES

CHAPTER 1.

1-1   Onnes, H.K.   "Disappearance of the electrical resistance of
                    mercury at helium temperatures". Konik.Akad.
                    Wet. Amsterdam 14, (1911), 113-115.

1-2   Bardeen, J., Cooper, L.N. and Shriefer, J.R., "Theory of superconduct-
                    ivity".   Physics Review 108, 5(1957), 1175-1204.

1-3   Kunzler, J.E., Buchler, E. and Warwick, J.H.
                    "Superconductivity in Nb$_3$Sn of high current density
                    in a magnetic field of 88 gauss". Phys.Rev.Lett. 6,
                    (1961), 89-91.

1-4   Montgomery, D.B. "Superconducting magnets".
                    I.E.E.E.Spectrum 1, 2(1964), 103-113.

1-5   Atherton, D.L. "Superconducting D.C. generators and motors".
                    I.E.E.E.Spectrum 1, 2 (1964), 67-71.

1-6   Wipf, S.L.   "Superconducting D.C. generator". Cryogenic Eng.
                    Conf.Proc., (1963), 342-348.

1-7   Jones, J.D. and Matthews, P.W.   "Three phase superconducting
                    motor". Rev.Sci.Inst. 35, 5(1964), 630-633.

1-8   Garwin, R.L. and Matisoo, J. "Superconducting lines for the
                    transmission of large amounts of electrical power over
                    great distances".   I.E.E.E.Proc. 55, 4(1967),
                    538-548.

1-9   Redmond, J.H. and Boot, F.W. 'Cryogenically cooled motors".
                    Electro-Technology, July 1964, 83-89.

1-10   Stekley, Z.J.J. and Zar, J.L. "Stable superconducting coils".
                    I.E.E.E. Trans. on Nuclear Sc. NS12, 3(1965),
                    367-372.

1-11   Lynton, E.A. "Superconductivity". London, Methuen;
                    New York, Wiley, 1964.

1-12   Taylor, A.W.B. "Superconductivity". London, Wykenham, 1970.

1-13   Sychev, V.V.   "Superconducting magnet system, field windings,
                    and inductors". Arlington, Virginia Joint
                    Publications Research Service, 1972.

1-14   Gregory, W.D., Mathews, W.N. and Edelsack, E.A.
                    "The science and technology of superconductivity".
                    New York, Plenum Press, 1973.

1-15   Timmerhaus, K.D. "Advances in cryogenic engineering".
                    Cryogenic Eng.Conf., New York, Plenum Press, 1960.

1-16 Arp, V.D., Ciark, A.F. and Flynn, T.M. "Some applications of cryogenics to high speed ground transport". U.S. Dept. of Commerce, Nat.Bur.Standards, 1973.

1-17 Haselden, G.G. "Cyrogenic fundamentals". London, New York, Academic Press, 1971.

1-18 Croft, A.J. "Cryogenic laboratory equipment". New York, Plenum Press, 1970.

1-19 Savitskii, E.M. "Superconducting materials". New York, Plenum Press, 1973.

1-20 Williams, J.E.C. "Superconductivity and its applications". Pion applied physics series, no.4.

1-21 Barron, R.F. "Cyrogenic systems". New York, McGraw-Hill, 1966.

1-22 Bell, J.H. "Cryogenic engineering". Englewood Cliffs, N.J., Prentice-Hall, 1963.

1-23 Scott, R.B. "Cryogenic engineering", Princeton, N.J. Van Norstrand, 1959.

1-24 Vance, R.W. "Cryogenic technology". New York, Wiley, 1963.

1-25 Bremer, J.W. "Superconductive devices". New York, McGraw-Hill, 1962.

1-26 Firth, I. "Superconductivity". London, Mills and Boon, 1972.

1-27 Fishlock, D. "A guide to superconductivity". London, Macdonald; New York, American Elsevier, 1969.

1-28 Kuper, C.G. "An introduction to superconductivity". Oxford, Clarendon Press, 1968.

1-29 McFee, R. "Applications of superconductivity to the generation and distribution of electric power". Elec.Eng. 81, (1962), 122-129.

1-30 Lorch, H.H. "The feasibility of superconducting power transformers". Cyrogenics 9, (1969), 354-361.

1-31 Hadlow, M.E.G., Baylis, J.A. and Lindley, B.C. "Superconductivity and its application to power engineering". Proc.I.E.E., I.E.E. Reviews 119, 8R(1972), 1003-1032.

1-32 Appleton, A.D. "Motors, generators and flux pumps". Cyrogenics 9, 3(1969), 147-157.

1-33 Woodson, H.H., Smith, J.L., Thullen, P. and Kirtley, J.L. "The application of superconductors in the field windings of large synchronous machines". I.E.E.E.Trans., P.A.S.90, 2(1971), 620-627.

1-34 Doyle, T.J. "Superconductive propulsion motor". Mechanical Engineer, January 1977, 48-53.

1-35 Fukasawa, M. "Development of cryogenic cable". Hitachi Review
          22, 10, 430-434.

1-36 Mole, C.J., Haller, H.E. and Litz, D.C. "Superconductor
          synchronous generators". 1972 Applied super-
          conductivity conference.

1-37 Komarek, P. "Superconducting magnets in the world of energy -
          especially fusion power". Cryogenics 16, 3(1976),
          131-141.

1-38 Meyerhoff, R.W. "Superconducting power transmission".
          Cyrogenics 11, (1971), 91-101.

1-39 Powell, J.R. and Danby. "Magnetic suspension for levitated
          tracked vehicles". Cryogenics 11, (1971),
          192-204.

1-40 Foner, S. and Schwartz, B.B. "Superconducting machines and
          devices, Large Systems Applications".
          NATO Advanced Study Institute, Entreves, Italy, 1973.
          NATO Advanced Study Institutes Series: Series B,
          Physics; VI.
          New York, Plenum Press, 1974.

1-41 Mulhall, B.E. "Superconducting electrical machines".
          Rev.of Phys. in Technology 3, 2(1972), 108-129.

1-42 Rogers, E.C., Cave E.C. and Grisby, R.
          "A superconducting link for laboratory tests on
          conductors for superconducting cables".
          Proc.Int.Inst. of Refrigeration conference on
          low temperatures and electric power, London, 1969,
          127-133.

1-43 Northeastern University U.S.A. Dept. Elec.Eng.
          "Superconducting transformer for power system
          applications". Proposal to E.R.D.A.

1-44 Maladain, A. "Superconductivity-present situation and outlook".
          Brown Boveri Review, 1(1971), 34-40.

1-45 Ogasawara, T. "Effective resistance of current carrying super-
          conducting wire in oscillating magnetic fields -
          Parts 1 and 2".
          Cyrogenics 16, 1(1976), 33-35 and 16, 2(1976), 89-96.

1-46. Bogner, G. and Kullman, D. "Electrical machines with superconduct-
          ing field windings - Parts 1, 2, 3".
          Siemens Forsch 4, 5(1975), 305-309,
          4, 6(1975), 368-372, 5, 1(1977), 10-16.

1-47 Appleton, A.D. "Development of superconducting D.C. machines at
          I.R.D. Co. Ltd.". Proc.I.E.E. 61, 1(1973), 106-111.

1-48 Goldsmid, H.J. "Superconducting magnets". G.E.C. Journal 3,
          3(1963), 114-121.

1-49 Kazovskiy, Kartsev and Shaktarin,   "Superconducting magnet
            systems". Science Publishing Co., Lengingrad,
            1967, 186-190.

1-50 Zizek, F. and Kurka, J.   "Research on application of superconduct-
            ivity in the Skoda Concern". Skoda Review No.2,
            1979, 25-31.

1-51 Beresford, J.E. and Green, M.J.I.   "D.C. heteropolar machine with
            superconducting field windings". Cryogenics 15,
            4(1975), 228.

1-52 Beresford, J.E. and Green, M.J.I.   "Letter to the editor",
            Cryogenics 17, 5(1977), 308.

1-53 Kropschot, R.H. "Cryogenic insulation". Ame.Soc.Heat Refrig.
            and Air Cond.Eng.Journal 3, 9(1959), 48-54.

1-54 Glaser, P.E. "Cryogenic insulations", Machine Design, August 17,
            1967, 146-152.

1-55 Scurlock, R.G. and Sauli, B.   "Development of multilayer
            insulations with thermal conductivities below $0.1\mu W$-
            cm^{-1}-K^{-1}".   Cryogenics 16, 5(1976), 303-311.

1-56 N.A.S.A. report SP-5027.   "Thermal insulation systems".

CHAPTER 5.

5-1   Scurlock, R.G. and Sauli, B.   "Development of multilayer
            insulations with thermal conductivities below $0.1\mu W$
            $-cm^{-1}$-K^{-1}".   Cyrogenics 16, 5(1976), 303-311.

5-2   Durham, T.F., McClintock, R.M. and Reed, R.P.
            "Cyrogenic materials data handbook".
            Cyrogenic Engineering Laboratory, Boulder, Colorado.
            Air Force Ballistic Missile Division, Contract AFO4(647)
            -59-3.
            U.S. Department of Commerce, National Bureau of
            Standards, 1962.

5-3   Hultgren, R., Orr, R.L. Anderson, P.D., Kelley, K.K.
            "Selected values of thermodynamic properties of
            metals and alloys". New York, Wiley, 1963.

5-4   Perry, J.H.   "Chemical engineers handbook 4th ed.".
            McGraw-Hill, Chemical Eng.Series, 1974.

CHAPTER 6.

6-1   Scott, J.P.   "Current leads for use in liquid-helium cryostats".
            Third international cyrogenic engineering conference
            proceedings, Berlin, 1970, 176-196.

6-2   Rauh, M.   "Optimum dimensions of current-carrying leads to
                      cryogenic apparatus".   Ibid.,182-186.

6-3   Gusewell, D. and Haebel, E.U.   "Current leads for refrigerator-
                      cooled large superconducting magnets".   Ibid.,
                      187-191.

6-4   Hohler, J.W.L., Prast, G. and DeJonge, A.K.   "Calculation of
                      losses induced by current-carrying leads in cryogenic
                      installations".   Ibid., 192-196.

6-5   Berard, P.   "Connexions electriques cryogeniques, aspects
                      theoriques".   Proc. XIIth Int.Congr.Ref., Madrid,
                      1967, 157-171.

6-6   Deiness, S.   "The production and optimization of high current
                      leads".   Cryogenics 5, (1965), 269-271.

6-7   Williams, J.E.C.   "Counterflow current leads for cryogenic
                      applications".   Cryogenics 3, 4(1963), 234-238.

6-8   Lange, F.   "The theoretical minimum for the heat influx in
                      cyrostats caused by current leads".
                      Cryogenics 10, 10(1970), 398-401.

6-9   Carbonell, E., Renard, M. and Bernard, P.
                      "Thermodynamic optimum for electrical connections
                      at cryogenic temperatures".   Cryogenics 8, 10(1968),
                      314-316.

6-10 Tsao, C.K.   "Power loss and temperature distribution of a gas
                      cooled cryogenic current lead".
                      Cyrogenics 14, 11(1974).

CHAPTER   13.

13-1 Clayton, A.E. and Hancock, N.N.   "The performance and design of
                      D.C. machines".   Engineering Degree Series,
                      Third Revised Edition, Pitman, 1959.

13-2 Hindmarsh, J.   "Fundamental ideas on large D.C. machines".
                      Electrical Times, 7 August, 1958, 187-192.

13-3 Hindmarsh, J.   "Volts per bar limit on large D.C. machines".
                      Electrical Times, 25 September, 1958, 461-463.

13-4 Fink, D.J. and Carroll, J.M.   "Standard handbook for electrical
                      engineers - 10th edition".
                      International Student Edition. McGraw-Hill, 1968.

13-5 Pratt, J.W.   "Operating limits of D.C. machines".   Electronics
                      and Power, 6 September 1973, 366-368.

13-6 Skenfield, B.   "Large D.C. machines".   Commutation in rotating
                      machinery - chapter 8. Conference on commutation
                      in rotating machinery, London, 1964.

13-7 Bruderlink, R. and Sauer, H.G. "Stromwender für hohe stegspannungen".
E.T.Z., Edn. B5, 10(1953), 327-330.

13-8 Appleton, A.D. "Motors, generators and flux pumps".
Cryogenics 9, 6(1969), 147-157.

13-9 Foner, S. and Schwartz, B.B. "Superconducting machines and devices,
Large Systems Applications".
NATO Advanced Study Institute, Entreves, Italy, 1973.
NATO Advanced Study Institutes Series: Series B,
Physics; VI.
New York, Plenum Press, 1974.

13-10 Kendall, P.W "Liquid metal brushes for homopolar generators".
Electrical Review, 19 January, 1973, 96-99.

13-11 McNab, I.R. and Wilkin, G.A. "Carbon-fibre brushes for superconduct-
ing machines". Electronics and Power, January,
1972, 8-10.

13-12 Timoshenko and Goodier. "Theory of elasticity". Third Revised
Edition, McGraw-Hill, 1970.

13-13 Grover, F.W. "Inductance calculations, working formulas and
tables". D. Van Norstrand Co., 1946.

13-14 Taylor, P.L. "Improving commutation in D.C.machines by the
use of flux traps". Proc.I.E.E. 117, 7(1970),
1269-1276.

13-15 Hodge, W. and Nippert, P.W. "Zirconium copper raises level of
commutator performance". Electro Technology
Newsletter 57, (1956), 95-97.

13-16 Lynn, C. and Elsey, H.M. "Effects of commutator surface film
conditions on commutation". A.I.E.E.Trans. 68,
(1949), 106-112.

13-17 Van Brunt, C. and Savage, R.H. "Carbon-brush contact films".
General Electric Review, July, 1944, 16-19.

13-18 Baker, R.M. "Commutation and current collection in hydrogen".
Winter convention A.I.E.E., N.Y., January, 1931,
714-717.

13-19 Savage, R.H. "Carbon-brush contact films". General Electric
Review, October, 1945, 13-20.

13-20 Marsden, J. and Savage, R.H. "Effects of silicone vapour on
brush wear". A.I.E.E. Transactions 67, (1949).

13-21 Elsey, H.M., Moberly, L.E. and Johnson, J.L. "Air humidity and
brush contact drop: The effect of water vapour,
sulphur dioxide and hydrogen sulphide".
A.I.E.E. general meeting, October, 1954, 1383-1389.

13-22 Dobson, J.V. "The effect of humidity on brush operation".
Electric Journal 32, 12(1935), 527-528.

13-23 Kalb, W.C.   "For good brush performance commutator surface
                     must be right". Power, November, 1944, 107-113.

13-24 Kalb, W.C.   "For good brush performance machine conditions
                     must be right". Power, December, 1944, 103-105.

13-25 Mayeur, M.R.   "Commutation par balais a deux tranches dans
                     les machines a courant continu".
                     Revue Generale de L'Electricite, September, 1950,
                     400-405.

13-26 Ludwig, L.R. and Baker, R.M. "Influence on commutation of
                     brush contact drop". A.I.E.E. Trans., December,
                     1932, 959-965.

13-27 Bates, J.J. and Powell, R. "Relative current-switching properties
                     carbon-fibre brushes and solid brushes and the
                     implications for commutator machines".
                     I.E.E. Proc. 118, 3/4(1971), 604-608.

13-28 Andrews, H.I. "Development of an electrically commutated motor
                     with laminated brushes". I.E.E. Proc. 116,5(1969),
                     763-768.

13-29 Bates, J.J., Stanway, J. and Sansum, R.F.
                     "Contact problems in machines using thyristor-
                     assisted commutation". I.E.E.Proc. 117, 2(1970),
                     387-397.

13-30 Bates, J.J.   "Using thyristors and diodes to improve commutation".
                     I.E.E.E. Spectrum, January, 1971, 38-47.

13-31 "New brush sweeps clean".   Electronics and Power, April/May,
                     1971, 175.

13-32 Robinson, A. "New brush sweeps clean". Electronics and Power,
                     July, 1971, 278.

13-33 Bates, J.J. and Stanway, J.   "Development of a 300kW, 3000rpm,
                     D.C. machine using thyristor-assisted commutation".
                     I.E.E. Proc. 123, 1(1976), 76-80.

13-34 Bates, J.J. and Stanway, J.   "Terminal characteristics of
                     machines with thryistor-assisted commutation".
                     I.E.E. Proc. 123, 1(1976), 85-88.

13-35 Inagaki, J., Kuniyoshi, M. and Tadakuma, S.   "Commutators get
                     the brush off". I.E.E.E Spectrum, June, 1973, 52-58.

13-36 Davis, R.M. and Jones, D.A.   "Conventional or electronic
                     commutation?" Commutation in rotating machines.
                     I.E.E. Conf.Publ.,no.11, 93-97.

13-37 Doyle, T.J.   "Superconductive propulsion motors".
                     Mechanical Engineer, January, 1977, 48-53.

INVESTIGATIONS INTO THE ABILITY TO CARRY OUT CRYOGENIC RESEARCH

A. Much of the initial investigation into the practical and financial
aspects of the porposed project were conducted during the final year of
the author's B.E. course by the author.

The problems investigated were as follows:

(a) The availability of cryogenic coolants, that is of
liquid helium and liquid nitrogen.

(b) The cost and availability of superconductor wire.

(c) The quantities of cryogenic coolant required to produce
the required conditions for acceptable lengths of time.

(d) The cost of peripheral equipment such as helium and
nitrogen containers, vacuum pumps and monitoring
equipment.

(e) The availability of the materials required in constructing
low temperature equipment.

A-1 Availability of Liquid Nitrogen and Helium

Liquid nitrogen was readily obtainable from the Chemistry Department
of the University of Tasmania at no cost to the Electrical Engineering
Department and without delay; hence at the investigation stage it was
envisaged that much of the work would make use of liquid nitrogen.

The availability of liquid helium was another problem as there were
no helium liquefaction plants in Tasmania. The only possible sources
of liquid helium were interstate which meant air freight across land
and sea would be necessary. The possible sources were either mainland
universities or the Commonwealth Industrial Gases Ltd. The universities

as a source of helium were eliminated because of the associated admin-istration difficulties and hence C.I.G. was the only supplier.

The possibility of purchasing a helium liquefaction unit was considered but the cost of such equipment was far in excess of the budget. The costing of the liquid helium was as follows:

$9-00 per litre for the first 25 litres taken in one month

$5-00 per litre for the balance taken out in the same month

These prices indicated that the helium cost would be substantial but within the budget. Freight charges doubled the landed cost of the liquid helium.

A-2 Availability of Superconductor

Superconducting wire is produced commercially in overseas countries and it is available in Australia with a delivery time of approximately one month.

At the present time superconducting wire is expensive because it is not manufactured on a very large scale. Data obtained from Imperial Metals Industry Australia Limited indicated that a suitable niobium-titanium wire would cost in the vicinity of $1,500 per kilometre. This price limited the use of superconducting wire to about 1000 metres a year; hence the importance of using 100 metres per coil initially and one reason for the change from the investigation of homopolar to the heteropolar machine.

Alternative superconductor suppliers are General Electric Company of the U.S.A. for niobium-tin tape or the Carborundum Company of the U.S.A. for niobium-carbonitride yarn. The costing of the previously mentioned items indicated that it was possible, from financial considerations, to conduct a cryogenic research project. The readily available liquid nitrogen meant that expertise in construction of

suitable containers could be achieved and heat inleak testing be conducted without purchasing helium.

A-3 Quantities of Helium Required

The quantity of helium required for each test was estimated from the following considerations:

(a) The latent heat of vaporization of helium.

(b) Equipment pre-cooled to 77K using liquid nitrogen.

(c) The length of superconductor to be cooled - approximately 200 metres.

(d) The amount of stainless steel to be cooled - approximately 5 kg. from envisaged sizes of the field coils wound from 100 metres of wire and the cryostat chambers required to house them.

(e) The total heat inleak to the cryostats - 1.5 watts.

From considerations in Appendix B on cryostat cooldown, helium requirements are 2.38 litres to cool 200 metres of wire and 6.36 litres to cool 5 kg. of stainless steel. An approximate total of ten litres of liquid helium are required to cool down the above quantities of materials.

With a heat inleak of 1.5 watts liquid helium is lost at the rate of 1.4 litres per hour. To give a period of not less than five hours operation required a minimum of 17 litres of liquid helium. This amount showed that the cost of the helium would be acceptable.

A-4 Peripheral Equipment

Basic peripheral equipment necessary for research on superconductivity and their 1975 prices are listed below.

Temperature monitoring equipment	2.2K - 4.2K	
	4.2K - 77K - 300K	$60
carbon resistance type	4.2K - 300K	
	77K - 300K	60
2.4 litre liquid nitrogen vessel		90
25 litre liquid nitrogen dewar and stand		300
30 litre liquid helium dewar		1,370
liquid helium transfer tube		200
liquid nitrogen level gauge		77
vacuum pump system capable of better than 10^{-7} torr		1,250
Penning type vacuum gauges 10^{-2} to 10^{-7} torr		400
Argon arc welder (debited to workshop costs)		933
safety equipment		50
	Total	$4,790
	Total excluding welder	$3,757

The items listed above were basic essentials for a small cryogenic laboratory to operate successfully. A further costly item that could have been purchased was an adequate leak detector; for example, a helium mass spectrometer detector. Fortunately the methods adopted for vacuum sealing and continuous pumping negated the need for such an item.

A-5 Availability of Materials

The materials required ranged from stainless steel tubing to vacuum greases to indium wire. There are a number of sources of stainless steel tubing overseas, for example Tubesales in the U.S.A. and Oxford Instruments in the U.K., that have delivery times in excess of six weeks. Australian suppliers have a very limited range of stainless steel tubing, hence most purchases were made from overseas firms.

Vacuum greases and special solders were obtained from Oxford Instruments. Edwards vacuum components were obtained through a local agent, Selby's Scientific.

A-6 <u>Running Costs</u>

It was envisaged that helium and superconductor requirements for the initial years of the laboratory would be about 60 litres of helium and 500 metres of superconductor per annum with an associated cost of near $1750 which was within the budget allowed.

A-7 <u>Conclusion</u>

The estimates of the annual running costs and of the capital outlay required for the purchase of essential equipment necessary for research into cryogenic engineering indicated that the costs were within the resources of the Electrical Engineering Department of the University of Tasmania.

APPENDIX B

CRYOSTAT COOLDOWN

B. Helium Consumption

The availability of liquid nitrogen meant that cryostats could be pre-cooled to 77K before introducing the liquid helium to cool to 4.2K. The pre-cooling with liquid nitrogen was essential as it meant a 94 percent reduction in the cooldown loss of liquid helium.

To calculate the quantity of liquid helium required to reduce the temperature of the cryostat and superconductor to 4.2K required the heat capacity, or the enthalpy difference, of the materials between 77K and 4.2K. These values were obtained by integration of specific heats over the range 4.2K to 77K. The results are summarized below:

| Material | Enthalpy difference between | |
	4.2K and 77K (Joule/gm)	77K and 290K (Joule/gm)
Magnesium	4.94	81.4
Chromium	2.41	76.0
Iron	3.32	77.5
Copper	5.27	74.9
Titanium	5.47	95.9
Niobium	4.64	52.7
Superconductor Niomax FM	4.92	75.9

Superconducting wire: 14.9% by weight niobium,

18.6% by weight titanium,

66.8% by weight copper, and its weight

per unit length is 6.3kg/km.

If only the latent heat of vaporization of the liquid helium (C_L = 20.9J/gm = 2.61J/cc at one atmosphere pressure) is used for cooling then the quantity of liquid helium used during the cooldown of the initial machine cryostats would be:

(a) Stainless steel - heat removed on cooling from 77K to 4.2K

For five kilograms of stainless steel (assuming that it is all iron) the heat removed during cooldown from 77K to 4.2K is given by 3.32 * 5000 Joules = 16.6kJ.

(b) Superconductor - heat removed on cooling from 77K to 4.2K

For 200 metres of superconductor the heat removed during cooldown from 77K to 4.2K is given by 4.92 * 6300 * 0.2 Joules = 6.2kJ.

(c) Helium used

To cool five kilograms of stainless steel = $\frac{16.6}{2.61}$ litres

= 6.36 litres

To cool 200 metres of superconductor = $\frac{6.2}{2.61}$ litres

= 2.38 litres

In actual fact the amount of liquid helium used for cooldown should be less than the above values because of the additional heat removed by increases in the temperature of the boil-off gases.

APPENDIX C

EFFECTS OF CRYOGENIC TEMPERATURES UPON SELECTED MATERIALS

C. Initial work investigating the effects of liquid nitrogen on selected

materials and gaining experience into handling techniques of liquid nitrogen

proved to be important as it revealed, quite dramatically in cases, which

materials could and could not be used or combined in cold sections of

cryostats.

Many materials, with the exception of household string, became solid

and brittle at cryogenic temperatures, in particular greases and rubber

which vitiates their use except in certain circumstances. For example,

surgical rubber was found adequate to transfer liquid nitrogen from a dewar

to a cryostat even though it became solid.

Many forms of demountable seals were tested and found to be deficient

mainly because of differing thermal contraction rates which caused

fracturing of materials or separation of joined components.

Rubber "O" rings proved to be useless as a method of vacuum sealing at

reduced temperature, even exposure to the boil off gases during initial

cooldown of apparatus caused their failure.

For demountable seals at cryogenic temperatures teflon ribbon between

bolted plates proved to give a seal but this method was not adopted as

indium, which retains its malleability at cryogenic temperatures, was found

to give better results and it could be reused many times.

Instead of listing the materials tested at liquid nitrogen temperatures

and the results it would suffice to say that most plastic type materials

became brittle and hence are not suitable for work at cryogenic temperatures.

Components of equipment which are exposed to reduced temperatures should be

made from the one material except where thermal contraction can be matched or where movement between sections can be tolerated or allowed for.

MODEL FIELD FLUX DISTRIBUTIONS AND CALCULATIONS

D. The voltage ratings for the initial test machine configurations were estimated from the field pole fluxes calculated from the field flux density distributions of the model. To obtain the required field flux, as given by equation D-1, the surface of the armature was divided into bands similar to those given in figures D-1 and D-2. The flux density curves were integrated over these bands using approximations similar to equation D-2.

$$\Phi_p = \oint \underline{B} \cdot dA$$

$$= \int_0^h \int_0^{2\pi} Br(\theta, x) \, r \, d\theta \, dx \qquad \ldots \text{D-1}$$

Where $Br(\theta, x)$ equals the radial component of the field flux density as a function of height and angular position in the region of a field pole.

$$\Phi_p = \frac{rh}{4} \left[\int_0^{2\pi} B_0 \, d\theta + 2\int_0^{2\pi} B_1 \, d\theta + \int_0^{2\pi} B_2 \, d\theta \right] \qquad \ldots \text{D-2}$$

Approximation D-2 applies for figure D-1 with only one field coil energised; B_0, B_1, and B_2 are the average radial field flux densities in the bands 0, 1, and 2 respectively. Care was required with the signs of B_0, B_1, and B_2 as the integrations passed from a north pole region to a south pole region.

D-1 Iron Core and Yoke

The following results were obtained from the curves of figure 4-21. The bands used were as given in figure D-1.

scaling factor $1cm^2 \equiv 3.67 * 0.3142$ gauss-rad $= 1.153$ gauss-rad

armature radium $= 3cm$ armature height $= 6cm$

ARMATURE SURFACE
SEGMENTATIONS

FIG D-1

$h_{1/8}$
$h_{1/4}$
$h_{1/4}$
$h_{1/4}$
$h_{1/8}$

"0"
"1"
"2"

x

r

FIG D-2

2 $h_{1/5}$
1 $h_{1/5}$
0 $h_{1/5}$
1 $h_{1/5}$
2 $h_{1/5}$
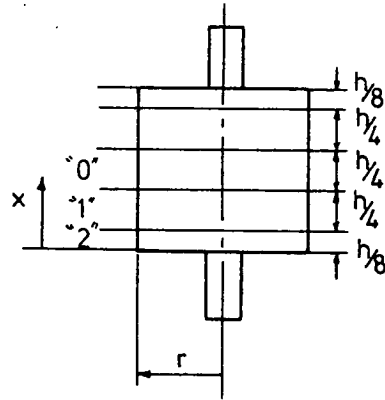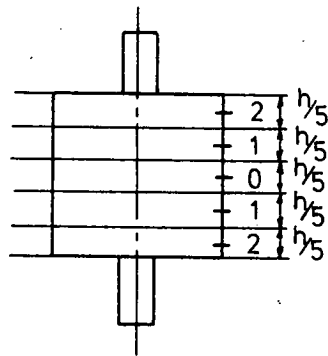
Position	Area under Curve cm^2	$\int Bd\theta$ gauss	Current ampere
0	26.6	30.7	2
1	19.4	22.3	2
2	11.5	13.3	2

B_{max} = 15 gauss with 1 ampere field current

$$\Phi_p = \frac{0.03 * 0.06}{4} (13.3 + 44.6 + 30.7) * 10^{-4} \text{ weber}$$

= 3.99 μweber at 2 amperes current

= 2 weber at 1 ampere current

Thus the average field flux density was 3.54 gauss with a field excitation current of 1 ampere.

D-2 Iron Yoke, Core and Pole Faces

The following results were obtained from the curves of figure 4-22. The bands used were as given in figure D-2.

scaling factor 1cm^2 = 0.927 gauss-radian

armature radius = 3cm   armature height = 6cm

Position	Area under Curve cm^2	$\int Bd\theta$ gauss	Current ampere
0	45.2	41.9	2.5
1	45.2	41.9	2.5
2	36.5	33.8	2.5

B_{max} = 9.8 gauss with 1 ampere field current

$$\Phi_p = \frac{0.03 * 0.06}{5} (2 \times 41.9 + 2 \times 33.8 + 41.9) * 10^{-4} \text{ weber}$$

= 6.96 μweber with 2.5 amperes field current

= 2.78 μweber with 1 ampere field current

Thus the average field flux density was 4.84 gauss with a field excitation current of one ampere.

D-3 Iron Yoke Only

The following results were obtained from the curves of figure 4-23. The bands used were as given in figure D-1.

scaling factor $1cm^2 \equiv 0.902$ gauss-radian

armature radius = 3cm   armature height = 6cm

Position	Area under Curve cm^2	$\int Bd\theta$ gauss	Current ampere
0	19	17.1	2
1	15.8	14.3	2
2	8.9	8.03	2

B_{max} = 9.14 gauss with 1 ampere field current

$$\Phi_p = \frac{0.03 * 0.06}{5} (2 \times 14.3 + 2 \times 8.03 + 17.1) * 10^{-4} \text{ weber}$$

= 2.22 μweber with 2 amperes field current

= 1.11 μweber with 1 ampere field current

Thus the average field flux density was 1.96 gauss with one ampere field excitation current.

D-4 Iron Pole Faces and Yoke

The following results were obtained from the curves of figure 4-24. The bands used were as given in figure D-1.

scaling factor $1 cm^2 \equiv 0.9$ gauss-radian

armature radium = 3cm   armature height = 6cm

Position	Area under Curve cm^2	$\int Bd\theta$ gauss	Current ampere
0	23.7	21.3	3
1	22.9	20.6	3
2	24.2	21.8	3

B_{max} = 4.35 gauss with 1 ampere field current

$$\phi_p = \frac{0.03 * 0.06}{5} (2 \times 21.8 + 2 \times 20.6 + 21.3) * 10^{-4} \text{ weber}$$

= 3.82 μweber with 3 amperes field current

= 1.27 μweber with 1 ampere field current

Thus the average field flux density was 2.25 gauss with one ampere field excitation current.

RESULTS AND DATA FOR THE DESIGN OF A SET OF COUNTERFLOW
CRYOGENIC CURRENT LEADS

E. The following tables are the results obtained from the expressions developed for the analysis of the counter flow cryogenic current leads which carried the excitation current to the superconducting field coil - Chapter 6.

Also included are the electrical resistivity and thermal conductivity data for 99.95 per cent pure copper and the equations which were fitted to this data.

The results of table E-7 indicate the differences between the design and performance of the leads when the Wiedemann-Franz Law was used in conjunction with the constant specific heat of helium gas approximation and when an iterative technique involving the tabulated data directly was used.

The expressions used to describe these properties in the iteration solution were:

<u>Thermal conductivity (K watt-cm^{-1}-kelvin^{-1})</u>

T $\leqslant$ 20 kelvin $\qquad$ K = 0.459T

20 kelvin <T$\leqslant$ 40 kelvin $\qquad$ K = A T^5 + B T^4 + C T^3 + D T^2 + E T + F

T > 40 kelvin $\qquad$ K = K$_0$ + EXP(M-T/N)

where

A = -1.6786162 * 10^{-5}

B = 2.5000836 * 10^{-3}

C = -1.4532134 * 10^{-1}

D = 4.0968286

E = -55.60221

F = 298.76725

A fifth degree polynomial was chosen for this region so that the value of thermal conductivity and the temperature derivatives were satisfied at the boundaries; that is, T = 20K and 40K and where $\frac{dK}{dT}$ = 0. The coefficients had to be calculated to the number of significant figures given to eliminate large calculation errors due to the fact that the result obtained was significantly smaller than each term involved

for T > 40 kelvin   K = 3.95 + EXP(3.364 - T/26.25)

Electrical resistivity ratio $\rho_T|\rho_{300}$ = R

The expressions used for the electrical resistivity ratio were:

T < 40 kelvin $R = 3.025 * 10^{-4} * T + 0.0031$

40 kelvin < T < 70 kelvin $R = 2.93 * 10^{-3} * T - 0.102$

T > 70 kelvin $R = 3.9 * 10^{-3} * T - 0.17$

$\rho_{300} = 1.72 * 10^{-6} \Omega\text{-cm.}$

TABLE E-1

COUNTER FLOW CRYOGENIC LEAD Z TEMPERATURE PROFILES

D	0	0.25	0.31	0.315	0.32	0.34
Z			TEMPERATURE (K)			
0	4.2	4.2	4.2	4.2	4.2	4.2
1	11	10	9.65	9	9	9
2	19	21	19.5	19	18.5	19
3	78	43	36	35.5	35	32
4	213	84	62.4	61	59	52.5
5	579	160	101	97	93	77
6	1570	300	155	145	135	98
7		556	221	198	178	101
8		1015	284	230	198	52
9			309	225	148	
10			216	675		

TABLE E-2

THERMAL CONDUCTIVITY AND ELECTRICAL RESISTIVITY OF COPPER
99.95% PURE

TEMPERATURE	THERMAL CONDUCTIVITY	$\rho_T | \rho_{300}$	$\rho_{300} = 1.7\mu\Omega$-cm
kelvin	watt-cm^{-1}-kelvin^{-1}	N.D.	$T = 300$ $\int kdT = 1490$w/cm $T = 4.2$
0	0		
5	2.25	0.0034	
10	4.57	0.0038	
15	6.88	0.0046	
20	9.18	0.0060	
25	11.3	0.0068	
27.5	11.5	0.00772	
30	11.45	0.0085	
35	11.05	0.0113	
40	10.25	0.0156	
50	8.3	0.0369	
70	5.92	0.1	
100	4.55	0.216	
150	4.07	0.419	
200	3.97	0.615	
250	3.87	0.704	
300	3.8	1.0	

TABLE E-3

TEMPERATURE PROFILE FOR OPTIMIZED LEADS WITH $Q_A = 0$

$$x = \frac{2A}{nc_p} \int K dZ$$

Z	T	K	$\int K dZ$	x
N.D.	kelvin	w-cm^{-1}-kelvin^{-1}	w-cm^{-1}-kelvin^{-1}	cm
0	4.2	1.9	0	0
1	9.65	4.4	2.96	3.85
2	19.5	8.9	9.32	12
2.5	28	11.5	14	18.1
3	36	11.2	20	26
4	62.4	6.6	28.7	37
5	101	4.5	33.9	44
6	155	4.1	38.2	50
7	220	3.95	42.2	55
8	284	3.8	46.1	60
9	309	3.75	49.9	65

TABLE E-4

EFFECTS OF AMBIENT HEAT INLEAK

Z TEMPERATURE PROFILES

Z	D=0.31 N=0	0.31 0.2	0.2 0	0.2 0.5
	TEMPERATURE (Kelvin)			
0	4.2	4.2	4.2	4.2
0.5	6.50	6.00	6.58	5.33
1	9.65	8.38	10.0	6.84
1.5	13.8	11.4	15.2	8.91
2	19.4	15.4	22.6	11.7
2.5	26.7	20.3	33.5	15.6
3	36.0	26.4	49.2	21.0
3.5	47.7	33.9	72.0	28.6
4	62.3	42.8	104.8	39.2
4.5	80.2	53.2	152.2	54.2
5	101.5	65.0	220.5	75.4
5.5	126.6	78.0	318.9	105.5
6	155.3	91.7	460.4	148.3
6.5	187.1	105.0	664.1	209.3
7	220.1	116.5	956.9	296.4
7.5	254.4	123.8	1377.9	470.7
8	284.3	123.4	1983.0	598.6
8.5	305.2	110.5		
9	309.1	78.1		
9.5	284.7	17.0		
10	216.0	-85.5		

TABLE E-5

OPTIMUM "D" FOR GIVEN "N"

CYROGENIC CURRENT LEADS

		Modified Heat Inleaks		
		Total	Lead	Ambient
N	D	$\dfrac{C_p\,Q_T}{2I\,LC}\,K^2$	$\dfrac{C_p\,Q_L}{2I\,LC_L}\,K^2$	$\dfrac{C_p\,Q_A}{2I\,LC_L}\,K^2$
N.D	N.D			
0	0.31	1.8	1.8	0
0.25	0.29	1.85	1.39	0.46
0.42	0.27	1.92	1.11	0.81
0.48	0.26	1.96	1.02	0.94
0.51	0.25	2	0.98	1.02

TABLE E-6

OPTIMUM LEAD WITH AMBIENT HEAT INLEAK OF 0.2 WATT

$N = 0.27$ $D = 0.2877$

Z	T	K	$\int KdZ$
N.D.	Kelvin	watt-cm^{-1}-Kelvin	watt-cm^{-1}-Kelvin
0	4.2	1.9	0
1	8	3.2	2.4
2	14.5	6.65	7
3	25.2	11.3	16.1
4	42	10.25	27.2
5	67.6	6.1	35
6	104	4.45	40
7	154	4.05	44.3
8	213	3.95	48.5
9	274	3.8	52.2
10	305	3.8	56

TABLE E-7

HEAT INLEAKS WITH 300 AMPERE OPTIMISED
LEADS CARRYING DIFFERENT CURRENTS

Process:

    (a) choose a value of "D"

    (b) evaluate the integral $\int KdZ$ from Z Temperature Profile

    (c) calculate n from the integral

    (d) calculate value of I from n and D

	Wiedemann-Franz Law			Computer Program with Tabulated values of K and ρ	
D	I	Q_T	T_{MAX}	I	Q_T
N.D.	amp	watt	Kelvin	amp	watt
0	0	0.311	300	0	0.329
0.1	92.6	0.352	300	50	0.332
0.2	155	0.417	300	100	0.342
0.25	189	0.453	300	150	0.358
0.309	310} 280}	0.671} 0.604}	326} 300} $I > I_{opt}$	200	0.384
0.308	315} 275}	0.683} 0.596}	345} 300} $I < I_{opt}$	250	0.425
0.31	300	0.636	300	270(optimum)	0.45

APPENDIX F

TESTING THE COUNTERFLOW CRYOGENIC CURRENT LEADS

F.   In situations where the theory is known to be reliable final designs

should perform according to the specifications;   however, when the theory

is questionable extensive testing is necessary to verify the performance of

a component and, where necessary, modifications made before it can be

confidently put into reliable service.   The latter was the situation, as

seen by the author, with the adopted fin design for the counterflow cryogenic

current leads which supplied the excitation current to the superconducting

coil and provided the transition from normal conduction to superconduction.

F-1 Testing with Liquid Nitrogen

For economical reasons the testing of the leads was restricted to the

measurement of the heat introduced to liquid nitrogen in a properly

insulated cryostat via leads terminated with a short circuit (simulating

the superconducting coil) and carrying different currents.

To obtain data as accurately as possible the heat inleaks were measured

as the level of the liquid nitrogen fell from approximately 350mm to 700mm

from the room temperature extremity of the 650mm long leads.

The method adopted for obtaining the heat inleaks was to measure the

time taken by the boil off gases to displace a predetermined volume of water

from under an upturned beaker.   Allowances for the water temperature, the

water vapour pressure, and the prevailing atmospheric pressure were made

when calculating the heat inleak to the liquid nitrogen.

In successful cryostats the ambient heat inleak to the liquid nitrogen

when the leads were not in position was found to be small in comparison with

that from the leads.

F-2 <u>Prediction of the Lead Heat Inleak</u>

A program, which relied upon tabulated data (Appendix E), was developed to calculate the lead heat inleak and the temperature profile of the lead when it is terminated with a short circuit immersed in liquid nitrogen.

Because of the high latent heat of vaporization of liquid helium the leads had to be de-rated considerably for the operation into liquid nitrogen. For example, the leads optimised to supply 300 ampere into liquid helium are the optimum leads for the supply of 80 ampere into liquid nitrogen.

F-3 <u>Comparison of Results</u>

The calculated and the measured results are tabulated below (Table F-1) and also plotted - figure 6-13. The two sets of results compared favourably hence it was known that the leads would operate satisfactorily when supplying the higher currents to the superconducting coil.

<u>TABLE F-1</u>

300 AMPERE LEAD HEAT INLEAK TESTS TO LIQUID NITROGEN

CURRENT (ampere)	<u>HEAT INLEAKS</u> (watts)			
	PREDICTED (calculated using the computer program)		MEASURED	
			1st SET unsuccessful cryostat	2nd SET successful cryostat
0	2.06		1.61 to 2.4	2.09
20	2.14		2.1 to 2.3	
40	2.4		2.3 to 3.05	
60	2.9		3.67	
optimum→80	3.69	4.1	4.19 to 4.47	
100	4.95		6.4	
120	6.9			
		calculated using the Wiedemann-Franz Law approximation		

APPENDIX G

PRELIMINARY TESTS ON THE INITIAL MACHINE

G.   The preliminary tests on the initial machine were performed so
that the operating characteristics of the armature were known prior to
the use of the superconducting field windings. Tests on the field flux
density and armature reaction flux density in the vicinity of the field
windings were necessary to determine whether the critical flux density of
the niobium-titanium superconductor would be exceeded.

G-1   Open circuit voltage

Two field coils of dimensions similar to the envisaged superconduct-
ing field coils were wound with 400 turns each from 21 B & S copper wire.
The armature was driven at 940 rpm and the following results (Table G.1)
of open circuit voltage versus field current were obtained.

Using linear interpolation to a field current of 300 amps the
voltage of the initial machine at 1500 rpm would be:

$$E = \frac{1.505 - 0.01}{10} * \frac{1500}{940} * 300 \text{ volts}$$

$$E = 71.5 \text{ volts.}$$

G-2   Field flux density

The field flux density was measured at the inner radius of the
field coil for different field currents - Table G-1. The measurements
were made at the inner radius because the field flux density was at its
greatest value at that radius.

Linear interpolation was used (see below) to calculate the peak
field flux density in the region of the superconductor.

$$\text{Peak flux density} = 940 * \frac{300}{10} * 10^{-4} \text{ tesla}$$

$$= 2.82 \text{ tesla}$$

The critical flux density for the superconductor used (Niomax FM C361) at 300 amps is 6.5 tesla hence quenching due to excessive flux densities should not be a problem. Plotting the load line of the field coils on the critical current curve of the superconductor indicated that a field current of up to 460 amps should be possible before quenching due to excessive flux density would occur.

TABLE G-1

INITIAL MACHINE TEST RESULTS

| Field Current (amp)	Open circuit Voltage (940rpm)(volts)	Inner radius of field coil gauss	Centre of field coil gauss
0	0.01	0	0
2	0.305	189	100
4	0.606	378	203
6	0.895	565	306
8	1.19	760	410
10	1.505	940	512

APPENDIX   H

SUPERCONDUCTOR PROPERTIES

H.   The particular superconductor used during the course of the
study was an Imperial Metals Industries (Kynoch) Limited intrinsically-
stable niobium-titanium alloy superconductor. This superconductor has
361 very fine alloy filaments embedded in a high-conductivity copper
matrix.

The critical parameters used for the conductor are given in
figure H-1.

Figure H-1 illustrates the critical parameters assumed for
the conductor and used for all appropriate calculations.

FIG H-1
CRITICAL PARAMETERS
NIOBIUM-TITANIUM ALLOY
SUPERCONDUCTOR
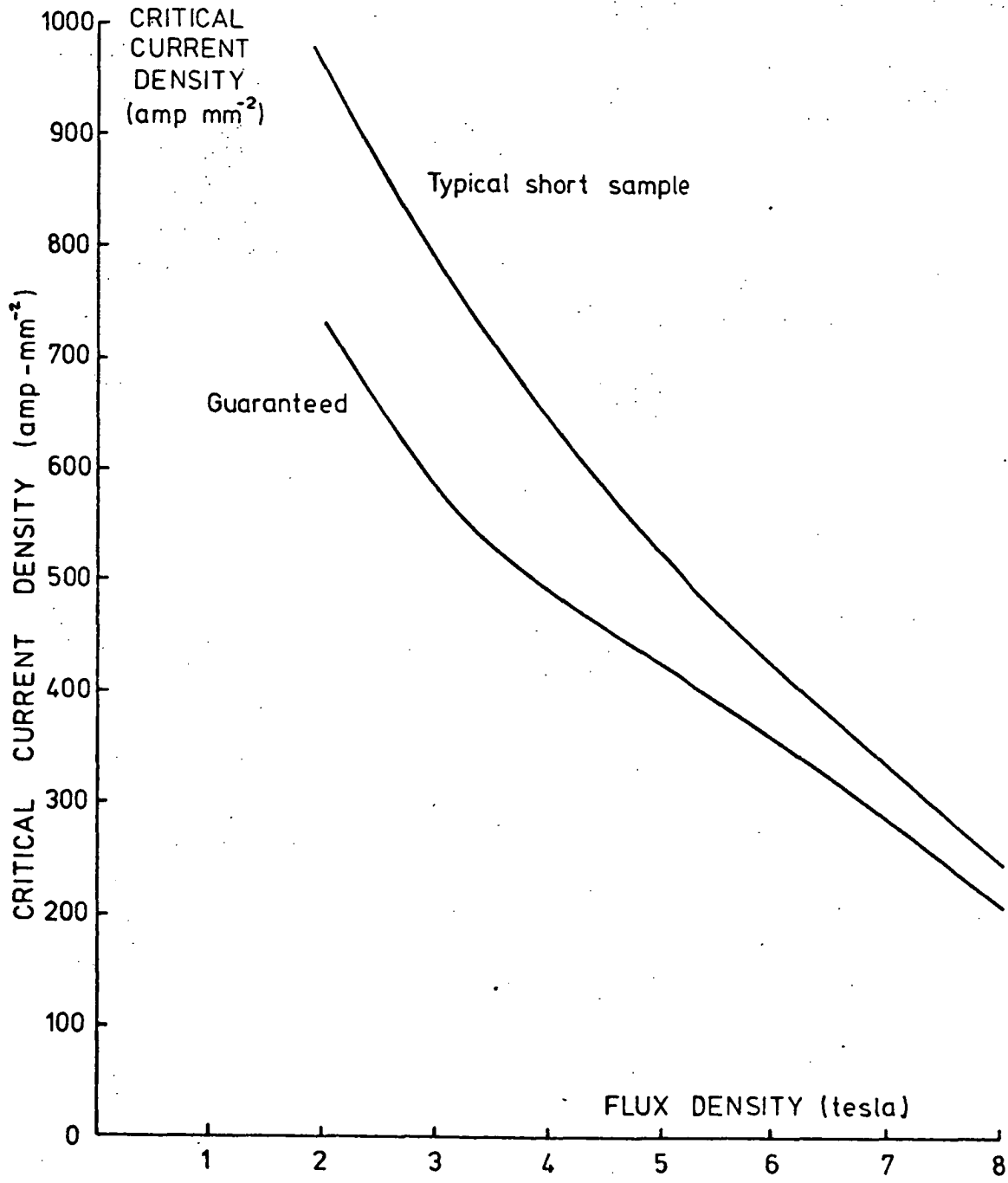
GENERAL FLUX DENSITY OF A CIRCULAR COIL
WITH A RECTANGULAR CROSS SECTION

I. Single Turn Coil

With a reference to figure I-1, the radial and axial components
of the flux density are given by equations I-1 and I-2 respectively.

$$B = \frac{\mu_0 i}{4\pi} \int \frac{d\ell \times \hat{r}}{r^2}$$

$$= \frac{\mu_0 i}{4\pi} \int \frac{d\ell \times (c\,\hat{r}_1 + b\,\hat{r}_2)}{r^3}$$

$$B_r = \frac{\mu_0 i}{4\pi r_0} \int_0^{2\pi} \frac{b/r_0 \cos\theta \, d\theta}{[(a/r_0)^2 + (b/r_0)^2 + 1 - 2a/r_0 \cos\theta]^{3/2}} \qquad (I\text{-}1)$$

$$B_a = \frac{\mu_0 i}{4\pi r_0} \int_0^{2\pi} \frac{(1 - a/r_0 \cos\theta) \, d\theta}{[(a/r_0)^2 + (b/r_0)^2 + 1 - 2A/r_0 \cos\theta]^{3/2}} \qquad (I\text{-}2)$$

I-1 Rectangular Cross Sectioned Coil

With reference to figure I-2 and using equations I-1 and I-2
the radial and axial components of flux density for the general coil are
given by equations I-3 and I-4 respectively.

$$B_r(a,b,) = \frac{\mu_0 J R_0}{4\pi} \int_{-B/R_0}^{B/R_0} \int_1^{1+2A/R_0} \int_0^{2\pi} \frac{\alpha(b/R_0 - \beta)\cos\theta \, d\theta \, d\alpha \, d\beta}{[(b/R_0 - \beta)^2 + (a/R_0)^2 + \alpha^2 - 2a/R_0 \alpha \cos\theta]^{3/2}}$$
$$(I\text{-}3)$$

$$B_a(a,b,) = \frac{\mu_0 J R_0}{4\pi} \int_{-B/R_0}^{B/R_0} \int_1^{1+2A/R_0} \int_0^{2\pi} \frac{\alpha(\alpha - a/R_0 \cos\theta) \, d\theta \, d\alpha \, d\beta}{[(b/R_0 - \beta)^2 + (a/R_0)^2 + \alpha^2 - 2a/R_0 \alpha \cos\theta]^{3/2}}$$
$$(I\text{-}4)$$

where $\alpha = a/R_0$ and $\beta = y/R_0$.

Special care had to be taken when evaluating the maximum coil
flux density ($\alpha=1$, $\beta=0$) as both the numerator and denominator went to zero
simultaneously. A program was written which evaluated the integrals
from the expression given by equations I-5 and I-6.

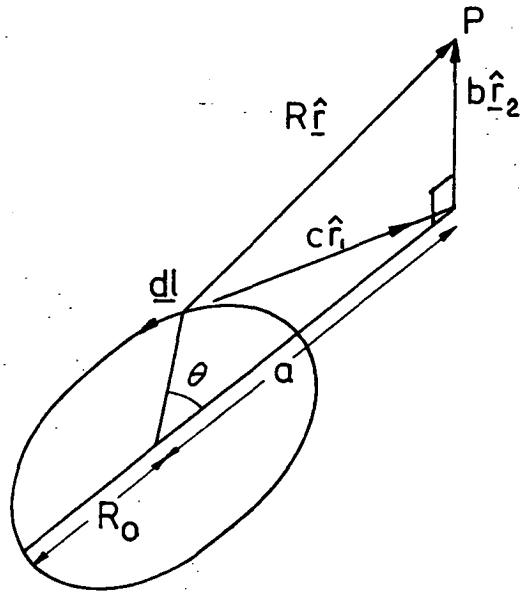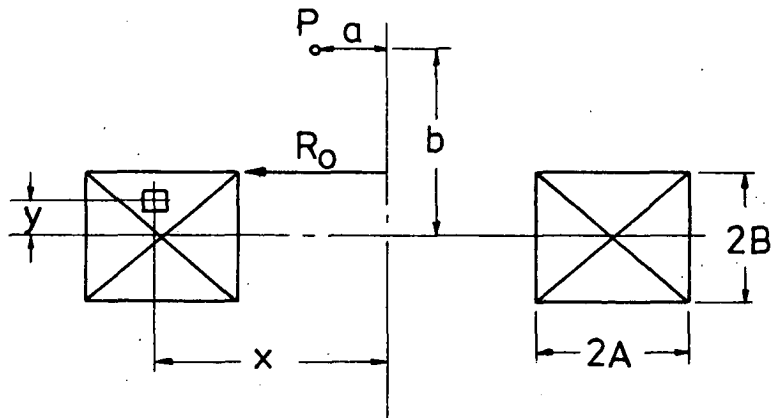# FIG I-1
FLUX DENSITY OF A
SINGLE TURN COIL

FIG I-2
FLUX DENSITY OF A COIL WITH
RECTANGULAR CROSS SECTION

$$B_a(a,b) = \frac{\mu_o *(\text{Ampere Turns})}{R_o} * \frac{1}{2LMN} \sum_{i=1-N/2}^{i=N/2} \sum_{j=1}^{M} \sum_{k=1}^{L} \frac{\alpha(\alpha - a/R_o \cos\theta)}{R^3} \qquad (I-5)$$

$$B_r(a,b) = \frac{\mu_o *(\text{Ampere Turns})}{R_o} * \frac{1}{2LMN} \sum_{i=1-N/2}^{i=N/2} \sum_{j=1}^{M} \sum_{k=1}^{L} \frac{\alpha(b/R_o - \beta)\cos\theta}{R^{3/2}} \qquad (I-6)$$

where:

$$\alpha = 1 + (j - 0.5)d\alpha \qquad\qquad d\alpha = 2A/R_o * \frac{1}{M}$$
$$\beta = (i - 0.5)d\beta \qquad\qquad d\beta = 2B/R_o * \frac{1}{N}$$
$$\theta = (k - 0.5)d\theta \qquad\qquad d\theta = 2\pi/L$$
$$R = (b/R_o - \beta)^2 + (a/R_o)^2 + \alpha^2 - 2a/R_o\,\alpha\cos\theta$$

It was found that, for the best accuracy, $d\alpha$, $d\beta$, and $d\theta$ should be as near to equal as possible.

I-2   On Axis Coil Flux Density

With $a = 0$ in equation I-3 it was apparent that the radial component is zero. From equation I-4 with $a = 0$ the axial component is given by equation I-7 as derived below.

$$B_a(a,b) = \frac{\mu_o JR_o}{4\pi} \int_{-B/R_o}^{B/R_o} \int_{1}^{1+2A/R_o} \int_{0}^{2\pi} \frac{\alpha^2\, d\theta\, d\alpha\, d\beta}{[(b/R_o - \beta)^2 + \alpha^2]^{3/2}}$$

$$= \frac{\mu_o JR_o}{2} \int_{-B/R_o}^{B/R_o} \int_{1}^{1+2A/R_o} \frac{\alpha^2\, d\alpha\, d\beta}{[(b/R_o - \beta)^2 + \alpha^2]^{3/2}}$$

$$= \frac{\mu_o JR_o}{2} [F(x_1, \psi) - F(x_2, \psi)] \qquad (I-7)$$

where $F(x, \psi) = \frac{1}{x} \log_e \left[\frac{\psi + (x^2 + \psi^2)^{1/2}}{1 + (x^2 + 1)^{1/2}} \right]$

$$x_1 = \frac{B + b}{R_o} \qquad x_2 = \frac{b - B}{R_o}$$

$$\psi = 1 + 2A/R_o$$

The evaluation of the double integral was achieved by noting that:

$$\int \frac{1}{(Z^2 + 1)^{\frac{1}{2}}} \, dZ = \log_e [Z + \sqrt{1 + Z^2}]$$

$$\int \frac{1}{(Z^2 + 1)^{3/2}} \, dZ = Z/(Z^2 + 1)^{\frac{1}{2}}$$

VOLUME OPTIMIZATION OF CIRCULAR COILS WITH
A RECTANGULAR CROSS SECTION

J.   Introduction

Optimization aim: to design a coil, with a predetermined average current density and inner radius, of minimum conductor volume to produce a required central flux density.

J-1   Optimization

The volume of a coil with reference to figure I-2 is given by equation J-1.

$$V/R_o^3 = \pi \; 2B/R_o \; 2A/R_o \; [2 + 2A/R_o] \tag{J-1}$$

From equation I-7 the coil central flux density, a = 0, b = 0, is given by equation J-2.

$$B_a = \mu_o \; J \; B \; \log_e F \tag{J-2}$$

where

$$F = \frac{1 + 2A/R_o + \{(1 + 2A/R_o)^2 + (B/R_o)^2\}^{\frac{1}{2}}}{1 + \{1 + (B/R_o)^2\}^{\frac{1}{2}}}$$

Rearranging equation J-2 and introducing the coil ampere-turns I = J*2A*2B resulted in equation J-3.

$$\frac{B_a R_o}{\mu_o I} = \frac{2A}{R_o} \log_e F \tag{J-3}$$

With the aid of a search type computer program the right hand side of equation J-3 was maximised for a given value of the non-dimensional coil volume, V/R_o^3.

For a given coil inner radius and central flux density the results (table J-1) represent the minimum coil ampere turns required for a given volume. The corresponding minimum average coil current density can then be calculated. This was however the reverse of the required process; that is, given the average coil current density it was necessary to find the minimum required coil volume to produce the central flux density.

A solution technique which gives the desired results is as follows:

<u>Data</u>

Central Flux Density	B_a	tesla
Coil Inner Radius	R_o	metres
Coil Average Flux Density	J	amp/metre^2

<u>Technique</u>

a)   Guess a value of $2A/R_o$ or V/R_o^3

b)   From table J-1 obtain the corresponding value of V/R_o^3 or $2A/R_o$

c)   Calculate $2B/R_o = V/R_o^3 * \dfrac{1}{\pi\, 2A/R_o\, (2 + 2A/R_o)}$

d)   Calculate $\dfrac{B_o R_o}{\mu_o I} = \dfrac{B_o}{\mu_o R_o\, J\, 2A/R_o\, 2B/R_o}$

e)   Compare the value of $\dfrac{B_o R_o}{\mu_o I}$ with the corresponding value for the guess value of $2A/R_o$ or V/R_o^3

f)   If agreement is good, then one has the required result: otherwise another guess value of $2A/R_o$ or V/R_o^3 would be required.

Table J-1 also gives the data required for the calculation of the maximum flux density within the coil so that a check to see if the critical flux density is exceeded can be made.

COIL OPTIMIZATION

Table J-1

Volume V/R_o^3	Radial Thickness $2A/R_o$	Axial Length $2B/R_o$	Maximum Central Flux Density $B_o\, R_o/\mu_o\, I$	Coil Maximum Flux Density $B_{MAX}\, R_o/\mu_o\, I$
0.01	0.01072	0.14767	0.496	2.883
0.02	0.01722	0.18330	0.4937	2.566
0.05	0.03162	0.24770	0.4886	2.091
0.10	0.04960	0.3131	0.4824	1.689
0.20	0.07829	0.3913	0.4731	1.389
0.50	0.14219	0.5225	0.4541	1.038
1.	0.223	0.64214	0.4334	0.856

STRENGTH DISC DESIGN OF A DISC TYPE
HOMOPOLAR MACHINE

K.   Introduction

The armature conductors of a disc type homopolar machine are supported by a strength disc. The disc has to withstand stresses which arise from the machine load torque and the rotation of the armature.

The thickness of the strength disc was assumed to be constant and was selected on the basis of maintaining the maximum stress below a predetermined upper limit.

K-1   Strength Disc Design

With reference to figure K-1 the maximum radial and maximum circumferential stresses due to rotation are given by equations (K-1) and (K-2) respectively.

$$\sigma_{rMAX} = \frac{3 + \nu}{8} \rho \, \omega^2 \, (b - a)^2 \tag{K-1}$$

$$\sigma_{cMAX} = \frac{3 + \nu}{4} \rho \, \omega^2 \, (b^2 + \frac{1 - \nu}{3 + \nu} \, a^2) \tag{K-2}$$

The maximum radial stress occurs at $r = \sqrt{ab}$ and the maximum circumferential stress occurs at $r = a$. From the inspection of equations K-1 and K-2 the maximum circumferential stress is always greater than the maximum radial stress. Hence the design of the disc considers the stresses at the inner disc radius where the maximum circumferential stress and the full machine torque occurs. The radial stress at the inner radius is zero.

At the inner disc radius the machine torque manifests itself as a shear stress which, combined with the circumferential stress results in the total disc stress.

The resultant principal stresses and the maximum shear stress were calculated using Mohr's Circle theory.

The shear stress at the inner radius due to the load torque is given by equation K-3.

FIG K-1
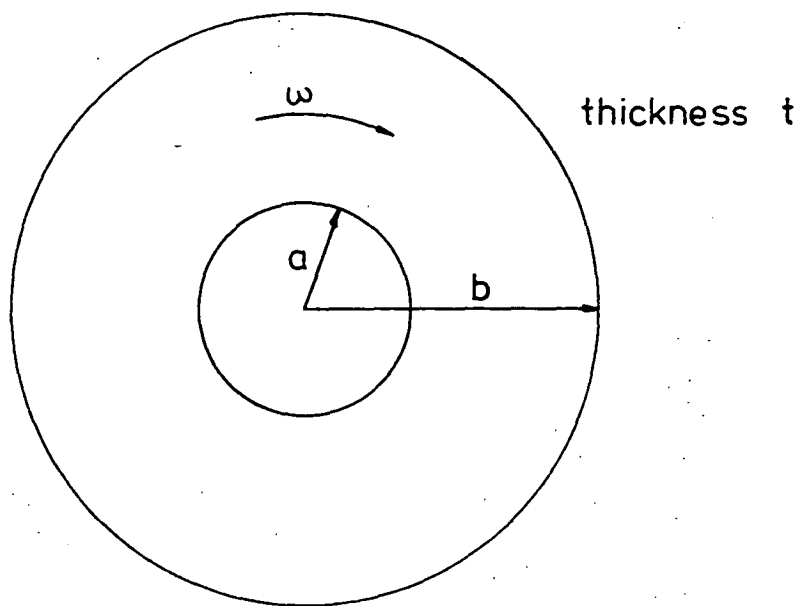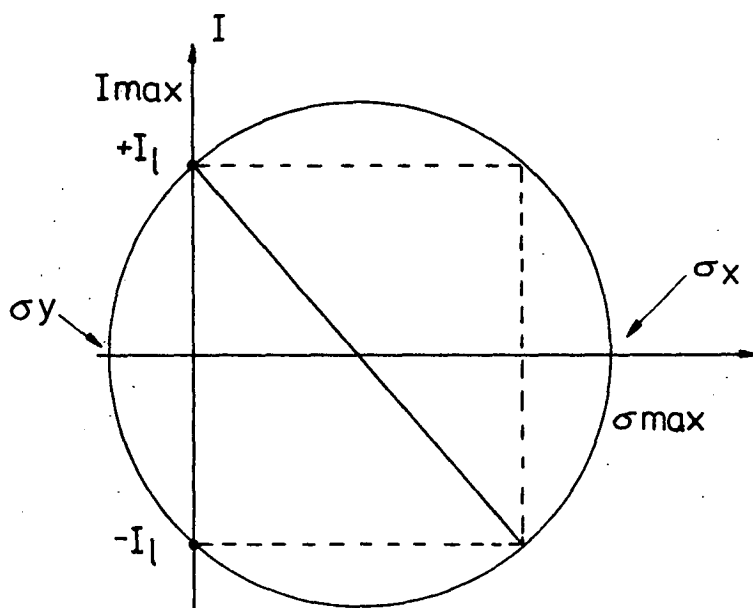HOMOPOLAR MACHINE STRENGTH DISC

FIG K-2
MOHR'S CIRCLE AT THE INNER
RADIUS OF A STRENGTH DISC

$$I_\ell = \frac{T}{2\pi t a^2} \qquad \text{(K-3)}$$

I_ℓ = shear stress (Newton-metre^{-2})

T = load torque (Newton-metre)

t = disc thickness (metres)

a = disc inner radius (metres)

With reference to figure K-2 the principal stresses and the maximum shear stresses are given by equations K-4, K-5 and K-6 respectively.

$$\sigma_x = \frac{\sigma_{cMAX}}{2} + \left(I_\ell^2 + \frac{\sigma^2_{cMAX}}{4} \right)^{\frac{1}{2}} \qquad \text{(K-4)}$$

$$\sigma_y = \frac{\sigma_{cMAX}}{2} - \left(I_\ell^2 + \frac{\sigma^2_{cMAX}}{4} \right)^{\frac{1}{2}} \qquad \text{(K-5)}$$

$$I_{MAX} = \left(I_\ell^2 + \frac{\sigma^2_{cMAX}}{4} \right)^{\frac{1}{2}} \qquad \text{(K-6)}$$

The effective density of the disc, which is used in equations K-1 and K-2, takes into account the armature conductors and is given by equation K-7.

$$\rho_\ell = \rho + \rho_c \frac{t_c}{t} \qquad \text{(K-7)}$$

ρ = disc material density (Kg-metre^{-3})

ρ_c = armature conductor density (Kg-metre^{-3})

t = disc material thickness (metre)

t_c = armature conductor total thickness (metre)

The thickness of the disc was selected so that the upper limits of the stresses were not exceeded.

APPENDIX L

ARMATURE TYPE FIELD AND ARMATURE REACTION

FLUX CALCULATIONS

L.   Introduction

The following develops formulae which were used to estimate the radial and circumferential flux density components due to current flow in armature type windings. The armature reaction fluxes were calculated to ascertain their effect upon the operation of a superconducting field system in a prototype machine of the format finally selected. The formulae also apply to the calculation of the field flux densities of the field system format selected.

L-1   Approximation

The approximation made to ease the calculations assumed that the armature length was infinite. This resulted in the over estimation of both the armature reaction and field flux densities.

With reference to figure L-1, the flux density of a wire of finite length, as a fraction of that produced by an infinite wire, is given by equation L-1.

$$B/B_\infty = (\cos \theta_1 + \cos \theta_2)/2 \qquad\qquad (L-1)$$

For small values of θ_1 and θ_2 the approximation is evidently justified; but for increasing values of θ_1 and θ_2 the accuracy for a single wire decreases considerably. However, when in close proximity to the winding (as is the case with the armature conductors and the field winding) the contribution to the flux density by distant wires is considerably less than that of the wires where the assumption that $B/B_\infty = 1$ is applicable. This reduces errors that could occur when the approximation is not appropriate.

When considering the armature reaction fluxes the over estimation of the flux densities results in calculations which are on the safe side. However, when considering the armature type field winding fluxes, the over estimation of the total pole flux in the region of the active portion of the armature conductors would result in terminal voltages below those designed for. This is offset because the flux densities in the region of the armature end windings has not been taken into account. The added voltage generated
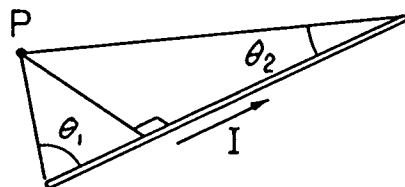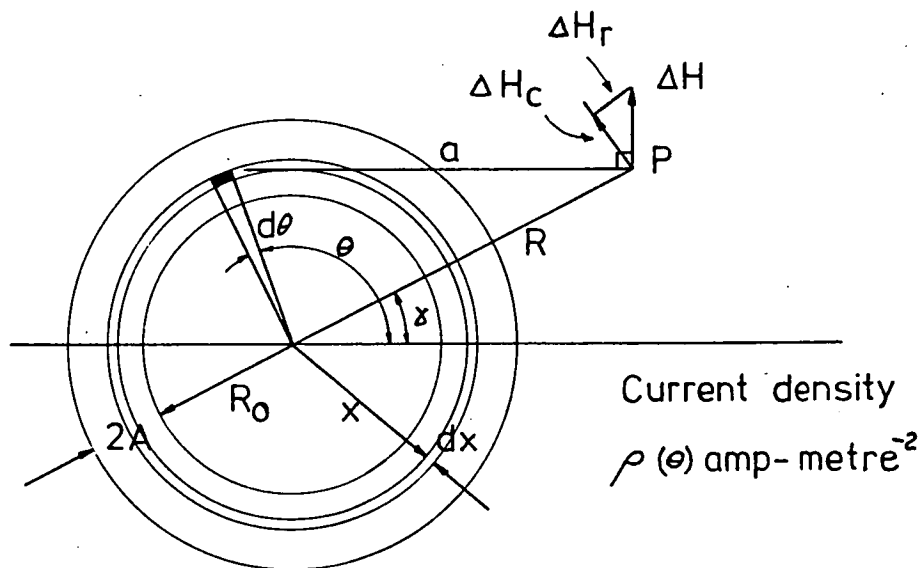
FIG L-1
FLUX DENSITY OF A WIRE
OF FINITE LENGTH

FIG L-2
FLUX DENSITY OF A CURRENT SHEET
OF FINITE THICKNESS

Current density

$\rho\ (\theta)$ amp-metre^{-2}

in the end connections could produce terminal voltages greater than the design value.

L-2 Calculations of Flux Densities

With reference to figure L-2, the circumferential and radial components of the flux density are given by equations L-2 and L-3 respectively.

$$B_c = \frac{\mu_o}{\pi} \int_{R_o}^{R_o+2A} \int_0^{2\pi} \frac{\rho(\theta) \; x \; (R^2 - Rx \cos(\theta - \chi))}{R(R^2 + x^2 - 2Rx \cos(\theta - \chi))} \; d\theta \; dx \qquad (L-2)$$

$$B_r = \frac{\mu_o}{\pi} \int_{R_o}^{R_o+2A} \int_0^{2\pi} \frac{\rho(\theta) \; x^2 \sin(\theta - \chi)}{[R^2 + x^2 - 2Rx \cos(\theta - \chi)]} \; d\theta \; dx \qquad (L-3)$$

$\rho(\theta)$ equals the winding average current density in ampere/metre^2 and varies with angle only and not radius.

The inner radius of the winding, R_o, was used to non-dimensionalise the integrations. This results in equations L-4 and L-5 for B_c and B_r respectively.

$$B_c = \frac{\mu_o R_o}{\pi} \int_1^{1+2A/R_o} \int_0^{2\pi} \frac{\rho(\theta) \; r \; (r^2 - r\alpha\cos(\theta - \chi))}{\alpha[r^2 + \alpha^2 - 2r\alpha\cos(\theta - \chi)]} \; d\theta \; d\alpha \qquad (L-4)$$

$$B_r = \frac{\mu_o R_o}{\pi} \int_1^{1+2A/R_o} \int_0^{2\pi} \frac{\rho(\theta) \; \alpha^2 \sin(\theta - \chi)}{[r^2 + \alpha^2 - 2r\alpha\cos(\theta - \chi)]} \; d\theta \; d\alpha \qquad (L-5)$$

Equation L-4 is elliptic hence its evaluation requires either tables or lengthy computations.

For an armature type winding the current density, $\rho(\theta)$, is a square wave function of the angle θ. The period of the square wave is determined by the number of poles in the winding as given by equation L-6.

$$\theta_p = 2\pi/n \qquad (L-6)$$

θ_p = square wave period (radians)
n = number of poles.

Integration of equation L-5 with respect to theta thus results in equation L-7.

$$H_r = \frac{\mu_o R_o \rho}{\pi r} \sum_{j=1}^{n} (-1)^j \int_1^{1+2A/R_o} \alpha \ln [r^2 + \alpha^2 - 2r\alpha \cos\phi] \, d\alpha \qquad (L-7)$$

where $\phi = 2\pi(j-1)/n - \chi$, ρ = current density (amp-metre^{-2}).

The indefinite integral of equation L-7 is given by equation L-8 and H_r is given by equation L-9.

$$I(\alpha) = \tfrac{1}{2}[\alpha^2 - r^2 \cos 2\phi) * \log_e (\alpha^2 + r^2 - 2\alpha r \cos\phi) - \alpha^2 - 2\alpha r \cos\phi$$

$$+ 2r^2 \sin 2\phi * \arctan \frac{\alpha - r \cos\phi}{r \sin\phi}] \qquad (L-8)$$

$$H_r = \frac{\mu_o R_o \rho}{2\pi r} \sum_{j=1}^{n} (-1)^j (I(1+2A/R_o) - I(1)) \qquad (L-9)$$

The evaluation of equation L-9 has one problem which occurs when $\cos\phi = 1$ and r equals one of the limits; that is unity or $1+2A/R_o$. This was resolved with the observation that:

$$(\alpha - r) \ln (\alpha - r) \to 0 \text{ as } \alpha \to r$$

$$\sin 2\phi * \arctan \left(\frac{\alpha - r \cos\phi}{r \sin\phi}\right) = 0 \text{ when } \sin\phi = 0$$

L-3   Effect of Armature End Windings

If the approximation was considered not to be appropriate, then to justify the added complication of the resulting calculations, the effect of the end windings would also require consideration.

With reference to figure L-3, which represents the directions of the armature currents in an actual winding, the total longitudinal and circumferential currents in the end winding regions are given by equations L-10 and L-11 respectively.
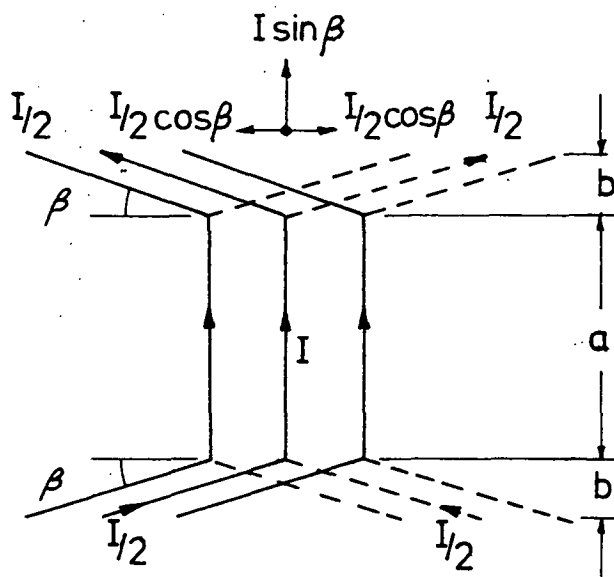
$$i_\ell = i \sin \beta \qquad (L-10)$$
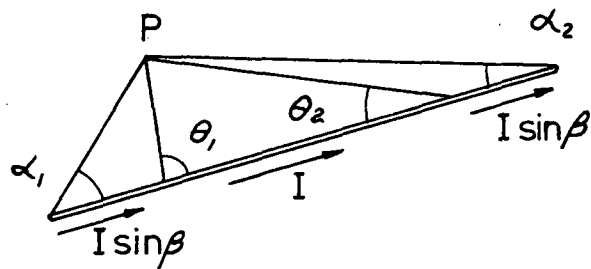
$$i_c = 0 \qquad (L-11)$$

The flux density of an equivalent armature conductor (figure L-3) which included the effects of the end winding, is given by equation L-12.

$$B/B_\infty = \tfrac{1}{2}[(\cos \theta_1 + \cos \theta_2)*(1 - \sin \beta) + (\cos \alpha_1 + \cos \alpha_2)*\sin \beta] \qquad (L-12)$$

It can be seen that allowance for this refinement in equations L-2

Armature representation

Equivalent Armature Conductor

FIG L-3
EFFECT OF ARMATURE
END WINDINGS

and L-3 leads to involved expressions which would require digital techniques to solve. Even though the refinement would be "messy", the author considered that there would be little difficulty in evaluating the expressions and that the added accuracy was not warranted for his purposes.

L-4 Accuracy of Calculation

To test the validity of equation L-9, the flux density distribution of a winding with the following specifications was measured and calculated. The results for the peak flux densities are plotted in figure L-4 for comparison.

internal diameter	190.5 mm
thickness of winding	7.4 ± 0.2 mm
number of poles	4
number of turns per pole	200
conductor diameter	1 mm
active length	190.5 mm
total length	340 mm

The results compare favourably and the calculated values indicate an over-estimation of the actual maximum winding flux density, which gives a conservative design when considering quench flux densities.

Equation L-4 was thus considered to be sufficiently accurate for flux density distribution calculations.

FIG L-4
PEAK RADIAL FLUX DENSITY
Current = 3amp
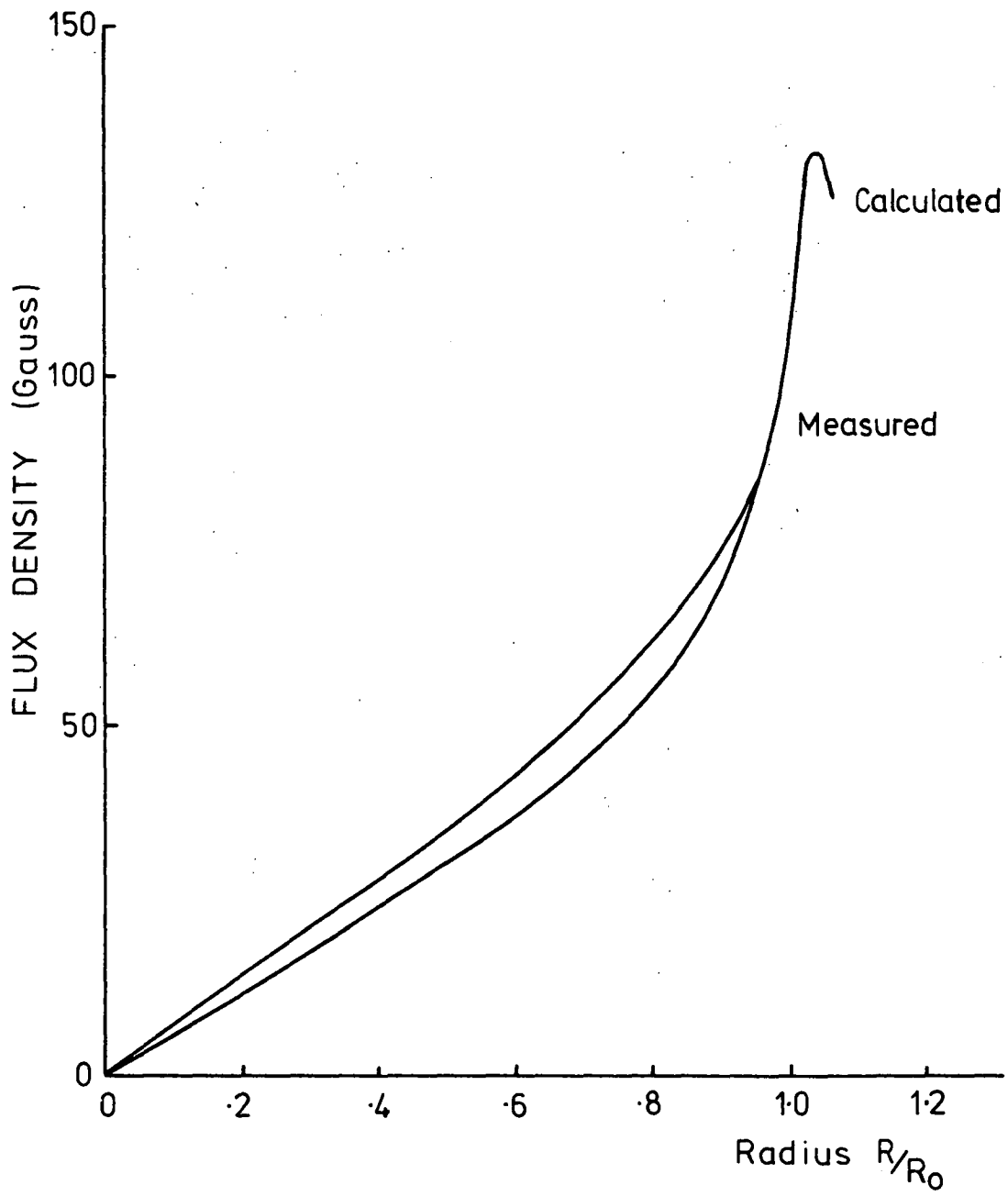
COIL MUTUAL AND SELF INDUCTANCE CALCULATIONS

M. Introduction

An estimation of the self inductances of armature coils was achieved with the aid of the guidelines set out in reference 13-13. There was not an expression for the mutual inductance of rectangular coils in the above reference hence a suitable expression was derived.

M-1 Single Turn Rectangular Coils

With reference to figure M-1 the mutual inductance of the coils is given by equation M-1.

$$M_{12} = \Phi_{12}/I_2 \qquad\qquad (M-1)$$

The flux linking circuit (1) due to the current in circuit (2), Φ_{12}, can be divided into the flux linkages from the four sides of circuit (2) and as sides AB and CD are equivalent equation M-2 results

$$\Phi_{12} = \Phi_{1AB} + \Phi_{1BC} + \Phi_{1CD} + \Phi_{1DA}$$

$$\Phi_{12} = 2\Phi_{1AB} + \Phi_{1BC} + \Phi_{1CD} \qquad\qquad (M-2)$$

The three flux linkages, Φ_{1AB}, Φ_{1BC}, Φ_{1DA}, are given by equations M-3, M-4, and M-5 respectively.

$$\Phi_{1AB} = \int_0^b \int_e^{c+a} \frac{\mu_0 I_2}{4\pi} \frac{1}{y} \left[\frac{a+x}{[y^2 + (a+c)^2]^{\frac{1}{2}}} - \frac{x}{[x^2 + y^2]^{\frac{1}{2}}} \right] dx\, dy \qquad (M-3)$$
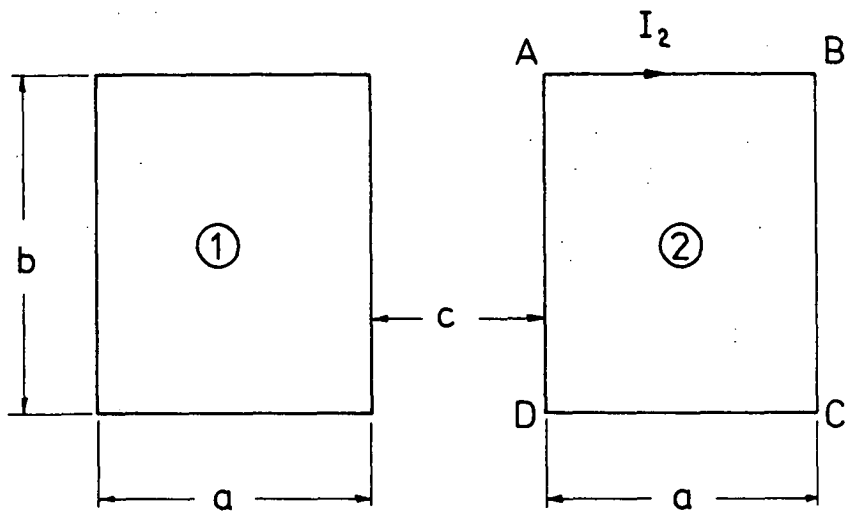
$$\Phi_{1BC} = \int_{a+c}^{2a+c} \int_0^b \frac{\mu_0 I_2}{4\pi} \frac{1}{y} \left[\frac{x}{[x^2 + y^2]^{\frac{1}{2}}} + \frac{b-x}{[(b-x)^2 + y^2]^{\frac{1}{2}}} \right] dx\, dy \qquad (M-4)$$

$$\Phi_{1DA} = \int_c^{c+a} \int_0^b \frac{\mu_0 I_2}{4\pi} \frac{1}{y} \left[\frac{x}{[x^2 + y^2]^{\frac{1}{2}}} + \frac{b-x}{[(b-x)^2 + y^2]^{\frac{1}{2}}} \right] dx\, dy \qquad (M-5)$$

With the aid of equations M-6 and M-7 the double integrals were evaluated. The resulting expression for the mutual inductance is given by equation M-8.

$$\int \frac{\alpha}{(\alpha^2 + 1)^{\frac{1}{2}}} \, d\alpha = (\alpha^2 + 1)^{\frac{1}{2}} \qquad\qquad (M-6)$$

FIG M-1
RECTANGULAR COIL
MUTUAL INDUCTANCE

$$\int \frac{(\beta^2 + 1)^{\frac{1}{2}}}{\beta} \, d\beta = \beta - \tfrac{1}{2} \log_e \left(\frac{\beta + 1}{\beta - 1}\right) \tag{M-7}$$

$$M_{12} = 2 * 10^{-7} * b \left[\sum_{i=1}^{2} x(i) - \sum_{j=1}^{3} F(j) \right] \tag{M-8}$$

where

$$x(i) = y(i) [b(i) - a(i)] = \log_e \frac{c(i) \, (1 + b(i))}{d(i) \, (1 + a(i))}$$

$$F(j) = x(j) [e(j) - \log_e \frac{1 + e(j)}{2}]$$

$$y(1) = 1 \qquad\qquad\qquad y(2) = -1$$

$$a(1) = [1 + (c/b)^2]^{\frac{1}{2}} \qquad\qquad a(2) = [1 + (\frac{c + a}{b})^2]^{\frac{1}{2}}$$

$$b(1) = [1 + (\frac{c + a}{b})^2]^{\frac{1}{2}} \qquad\qquad b(2) = [1 + (\frac{c + 2a}{b})^2]^{\frac{1}{2}}$$

$$c(1) = c/b \qquad\qquad\qquad c(2) = (c + a)/b$$

$$d(1) = (c + a)/b \qquad\qquad d(2) = (c + 2a)/b$$

$$x(1) = (c + 2a)/b \qquad x(2) = -2(c + a)/b \qquad x(3) = c/b$$

$$e(1) = [1 + \frac{b}{(c + 2a)^2}]^{\frac{1}{2}} \quad e(2) = [1 + (\frac{b}{c + a})^2]^{\frac{1}{2}} \quad e(3) = [1 + (\frac{b}{c})^2]^{\frac{1}{2}}$$

The evaluation of the mutual inductance appears to be involved, but in the above form is suited to a simple computer program.

APPENDIX N

HEAT TRANSFER BETWEEN THE CRYOGENIC
CURRENT LEADS AND THE ESCAPING HELIUM
GAS.

N. Introduction

To enhance the transfer of heat from the cryogenic current leads to the escaping helium gas fins were soldered onto the lead conductors. To estimate the effectiveness of the designs adopted the temperature difference between the leads and the escaping gas was estimated using the method given in reference 1.21.

N-1 Estimate of Temperature Difference

With reference to figure 14-2 and considering a section of the lead between cooling fins the following data applies:

copper conductor area	$15.8mm^2$
gas flow area	$596 mm^2$
wetted perimeter	$177 mm$

$$\text{hydraulic mean radius} = \frac{\text{flow area}}{\text{wetted perimeter}}$$

$$= 3.37mm$$

characteristic dimension for Reynold's Number

$$De_{Re} = 4 * \text{hydraulic mean radius}$$

$$= 13.5mm$$

heat transfer area per lead section

at the lead bottom	$906.5mm^2$
at the lead top	$866.6mm^2$

heat transfer characteristic dimension

$$De = 4 * \frac{\text{flow area}}{\text{heat transfer area}} * \text{length}$$

fin spacing at lead bottom	5mm
fin spacing at lead top	4mm

De at lead bottom 13.1mm

De at lead top   11 mm

With the leads operating at the design current of 430 amperes the heat inleak to the liquid helium is 0.912 watts. Assuming the heat of vaporisation of liquid helium at one atmosphere pressure (20.8 joule per gram) a helium loss of 0.0438 gram per second would occur.

Lead Bottom

At the lead bottom the temperature is assumed to be near 4.2K.

At a temperature of 4.2K the following data applies:

viscosity of gaseous helium $1.28 * 10^{-6}$ g/mm-sec

Prandtl Number for gaseous helium 0.9

copper electrical conductivity $5.78 * 10^{-8}$ Ω-mm

thermal conductivity of gaseous helium $9.69 * 10^{-6}$ watt/mm-K

specific heat at constant pressure for helium gas 6.82 J/g-K.

As estimated in Chapter 6 the temperature gradient at the lead bottom is 0.12K/mm, thus the temperature drop over the last segment of the lead is 0.6K.

Thus, the rate of heat transfer to the helium gas

$$= 0.0438 * 6.82 * 0.6 \text{ watts}$$

$$= 0.179 \text{ watt}$$

$$\text{Reynold's Number} = \frac{\text{flow rate}}{\text{flow area}} * \frac{\text{characteristic dimension}}{\text{viscosity}}$$

$$= \frac{0.0438}{596} * \frac{13.5}{1.28*10^{-6}}$$

$$= 775$$

At a Reynold's Number of 775 the flow will be laminar and the Nusselt Number is given by

$$N_{Nu} = 3.65 + \frac{0.0668 * \frac{De}{L} * N_{Re} * N_{Pr}}{1 + 0.04 * [\frac{De}{L} * N_{Re} * N_{Pr}]^{2/3}}$$

$$= 21.1$$

Thus, the heat transfer coefficient

$$= 21.1 * 9.69 * 10^{-6}/13.1 \text{ watt/mm}^2\text{-K}$$

$$= 1.56 * 10^{-5} \text{ watt/mm}^2\text{-K}$$

Thus, the temperature difference between the lead and the helium gas

$$= 0.179/(1.56 * 10^{-5} * 906.5) \text{ K}$$

$$= 12.7 \text{ K}$$

Lead Top

A similar calculation at the lead top gives the following:

rate of heat transfer to the helium gas $= 1.27$ watt

Reynold's Number $= 49.4$ (i.e. laminar flow)

Prandtl Number $= 0.686$

Nusselt Number $= 7.07$

heat transfer coefficient $= 9.76 * 10^{-5} \text{ watt/mm}^2\text{-K}$

temperature difference between the lead and the helium gas $= 18.8$ K

N-2 Conclusion

The cyrogenic current lead design adopted was considered satisfactory because the estimated temperature differences between the lead and the escaping helium were sufficiently small.